UNIVERSITY OF CALIFORNIA
RIVERSIDE

Multiple Strategies for a Selective Detection Task in Mice: Stimulus Attenuation, Prestimulus State, Object-Based and Temporal Transitions with Intermediates Across Learning

A Dissertation submitted in partial satisfaction
of the requirements for the degree of

Doctor of Philosophy

in

Neuroscience

by

Krista C. Marrero

March 2023

Dissertation Committee:
Dr. Edward Zagha, Chairperson
Dr. Anubhuti Goel
Dr. Hongdian Yang

The Dissertation of Krista C. Marrero is approved:

_____

_____

_____

Committee Chairperson

University of California, Riverside

ACKNOWLEDGEMENTS

Included in this dissertation are Chapters 2, 3, and 4, adaptations from previously published materials (Aruljothi et al., 2020; Marrero et al., 2021, 2022; Marrero et al., 2023). Primary contributions, additions, or changes are noted at the beginning of their respective chapters.

I thank my committee members, Dr. Edward Zagha, Dr. Hongdian Yang, and Dr. Anubhuti Goel. I have enjoyed our discussions throughout my research experience. I have found them to be both encouraging and enlightening. Additionally, I thank all the faculty members in the Interdepartmental Ph.D. Program in Neuroscience at UCR for endless inspiring and productive interactions, including professional talks, formal critiques, and casual discussions. Specifically, I thank Dr. Michael Adams, Dr. Monica Carson, Dr. Sachiko Haga-Yamanaka, Dr. Peter Hickmott, Dr. Xiaoping Hu, Dr. Kelly Huffman, Dr. Edward Korzus, Dr. Kalina Michalska, Dr. Khaleel Razak, Dr. Martin Riccomagno, Dr. Viji Santhakumar, and Dr. Aaron Seitz. In one way or another, whether by lab rotations, neuroscience colloquia, special topics courses, or side conversations, you have shaped my academic experience through your mentorship and/or your experimental approach. I thank the Psychology department staff, Renee Young, Jay Melashenko, Sarah Turnbull, and Kirsten Alonso for administrative efforts. I give extra thanks to the Graduate Neuroscience Program Student Advisors: Margarita Roman, Antonio Knox, and Nikita McWells; you have been a lifeline in academic crises and routine graduate affairs.

Most of all, I thank my principal investigator and graduate mentor, Dr. Edward Zagha. You have been reliable and steadfast in your rigor and enthusiasm of all neuroscientific endeavors. I have been the humble recipient of world class mentorship, whether you acknowledge yourself as such or not. I appreciate all the discussions on hypothesis-based experimental research. Your iterative critique of the scientific field has framed my personal ability to ask critical scientific questions, to develop approaches to solving related problems, to convey excitement for the potential impact of my work, and to prioritize findings as they are relevant to the investigation at hand. I have truly benefitted in the first years of your faculty mentorship; I look forward to years of academic discourse as you revolutionize the neuroscience field.

DEDICATIONS

First and foremost, I dedicate this piece to my God: my Heavenly Father, my Lord and Savior Jesus Christ, my Counselor and Confidant Holy Spirit. You have designed me with a passion and a purpose. You truly know me and still love me unconditionally. You have sacrificed all so that I would experience the blessing and grace that I do not deserve. You have guided me step by step according to the amazing plans and purposes that You have for me.

To my husband: Mark Stephen Marrero. I commit my love and respect to you. You have loved me wholly and sacrificially. How could I ask for anything else? Thank you for your diligence and faithfulness as I embarked onto unfamiliar waters. You have been my heart, my love, my one, my only, my partner, and all amidst joy and pain in the building of our life together. I love you. Love, me.

To my inspirational children: Caitlyn Abigayle and Asher Isaac. I devote my life ambition to you. You are the reason I have pursued the path that I have chosen. How can I express the infinite love that you deserve in my limited mother's love capacity? I only hope that you have seen the commitment, perseverance, and sacrifice that an imperfect mother can offer. I strive to be the best version of myself that I can be to love and support my family; I pray that this is the example that you carry into your life experience as well.

For my family: Mom, Dad, little Sis, and big Brother. Thank you for supporting me in all my scientific endeavors. Even when you didn't understand, you always knew the value. For my friend, my spiritual mentor, my pastor, Dr. Rob Spina: thank you for being

my biggest cheerleader. I've made it this far in my process and I have more to go. For all those I love and all those I miss: I would like to share a blessing that my father always prayed over me before he said 'goodbye':

> 'The Lord bless you and keep you; the Lord make His face to shine upon you and be gracious to you; the Lord lift up His countenance upon you and give you peace.'
>
> The priestly blessing, Number 6:24-26 ESV

Finally, for my lab family: the Zaghies – Krithiga, Manas, Angelina, Behzad, and Joanne. It's been real and it's been fun. There is still more to come. Thank you for growing, learning, and understanding as you search for your passion and purpose.

ABSTRACT OF THE DISSERTATION

Multiple Strategies for a Selective Detection Task in Mice: Stimulus Attenuation, Prestimulus State, Object-Based and Temporal Transitions with Intermediates Across Learning

by

Krista C. Marrero

Doctor of Philosophy, Graduate Program in Neuroscience
University of California, Riverside, March 2023
Dr. Edward Zagha, Chairperson

Strategies for optimized performance in any task do not spontaneously occur. They develop over time. Across learning, our first strategy may be a successful strategy. On the other hand, we may require multiple strategies to succeed in a task. In this body of work, we examine spatial and temporal behavioral and neuronal strategies relevant to reward driven decision making using a whisker-based selective detection paradigm where mice learn to selectively respond to a preferred (target) stimulus and selectively ignore a nonpreferred (distractor) stimulus. Through widefield calcium imaging of task-relevant sensory and motor cortices, we first identified comparable target and distractor stimulus encoding in sensory regions, followed by attenuation of distractor and propagation of target encoding in motor regions. We interpret this localized attenuation filter as a

functional, potentially reactive, neural strategy for the selection process after stimulus presentation and before a planned motor response. Then we found that a global cortical state of low activity and low variability in a prestimulus epoch predicted response outcomes. We interpret the global prestimulus profile as a preemptive, potentially proactive, neural strategy before stimulus presentation. Finally, longitudinal investigation across learning behavior revealed that mice used both object-based and temporal strategies to transition from naïve to expert performance in the selective detection task. Furthermore, we found that the transition strategies differed between male and female mice such that male mice overlapped their response and temporal strategies before improving their object-based performance and that female mice improved their performance through sequential temporal and object-based intermediate strategies. We find evidence that supports development of multiple strategies across learning, transitioning mice from suboptimal to optimal performance in the selective detection task. In conjunction with the neural findings of expert behaving mice, we can further our understanding of how behavioral strategies form across learning to maximize successful outcomes.

TABLE OF CONTENTS

LIST OF ABBREVIATIONS

ADHD – Attention Deficit Hyperactive Disorder
ASD – Autism Spectrum Disorder
ALM – Anterior Lateral (anterolateral) Motor Cortex
AUC – Area Under the Curve
Ca^{2+} – Calcium,
CR – Correct Rejections
GFP – Green Fluorescent Protein
GCaMP6s – GFP Calmodulin M13 Protein 6 Slow
FA – False Alarm
ITI – Intertrial Interval
ILI – Interlick Interval
LFP – Local Field Potential
Preme – Premature
Resp – Response
ROC – Receiver Operating Characteristic
ROI – Region of Interest
RT – Reaction Time
S1 – Primary Whisker Somatosensory Cortex
Snap25 – Synaptosome Associated Protein
Spont – Spontaneous
wMC – Primary Whisker Motor Cortex
WME – Whisker Motion Energy

LIST OF EQUATIONS

LIST OF FIGURES

Chapter 1: Introduction and Background

Age-old debates of nature versus nurture occur as far back as the Greek philosophers: Socrates, Plato, and Aristotle. Latter philosophical dichotomies feature the empiricists and the transcendentalists; Immanuel Kant suggested that experiences are not learned but inherent, derived from within a preexisting framework, while John Locke suggested that experience-dependent sensory inputs are acquired and accumulated onto an initially blank slate (Bird, 2023; Rogers, 2023). Thus, the discussion on how the brain processes space and time based on sensory inputs continues. Current investigations, of course, consider both nurture and nature as key aspects in an individual's spatiotemporal perception; though they coexist, the spatial percept has been comprehensively studied compared with the understudied temporal percept. Even so, spatial versus temporal percepts are often distinctly investigated (Dent 2012, Richter 2020). In consideration of mental health disorders such as autism spectrum (ASD), attention deficit (ADHD), learning, and schizophrenic disorders, where atypical behavior both influences and is influenced by complex and dynamic spatiotemporal environments, behavior paradigms can be designed to investigate collective strategic measures instead of isolated cognitive variables (Krakauer et al., 2017; Voelkl et al., 2020; Wurbel et al., 2020).

Neuroscience provides further insight into how the brain processes space and time; throughout this text, spatial and temporal features will be used analogously. Spatial attention is not investigated here. Neither is temporal attention investigated. Instead, we attempt to address the necessary features, including learning aspects, of spatial (object-

based) and temporal (waiting, timing, withholding through a duration) features required for one to selectively detect a preferred stimulus. By investigating and interpreting spatial and temporal features in tandem, we suitably address behavioral and neural components observed in the process of selective detection: selectively ignoring nonpreferred (unrewarded, distractor) stimuli and selectively responding to preferred (rewarded, target) stimuli. Such processes can be further explored regarding various paradigms, animal models, and mental health disorders. The ongoing discussion of whether spatiotemporal processes are natural and inherently preexistent or whether nurtured experience is required for the learning of spatiotemporal paradigms is yet to be satisfied. Hence, the necessity of this body of work, which will explore the object-based features of selective detection, the selective detection 'state', and the unexpected temporal features that became apparent for a whisker-based selective detection paradigm in mice.

Current paradigms investigate various object-based and temporal features. Strategies can include expert performance or developed performance across learning of object-based features; individual strategy contributions to the learning of temporal features, however, are comparatively understudied and need to be further investigated. Object-based goal directed sensory and motor paradigms include tasks for detection (Huber et al., 2012), discrimination (Erlich et al., 2011; Pai et al., 2011; Rudebeck & Murray, 2008; Song et al., 2020), categorization (Baunez & Robbins, 1997, 1999; Freedman et al., 2003; Reinert et al., 2021), and sequencing (Jin & Costa, 2010; Smits-Bandstra & De Nil, 2007), but such tasks also involve non-feature components such as

anticipation (Chen et al., 2017; Grabenhorst et al., 2019; McClure et al., 2003), attention (Katzner et al., 2009; Robbins, 2002), aversion (Chowdhury et al., 2019; Kutlu et al., 2020), confidence (Lak et al., 2014; Lak et al., 2020), emotion (Dolensek et al., 2020; Droit-Volet & Meck, 2007), evidence accumulation (Churchland et al., 2011; Erlich et al., 2015; Roitman & Shadlen, 2002), exploration and exploitation (Gagnon et al., 2016; Gagnon et al., 2018; Pisupati et al., 2021), flexibility (Duan et al., 2021; Nakayama et al., 2018), impulse control (Peterson et al., 1999; Robbins, 2002), reward discounting (Kable & Glimcher, 2007; Mar et al., 2011; Mobini et al., 2002), starting and stopping (Bari & Robbins, 2013; Hanisch et al., 2006), and uncertainty (Daw et al., 2005; Fiorillo et al., 2003; Lawson et al., 2021; Mendonça et al., 2020). These components represent variable mixes of allocentric or egocentric, internal and external, and both object-based and temporal elements that models use while forming strategies (Chen et al., 2021; Guitart-Masip et al., 2012; Reynolds et al., 2001). Optimal strategies for such multi-faceted tasks would involve knowledge of task consistency, restraint, sensorimotor integration, and structure, both spatially and temporally (Harvey et al., 2012; Jimenez-Gomez et al., 2009; McDannald et al., 2011; Walton et al., 2010). For example, in a stop-signal reaction time task, an optimal temporal strategy may include fast ‘stop’ reaction times but is concurrently influenced by known suboptimal phenotypes involving hazard (faster ‘go’ reaction times for longer waits) and motivation (slower overall reaction times upon disengagement) in performance (Hardung et al., 2017; Janssen & Shadlen, 2005; McBurney-Lin et al., 2020; Narayanan & Laubach, 2009). Potential suboptimal temporal

strategies are evidenced in behavioral phenotypes such as fast reaction times for a waiting paradigm (Kopec et al., 2015; Narayanan et al., 2006; Reyes et al., 2020), history-based “win-stay, lose-switch” for a probabilistic paradigm (Chen et al., 2021; Daw et al., 2006; International Brain et al., 2021), choice-based “perseverance” for a block switch paradigm (Ashwood et al., 2022; Busse et al., 2011; Duan et al., 2015; Lak et al., 2020), or withholding response for a target epoch paradigm (Makino & Komiyama, 2015; Tremblay & Schultz, 2000b). For a detection task, temporal strategies transition from suboptimal to optimal, such as naïve “sampling” (Kawai et al., 2015; O'Doherty, 2004; Soon et al., 2008) to expert stimulus-driven “timing” (Romo & Schultz, 1990), and may compete with or synergize with object-based detection strategies (Laubach et al., 2000). The ultimate benefit of temporal transitions in learning converges with that of object-based transitions: competitive edge, efficiency, sensorimotor fluidity, success (Barraclough et al., 2004; O'Doherty et al., 2003; Sakai & Fukai, 2008; Tremblay & Schultz, 2000a).

Paradigm for Selective Detection

Object-based and temporal behavior strategies certainly intertwine throughout the research: their dissociation is, at best, tricky. The temporal features, waiting and timing, may still be determined through object-based paradigms. Correspondingly, we would expect that object-based features, detection and discrimination, may be determined through temporal paradigms (Murakami et al., 2017; Toda et al., 2017). To that end, understanding object-based and temporal strategy transitions in behavioral shaping adds essential elements to the interpretation of naïve, learning, and expert behavior. We draw

our attention to the selective detection task. The selective detection behavior paradigm involves selectively not responding to a distractor stimulus and selectively responding to a target stimulus. The task extends beyond basic detection of a sensory stimulus to the cognitive process of ignoring irrelevant stimuli while responding to relevant stimuli (Aruljothi et al., 2020; Marrero et al., 2021; Zareian et al., 2023).

As mentioned, attention is not evaluated in the selective detection task. Attention can only be examined when a mouse attends and ignores flexibly; this imposes the requirement of switching target and distractor assignments to observe whether one truly attends versus ignores. Measures such as detection and discrimination are used for standard attention paradigms in the field. These are well-established in literature, primarily in primates, and we can leverage standardized signal detection measures to determine selectivity of detection (K. Britten et al., 1992; Britten et al., 1996a; Luck et al., 1997). Selective detection is not explored as extensively in mice; still, the whisker barrel system in mice is ideal for sensory stimuli due to its barrel-specificity, spatial laterality, and prevalence in the natural rodent environment. Also, extensive transgenic methods are utilized involving the whisker barrel system as it maps distinctly onto the smooth surface of the mouse cortex and can therefore be leveraged in the selective detection task (Petersen, 2019). As one can imagine, the benefits of studying how we ignore irrelevant information and respond to relevant information would apply to mental health conditions such as ADHD and ASD.

Stimulus Attenuation Strategy

Stimulus attenuation has been proposed as a framework by which one prevents irrelevant sensory information from influencing decisions based on relevant stimulus information. Effective strategies involve blocking or filtering of specific stimulus information in the cognitive stream of behavior. In the attenuation framework, both target and distractor sensory signals reach lower orders of the cognitive process. The relevant signal is then allowed to propagate to higher orders of the cognitive process, necessary for successful goal-directed behavior. Broadbent proposed that irrelevant signals in the signal processing stream are blocked by an attenuation filter (Broadbent, 1958). Treisman recognized that this, however, did not explain the 'cocktail effect', a well-known phenomenon by which select information (an individual's name) still reaches a higher order process (auditory recognition) by way of the filter despite successful ignoring of ambient noise (Anne M. Treisman, 1964). The nuance seems trivial, but the discussion was essential in fundamental debates regarding attention and the attenuating filter. In chapter 2, we explore the sensory to motor transformation process, providing evidence of the Treisman framework in the mouse whisker system. Importantly, we found a localized attenuation filter between task-related cortical regions, which predicted success in the selective detection task. The discovery of this stimulus attenuation filter is seminal in ongoing investigations into selective behavior and its neural correlates.

Prestimulus State Strategy

The prestimulus period is the short epoch preceding the presentation of an expected stimulus. The overall perspective of an individual in the prestimulus period is termed a 'state' in this body of work and can be imagined as a determinant in any post-stimulus outcome. For a subject in a performance task, the properties of a potential stimulus in the prestimulus epoch are still unknown. Still, the absence of a stimulus in this period can be just as informative in the accumulation of evidence as the presence of the stimulus in the post-stimulus period. Relevant evidence indicates favorable outcomes for in-task success. In this way, the prestimulus state influences perception in a behavior task. Investigations into various paradigms can use this epoch to explore certainty versus uncertainty, anticipation versus surprise, positive versus negative valence, and baseline performance in the prestimulus period. The prestimulus epoch is also used as a proxy for attention, termed the 'fixation period.' For instance, preparatory behavior occurs due to fixation, when the eminence of a stimulus is disclosed before the stimulus occurs; this can be differentiated from an uncued prestimulus epoch.

Although successful selectivity can rely on an individual's prestimulus state as a strategy, research is scarce regarding prestimulus activity in the selective detection goal-directed behavior. Investigation into the prestimulus state began in anesthetized animals, neglecting the overarching goal of understanding the cognitive process of perception (Arieli, 1995, 1996). Prestimulus states have been observed, albeit underreported, in other detection tasks; this is likely due to the object-based feature of the paradigms

employed, which focus on the post-stimulus features of a detected stimulus (S. Crochet & C. C. H. Petersen, 2006; Poulet et al., 2012; Poulet & Petersen, 2008; Zagha et al., 2015). To this end, we question whether a prestimulus state in awake behaving mice determines outcomes for the selective detection task in chapter 3, where we found that global prestimulus activity predicted trial outcomes. Thus, we defined an optimal neural state of low variability with a distinct component profile. The prestimulus state gives insight into determinants for cognitive goal-directed outcomes, which we can further pursue in optimizing conditions for learning and for improved performance in naïve versus expert behavior.

Regions of Interest for Strategies

The strategies investigated here are first seen in behavioral paradigms. Consequently, the neural correlates for successful stimulus attenuation and an optimal prestimulus state are studied only after behavior is established. Neural correlates of behavior are found in the topic of neural cognitive 'maps', which won a Nobel prize for its great impact on both hippocampal and broader neuroscientific communities (Burgess, 2014; McNaughton et al., 2006). Similarly, cortical involvement in cognitive paradigms of behavior is well supported by the literature. Investigations into the primate visual system indicate that early attenuation begins in the thalamus (Crick, 1984a). Some investigations localize attenuation within cortex (Moran & Desimone, 2010). Still others suggest that attenuation occurs within prefrontal cortex (Mante et al., 2013). It is well-established that detected stimulus signals reach primary sensory cortices and that task-related pathways

extend into motor cortices (Shubhodeep Chakrabarti & Cornelius Schwarz, 2018; Chen et al., 2017; Ferezou et al., 2007; Zagha et al., 2015). Specialized cortices are indicated in preparatory signaling, potentially functioning via competing or counterbalanced accumulation mechanisms, which optimizes signal to noise gain to reach internal neural "bounds" (de Lange et al., 2013). For a true prestimulus network, the cortical network closest to a favorable bound would result in a favorable outcome. Therefore, cortex is justified as a critical structure of interest for investigation into the selective detection task. For this body of work, simultaneous visualization of attenuation or prestimulus activity across cortex is made possible by widefield calcium (Ca^{2+}) imaging, which reveals Ca^{2+}-related population neural activity during awake behavior (Guo et al., 2014; Makino et al., 2017; Musall et al., 2019).

Brain regions other than cortex have been considered in cognitive literature. Prefrontal cortices (PFCs) receive the most attention regarding decision making, premature responding, response inhibition, and waiting (Aron et al., 2003; Donnelly et al., 2015; Hayton et al., 2010; Hayton et al., 2011; Pardey et al., 2013). Delay (duration) signals have been shown to persist in motor cortices (M1/M2) and medial PFCs (Finkelstein et al., 2021; Narayanan et al., 2013; Narayanan et al., 2006; Narayanan & Laubach, 2006, 2009; Smith et al., 2010). Other subcortical structures are involved in many aspects of our selective detection paradigm, including anticipation and prediction, premature responding, processing value and reward association, waiting and wait erroring (Fiorillo et al., 2008; Galtress & Kirkpatrick, 2010; Guitart-Masip et al., 2012; Koch et al., 2009;

Miyazaki et al., 2012; Totah et al., 2009; Wiener et al., 2008). For example, striatum is a popular region of interest for stimulus encoding and premature response, both factors in our selective detection task, and is surely indicated in reward processing (Matell & Meck, 2000; Matell & Meck, 2004; Merchant et al., 2013; Zareian et al., 2023). Even though prefrontal and subcortical regions are worth investigating, widefield imaging has yielded cortical sensory to motor 'maps' that can be further investigated for both learning and performance regarding the selective detection task (Aruljothi et al., 2020; Marrero et al., 2021).

Waiting as a Temporal Strategy

We predetermine as a logical premise that waiting is a strategy in the prestimulus period, especially for success in the selective detection task, and that the wait strategy is shaped by reward association. To defend a waiting strategy, as is the case for any other cognitive process, we must agree on the fundamental definition of waiting. Waiting is defined as withholding for a temporal duration (usually for an expected reward or to prevent an impending punishment); it requires temporal recognition of a duration and temporal navigation throughout the duration. Waiting in the selective detection task occurs before stimulus presentation and is motivated by the expectation of reward.

The motivation to wait can be interrupted by several processes. The classic Stanford marshmallow experiment, which investigated children's ability to wait in a delayed gratification task, gives a fun introspection into one aspect that interrupts the motivation to wait (Mischel & Ebbesen, 1970). It was found that the longer the delay, the

less likely a child was motivated to wait for a preferred reward. The test is also referenced as a proxy for impulsivity, a process that interrupts the ability to wait. To ensure voluntary task engagement, the selective detection task required waiting. The waiting strategy can be shaped by punishing impulsive 'premature' responses (Robbins, 2002). Paradigms that allow premature responses do not report waiting (Parker et al., 2014).

The motivation to wait can also be driven by other processes. In an effort to reduce processes down to their essential contributions to motivation, the Piers-Steel "Temporal Motivation Theory" explains motivation through the procrastination equation (Steel, 2007; Steel & König, 2006), a function of expectancy, value, delay, and impulsiveness:

$$Motivation = \frac{Expectancy \times Value}{Impulsiveness \times Delay}$$

Motivation - Equation 1

With these in mind, we can determine the motivation to wait in the selective detection task: before the stimulus presentation, mice must learn strategies based on the expectation of a stimulus, the understanding of reward value, the withholding of impulsive action, and the knowledge the temporal restriction of waiting through a delay. Hence, waiting is a strategy and must develop across learning.

Timing as a Temporal Strategy

We apply similar logic to the temporal strategy of timing. We predetermine that timing is a strategy after stimulus presentation for success in the selective detection task, also shaped by reward association. To defend a timing strategy, we must agree on the

fundamental definition: timing is defined as withholding until a target duration (for an expected reward or to prevent punishment); it requires temporal recognition of the target duration and requires temporal navigation for the target execution. Timing in the selective detection task occurs after stimulus presentation, motivated by the expectation of reward.

The selective detection task attempted to remove temporal confounds such as timing (and waiting). For this discussion, timing behavior involves a stimulus and a response. Different tasks vary in temporal aspects, but if there is no stimulus, there is no target timing. Withholding through a duration sans stimulus is still considered waiting. In addition to object-based strategies, in chapter 4, we approach waiting and timing directly as unexpected strategies exhibited by the mice.

Before timing strategies form, reward association must be shaped with classical conditioning: a stimulus is delivered, then a reward is delivered, independent of response activity (Bakhurin et al., 2017). Developing a strategy for target timing recruits operant conditioning: a stimulus is delivered and a reward is only delivered if the subject responds (Kawai et al., 2015). The response behavior is arbitrary when a subject learns a timing task (Reyes et al., 2020; Tunes et al., 2022). If we revisit the procrastination equation, we can determine the motivation to time in the selective detection task: mice must learn strategies based on the expectation of a reward, the understanding of the reward value, the withholding of impulsive reaction, and the temporal knowledge the target delay. Separate from waiting, timing is a strategy and must develop across learning.

Strategies across Learning

Because the decision making process incorporates multiple strategies to transform incoming stimuli into outgoing choices, optimizing performance across learning must employ multiple, dynamic, evolving strategies or readouts. As a subject learns to transition their performance from naïve behavior to expert behave, it takes into consideration the relevance, salience, structure, and readouts of a task paradigm; both object-based and temporal features are integrated into optimal strategies (Emmons et al., 2017; Kar & DiCarlo, 2021; Ni et al., 2018; Ruff & Cohen, 2019).

For our task, after mice have learned stimulus and response reward associations through classical and operant conditioning, they are introduced to the full measure of the selective detection paradigm. In naïve behavior before a stimulus presentation, mice exhibit sampling as spontaneous licking (Dickinson & Balleine, 1994; O'Doherty et al., 2003). They must learn to withhold this prepotent response for a stimulus presentation. In naïve behavior after a stimulus presentation, mice exhibit sampling as randomized responses to a stimulus (Laubach et al., 2000; van Maanen et al., 2012). They must learn to withhold a reactive response immediately after a stimulus presentation.

Learning strategies are known to change across sessions, within sessions, from trial to trial, and, indeed, across animal models (International Brain et al., 2021; Musall et al., 2019; Parker et al., 2015; Roy et al., 2021; Tanaka et al., 2004). Yet, the order of learning for these strategy transitions is frequently overlooked across investigations. Furthermore, the manner and order in which strategies are learned is useful when

investigating neuronal and behavioral correlates, especially when temporal performance is known to be compromised over spatial performance as in ADHD (Pardey et al., 2009; Rubia et al., 2009; Toplak et al., 2006), ASD (Meilleur et al., 2020), learning disorders (Eden et al., 1995), and schizophrenia (Carroll et al., 2009; Lee et al., 2009).

Lastly, it is unknown how, whether, or why male versus female strategies differ. The concern over whether genders are investigated equally has become more and more prevalent in ongoing investigations. It has been found that executive functioning is invariable between genders, positive reinforcement learning affects genders similarly, and that cognitive flexibility paradigms show no differences when comparing genders (Grissom & Reyes, 2019). However, gender differences have been found in avoidance behavior, novel environment navigation, risk, switch and preferential sampling behavior in uncertain conditions, and sensitivity in probabilistic versus certain punishment outcomes (Chen et al., 2021; Gagnon et al., 2016; Gagnon et al., 2018). Consequently, some gender differences have been found to influence efficiency and success depending on the paradigm. It may be that genders show differences in behavior due to an intrinsic prestimulus state, the ability to attenuate a stimulus, initial conditions before learning, final resolutions after learning, or a difference in the learning transition from naïve to expert behavior for the selective detection task.

Relevance of Research

In this body of work, we explore expert performance in awake behaving mice, task-related cortical correlates during this expert behavior, and a longitudinal analysis indicating that

mice use multiple learning strategies as they transition from naïve to expert behavior. The examination of multiple learning strategies regarding behavior adapts a more comprehensive interpretation to ongoing investigations into neural correlates of learning behavior across animal models and task paradigms.

References

Arieli, A. (1995). Coherent Spatiotemporal Patterns of Ongoing Activity Revealed by Real-Time Optical Imaging Coupled With Single-Unit Recording in the Cat Visual Cortex.

Arieli, A. (1996). Dynamics of Ongoing Activity: Explanation of the Large Variability in Evoked Cortical Responses.

Aron, A. R., Fletcher, P. C., Bullmore, E. T., Sahakian, B. J., & Robbins, T. W. (2003). Stop-signal inhibition disrupted by damage to right inferior frontal gyrus in humans. *Nat Neurosci*, *6*(2), 115-116. https://doi.org/10.1038/nn1003

Aruljothi, K., Marrero, K., Zhang, Z., Zareian, B., & Zagha, E. (2020). Functional Localization of an Attenuating Filter within Cortex for a Selective Detection Task in Mice. *The Journal of Neuroscience*, *40*(28), 5443-5454. https://doi.org/10.1523/jneurosci.2993-19.2020

Ashwood, Z. C., Roy, N. A., Stone, I. R., International Brain, L., Urai, A. E., Churchland, A. K., Pouget, A., & Pillow, J. W. (2022). Mice alternate between discrete strategies during perceptual decision-making. *Nat Neurosci*, *25*(2), 201-212. https://doi.org/10.1038/s41593-021-01007-z

Bakhurin, K. I., Goudar, V., Shobe, J. L., Claar, L. D., Buonomano, D. V., & Masmanidis, S. C. (2017). Differential Encoding of Time by Prefrontal and Striatal Network Dynamics. *J Neurosci*, *37*(4), 854-870. https://doi.org/10.1523/JNEUROSCI.1789-16.2016

Bari, A., & Robbins, T. W. (2013). Inhibition and impulsivity: behavioral and neural basis of response control. *Prog Neurobiol*, *108*, 44-79. https://doi.org/10.1016/j.pneurobio.2013.06.005

Barraclough, D. J., Conroy, M. L., & Lee, D. (2004). Prefrontal cortex and decision making in a mixed-strategy game. *Nat Neurosci*, *7*(4), 404-410. https://doi.org/10.1038/nn1209

Baunez, C., & Robbins, T. W. (1997). Bilateral Lesions of the Subthalamic Nucleus Induce Multiple Deficits in an Attentional Task in Rats [https://doi.org/10.1111/j.1460-

9568.1997.tb01376.x]. *European Journal of Neuroscience*, *9*(10), 2086-2099. https://doi.org/https://doi.org/10.1111/j.1460-9568.1997.tb01376.x

Baunez, C., & Robbins, T. W. (1999). Effects of transient inactivation of the subthalamic nucleus by local muscimol and APV infusions on performance on the five-choice serial reaction time task in rats. *Psychopharmacology*, *141*(1), 57-65. https://doi.org/10.1007/s002130050806

Bird, O. A. D., Brian. (2023). Immanuel Kant. In *Encyclopedia Britannica*.

Britten, K., Shadlen, M., Newsome, W., & Movshon, J. (1992). The analysis of visual motion: a comparison of neuronal and psychophysical performance. *The Journal of Neuroscience*, *12*(12), 4745-4765. https://doi.org/10.1523/jneurosci.12-12-04745.1992

Britten, K. H., Newsome, W. T., Shadlen, M. N., Celebrini, S., & Movshon, J. A. (1996). A relationship between behavioral choice and the visual responses of neurons in macaque MT. *Visual Neuroscience*, *13*(1), 87-100. https://doi.org/10.1017/s095252380000715x

Broadbent, D. E. (1958). CHAPTER 2 - SELECTIVE LISTENING TO SPEECH. In D. E. Broadbent (Ed.), *Perception and Communication* (pp. 11-35). Pergamon. https://doi.org/https://doi.org/10.1016/B978-1-4832-0079-8.50004-9

Burgess, N. (2014). The 2014 Nobel Prize in Physiology or Medicine: a spatial model for cognitive neuroscience. *Neuron*, *84*(6), 1120-1125. https://doi.org/10.1016/j.neuron.2014.12.009

Busse, L., Ayaz, A., Dhruv, N. T., Katzner, S., Saleem, A. B., Scholvinck, M. L., Zaharia, A. D., & Carandini, M. (2011). The detection of visual contrast in the behaving mouse. *J Neurosci*, *31*(31), 11351-11361. https://doi.org/10.1523/JNEUROSCI.6689-10.2011

Carroll, C. A., O'Donnell, B. F., Shekhar, A., & Hetrick, W. P. (2009). Timing dysfunctions in schizophrenia as measured by a repetitive finger tapping task. *Brain Cogn*, *71*(3), 345-353. https://doi.org/10.1016/j.bandc.2009.06.009

Chakrabarti, S., & Schwarz, C. (2018). Cortical modulation of sensory flow during active touch in the rat whisker system. *Nature Communications*, *9*(1). https://doi.org/10.1038/s41467-018-06200-6

Chen, C. S., Ebitz, R. B., Bindas, S. R., Redish, A. D., Hayden, B. Y., & Grissom, N. M. (2021). Divergent Strategies for Learning in Males and Females. *Curr Biol*, *31*(1), 39-50 e34. https://doi.org/10.1016/j.cub.2020.09.075

Chen, T. W., Li, N., Daie, K., & Svoboda, K. (2017). A Map of Anticipatory Activity in Mouse Motor Cortex. *Neuron*, *94*(4), 866-879 e864. https://doi.org/10.1016/j.neuron.2017.05.005

Chowdhury, T. G., Wallin-Miller, K. G., Rear, A. A., Park, J., Diaz, V., Simon, N. W., & Moghaddam, B. (2019). Sex differences in reward- and punishment-guided actions. *Cogn Affect Behav Neurosci*, *19*(6), 1404-1417. https://doi.org/10.3758/s13415-019-00736-w

Churchland, A. K., Kiani, R., Chaudhuri, R., Wang, X. J., Pouget, A., & Shadlen, M. N. (2011). Variance as a signature of neural computations during decision making. *Neuron*, *69*(4), 818-831. https://doi.org/10.1016/j.neuron.2010.12.037

Crick, F. (1984). Function of the thalamic reticular complex: the searchlight hypothesis. *Proceedings of the National Academy of Sciences*, *81*(14), 4586-4590. https://doi.org/10.1073/pnas.81.14.4586

Crochet, S., & Petersen, C. C. H. (2006). Correlating whisker behavior with membrane potential in barrel cortex of awake mice. *Nature Neuroscience*, *9*(5), 608-610. https://doi.org/10.1038/nn1690

Daw, N. D., Niv, Y., & Dayan, P. (2005). Uncertainty-based competition between prefrontal and dorsolateral striatal systems for behavioral control. *Nat Neurosci*, *8*(12), 1704-1711. https://doi.org/10.1038/nn1560

Daw, N. D., O'Doherty, J. P., Dayan, P., Seymour, B., & Dolan, R. J. (2006). Cortical substrates for exploratory decisions in humans. *Nature*, *441*(7095), 876-879. https://doi.org/10.1038/nature04766

Dickinson, A., & Balleine, B. W. (1994). Motivational control of goal-directed action. *Animal Learning & Behavior*, *22*, 1-18.

Dolensek, N., Gehrlach, D. A., Klein, A. S., & Gogolla, N. (2020). Facial expressions of emotion states and their neuronal correlates in mice. *Science*, *368*(6486), 89-94. https://doi.org/10.1126/science.aaz9468

Donnelly, N. A., Paulsen, O., Robbins, T. W., & Dalley, J. W. (2015). Ramping single unit activity in the medial prefrontal cortex and ventral striatum reflects the onset of waiting but not imminent impulsive actions. *Eur J Neurosci*, *41*(12), 1524-1537. https://doi.org/10.1111/ejn.12895

Droit-Volet, S., & Meck, W. H. (2007). How emotions colour our perception of time. *Trends Cogn Sci*, *11*(12), 504-513. https://doi.org/10.1016/j.tics.2007.09.008

Duan, C. A., Erlich, J. C., & Brody, C. D. (2015). Requirement of Prefrontal and Midbrain Regions for Rapid Executive Control of Behavior in the Rat. *Neuron*, *86*(6), 1491-1503. https://doi.org/10.1016/j.neuron.2015.05.042

Duan, C. A., Pagan, M., Piet, A. T., Kopec, C. D., Akrami, A., Riordan, A. J., Erlich, J. C., & Brody, C. D. (2021). Collicular circuits for flexible sensorimotor routing. *Nat Neurosci*, *24*(8), 1110-1120. https://doi.org/10.1038/s41593-021-00865-x

Eden, G. F., Stein, J. F., Wood, H. M., & Wood, F. B. (1995). Temporal and Spatial Processing in Reading Disabled and Normal Children. *Cortex*, *31*(3), 451-468. https://doi.org/https://doi.org/10.1016/S0010-9452(13)80059-7

Emmons, E. B., De Corte, B. J., Kim, Y., Parker, K. L., Matell, M. S., & Narayanan, N. S. (2017). Rodent Medial Frontal Control of Temporal Processing in the Dorsomedial Striatum. *J Neurosci*, *37*(36), 8718-8733. https://doi.org/10.1523/JNEUROSCI.1376-17.2017

Erlich, J. C., Bialek, M., & Brody, C. D. (2011). A cortical substrate for memory-guided orienting in the rat. *Neuron*, *72*(2), 330-343. https://doi.org/10.1016/j.neuron.2011.07.010

Erlich, J. C., Brunton, B. W., Duan, C. A., Hanks, T. D., & Brody, C. D. (2015). Distinct effects of prefrontal and parietal cortex inactivations on an accumulation of evidence task in the rat. *Elife*, *4*. https://doi.org/10.7554/eLife.05457

Ferezou, I., Haiss, F., Gentet, L. J., Aronoff, R., Weber, B., & Petersen, C. C. (2007). Spatiotemporal dynamics of cortical sensorimotor integration in behaving mice. *Neuron*, *56*(5), 907-923. https://doi.org/10.1016/j.neuron.2007.10.007

Finkelstein, A., Fontolan, L., Economo, M. N., Li, N., Romani, S., & Svoboda, K. (2021). Attractor dynamics gate cortical information flow during decision-making. *Nat Neurosci*, *24*(6), 843-850. https://doi.org/10.1038/s41593-021-00840-6

Fiorillo, C. D., Newsome, W. T., & Schultz, W. (2008). The temporal precision of reward prediction in dopamine neurons. *Nat Neurosci*, *11*(8), 966-973. https://doi.org/10.1038/nn.2159

Fiorillo, C. D., Tobler, P. N., & Schultz, W. (2003). Discrete Coding of Reward Probability and Uncertainty by Dopamine Neurons. *Science*, *299*(5614), 1898-1902. https://doi.org/10.1126/science.1077349

Freedman, D. J., Riesenhuber, M., Poggio, T., & Miller, E. K. (2003). A Comparison of Primate Prefrontal and Inferior Temporal Cortices during Visual Categorization. *The Journal of Neuroscience*, *23*(12), 5235-5246. https://doi.org/10.1523/jneurosci.23-12-05235.2003

Gagnon, K. T., Cashdan, E. A., Stefanucci, J. K., & Creem-Regehr, S. H. (2016). Sex Differences in Exploration Behavior and the Relationship to Harm Avoidance. *Hum Nat*, *27*(1), 82-97. https://doi.org/10.1007/s12110-015-9248-1

Gagnon, K. T., Thomas, B. J., Munion, A., Creem-Regehr, S. H., Cashdan, E. A., & Stefanucci, J. K. (2018). Not all those who wander are lost: Spatial exploration patterns and their relationship to gender and spatial memory. *Cognition*, *180*, 108-117. https://doi.org/10.1016/j.cognition.2018.06.020

Galtress, T., & Kirkpatrick, K. (2010). The role of the nucleus accumbens core in impulsive choice, timing, and reward processing. *Behav Neurosci*, *124*(1), 26-43. https://doi.org/10.1037/a0018464

Grabenhorst, M., Michalareas, G., Maloney, L. T., & Poeppel, D. (2019). The anticipation of events in time. *Nature Communications*, *10*(1), 5802. https://doi.org/10.1038/s41467-019-13849-0

Grissom, N. M., & Reyes, T. M. (2019). Let's call the whole thing off: evaluating gender and sex differences in executive function. *Neuropsychopharmacology*, *44*(1), 86-96. https://doi.org/10.1038/s41386-018-0179-5

Guitart-Masip, M., Huys, Q. J. M., Fuentemilla, L., Dayan, P., Duzel, E., & Dolan, R. J. (2012). Go and no-go learning in reward and punishment: Interactions between affect and effect. *Neuroimage*, *62*(1), 154-166. https://doi.org/https://doi.org/10.1016/j.neuroimage.2012.04.024

Guo, Z. V., Li, N., Huber, D., Ophir, E., Gutnisky, D., Ting, J. T., Feng, G., & Svoboda, K. (2014). Flow of cortical activity underlying a tactile decision in mice. *Neuron*, *81*(1), 179-194. https://doi.org/10.1016/j.neuron.2013.10.020

Hanisch, C., Radach, R., Holtkamp, K., Herpertz-Dahlmann, B., & Konrad, K. (2006). Oculomotor inhibition in children with and without attention-deficit hyperactivity disorder (ADHD). *J Neural Transm (Vienna)*, *113*(5), 671-684. https://doi.org/10.1007/s00702-005-0344-y

Hardung, S., Epple, R., Jackel, Z., Eriksson, D., Uran, C., Senn, V., Gibor, L., Yizhar, O., & Diester, I. (2017). A Functional Gradient in the Rodent Prefrontal Cortex Supports Behavioral Inhibition. *Curr Biol*, *27*(4), 549-555. https://doi.org/10.1016/j.cub.2016.12.052

Harvey, C. D., Coen, P., & Tank, D. W. (2012). Choice-specific sequences in parietal cortex during a virtual-navigation decision task. *Nature*, *484*(7392), 62-68. https://doi.org/10.1038/nature10918

Hayton, S. J., Lovett-Barron, M., Dumont, E. C., & Olmstead, M. C. (2010). Target-specific encoding of response inhibition: increased contribution of AMPA to NMDA receptors at excitatory synapses in the prefrontal cortex. *J Neurosci*, *30*(34), 11493-11500. https://doi.org/10.1523/JNEUROSCI.1550-10.2010

Hayton, S. J., Olmstead, M. C., & Dumont, E. C. (2011). Shift in the intrinsic excitability of medial prefrontal cortex neurons following training in impulse control and cued-responding tasks. *PLoS One*, *6*(8), e23885. https://doi.org/10.1371/journal.pone.0023885

Huber, D., Gutnisky, D. A., Peron, S., O'Connor, D. H., Wiegert, J. S., Tian, L., Oertner, T. G., Looger, L. L., & Svoboda, K. (2012). Multiple dynamic representations in the

motor cortex during sensorimotor learning. *Nature*, *484*(7395), 473-478. https://doi.org/10.1038/nature11039

International Brain, L., Aguillon-Rodriguez, V., Angelaki, D., Bayer, H., Bonacchi, N., Carandini, M., Cazettes, F., Chapuis, G., Churchland, A. K., Dan, Y., Dewitt, E., Faulkner, M., Forrest, H., Haetzel, L., Hausser, M., Hofer, S. B., Hu, F., Khanal, A., Krasniak, C., . . . Zador, A. M. (2021). Standardized and reproducible measurement of decision-making in mice. *Elife*, *10*. https://doi.org/10.7554/eLife.63711

Janssen, P., & Shadlen, M. N. (2005). A representation of the hazard rate of elapsed time in macaque area LIP. *Nat Neurosci*, *8*(2), 234-241. https://doi.org/10.1038/nn1386

Jimenez-Gomez, C., Podlesnik, C. A., & Shahan, T. A. (2009). Effects of initial-link duration on preference and resistance to change in concurrent-chains schedules. *Behav Processes*, *81*(2), 223-226. https://doi.org/10.1016/j.beproc.2009.02.011

Jin, X., & Costa, R. M. (2010). Start/stop signals emerge in nigrostriatal circuits during sequence learning. *Nature*, *466*(7305), 457-462. https://doi.org/10.1038/nature09263

Kable, J. W., & Glimcher, P. W. (2007). The neural correlates of subjective value during intertemporal choice. *Nat Neurosci*, *10*(12), 1625-1633. https://doi.org/10.1038/nn2007

Kar, K., & DiCarlo, J. J. (2021). Fast Recurrent Processing via Ventrolateral Prefrontal Cortex Is Needed by the Primate Ventral Stream for Robust Core Visual Object Recognition. *Neuron*, *109*(1), 164-176 e165. https://doi.org/10.1016/j.neuron.2020.09.035

Katzner, S., Busse, L., & Treue, S. (2009). Attention to the Color of a Moving Stimulus Modulates Motion-Signal Processing in Macaque Area MT: Evidence for a Unified Attentional System. *Front Syst Neurosci*, *3*, 12. https://doi.org/10.3389/neuro.06.012.2009

Kawai, R., Markman, T., Poddar, R., Ko, R., Fantana, A. L., Dhawale, A. K., Kampff, A. R., & Olveczky, B. P. (2015). Motor cortex is required for learning but not for executing

a motor skill. *Neuron*, *86*(3), 800-812. https://doi.org/10.1016/j.neuron.2015.03.024

Koch, G., Oliveri, M., & Caltagirone, C. (2009). Neural networks engaged in milliseconds and seconds time processing: evidence from transcranial magnetic stimulation and patients with cortical or subcortical dysfunction. *Philos Trans R Soc Lond B Biol Sci*, *364*(1525), 1907-1918. https://doi.org/10.1098/rstb.2009.0018

Kopec, C. D., Erlich, J. C., Brunton, B. W., Deisseroth, K., & Brody, C. D. (2015). Cortical and Subcortical Contributions to Short-Term Memory for Orienting Movements. *Neuron*, *88*(2), 367-377. https://doi.org/10.1016/j.neuron.2015.08.033

Krakauer, J. W., Ghazanfar, A. A., Gomez-Marin, A., MacIver, M. A., & Poeppel, D. (2017). Neuroscience Needs Behavior: Correcting a Reductionist Bias. *Neuron*, *93*(3), 480-490. https://doi.org/10.1016/j.neuron.2016.12.041

Kutlu, M. G., Zachry, J. E., Brady, L. J., Melugin, P. R., Kelly, S. J., Sanders, C., Tat, J., Johnson, A. R., Thibeault, K., Lopez, A. J., Siciliano, C. A., & Calipari, E. S. (2020). A novel multidimensional reinforcement task in mice elucidates sex-specific behavioral strategies. *Neuropsychopharmacology*, *45*(9), 1463-1472. https://doi.org/10.1038/s41386-020-0692-1

Lak, A., Costa, G. M., Romberg, E., Koulakov, A. A., Mainen, Z. F., & Kepecs, A. (2014). Orbitofrontal cortex is required for optimal waiting based on decision confidence. *Neuron*, *84*(1), 190-201. https://doi.org/10.1016/j.neuron.2014.08.039

Lak, A., Okun, M., Moss, M. M., Gurnani, H., Farrell, K., Wells, M. J., Reddy, C. B., Kepecs, A., Harris, K. D., & Carandini, M. (2020). Dopaminergic and Prefrontal Basis of Learning from Sensory Confidence and Reward Value. *Neuron*, *105*(4), 700-711.e706. https://doi.org/https://doi.org/10.1016/j.neuron.2019.11.018

Laubach, M., Wessberg, J., & Nicolelis, M. A. L. (2000). Cortical ensemble activity increasingly predicts behaviour outcomes during learning of a motor task. *Nature*, *405*(6786), 567-571. https://doi.org/10.1038/35014604

Lawson, R. P., Bisby, J., Nord, C. L., Burgess, N., & Rees, G. (2021). The Computational, Pharmacological, and Physiological Determinants of Sensory Learning under

Uncertainty. *Curr Biol*, *31*(1), 163-172 e164. https://doi.org/10.1016/j.cub.2020.10.043

Lee, K. H., Bhaker, R. S., Mysore, A., Parks, R. W., Birkett, P. B., & Woodruff, P. W. (2009). Time perception and its neuropsychological correlates in patients with schizophrenia and in healthy volunteers. *Psychiatry Res*, *166*(2-3), 174-183. https://doi.org/10.1016/j.psychres.2008.03.004

Luck, S. J., Chelazzi, L., Hillyard, S. A., & Desimone, R. (1997). Neural Mechanisms of Spatial Selective Attention in Areas V1, V2, and V4 of Macaque Visual Cortex. *Journal of Neurophysiology*, *77*(1), 24-42. https://doi.org/10.1152/jn.1997.77.1.24

Makino, H., & Komiyama, T. (2015). Learning enhances the relative impact of top-down processing in the visual cortex. *Nat Neurosci*, *18*(8), 1116-1122. https://doi.org/10.1038/nn.4061

Makino, H., Ren, C., Liu, H., Kim, A. N., Kondapaneni, N., Liu, X., Kuzum, D., & Komiyama, T. (2017). Transformation of Cortex-wide Emergent Properties during Motor Learning. *Neuron*, *94*(4), 880-890 e888. https://doi.org/10.1016/j.neuron.2017.04.015

Mante, V., Sussillo, D., Shenoy, K. V., & Newsome, W. T. (2013). Context-dependent computation by recurrent dynamics in prefrontal cortex. *Nature*, *503*(7474), 78-84. https://doi.org/10.1038/nature12742

Mar, A. C., Walker, A. L., Theobald, D. E., Eagle, D. M., & Robbins, T. W. (2011). Dissociable effects of lesions to orbitofrontal cortex subregions on impulsive choice in the rat. *J Neurosci*, *31*(17), 6398-6404. https://doi.org/10.1523/JNEUROSCI.6620-10.2011

Marrero, K., Aruljothi, K., Zareian, B., Gao, C., Zhang, Z., & Zagha, E. (2021). Global, Low-Amplitude Cortical State Predicts Response Outcomes in a Selective Detection Task in Mice. *Cereb Cortex*. https://doi.org/10.1093/cercor/bhab339

Matell, M. S., & Meck, W. H. (2000). Neuropsychological mechanisms of interval timing behavior. *BioEssays*, *22*(1), 94-103. https://doi.org/10.1002/(SICI)1521-1878(200001)22:1<94::AID-BIES14>3.0.CO;2-E

Matell, M. S., & Meck, W. H. (2004). Cortico-striatal circuits and interval timing: coincidence detection of oscillatory processes. *Brain Res Cogn Brain Res*, *21*(2), 139-170. https://doi.org/10.1016/j.cogbrainres.2004.06.012

McBurney-Lin, J., Sun, Y., Tortorelli, L. S., Nguyen, Q. A. T., Haga-Yamanaka, S., & Yang, H. (2020). Bidirectional pharmacological perturbations of the noradrenergic system differentially affect tactile detection. *Neuropharmacology*, *174*, 108151. https://doi.org/10.1016/j.neuropharm.2020.108151

McClure, S. M., Berns, G. S., & Montague, P. R. (2003). Temporal Prediction Errors in a Passive Learning Task Activate Human Striatum. *Neuron*, *38*(2), 339-346. https://doi.org/10.1016/S0896-6273(03)00154-5

McDannald, M. A., Lucantonio, F., Burke, K. A., Niv, Y., & Schoenbaum, G. (2011). Ventral striatum and orbitofrontal cortex are both required for model-based, but not model-free, reinforcement learning. *J Neurosci*, *31*(7), 2700-2705. https://doi.org/10.1523/JNEUROSCI.5499-10.2011

McNaughton, B. L., Battaglia, F. P., Jensen, O., Moser, E. I., & Moser, M. B. (2006). Path integration and the neural basis of the 'cognitive map'. *Nat Rev Neurosci*, *7*(8), 663-678. https://doi.org/10.1038/nrn1932

Meilleur, A., Foster, N. E. V., Coll, S. M., Brambati, S. M., & Hyde, K. L. (2020). Unisensory and multisensory temporal processing in autism and dyslexia: A systematic review and meta-analysis. *Neurosci Biobehav Rev*, *116*, 44-63. https://doi.org/10.1016/j.neubiorev.2020.06.013

Mendonça, A. G., Drugowitsch, J., Vicente, M. I., DeWitt, E. E. J., Pouget, A., & Mainen, Z. F. (2020). The impact of learning on perceptual decisions and its implication for speed-accuracy tradeoffs. *Nature Communications*, *11*(1), 2757. https://doi.org/10.1038/s41467-020-16196-7

Merchant, H., Harrington, D. L., & Meck, W. H. (2013). Neural basis of the perception and estimation of time. *Annu Rev Neurosci*, *36*, 313-336. https://doi.org/10.1146/annurev-neuro-062012-170349

Mischel, W., & Ebbesen, E. B. (1970). Attention in delay of gratification. *Journal of Personality and Social Psychology*, *16*, 329-337. https://doi.org/10.1037/h0029815

Miyazaki, K. W., Miyazaki, K., & Doya, K. (2012). Activation of dorsal raphe serotonin neurons is necessary for waiting for delayed rewards. *J Neurosci*, *32*(31), 10451-10457. https://doi.org/10.1523/JNEUROSCI.0915-12.2012

Mobini, S., Body, S., Ho, M. Y., Bradshaw, C. M., Szabadi, E., Deakin, J. F., & Anderson, I. M. (2002). Effects of lesions of the orbitofrontal cortex on sensitivity to delayed and probabilistic reinforcement. *Psychopharmacology (Berl)*, *160*(3), 290-298. https://doi.org/10.1007/s00213-001-0983-0

Moran, J., & Desimone, R. (2010). Selective Attention Gates Visual Processing in the Extrastriate Cortex Author (s): Jeffrey Moran and Robert Desimone Published by : American Association for the Advancement of Science Stable URL : http://www.jstor.org/stable/1696121. *Advancement Of Science*, *229*(4715), 782-784.

Murakami, M., Shteingart, H., Loewenstein, Y., & Mainen, Z. F. (2017). Distinct Sources of Deterministic and Stochastic Components of Action Timing Decisions in Rodent Frontal Cortex. *Neuron*, *94*(4), 908-919 e907. https://doi.org/10.1016/j.neuron.2017.04.040

Musall, S., Kaufman, M. T., Juavinett, A. L., Gluf, S., & Churchland, A. K. (2019). Single-trial neural dynamics are dominated by richly varied movements. *Nat Neurosci*, *22*(10), 1677-1686. https://doi.org/10.1038/s41593-019-0502-4

Nakayama, H., Ibanez-Tallon, I., & Heintz, N. (2018). Cell-Type-Specific Contributions of Medial Prefrontal Neurons to Flexible Behaviors. *J Neurosci*, *38*(19), 4490-4504. https://doi.org/10.1523/JNEUROSCI.3537-17.2018

Narayanan, N. S., Cavanagh, J. F., Frank, M. J., & Laubach, M. (2013). Common medial frontal mechanisms of adaptive control in humans and rodents. *Nat Neurosci*, *16*(12), 1888-1895. https://doi.org/10.1038/nn.3549

Narayanan, N. S., Horst, N. K., & Laubach, M. (2006). Reversible inactivations of rat medial prefrontal cortex impair the ability to wait for a stimulus. *Neuroscience*, *139*(3), 865-876. https://doi.org/10.1016/j.neuroscience.2005.11.072

Narayanan, N. S., & Laubach, M. (2006). Top-down control of motor cortex ensembles by dorsomedial prefrontal cortex. *Neuron*, *52*(5), 921-931. https://doi.org/10.1016/j.neuron.2006.10.021

Narayanan, N. S., & Laubach, M. (2009). Delay activity in rodent frontal cortex during a simple reaction time task. *J Neurophysiol*, *101*(6), 2859-2871. https://doi.org/10.1152/jn.90615.2008

Ni, A. M., Ruff, D. A., Alberts, J. J., Symmonds, J., & Cohen, M. R. (2018). Learning and attention reveal a general relationship between population activity and behavior. *Science*, *359*(6374), 463-465. https://doi.org/10.1126/science.aao0284

O'Doherty, J. P. (2004). Reward representations and reward-related learning in the human brain: insights from neuroimaging. *Curr Opin Neurobiol*, *14*(6), 769-776. https://doi.org/10.1016/j.conb.2004.10.016

O'Doherty, J. P., Dayan, P., Friston, K., Critchley, H., & Dolan, R. J. (2003). Temporal Difference Models and Reward-Related Learning in the Human Brain. *Neuron*, *38*(2), 329-337. https://doi.org/10.1016/S0896-6273(03)00169-7

Pai, S., Erlich, J. C., Kopec, C., & Brody, C. D. (2011). Minimal impairment in a rat model of duration discrimination following excitotoxic lesions of primary auditory and prefrontal cortices. *Front Syst Neurosci*, *5*, 74. https://doi.org/10.3389/fnsys.2011.00074

Pardey, M. C., Homewood, J., Taylor, A., & Cornish, J. L. (2009). Re-evaluation of an animal model for ADHD using a free-operant choice task. *J Neurosci Methods*, *176*(2), 166-171. https://doi.org/10.1016/j.jneumeth.2008.09.009

Pardey, M. C., Kumar, N. N., Goodchild, A. K., & Cornish, J. L. (2013). Catecholamine receptors differentially mediate impulsive choice in the medial prefrontal and orbitofrontal cortex. *J Psychopharmacol*, *27*(2), 203-212. https://doi.org/10.1177/0269881112465497

Parker, K. L., Chen, K. H., Kingyon, J. R., Cavanagh, J. F., & Narayanan, N. S. (2014). D1-dependent 4 Hz oscillations and ramping activity in rodent medial frontal cortex during interval timing. *J Neurosci*, *34*(50), 16774-16783. https://doi.org/10.1523/JNEUROSCI.2772-14.2014

Parker, K. L., Chen, K. H., Kingyon, J. R., Cavanagh, J. F., & Narayanan, N. S. (2015). Medial frontal approximately 4-Hz activity in humans and rodents is attenuated in PD patients and in rodents with cortical dopamine depletion. *J Neurophysiol*, *114*(2), 1310-1320. https://doi.org/10.1152/jn.00412.2015

Petersen, C. C. H. (2019). Sensorimotor processing in the rodent barrel cortex. *Nat Rev Neurosci*, *20*(9), 533-546. https://doi.org/10.1038/s41583-019-0200-y

Peterson, B. S., Skudlarski, P., Gatenby, J. C., Zhang, H., Anderson, A. W., & Gore, J. C. (1999). An fMRI study of stroop word-color interference: evidence for cingulate subregions subserving multiple distributed attentional systems. *Biological Psychiatry*, *45*(10), 1237-1258. https://doi.org/https://doi.org/10.1016/S0006-3223(99)00056-6

Pisupati, S., Chartarifsky-Lynn, L., Khanal, A., & Churchland, A. K. (2021). Lapses in perceptual decisions reflect exploration. *Elife*, *10*. https://doi.org/10.7554/eLife.55490

Poulet, J. F., Fernandez, L. M., Crochet, S., & Petersen, C. C. (2012). Thalamic control of cortical states. *Nat Neurosci*, *15*(3), 370-372. https://doi.org/10.1038/nn.3035

Poulet, J. F., & Petersen, C. C. (2008). Internal brain state regulates membrane potential synchrony in barrel cortex of behaving mice. *Nature*, *454*(7206), 881-885. https://doi.org/10.1038/nature07150

Reinert, S., Hubener, M., Bonhoeffer, T., & Goltstein, P. M. (2021). Mouse prefrontal cortex represents learned rules for categorization. *Nature*, *593*(7859), 411-417. https://doi.org/10.1038/s41586-021-03452-z

Reyes, M. B., de Miranda, D. H., Tunes, G. C., Cravo, A. M., & Caetano, M. S. (2020). Rats can learn a temporal task in a single session. *Behav Processes*, *170*, 103986. https://doi.org/10.1016/j.beproc.2019.103986

Reynolds, J. N. J., Hyland, B. I., & Wickens, J. R. (2001). A cellular mechanism of reward-related learning. *Nature*, *413*(6851), 67-70. https://doi.org/10.1038/35092560

Robbins, T. W. (2002). The 5-choice serial reaction time task: behavioural pharmacology and functional neurochemistry. *Psychopharmacology (Berl)*, *163*(3-4), 362-380. https://doi.org/10.1007/s00213-002-1154-7

Rogers, G. A. J. (2023). John Locke. In *Encyclopedia Britannica.* .

Roitman, J. D., & Shadlen, M. N. (2002). Response of Neurons in the Lateral Intraparietal Area during a Combined Visual Discrimination Reaction Time Task. *The Journal of*

Neuroscience, *22*(21), 9475-9489. https://doi.org/10.1523/jneurosci.22-21-09475.2002

Romo, R., & Schultz, W. (1990). Dopamine neurons of the monkey midbrain: contingencies of responses to active touch during self-initiated arm movements. *Journal of Neurophysiology*, *63*(3), 592-606. https://doi.org/10.1152/jn.1990.63.3.592

Roy, N. A., Bak, J. H., International Brain, L., Akrami, A., Brody, C. D., & Pillow, J. W. (2021). Extracting the dynamics of behavior in sensory decision-making experiments. *Neuron*. https://doi.org/10.1016/j.neuron.2020.12.004

Rubia, K., Halari, R., Christakou, A., & Taylor, E. (2009). Impulsiveness as a timing disturbance: neurocognitive abnormalities in attention-deficit hyperactivity disorder during temporal processes and normalization with methylphenidate. *Philos Trans R Soc Lond B Biol Sci*, *364*(1525), 1919-1931. https://doi.org/10.1098/rstb.2009.0014

Rudebeck, P. H., & Murray, E. A. (2008). Amygdala and orbitofrontal cortex lesions differentially influence choices during object reversal learning. *J Neurosci*, *28*(33), 8338-8343. https://doi.org/10.1523/JNEUROSCI.2272-08.2008

Ruff, D. A., & Cohen, M. R. (2019). Simultaneous multi-area recordings suggest that attention improves performance by reshaping stimulus representations. *Nat Neurosci*, *22*(10), 1669-1676. https://doi.org/10.1038/s41593-019-0477-1

Sakai, Y., & Fukai, T. (2008). The actor-critic learning is behind the matching law: Matching versus optimal behaviors. *Neural Computation*, *20*(1), 227-251. https://doi.org/10.1162/neco.2008.20.1.227

Smith, N. J., Horst, N. K., Liu, B., Caetano, M. S., & Laubach, M. (2010). Reversible Inactivation of Rat Premotor Cortex Impairs Temporal Preparation, but not Inhibitory Control, During Simple Reaction-Time Performance. *Front Integr Neurosci*, *4*, 124. https://doi.org/10.3389/fnint.2010.00124

Smits-Bandstra, S., & De Nil, L. F. (2007). Sequence skill learning in persons who stutter: implications for cortico-striato-thalamo-cortical dysfunction. *J Fluency Disord*, *32*(4), 251-278. https://doi.org/10.1016/j.jfludis.2007.06.001

Song, Y.-H., Hwang, Y.-S., Kim, K., Lee, H.-R., Kim, J.-H., Maclachlan, C., Dubois, A., Jung, M. W., Petersen, C. C. H., Knott, G., Lee, S.-H., & Lee, S.-H. (2020). Somatostatin enhances visual processing and perception by suppressing excitatory inputs to parvalbumin-positive interneurons in V1. *Science Advances*, *6*(17), eaaz0517. https://doi.org/doi:10.1126/sciadv.aaz0517

Soon, C. S., Brass, M., Heinze, H. J., & Haynes, J. D. (2008). Unconscious determinants of free decisions in the human brain. *Nat Neurosci*, *11*(5), 543-545. https://doi.org/10.1038/nn.2112

Steel, P. (2007). The nature of procrastination: A meta-analytic and theoretical review of quintessential self-regulatory failure. *Psychological Bulletin*, *133*, 65-94. https://doi.org/10.1037/0033-2909.133.1.65

Steel, P., & König, C. J. (2006). Integrating Theories of Motivation. *Academy of Management Review*, *31*(4), 889-913. https://doi.org/10.5465/amr.2006.22527462

Tanaka, S. C., Doya, K., Okada, G., Ueda, K., Okamoto, Y., & Yamawaki, S. (2004). Prediction of immediate and future rewards differentially recruits cortico-basal ganglia loops. *Nat Neurosci*, *7*(8), 887-893. https://doi.org/10.1038/nn1279

Toda, K., Lusk, N. A., Watson, G. D. R., Kim, N., Lu, D., Li, H. E., Meck, W. H., & Yin, H. H. (2017). Nigrotectal Stimulation Stops Interval Timing in Mice. *Curr Biol*, *27*(24), 3763-3770 e3763. https://doi.org/10.1016/j.cub.2017.11.003

Toplak, M. E., Dockstader, C., & Tannock, R. (2006). Temporal information processing in ADHD: findings to date and new methods. *J Neurosci Methods*, *151*(1), 15-29. https://doi.org/10.1016/j.jneumeth.2005.09.018

Totah, N. K., Kim, Y. B., Homayoun, H., & Moghaddam, B. (2009). Anterior cingulate neurons represent errors and preparatory attention within the same behavioral sequence. *J Neurosci*, *29*(20), 6418-6426. https://doi.org/10.1523/JNEUROSCI.1142-09.2009

Treisman, A. M. (1964). Selective Attention in Man. *British Medical Bulletin*, *20*(1), 12-16. https://doi.org/10.1093/oxfordjournals.bmb.a070274

Tremblay, L., & Schultz, W. (2000a). Modifications of Reward Expectation-Related Neuronal Activity During Learning in Primate Orbitofrontal Cortex. *Journal of Neurophysiology*, *83*(4), 1877-1885. https://doi.org/10.1152/jn.2000.83.4.1877

Tremblay, L., & Schultz, W. (2000b). Reward-Related Neuronal Activity During Go-Nogo Task Performance in Primate Orbitofrontal Cortex. *Journal of Neurophysiology*, *83*(4), 1864-1876. https://doi.org/10.1152/jn.2000.83.4.1864

Tunes, G. C., Fermino de Oliveira, E., Vieira, E. U. P., Caetano, M. S., Cravo, A. M., & Bussotti Reyes, M. (2022). Time encoding migrates from prefrontal cortex to dorsal striatum during learning of a self-timed response duration task. *Elife*, *11*, e65495. https://doi.org/10.7554/eLife.65495

van Maanen, L., Grasman, R. P., Forstmann, B. U., & Wagenmakers, E. J. (2012). Pieron's Law and Optimal Behavior in Perceptual Decision-Making. *Front Neurosci*, *5*, 143. https://doi.org/10.3389/fnins.2011.00143

Voelkl, B., Altman, N. S., Forsman, A., Forstmeier, W., Gurevitch, J., Jaric, I., Karp, N. A., Kas, M. J., Schielzeth, H., Van De Casteele, T., & Würbel, H. (2020). Reproducibility of animal research in light of biological variation. *Nature Reviews Neuroscience*, *21*(7), 384-393. https://doi.org/10.1038/s41583-020-0313-3

Walton, M. E., Behrens, T. E., Buckley, M. J., Rudebeck, P. H., & Rushworth, M. F. (2010). Separable learning systems in the macaque brain and the role of orbitofrontal cortex in contingent learning. *Neuron*, *65*(6), 927-939. https://doi.org/10.1016/j.neuron.2010.02.027

Wiener, M., Magaro, C. M., & Matell, M. S. (2008). Accurate timing but increased impulsivity following excitotoxic lesions of the subthalamic nucleus. *Neurosci Lett*, *440*(2), 176-180. https://doi.org/10.1016/j.neulet.2008.05.071

Wurbel, H., Voelkl, B., Altman, N. S., Forsman, A., Forstmeier, W., Gurevitch, J., Jaric, I., Karp, N. A., Kas, M. J., Schielzeth, H., & Van de Casteele, T. (2020). Reply to 'It is time for an empirically informed paradigm shift in animal research'. *Nat Rev Neurosci*, *21*(11), 661-662. https://doi.org/10.1038/s41583-020-0370-7

Zagha, E., Ge, X., & McCormick, D. A. (2015). Competing Neural Ensembles in Motor Cortex Gate Goal-Directed Motor Output. *Neuron*, *88*(3), 565-577. https://doi.org/10.1016/j.neuron.2015.09.044

Zareian, B., Lam, A., & Zagha, E. (2023). Dorsolateral striatum is a bottleneck for responding to task-relevant stimuli in a learned whisker detection task in mice. *The Journal of Neuroscience*, JN-RM-1506-1522. https://doi.org/10.1523/JNEUROSCI.1506-22.2023

Chapter 2: Functional Localization of an Attenuating Filter

Multiple aspects were required for the first widefield imaging manuscript. First, it was important for our lab to establish the robustness of the selective detection task in mice. Behaviorally, this included response rates and discrimination, as these were considered when we qualified expert behavior in mice. To our chagrin, criterion bias was not reported here, even though this is an important feature to consider for animals performing for detection paradigms. Additionally, although the whisker system has been used as a standard somatosensory model in rodents, our selective detection paradigm yielded compelling and reliable evidence of the attenuation filter localized within cortex for the selective detection task in mice.

We also needed to demonstrate the widefield technique that produced our results. Although widefield calcium imaging has been used for rodent models performing in decision making paradigms, this manuscript introduced the techniques used in our lab environment. Finally, the establishment of an attenuating filter instead of a blocking filter addressed the Broadbent versus Treisman framework as discussed in the introduction. We were able to defend the latter framework as our widefield imaging did not completely block cortical signal between sensory to motor cortices, as evidenced by target versus distractor reduction but not elimination of stimulus encoding.

My contributions to this work included animal surgeries, behavioral training of mice used in imaging analyses, collection of widefield imaging data, and data analyses for fluorescence activity, stimulus encoding, choice encoding (see below), and seed

correlation. Visualization and quantification of stimulus encoding for target versus distractor sensory and motor cortices were key findings from this manuscript. In this way, our work was essential for subsequent analyses from the Zagha lab.

A major change has been made concerning this adapted chapter. Although we termed data from the preresponse frames 'choice probability', which proposes a percentage data output, the more accurate term for the quantification regarding preresponse frames, both for the preresponse frames and for the change in preresponse frames, is 'choice encoding'. Choice probability is usually reported as a probabilistic percentage, but our choice encoding extended choice probability a step further based on signal detection theory. In retrospect, the reported neurometric d' methods apply to both terms 'stimulus encoding' and 'choice encoding'. The neurometric d' for stimulus encoding refers to a stimulus present (fluorescence activity after a stimulus) signal as it compares to a stimulus absent (fluorescence activity before a stimulus) signal. The neurometric d' for choice encoding refers to a choice present (fluorescence activity for a response) signal as it compares to a choice absent (fluorescence activity for no response) signal. The results and resulting interpretations remain unchanged; only the terminology is addressed. The changes adapted are noted in blue.

Functional Localization of an Attenuating Filter

Adapted from:

Functional Localization of an Attenuating Filter within Cortex for a Selective Detection Task in Mice

Abbreviated title: Cortical attenuation during selective detection

Authors: Krithiga Aruljothi[1*], Krista Marrero[2*], Zhaoran Zhang[2], Behzad Zareian[1], Edward Zagha[1,2]

[1] Department of Psychology, [2] Neuroscience Graduate Program, University of California Riverside, 900 University Avenue, Riverside CA 92521 USA

* equal contributors

Correspondence to: edward.zagha@ucr.edu

Acknowledgements: This work was supported by the Whitehall Foundation (Research Grant 2017-05-71 to E.Z.) and the National Institutes of Health (R01NS107599 to E.Z.). We thank Trevor Stavropoulos for assistance with Arduino programming. We thank Shaida Abachi for collecting whisker imaging data. We thank Hongdian Yang, Martin Riccomagno, Aaron Seitz and Megan Peters for many helpful discussions throughout the project.

Abstract

An essential feature of goal-directed behavior is the ability to selectively respond to the diverse stimuli in one's environment. However, the neural mechanisms that enable us to respond to target stimuli while ignoring distractor stimuli are poorly understood. To study this sensory selection process, we trained male and female mice in a selective detection task in which mice learn to respond to rapid stimuli in the target whisker field and ignore identical stimuli in the opposite, distractor whisker field. In expert mice, we used widefield Ca^{2+} imaging to analyze target-related and distractor-related neural responses throughout dorsal cortex. For target stimuli, we observed strong signal activation in primary somatosensory cortex (S1) and frontal cortices, including both the whisker region of primary motor cortex (wMC) and anterior lateral motor cortex (ALM). For distractor stimuli, we observed strong signal activation in S1, with minimal propagation to frontal cortex. Our data support only modest subcortical filtering, with robust, step-like attenuation in distractor processing between mono-synaptically coupled regions of S1 and wMC. This study establishes a highly robust model system for studying the neural mechanisms of sensory selection and places important constraints on its implementation.

Significance Statement

Responding to task-relevant stimuli while ignoring task-irrelevant stimuli is critical for goal-directed behavior. Yet, the neural mechanisms involved in this selection process are poorly understood. We trained mice in a detection task with both target and distractor stimuli. During expert performance, we measured neural activity throughout cortex using widefield imaging. We observed responses to target stimuli in multiple sensory and motor cortical regions. In contrast, responses to distractor stimuli were abruptly suppressed beyond sensory cortex. Our findings localize the sites of attenuation when successfully ignoring a distractor stimulus and provide essential foundations for further revealing the neural mechanism of sensory selection and distractor suppression.

Introduction

We are constantly bombarded by sensory stimuli. To complete a given task, we must selectively respond to task-relevant stimuli while ignoring task-irrelevant stimuli. A framework for understanding stimulus selection is provided by the Treisman attenuation theory (Figure 2.1). According to this theory, both attended and unattended signals enter short-term storage. Responses to attended stimuli propagate forward for higher-order processing. Responses to unattended stimuli, however, are suppressed by an attenuating filter at some point along the processing stream (A. M. Treisman, 1964). The attenuation theory was originally developed to understand selection amongst conflicting speech patterns, yet has since been adapted to study sensory selection across multiple sensory modalities and species (Moran & Desimone, 1985; Sridharan et al., 2014; Wiederman & O'Carroll, 2013).

Where in the brain does attenuation occur and what are the neural mechanisms involved? Extensive studies in the primate visual system have identified stimulus filtering throughout multiple brain regions. Sensory selection was initially proposed to occur in the thalamus, mediated by the modulation of thalamic relay neuron activation by the reticular thalamus (Crick, 1984b). Recordings in behaving primates have demonstrated early-onset attentional modulations in thalamus (McAlonan et al., 2008), consistent with stimulus filtering prior to reaching cortex. However, earlier physiological studies demonstrated robust attentional filtering within cortex, between primary visual cortex and visual area V4 (Moran & Desimone, 1985). Alternatively, other studies argue for

filtering occurring primarily within prefrontal cortex (Mante et al., 2013). Potential 'top-down' pathways establishing an attenuating filter include cortical feedback and ascending neuromodulation (Miller & Cohen, 2001; Noudoost & Moore, 2011). Yet, these mechanisms are poorly understood, in part due to the apparent highly distributed filtering processes of the primate visual system.

Our goal in this study is to localize the attenuating filter for a simple sensory-motor task in the mouse whisker system. This model system benefits from extensive characterization of the sensory and motor regions and pathways involved, with significantly fewer hierarchical levels than the primate visual system (Guo et al., 2014; Kleinfeld et al., 1999; Petersen, 2019). Whisker deflection activates brainstem pathways which travel predominantly through the ventral posteromedial (VPM) thalamus and onto primary somatosensory (barrel) cortex (S1). From S1, there are robust, mono-synaptic connections to the whisker region of primary motor cortex (wMC) (Mao et al., 2011; Miyashita et al., 1994; Porter & White, 1983). Sensory responses in S1 rapidly propagate to wMC, under both anesthetized and awake conditions (Chakrabarti et al., 2008; Farkas et al., 1999; Ferezou et al., 2007; Kleinfeld et al., 2002; Zagha et al., 2015). Moreover, this pathway may be particularly important for input detection; S1-wMC projection neurons were found to be preferentially responsive to touch in an object detection task (Chen et al., 2013), which enhanced during task training (Chen et al., 2015). Recent studies in the rodent whisker system have reported sensory filtering within the thalamus (Rodenkirch et al., 2019) and brainstem (S. Chakrabarti & C. Schwarz, 2018). However, it remains

unknown to what extent these subcortical or cortical pathways contribute to filtering during a sensory selection task.

We designed a selective detection task with spatially and temporally distinct processing streams. Mice respond to rapid deflections of one whisker field (target) and ignore identical stimuli in the opposite, contralateral whisker field (distractor). Rather than presenting target and distractor stimuli together, as in the original studies on sensory selection (Moran & Desimone, 1985; A. M. Treisman, 1964), we present each stimulus individually on different trials. Thus, we can evaluate target and distractor processing separately across space (different hemispheres) and time (different trials). The motor response in our task is a straight-forward lick. As the sensory and motor content of our task is symmetric, the only asymmetry is the selection process. In expert performing mice, we used widefield Ca^{2+} population imaging (Wekselblatt et al., 2016) to simultaneously monitor neural activity bilaterally in sensory and motor regions. We then quantified the asymmetry in target aligned versus distractor aligned sensory processing streams to localize sites of attenuation.

Materials and Methods

Animal Subjects and Surgery

All experiments performed in this study were approved by the IACUC of University of California, Riverside. Mice were purchased from Jackson Laboratories (JAX). Task-related neural imaging data were obtained from GCaMP6s expressing Snap25-2A-GCaMP6s-D mice (JAX #025111). The SNAP25-2A-GCaMP6s mouse line expresses GCaMP6s pan-neuronally, in both excitatory and inhibitory neurons throughout the brain (Madisen et al., 2015). Transgenic mice were backcrossed into the BALB/cByJ (JAX 000651) background. Both male and female mice were used in these experiments. Recording sessions from male and female mice were similar according to behavioral performance (imaging experiments: 4 male mice, 32 sessions, 1 female mouse, 7 sessions; discriminability d': male 2.0 ± 0.1, female 1.9 ± 0.2, two sample t-test, p= 0.36, t(37)= 0.92; target stimulus reaction time (s): male 0.30 ± 0.01, female 0.32 ± 0.02 , two sample t-test, p= 0.70, t(37)= -0.38) and neural responses (data not shown), and therefore data were combined for grand average analyses. Mice were housed on a light cycle of 12 hours light/ 12 hours dark. All trainings and recordings were conducted on mice head-fixed in the behavioral apparatus. For headpost implantation, 2 to 5 months-old mice were placed under a combination of isoflurane (1-2%), ketamine (100 mg/kg), and xylazine (10 mg/kg) anesthesia. A 10 mm x 10 mm piece of scalp was resected to expose the skull. The exposed skull was cleared of connective tissue and a custom-built headpost was implanted onto the skull with cyanoacrylate glue. The lightweight titanium or stainless

steel headpost (3 cm in length and 1.5 grams in weight) had an 8 mm x 8 mm central window for imaging and recording. For in vivo widefield Ca^{2+} imaging, a thin layer of cyanoacrylate gap-filling medium (Insta-Cure, Bob Smith Industries) was applied to the window, to both seal the exposed skull and enhance skull transparency. Silicone elastomer (Reynolds Advanced Materials) was additionally applied above the imaging window. After surgery, mice were placed onto a heating pad to recover and administered meloxicam (0.3 mg/kg) and enrofloxacin (5 mg/kg) for three days post-op. Mice were given a minimum of three days to recover from surgery before water-restriction and behavioral training. Recordings under anesthesia were conducted immediately after headpost implantation.

Animal Behavior

Mice were trained in a Go/NoGo passive whisker selective detection task. During behavioral training mice were given food ad libitum but were water-restricted to a minimum of 1 mL per day. Weights were monitored daily to maintain over 85% of their initial post-surgery weights, and additional water was given as needed to maintain this level. The behavioral apparatus was controlled by Arduino and custom MATLAB (MathWorks) code. Piezo-controlled paddles (Physik Instrumente and Piezo.com) were placed bilaterally in the whisker fields, with each paddle contacting 2 to 4 whiskers. Paddle deflections of a triangle waveform had rising phases that ranged from 0.1 s (for large deflections) to 0.01 s (for small deflections), followed by an immediate falling phase. Deflection velocity was constant, therefore increased duration correlated with increased

deflection amplitude. The maximum amplitude, for 0.1 s deflections, was 1 mm. Stimulus duration and amplitude were varied with training with the goal of maintaining a 75% hit rate. This target hit rate was selected to maintain high reward rates while still operating within the dynamic range of each mouse's psychometric curve. Within every session, target and distractor stimulus strengths were identical. Directly below the mouse's snout was a central lick port. Each 'hit' trial was rewarded with ~5 mL of water delivered through the lick port.

Behavioral training consisted of three stages. Inter-trial intervals for all stages varied from 5 to 9 s with a negative exponential distribution to minimize potential timing strategies. Additionally, in all stages a 'lockout' period of 200 ms separated stimulus onset and the earliest opportunity for reward. Target and distractor whisker fields were assigned at Stage 1 and remained constant throughout training. Target/distractor assignment was varied across the population and analyzed separately (Figure 2.7A-C) before combining for grand average analyses. Each session lasted approximately 60 minutes and consisted of ~200 trials. (Stage 1) Classical conditioning: Unilateral (target) whisker deflection was paired with fluid reward; distractor whisker deflection was neither rewarded nor punished. Mice were trained on this stage for 1 to 3 days, 1 to 2 sessions per day. (Stage 2) Operant conditioning: Following unilateral (target) whisker deflection, mice were required to contact the lick port within a lick detection window of 1.5 s to initiate the fluid reward. Mice were trained on this stage for 2 to 3 days, 1 session per day. (Stage 3) Impulse control: Similar task structure as above, except all incorrect

responses (licking during the ITI, during the lockout period, or following distractor deflections) were punished by re-setting the ITI, effectively acting as a time-out. The response detection window was shortened to 1 s. Following full-length ITIs, trial types were selected randomly from a distribution of 80% distractor and 20% target. For distractor trials, not responding (*correct rejection*) was rewarded with a shortened ITI (2 to 4 s, negative exponential distribution) and a subsequent target trial. Licking to the distractor (*false alarm*) or not responding to the target (*miss*) initiated a subsequent full-length ITI. Responding to the target stimulus (*hit*) triggered a fluid reward, followed by a full-length ITI. Behavioral and neural imaging data for hit trials with and without preceding correct rejections were compared (Figure 2.7D, E) before combining for grand average analyses. For approximately half of the mice in this study, following full-length ITIs, catch trials without a whisker stimulus were interspersed at a rate of 10% of all stimulus trials.

A single, contiguous behavioral window was considered for analyses, from session onset until 120 s of no responding, which we interpreted as task disengagement. Hit rate, false alarm rate, spontaneous lick rate, and reaction times were all used to assess task performance. Foremost, we used the sensitivity or d-prime (d') framework from signal detection theory. Traditionally, d' is used as a measure of detection between stimulus present and stimulus absent conditions. Here, we implemented a discriminability d' between target detection and distractor detection [$d' = Z_{\text{hit rate}} - Z_{\text{false alarm rate}}$] where Z is the inverse of the normal cumulative distribution function. Mice were considered expert

in our task once they achieved a d'>1 for three consecutive days. The spontaneous lick rate was calculated as the response rate during the last 1 s of the full-length ITI.

Widefield Imaging

Widefield imaging was performed through-skull in head-fixed mice while they performed the selective detection task. Imaging was conducted through a Macroscope IIa (RedShirtImaging), beam diverter removed, 75 mm inverted lens with 0.7x magnification and 16 mm working distance. The lens (NA 0.4) was positioned directly over the cranial window, providing a 7 mm x 5.8 mm field of view, including most of dorsal parietal and frontal cortex bilaterally. Illumination was provided by a mounted 470 nm LED (Thorlabs M470L3), dispersed with a collimating lens (Thorlabs ACL2520-A), band-pass filtered (Chroma ET480/40x) and directed through the macroscope using a dichroic mirror (Chroma T510lpxrxt). Fluorescent light returning to the brain was band-pass filtered (Chroma ET535/50m) prior to reaching an RT sCMOS camera (SPOT Imaging). On camera 2x2 binning and post-processing image size reduction gave a final resolution of 142 x 170 pixels at 41 µm per pixel and 12-bit depth. Images were acquired at a temporal resolution of 10 Hz, aligned to the trial structure. TIF image sequences were imported to MATLAB for preprocessing and analysis.

Local field potential (LFP) recordings

LFP recordings were conducted through small (<0.5 mm diameter) craniotomies and durotomies positioned above S1 (from bregma: posterior 1.5 mm, lateral 3.5 mm), wMC (anterior 1 mm, lateral 1 mm) and ALM (anterior 2.5 mm, lateral 1.5 mm), in target aligned

and distractor aligned cortices. Recording sites were positioned 750 mm below the pial surface, targeting layer 5. Recordings were acquired with silicon probes (Neuronexus, A1x16-Poly2-5mm-50s-177), bandpass filtered from 0.1 Hz to 8 kHz and digitized at 32 kHz (Neuralynx). Further analyses were conducted in MATLAB.

Imaging of whisker movements

A CMOS camera (Thorlabs DCC3240M camera with Edmund Optics lens 33-301) was positioned directly above the mouse while performing the detection task. Field of view included both whisker fields and stimulus paddles. Images were captured at 8-bit depth continuously at 60 Hz (ThorCam) and imported to MATLAB for all analyses.

Data Analysis

All data analyses were performed in MATLAB using custom scripts.

Fluorescence Preprocessing and Trial-Based Neural Activity

Peri-stimulus trial imaging time windows included 1 s before stimulus onset and 1.2 s after stimulus onset, which included the lockout and response windows. The first step of image processing was to concatenate fluorescence activity from consecutive trials to create a raw movie F, where $F_n(i,j,f)$ shows the fluorescence of each pixel (i^{th} row, j^{th} column) in the f^{th} frame for each individual trial n. The pre-stimulus baseline fluorescence $F_o(i,j,n)$ was calculated by averaging pixelwise activity across the first 10 frames preceding the stimulus onset per trial n (1 s pre-stimulus).

Finally, relative fluorescent signal normalized to pre-stimulus baseline (dF/F) was calculated as

$$dF/F_0(i,j,n) = [F_n(i,j,f) - F_0(i,j,n)]/F_0(i,j,n)$$

Baseline Fluorescence - Equation 2

Average trial movies were created by indexing trials according to trial outcome (*hit*, *miss*, *false alarm*, *correct rejection*, *spontaneous*) and averaging activities at each pixel across the corresponding frame of each corresponding trial. Frame alignments were conducted both with reference to stimulus onset (stimulus aligned) and with reference to the first frame containing the response (response aligned) (see Figure 2.4). Spontaneous trials were those in which a response occurred during the 1 s pre-stimulus imaging period. Trials with responses during the lockout period were excluded from all further analyses.

Data were analyzed per session (n=39), per mouse (n=5), per target-distractor assignment (n=2) and across all experiments (grand average). For a session to be included in our analyses, our inclusion criteria were d'>1 for at least 10 minutes of continuous engagement. Only one engagement period per session was included. For qualitative analyses, trial movies from recording sessions were spatially aligned to bregma and averaged per mouse. These data were then averaged per target-distractor assignment (see Figure 2.7 for whisker deflection assignments). One target-distractor assignment dataset was then flipped horizontally (rostro-caudal axis) at bregma before the grand average dF/F. For quantitative analyses, the subsequent datasets were first flipped at

bregma according to target-distractor assignment (as before) and then averaged across all sessions.

Quantification of Stimulus Encoding

To quantify stimulus response magnitude, we calculated the neurometric d' (K. H. Britten et al., 1992) comparing activity pre-stimulus (stimulus absent) and post-stimulus (stimulus present), specifically during the lockout period. Neurometric d' was calculated separately for target and distractor trials and included all trials regardless of outcome (hit and miss trials for target and false alarm and correct rejection for distractor). Pre-stimulus (10 frames preceding stimulus onset) and post-stimulus activities were binned and plotted in an ROC (receiver operating characteristic) curve. The area under the curve (AUC) was converted to d' using the equation:

$$neurometric\ d' = \sqrt{2} * Z_{AUC}$$

d' Neurometric - Equation 3

In the context of this study, neurometric d' is the performance measurement of a pixel where d'>0 denotes more post-stimulus pixel activity and d'<0 denotes more pre-stimulus pixel activity. For each region of interest, we report the peak neurometric d' within the spatially defined region of interest (ROI). Subsequent analyses compared target stimulus encoding in target aligned cortices to distractor stimulus encoding in distractor aligned cortices.

Quantification of Choice Encoding

To quantify choice-related neural activity, we calculated choice encoding d' (Britten et al., 1996b) comparing activity on hit trials (response present) and miss trials (response absent), specifically during the lockout phase. Sessions were included in this analysis if they had 5 or more trials of each type. Trials with stimuli of different amplitudes were combined only if response rates for each amplitude-specific trial type were comparable (within 15%). Overall, 9 sessions were excluded from this analysis, due to too few miss trials (n=30, instead of n=39). Choice probability was calculated for activity within the pre-response frame (100 to 200 ms during the lockout) and for activity between the pre-response frames (change in activity, subtraction of activity in the 0 to 100 ms frame window from the 100 to 200 ms frame window during the lockout). In the context of this study, choice encoding d' is the performance measurement of a pixel where d'>0 denotes more response-related pixel activity and d'<0 denotes more no response-related pixel activity. Response present and response absent activities were binned and plotted in an ROC curve. The area under the curve was converted to d' as described above.

Seed Correlation Analysis

Correlation maps were generated separately for target and distractor hemispheres and for S1, wMC and ALM seed regions (generating six correlation maps per session). Baseline averaged fluorescence activity trajectories from all trial types (excluding spontaneous) were concatenated into a single time series. The following trial structures were analyzed separately: 1) full trial, including 10 frames pre-stimulus and 12 frames post-stimulus

including the lockout and response windows, 2) pre-stimulus only, including 10 frames pre-stimulus, 3) peri-stimulus and lockout, including 1 frame pre-stimulus and 2 frames post-stimulus during the lockout, and 4) response, including 10 frames after the lockout and during the response window. The seed was the average time series from all pixels in the indicated region of interest. Pairwise correlation coefficients were calculated between the seed and all other pixels. To reduce computation time, all trial movies were spatially down sampled 4-fold across both axes for a resolution of 36 x 43 pixels at 164 um per pixel prior to running the correlation analyses. We report r^2 values, as the square of the correlation coefficient. For each region of interest, we report the average correlation r^2 within the spatially defined region. Subsequent analyses compared target aligned intracortical correlations to distractor aligned intracortical correlations.

Evoked-potential analyses

Single-trial LFP recordings were aligned to target and distractor stimulus onset. To isolate the LFP signal, single-trial data were bandpass filtered from 0.2 Hz to 100 Hz using a second order Butterworth filter, then down sampled to a sampling frequency of 400 Hz. Following filtering and down sampling, single-trial data were averaged according to trial type. In Figure 2.9, stimulus artifacts at 0-10 ms post-stimulus were truncated when present.

Whisker movement analyses

Movies were parsed into regions of interest containing target or distractor whisker fields. Whisker motion energy (WME) within each region was calculated for each frame as the

temporal derivative for each pixel of the mean gray value from the previous frame. Values per pixel were normalized (squared) and summed across pixels, providing a single WME value. WME data from the movies were aligned to target and distractor stimulus onset and averaged across trial type.

Statistical Analyses

For neurometric d' and choice encoding d', statistical analyses were performed to determine whether each pixel value was significantly different than zero across sessions (one sample t-test). Data were spatially aligned across sessions as described above. The threshold for statistical significance was corrected for multiple comparisons using the Bonferroni correction [0.05/(142x170) = $2.1x10^{-6}$ for a single imaging session and 0.05/(156x194) = $1.7x10^{-6}$ across aligned imaging sessions]. For neurometric d' and seed correlation, we additionally conducted region of interest (ROI) analyses. For neurometric d', reduction in distractor encoding was calculated as: (target d' – distractor d') / target d', calculated separately for S1, wMC and ALM. Statistical analyses were performed to determine whether reduction in distractor encoding was significantly different than zero within each region across sessions (one sample t-test, significance threshold corrected for multiple comparisons 0.05/3 = 0.017). Additionally, comparison of reduction in distractor encoding between the three ROIs across sessions was conducted using ANOVA and post-hoc Tukey test. For seed correlation, comparison between the three ROIs across sessions and comparisons between different trial phases across sessions were conducted using ANOVA and post-hoc Tukey test. To quantify changes in whisker motion energy (WME),

post-stimulus values (each frame) were compared to average pre-stimulus (1 s baseline) values. Comparisons were conducted using paired t-test for each post-stimulus window, with a p-value threshold of 0.01 for significance. Average data are reported as mean ± standard error of the mean.

Results

Training mice in a selective detection task

To study the neural mechanisms of sensory selection, we developed a Go/NoGo passive whisker detection task in head-fixed mice (Figure 2.2). In this task, target stimuli are rapid deflections of multiple whiskers in one whisker field and distractor stimuli are identical deflections in the opposite whisker field (Figure 2.2A). Throughout training we quantified task performance as the separation (d') between hit rate and false alarm rate (Figure 2.2C). We considered mice 'expert' once they achieved a discriminability d'>1 on three consecutive sessions. Average time to expert performance was 11 days in the full task (see Methods) (Figures 2.2D and 2.2E) (number of sessions to expert performance: 11.2 ± 0.9, n=43 mice). Performance measures for the imaging sessions used in subsequent analyses are shown in Figure 2.2F (n=39 sessions across n=5 mice, hit rate (%), 80.4 ± 2.2; false alarm rate, 13.6 ± 1.1; spontaneous lick rate, 8.1 ± 0.5; d' comparing hit vs false alarm rates, 2.0 ± 0.1).

Two key features of this task facilitate the study of sensory selection. First, target and distractor stimuli are presented to contralateral whisker fields. Given the highly lateralized somatosensory whisker representation, we expect the target aligned and distractor aligned processing streams to be well separated across hemispheres. Second, we imposed a short (200 ms) lockout period after stimulus onset and before the response window. Responding during the lockout is punished with a time-out, and mice learn to withhold their licking responses through this period (e.g., Figure 2.2G). All analyses of

stimulus selection are conducted within this lockout period, which is post-stimulus onset and pre-reward, thereby isolating the selection process from reward-associated behavior.

Propagation of cortical activity during task performance

We used widefield calcium imaging (GCaMP6s Ca^{2+} sensor) to monitor neural activity broadly across dorsal cortex during task performance. We used a combination of anatomic landmarks and functional mapping to identify various cortical regions (Figures 2.3A and 2.3B). Whisker deflection in anesthetized mice was used to localize the primary somatosensory barrel field (S1) and the whisker region of primary motor cortex (wMC) (n=13, example session shown in Figure 2.3B, left). Reward-triggered licking in water-restricted yet task naïve mice was used to localize anterior lateral motor cortex (ALM), which has recently been identified as a pre-motor licking-related region (Chen et al., 2017; Guo et al., 2014) (n=6, example session shown in Figure 2.3B, right). Thus, our anatomic and functional mapping confirms that we can simultaneously monitor licking-related and whisker sensory and motor cortical regions bilaterally.

We imaged expert mice while they were performing the whisker detection task. Here, we show stimulus evoked cortical activity on target and distractor trials across all mice and all sessions (grand average: n=5 mice, n=39 sessions) (Figures 2.3C and 2.3D). The two sequential imaging frames both occurred within the lockout period, which is after stimulus onset and before the earliest allowed response time. As expected, for both trial types we observed activity initiation in S1 contralateral to the deflected whisker field. By the end of the lockout period, we observed strong S1 activity following both target and

distractor stimuli. On target trials we observed propagation of activity to wMC, ALM, and retrosplenial cortex (RSP). Note that the activity does not spread uniformly from the site of initiation, but rather emerges in discrete cortical regions. In contrast, on distractor trials the activity was largely contained within S1, with only mild activation of wMC.

In Figure 2.4, we show the grand average fluorescence signals across all trial types and outcomes, aligned to both stimulus onset and response onset. Notice that during the response (post-response onset for hit, false alarm and spontaneous licking trials) we observed strong signals that are widespread throughout dorsal cortex. However, in this study we are most interested in the activity initiating, and therefore preceding, the response. On hit trials (Figure 2.4A), we observed the propagation of activity from S1 to frontal and parietal regions post-stimulus (aligned to stimulus) and pre-response (aligned to response). On correct rejection trials (Figure 2.4E), we also saw strong activity in S1, but with very little propagation to other cortical regions. Propagation is not simply delayed on these trials, as we can track the resolution of distractor-evoked activity into the response window.

The incorrect trial types also showed distinct activation patterns. On both false alarm trials (Figure 2.4B) and miss trials (Figure 2.4D), in addition to lateralized S1 responses, we also observed prominent bilateral activity in the somatosensory limb regions. We interpret these neural signals as reflecting the self-motion of the mouse. Prior studies have shown that during passive whisker detection tasks, self-motion (quantified by whisking behavior) reduces detection probability (D. R. Ollerenshaw et al., 2012). Thus,

limb region activation observed here is consistent with self-motion contributing to incorrect, both miss and false alarm, trial outcomes. On spontaneous trials (responses not preceded by a whisker stimulus) we observed minimal pre-response cortical activity (Figure 2.4C).

Quantification of stimulus encoding and attenuation across cortex

The above analyses demonstrate, qualitatively, the differential propagation of cortical signals for target and distractor stimuli. Next, we sought to quantify these responses. To do this, we calculated the neurometric sensitivity index (d') (K. H. Britten et al., 1992) for each pixel in our imaging window (Figure 2.5). Across each session we compared the pre-stimulus activity (stimulus absent) to activity during the lockout period (stimulus present). Importantly, for this analysis we included all target trials and all distractor trials regardless of trial outcome (although excluding trials with responses during the lockout). We use d' rather than dF/F, as the former accounts for trial-by-trial variability and reflects the ability of an ideal observer to distinguish signal from noise on single trials. The d' maps from target and distractor stimuli largely match dF/F patterns described above; for target stimuli high d' values are observed in S1, wMC, ALM and RSP (Figure 2.5A, right) whereas for distractor stimuli, high d' values are only observed in S1 (Figure 2.5B, right). These regions show neurometric d' values significantly above zero (Figure 2.5C and 5D). We do observe a focal increase in d' for distractor wMC (Figure 2.5B, right), but this does not reach statistical significance after correction for multiple comparisons (Figure 2.5D).

Next, we quantified the propagation of stimulus responses for target versus distractor stimuli. We describe this analysis first for S1. For each session, we determined the peak neurometric d' for the target stimulus in target aligned S1 versus the peak neurometric d' for the distractor stimulus in distractor aligned S1. We plotted these data in Figure 2.6A. Data along the unity line indicate equal neurometric d' values for target and distractor stimuli for that session. For S1, the data are widely distributed, yet with a nonsignificant trend towards larger responses for target stimuli (n=39 sessions, 8.8 ± 7.9% reduction in distractor d', one sample t-test, p=0.27, t(38)= 1.12) (Figure 2.6D). We repeated these analyses for wMC and ALM. For these regions we find that neurometric d' values are consistently larger for target stimuli (Figures 2.6B and 2.6C). Reduction in distractor d' is 61.0±7.1% in wMC (one sample t-test, $p=1.76e^{-10}$, t(38)= 8.62) and 72.1 ± 6.9 % in ALM (one sample t-test, $p=8.83e^{-13}$, t(38)= 10.49) (Figure 2.6D). Additionally, reduction in distractor encoding is greater for wMC and ALM compared to S1 (ANOVA, $p=7.97e^{-9}$, F(1,38) = 54.2, with post-hoc Tukey comparison). Overall, these data demonstrate robust attenuation of distractor responses between the mono-synaptically connected regions of S1 and wMC.

Analyses of intrinsic lateralization, trial history, electrical activity, whisker movements and choice encoding

We performed a series of analyses to determine whether the neural activity described above reflects the selection process or can be accounted for by task or behavioral confounds. First, widespread cortical propagation in our task could reflect target selection

or an intrinsic lateralization of cortical activity (e.g., left-sided whisker deflections always evoke more widespread cortical activation). To distinguish between these possibilities, two cohorts of mice were trained with opposite target-distractor assignments. In previous analyses we aligned all data with respect to target-distractor orientation. Here, we show behavioral performance (Figure 2.7A) and neural activity separately according to target assignment (Figure 2.7B target aligned right hemisphere, n=3 mice and n=25 sessions; Figure 2.7C target aligned left hemisphere, n=2 mice, n=14 sessions). Note that propagation from S1 to frontal and other parietal cortices occurs selectively on target trials, irrespective of the side of target assignment. Therefore, these differential patterns of cortical activation reflect learned adaptations to our task, rather than intrinsic lateralization.

In our task, most target trials followed a correct rejection and shortened inter-trial interval (80%), while a minority of target trials was not preceded by a correct rejection and followed a long inter-trial interval (20%). It is possible that the mice in our task implemented a strategy of using the distractor stimulus to orient attention to the target whisker field rather than solely attending the target stimulus. To determine the likelihood of this strategy, we compared behavioral performance on target trials (Figure 2.7D) and hit-related neural activity (Figure 2.7E) separately according to the presence of a preceding correction rejection. The similar behavioral performance (hit rate, paired t-test, $p=0.63$, $t(38)=-0.49$; reaction time, paired t-test, $p=0.77$, $t(38)=0.29$) and neural activity suggest that the distractor stimulus was not utilized to enhance target detection.

Next, we sought to confirm our Ca^{2+} imaging findings with local field potential (LFP) recordings, which have much higher temporal resolution. We recorded LFP signals from layer 5 of S1, wMC and ALM, in target aligned and distractor aligned hemispheres (not simultaneously recorded). We compared target-evoked responses in target aligned cortices (Figure 2.8 A-C) to distractor-evoked responses in distractor aligned cortices (Figure 2.8 D-F). We find that early post-stimulus activity, likely reflecting the initial feedforward sensory sweep, is similar in target aligned and distractor aligned S1 and wMC (Figure 2.8 G, H; peak 1, occurring within 50 ms post-stimulus). Late activity does diverge in S1 and wMC between target and distractor recordings. In ALM, notably, the large post-stimulus activity in target recordings is nearly absent in distractor recordings. These LFP data support our Ca^{2+} imaging findings of minimal subcortical filtering of the sensory response followed by robust attenuation across cortex.

To further understand how neural activity relates to movements during the task, in four additional sessions we imaged whisker movements during task performance and analyzed task aligned whisker motion energy. We present two example sessions in Figure 2.9, in which we plot whisker motion energy for target and distractor whiskers aligned to target and distractor stimulus trials. We find that whisker movements increase on target trials in both target and distractor whiskers approximately 100 ms after stimulus onset (Figure 2.9 A, B, E, F) (latency, n=4; target whiskers: 100 +/- 10 ms; distractor whiskers: 129 +/- 4 ms). This increase in bilateral whisker movements is before the onset of licking (>200 ms, due to lockout window), and therefore appears to be part of a response motor

sequence (Musall et al., 2019). Whisker motion energy on distractor trials remained at pre-stimulus levels or increased late in the trial (Figure 2.9G, H), for target and distractor whiskers. In comparing the onset of neural signals (LFP) to the onset of behavior (whisking and licking) we find that the cortical signals precede overt behavior. Our data are therefore consistent with activation of wMC and ALM triggering a whisking and licking response sequence.

We conducted additional analyses of the widefield imaging data to determine whether the observed propagation to frontal cortex for target stimuli is predictive of response initiation. The alternative hypothesis is that propagation reflects a learned stimulus association that may be independent of responding. To distinguish between these hypotheses, we calculated choice encoding (Britten et al., 1996b) for each pixel (Figure 2.10), comparing activity on hit trials (response present) versus miss trials (response absent). The average spatial map of target stimulus choice encoding is shown in Figure 2.10A (left). This analysis revealed pixels with modest positive (increased on hit trials) and negative (increased on miss trials) values of choice encoding. However, none of the pixel values were significantly different than zero after correction for multiple comparisons (Figure 2.10A, right).

We reasoned that hit versus miss outcomes may depend on both the state of the mouse as well as the strength of the stimulus-evoked responses. To isolate the latter component, we recalculated choice encoding based on the difference in activity between early and late lockout period activity (see Methods). With this method, we observed large

and significant choice encoding values in target aligned wMC and bilateral ALM (Figure 2.10B). We also observed focal increases in choice encoding in target aligned S1 and RSP, but these regions did not reach statistical significance after correction for multiple comparisons (Figure 2.10B). Thus, cortical activation of frontal cortex on target trials is predictive of response initiation.

Quantification of functional connectivity across cortex

Finally, we sought to determine whether the differences in propagation for target versus distractor stimuli are reflected in the correlation patterns, or 'functional connectivity', between sensory and motor cortices. To do this, we created pixel-by-pixel correlation maps for S1, wMC, and ALM in target aligned or distractor aligned hemispheres as seed regions of interest (ROIs). We show the correlation maps for the full trial data, which include the pre-stimulus, peri-stimulus, and response windows for all stimulus trial types (Figures 2.11A-F). The most striking findings are regional structure and symmetry. The spatial correlation patterns are highly similar for wMC and ALM seeds, which are quite different from S1 seeds (compare Figures 2.11A/D with 2.11B/E, C/F). This regional structure illustrates that the correlation values reflect local neural activity rather than global imaging artifacts. Regarding symmetry, for all three cortical regions, the target aligned and distractor aligned seed maps are qualitatively extremely similar (compare Figure 2.11A-C with 2.11D-F).

Despite these similarities, we do find significant differences in correlations between S1 and wMC (r^2, target 0.84±0.01, distractor 0.76±0.01, paired t-test, $p=2.9e^{-7}$,

t(38)=6.2, n=39) and between S1 and ALM (r^2, target 0.80±0.01, distractor 0.68±0.02, paired t-test, $p=8.6e^{-10}$, t(38)=8.1, n=39). (Figure 2.11G). The largest differences in target aligned and distractor aligned correlations were between S1 and ALM (ANOVA, $p=1.6e^{-8}$, F(2,37)=30.3, with post-hoc Tukey comparison) (Figure 2.11G). To determine whether these differences are persistent or related to specific phases of the task, we ran the correlation analyses separately for the pre-stimulus, peri-stimulus, and response windows. We found that differences in correlations for target aligned versus distractor aligned S1 to wMC (Figure 2.11H) and S1 to ALM (Figure 2.11I) were significantly larger in the response phase compared to the pre-stimulus phase (ANOVA with post-hoc Tukey comparison, S1-wMC, p=0.0004; S1-ALM, p=0.0005). However, even in the pre-stimulus phase, there was a small yet significant increase in S1 to ALM correlation in target aligned compared to distractor aligned hemispheres (paired t-test, p=0.0018, t(38)=3.4) (Figure 2.11I). Overall, these data are inconsistent with large, global changes in synaptic plasticity or functional connectivity driving task performance, but rather implicate more focal, possibly pathway-specific, adaptations.

Discussion

We developed a Go/NoGo selective detection task to study the neural processes of sensory selection in the mouse somatosensory whisker system. Mice learned to respond to target whisker deflections and ignore contralateral, distractor whisker deflections, achieving expert performance within 2 to 3 weeks of training (Figure 2.2). The main finding of this study is robust attenuation of distractor compared to target stimulus processing between mono-synaptically coupled cortical regions S1 and wMC (Figures 2.3-2.6). We interpret this observation as reflecting the presence of an intra-cortical attenuating filter, suppressing higher order processing of unattended stimuli (A. M. Treisman, 1964).

We note important differences between our study and previous studies of the neural correlates of sensory selection. In our task, target and distractor receptive fields were assigned at the onset of training and remained constant throughout the learning process. This contrasts with previous studies in primates, in which the target and distractor assignments are cued each block or trial. Moreover, our target and distractor stimuli were always across hemispheres, rather than varying in proximity. Yet, despite differences in training, species, sensory modality, stimulus details, and recording technique, we do note remarkable similarities with previous studies. As in the primate visual system, we observe progressive distractor suppression along the cortical hierarchy (Figure 2.6D) (Moran & Desimone, 1985; Tootell et al., 1998; Treue, 2001). Comparing modulation amplitudes between studies is problematic because they vary widely

depending on task and stimulus details. However, generally, within thalamus and primary visual cortex, attentional modulations of approximately 10% have been reported (McAlonan et al., 2008; Motter, 1993; Tootell et al., 1998), which is similar to the 8.8% average modulation we observed in primary somatosensory cortex. Within higher order sensory cortices, attentional modulations of 50 to 65% have been reported (Moran & Desimone, 1985; Tootell et al., 1998), which is similar to the 61.0% and 72.1% average modulations we observed in wMC and ALM, respectively.

What is the nature of distractor suppression? One possibility is that suppression is reactive, that once a distractor is detected, another brain region initiates an inhibitory brake to prevent further processing. This type of transient activation is observed, for example, in prefrontal cortex during stop-signal reaction time tasks at the detection of a 'stop' signal (Aron & Poldrack, 2006; Hanes et al., 1998). A second possibility is that suppression is proactive, already deployed in the initial conditions of the brain regions receiving the distractor stimulus. Insofar as we do not observe additional transient activations for distractor stimuli, our data support the second explanation of proactive suppression.

Given our localization of an attenuating filter between S1 and wMC, there are multiple possible mechanisms for implementing this filter. The most direct mechanism would be bidirectional modulation of the S1-wMC intra-cortical projection pathway. Previous studies of whisker detection have identified increased sensory processing with learning in wMC and in specific S1-wMC projection neurons (Chen et al., 2015; Le Merre

et al., 2018). Whether this pathway decreases in strength when aligned with a distractor has not been studied. However, such a finding of bidirectional modulation would provide strong evidence for involvement of this pathway in specific stimulus selection, rather than general task engagement. Additionally, regulated propagation between S1 and wMC may involve subcortical loops through the striatum (Alloway et al., 2006) or posterior medial thalamus (Kleinfeld et al., 1999), or cortical feedback projections from PFC to wMC or from wMC to S1 (Xu et al., 2012; Zagha et al., 2013). For example, wMC to S1 feedback may strengthen (target aligned) or weaken (distractor aligned) the reciprocal S1 to wMC feedforward pathway. Strengthening or weakening may occur through feedback targeting of excitatory, inhibitory or disinhibitory S1 neurons (Kinnischtzke et al., 2014; S. Lee et al., 2013; Petreanu et al., 2009; Rocco & Brumberg, 2007; Zagha et al., 2013). Our task provides an excellent platform for studying the plasticity and cellular/circuit contributions of each of these mechanisms towards target enhancement and/or distractor suppression. Alternatively, our findings are inconsistent with strong reductions in ascending sensory drives to distractor aligned S1 (Figures 2.3-2.6 and 2.8) or large, global reductions in the structural or functional connectivity between distractor aligned S1 and the rest of cortex (Figure 2.11).

While our study identifies a sensory filtering process distal to S1, other studies have identified sensory gating in S1 and earlier subcortical structures. Previous studies of the rodent whisker system have examined differences in sensory processing during periods of whisking versus non-whisking. In general, these studies find reductions in

sensory responses during whisking (S. Chakrabarti & C. Schwarz, 2018; S. Crochet & C. C. Petersen, 2006; Fanselow & Nicolelis, 1999; Ferezou et al., 2007; Lee et al., 2008), which is already present in the first sensory brainstem relay (S. Chakrabarti & C. Schwarz, 2018). This sensory gating process is likely mediated by both top-down cortical (S. Chakrabarti & C. Schwarz, 2018; Lee et al., 2008) and neuromodulatory (Eggermann et al., 2014) inputs. Thus, modulations of sensory processing may occur all along the ascending sensory pathway, including brainstem, thalamus, and cortex. Why different behavioral contexts engage different mechanisms of sensory gating is currently unknown.

Finally, we currently do not know how wMC contributes to the sensory selection process. This cortical region has been studied extensively with respect to whisking, specifically in establishing its set-point, initiation, and amplitude modulation (Carvell et al., 1996; Hill et al., 2011). Consistent with this, we find that wMC activation on target trials correlates with bilateral increases in whisking (Figure 2.9). Alternatively, more recent studies have demonstrated roles for this same region in orienting behaviors and action suppression (Ebbesen et al., 2017; Erlich et al., 2011; Zagha et al., 2015). Our study demonstrates, at the representational level, a possible additional function of regulating the propagation of sensory processing for sensory selection. And yet, wMC is only one of the many routes by which a whisker stimulus can initiate a motor output (Kleinfeld et al., 1999). Defining how wMC contributes to sensory-motor processing in this task and in other behavioral contexts will be a major focus of future investigations.

References

Alloway, K. D., Lou, L., Nwabueze-Ogbo, F., & Chakrabarti, S. (2006). Topography of cortical projections to the dorsolateral neostriatum in rats: multiple overlapping sensorimotor pathways. *J Comp Neurol*, *499*(1), 33-48. https://doi.org/10.1002/cne.21039

Aron, A. R., & Poldrack, R. A. (2006). Cortical and subcortical contributions to Stop signal response inhibition: role of the subthalamic nucleus. *J Neurosci*, *26*(9), 2424-2433. https://doi.org/10.1523/JNEUROSCI.4682-05.2006

Britten, K. H., Newsome, W. T., Shadlen, M. N., Celebrini, S., & Movshon, J. A. (1996). A relationship between behavioral choice and the visual responses of neurons in macaque MT. *Vis Neurosci*, *13*(1), 87-100. https://doi.org/10.1017/s095252380000715x

Britten, K. H., Shadlen, M. N., Newsome, W. T., & Movshon, J. A. (1992). The analysis of visual motion: a comparison of neuronal and psychophysical performance. *J Neurosci*, *12*(12), 4745-4765. https://www.ncbi.nlm.nih.gov/pubmed/1464765

Carvell, G. E., Miller, S. A., & Simons, D. J. (1996). The relationship of vibrissal motor cortex unit activity to whisking in the awake rat. *Somatosens Mot Res*, *13*(2), 115-127. http://www.ncbi.nlm.nih.gov/pubmed/8844960

Chakrabarti, S., & Schwarz, C. (2018). Cortical modulation of sensory flow during active touch in the rat whisker system. *Nat Commun*, *9*(1), 3907. https://doi.org/10.1038/s41467-018-06200-6

Chakrabarti, S., Zhang, M., & Alloway, K. D. (2008). MI neuronal responses to peripheral whisker stimulation: relationship to neuronal activity in si barrels and septa. *J Neurophysiol*, *100*(1), 50-63. https://doi.org/10.1152/jn.90327.2008

Chen, J. L., Carta, S., Soldado-Magraner, J., Schneider, B. L., & Helmchen, F. (2013). Behaviour-dependent recruitment of long-range projection neurons in somatosensory cortex. *Nature*, *499*(7458), 336-340. https://doi.org/10.1038/nature12236

Chen, J. L., Margolis, D. J., Stankov, A., Sumanovski, L. T., Schneider, B. L., & Helmchen, F. (2015). Pathway-specific reorganization of projection neurons in somatosensory

cortex during learning. *Nat Neurosci*, *18*(8), 1101-1108. https://doi.org/10.1038/nn.4046

Chen, T. W., Li, N., Daie, K., & Svoboda, K. (2017). A Map of Anticipatory Activity in Mouse Motor Cortex. *Neuron*, *94*(4), 866-879 e864. https://doi.org/10.1016/j.neuron.2017.05.005

Crick, F. (1984). Function of the thalamic reticular complex: the searchlight hypothesis. *Proc Natl Acad Sci U S A*, *81*(14), 4586-4590. https://doi.org/10.1073/pnas.81.14.4586

Crochet, S., & Petersen, C. C. (2006). Correlating whisker behavior with membrane potential in barrel cortex of awake mice. *Nat Neurosci*, *9*(5), 608-610. https://doi.org/10.1038/nn1690

Ebbesen, C. L., Doron, G., Lenschow, C., & Brecht, M. (2017). Vibrissa motor cortex activity suppresses contralateral whisking behavior. *Nat Neurosci*, *20*(1), 82-89. https://doi.org/10.1038/nn.4437

Eggermann, E., Kremer, Y., Crochet, S., & Petersen, C. C. H. (2014). Cholinergic signals in mouse barrel cortex during active whisker sensing. *Cell Rep*, *9*(5), 1654-1660. https://doi.org/10.1016/j.celrep.2014.11.005

Erlich, J. C., Bialek, M., & Brody, C. D. (2011). A cortical substrate for memory-guided orienting in the rat. *Neuron*, *72*(2), 330-343. https://doi.org/10.1016/j.neuron.2011.07.010

Fanselow, E. E., & Nicolelis, M. A. (1999). Behavioral modulation of tactile responses in the rat somatosensory system. *J Neurosci*, *19*(17), 7603-7616. http://www.ncbi.nlm.nih.gov/entrez/query.fcgi?cmd=Retrieve&db=PubMed&dopt=Citation&list_uids=10460266

Farkas, T., Kis, Z., Toldi, J., & Wolff, J. R. (1999). Activation of the primary motor cortex by somatosensory stimulation in adult rats is mediated mainly by associational connections from the somatosensory cortex. *Neuroscience*, *90*(2), 353-361. https://doi.org/10.1016/s0306-4522(98)00451-5

Ferezou, I., Haiss, F., Gentet, L. J., Aronoff, R., Weber, B., & Petersen, C. C. (2007). Spatiotemporal dynamics of cortical sensorimotor integration in behaving mice. *Neuron*, *56*(5), 907-923. https://doi.org/10.1016/j.neuron.2007.10.007

Guo, Z. V., Li, N., Huber, D., Ophir, E., Gutnisky, D., Ting, J. T., Feng, G., & Svoboda, K. (2014). Flow of cortical activity underlying a tactile decision in mice. *Neuron*, *81*(1), 179-194. https://doi.org/10.1016/j.neuron.2013.10.020

Hanes, D. P., Patterson, W. F., 2nd, & Schall, J. D. (1998). Role of frontal eye fields in countermanding saccades: visual, movement, and fixation activity. *J Neurophysiol*, *79*(2), 817-834. http://www.ncbi.nlm.nih.gov/pubmed/9463444

Hill, D. N., Curtis, J. C., Moore, J. D., & Kleinfeld, D. (2011). Primary motor cortex reports efferent control of vibrissa motion on multiple timescales. *Neuron*, *72*(2), 344-356. https://doi.org/10.1016/j.neuron.2011.09.020

Kinnischtzke, A. K., Simons, D. J., & Fanselow, E. E. (2014). Motor cortex broadly engages excitatory and inhibitory neurons in somatosensory barrel cortex. *Cereb Cortex*, *24*(8), 2237-2248. https://doi.org/10.1093/cercor/bht085

Kleinfeld, D., Berg, R. W., & O'Connor, S. M. (1999). Anatomical loops and their electrical dynamics in relation to whisking by rat. *Somatosens Mot Res*, *16*(2), 69-88. https://doi.org/10.1080/08990229970528

Kleinfeld, D., Sachdev, R. N., Merchant, L. M., Jarvis, M. R., & Ebner, F. F. (2002). Adaptive filtering of vibrissa input in motor cortex of rat. *Neuron*, *34*(6), 1021-1034. https://doi.org/10.1016/s0896-6273(02)00732-8

Le Merre, P., Esmaeili, V., Charriere, E., Galan, K., Salin, P. A., Petersen, C. C. H., & Crochet, S. (2018). Reward-Based Learning Drives Rapid Sensory Signals in Medial Prefrontal Cortex and Dorsal Hippocampus Necessary for Goal-Directed Behavior. *Neuron*, *97*(1), 83-91 e85. https://doi.org/10.1016/j.neuron.2017.11.031

Lee, S., Carvell, G. E., & Simons, D. J. (2008). Motor modulation of afferent somatosensory circuits. *Nat Neurosci*, *11*(12), 1430-1438. http://www.ncbi.nlm.nih.gov/entrez/query.fcgi?cmd=Retrieve&db=PubMed&dopt=Citation&list_uids=19011625

Lee, S., Kruglikov, I., Huang, Z. J., Fishell, G., & Rudy, B. (2013). A disinhibitory circuit mediates motor integration in the somatosensory cortex. *Nat Neurosci*, *16*(11), 1662-1670. http://www.ncbi.nlm.nih.gov/entrez/query.fcgi?cmd=Retrieve&db=PubMed&dopt=Citation&list_uids=24097044

Madisen, L., Garner, A. R., Shimaoka, D., Chuong, A. S., Klapoetke, N. C., Li, L., van der Bourg, A., Niino, Y., Egolf, L., Monetti, C., Gu, H., Mills, M., Cheng, A., Tasic, B., Nguyen, T. N., Sunkin, S. M., Benucci, A., Nagy, A., Miyawaki, A., . . . Zeng, H. (2015). Transgenic mice for intersectional targeting of neural sensors and effectors with high specificity and performance. *Neuron*, *85*(5), 942-958. https://doi.org/10.1016/j.neuron.2015.02.022

Mante, V., Sussillo, D., Shenoy, K. V., & Newsome, W. T. (2013). Context-dependent computation by recurrent dynamics in prefrontal cortex. *Nature*, *503*(7474), 78-84. https://doi.org/10.1038/nature12742

Mao, T., Kusefoglu, D., Hooks, B. M., Huber, D., Petreanu, L., & Svoboda, K. (2011). Long-range neuronal circuits underlying the interaction between sensory and motor cortex. *Neuron*, *72*(1), 111-123. https://doi.org/10.1016/j.neuron.2011.07.029

McAlonan, K., Cavanaugh, J., & Wurtz, R. H. (2008). Guarding the gateway to cortex with attention in visual thalamus. *Nature*, *456*(7220), 391-394. https://doi.org/10.1038/nature07382

Miller, E. K., & Cohen, J. D. (2001). An integrative theory of prefrontal cortex function. *Annu Rev Neurosci*, *24*, 167-202. https://doi.org/10.1146/annurev.neuro.24.1.167

Miyashita, E., Keller, A., & Asanuma, H. (1994). Input-output organization of the rat vibrissal motor cortex. *Exp Brain Res*, *99*(2), 223-232. http://www.ncbi.nlm.nih.gov/pubmed/7523173

Moran, J., & Desimone, R. (1985). Selective attention gates visual processing in the extrastriate cortex. *Science*, *229*(4715), 782-784. http://www.ncbi.nlm.nih.gov/entrez/query.fcgi?cmd=Retrieve&db=PubMed&dopt=Citation&list_uids=4023713

Motter, B. C. (1993). Focal attention produces spatially selective processing in visual cortical areas V1, V2, and V4 in the presence of competing stimuli. *J Neurophysiol*, *70*(3), 909-919. https://doi.org/10.1152/jn.1993.70.3.909

Musall, S., Kaufman, M. T., Juavinett, A. L., Gluf, S., & Churchland, A. K. (2019). Single-trial neural dynamics are dominated by richly varied movements. *Nat Neurosci*, *22*(10), 1677-1686. https://doi.org/10.1038/s41593-019-0502-4

Noudoost, B., & Moore, T. (2011). The role of neuromodulators in selective attention. *Trends Cogn Sci*, *15*(12), 585-591. http://www.ncbi.nlm.nih.gov/entrez/query.fcgi?cmd=Retrieve&db=PubMed&dopt=Citation&list_uids=22074811

Ollerenshaw, D. R., Bari, B. A., Millard, D. C., Orr, L. E., Wang, Q., & Stanley, G. B. (2012). Detection of tactile inputs in the rat vibrissa pathway. *J Neurophysiol*, *108*(2), 479-490. https://doi.org/10.1152/jn.00004.2012

Petersen, C. C. H. (2019). Sensorimotor processing in the rodent barrel cortex. *Nat Rev Neurosci*, *20*(9), 533-546. https://doi.org/10.1038/s41583-019-0200-y

Petreanu, L., Mao, T., Sternson, S. M., & Svoboda, K. (2009). The subcellular organization of neocortical excitatory connections. *Nature*, *457*(7233), 1142-1145. https://doi.org/10.1038/nature07709

Porter, L. L., & White, E. L. (1983). Afferent and efferent pathways of the vibrissal region of primary motor cortex in the mouse. *J Comp Neurol*, *214*(3), 279-289. https://doi.org/10.1002/cne.902140306

Rocco, M. M., & Brumberg, J. C. (2007). The sensorimotor slice. *J Neurosci Methods*, *162*(1-2), 139-147. https://doi.org/10.1016/j.jneumeth.2007.01.002

Rodenkirch, C., Liu, Y., Schriver, B. J., & Wang, Q. (2019). Locus coeruleus activation enhances thalamic feature selectivity via norepinephrine regulation of intrathalamic circuit dynamics. *Nat Neurosci*, *22*(1), 120-133. https://doi.org/10.1038/s41593-018-0283-1

Sridharan, D., Schwarz, J. S., & Knudsen, E. I. (2014). Selective attention in birds. *Curr Biol*, *24*(11), R510-513. https://doi.org/10.1016/j.cub.2013.12.046

Tootell, R. B., Hadjikhani, N., Hall, E. K., Marrett, S., Vanduffel, W., Vaughan, J. T., & Dale, A. M. (1998). The retinotopy of visual spatial attention. *Neuron*, *21*(6), 1409-1422. https://doi.org/10.1016/s0896-6273(00)80659-5

Treisman, A. M. (1964). Selective Attention in Man. *Br Med Bull*, *20*, 12-16. https://doi.org/10.1093/oxfordjournals.bmb.a070274

Treue, S. (2001). Neural correlates of attention in primate visual cortex. *Trends Neurosci*, *24*(5), 295-300. https://doi.org/10.1016/s0166-2236(00)01814-2

Wekselblatt, J. B., Flister, E. D., Piscopo, D. M., & Niell, C. M. (2016). Large-scale imaging of cortical dynamics during sensory perception and behavior. *J Neurophysiol*, *115*(6), 2852-2866. https://doi.org/10.1152/jn.01056.2015

Wiederman, S. D., & O'Carroll, D. C. (2013). Selective attention in an insect visual neuron. *Curr Biol*, *23*(2), 156-161. https://doi.org/10.1016/j.cub.2012.11.048

Xu, N. L., Harnett, M. T., Williams, S. R., Huber, D., O'Connor, D. H., Svoboda, K., & Magee, J. C. (2012). Nonlinear dendritic integration of sensory and motor input during an active sensing task. *Nature*, *492*(7428), 247-251. http://www.ncbi.nlm.nih.gov/entrez/query.fcgi?cmd=Retrieve&db=PubMed&dopt=Citation&list_uids=23143335

Zagha, E., Casale, A. E., Sachdev, R. N., McGinley, M. J., & McCormick, D. A. (2013). Motor cortex feedback influences sensory processing by modulating network state. *Neuron*, *79*(3), 567-578. https://doi.org/10.1016/j.neuron.2013.06.008

Zagha, E., Ge, X., & McCormick, D. A. (2015). Competing Neural Ensembles in Motor Cortex Gate Goal-Directed Motor Output. *Neuron*, *88*(3), 565-577. https://doi.org/10.1016/j.neuron.2015.09.044

Figures and Legends

Figure 2.1: Treisman Attenuation Model

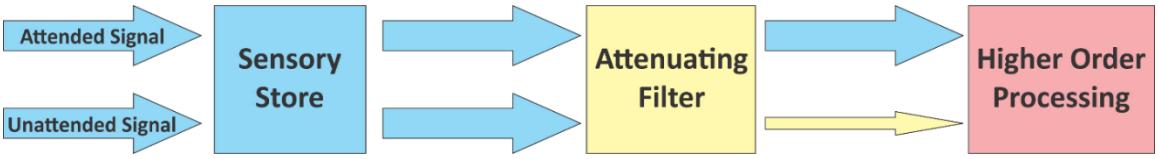

This model of selective attention proposes that both attended and unattended signals enter an early sensory store. At some point in the processing stream, however, an attenuating filter suppresses unattended signals while allowing attended signals to propagate forward for higher order processing.

Figure 2.2: Behavior Paradigm and Measures of Selective Detection

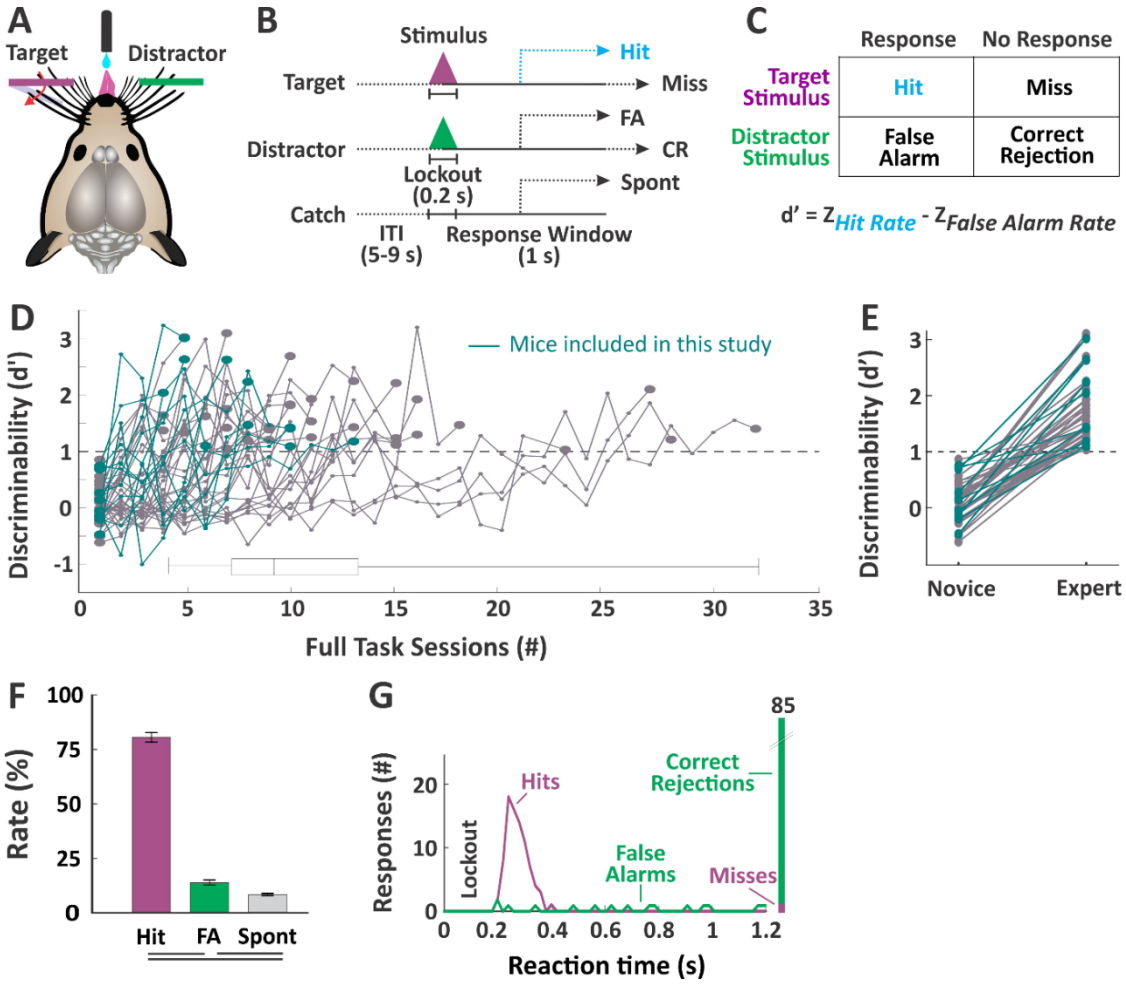

(A) Illustration of the behavioral setup. Mice are head-fixed in the behavioral rig with piezo-controlled paddles within their whisker fields bilaterally. Each paddle is assigned as target (purple) or distractor (green) at the start of training. Mice report stimulus detection and receive rewards from a central lickport. (B) Task structure. Each trial consists of an inter-trial interval, a stimulus and 200ms lockout, and a 1 s response window. Trial type as determined by the stimulus could be target, distractor or catch (no stimulus). (C) Calculation of discriminability d', as the separation between hit rate and false alarm rate. (D) Performance trajectories for all mice (n=43 mice) and box and whiskers summary plot. Those used for imaging studies (n=5 mice) are indicated in blue. Mice were considered expert once they achieved a d'>1 for three consecutive days. (E) Comparison of d' for novice mice (first day of training on impulse control) and expert mice (n=43 mice, paired sample t-test, $p=3.7e^{-20}$, t(42)=16.71). (F) Performance measures for the imaging sessions (n=39 sessions). Lines below plot denote statistical significance. (G) Example session data showing reaction time distributions for target and distractor trials.

Figure 2.3: Sensory and Motor Cortical Representations Using Widefield Imaging

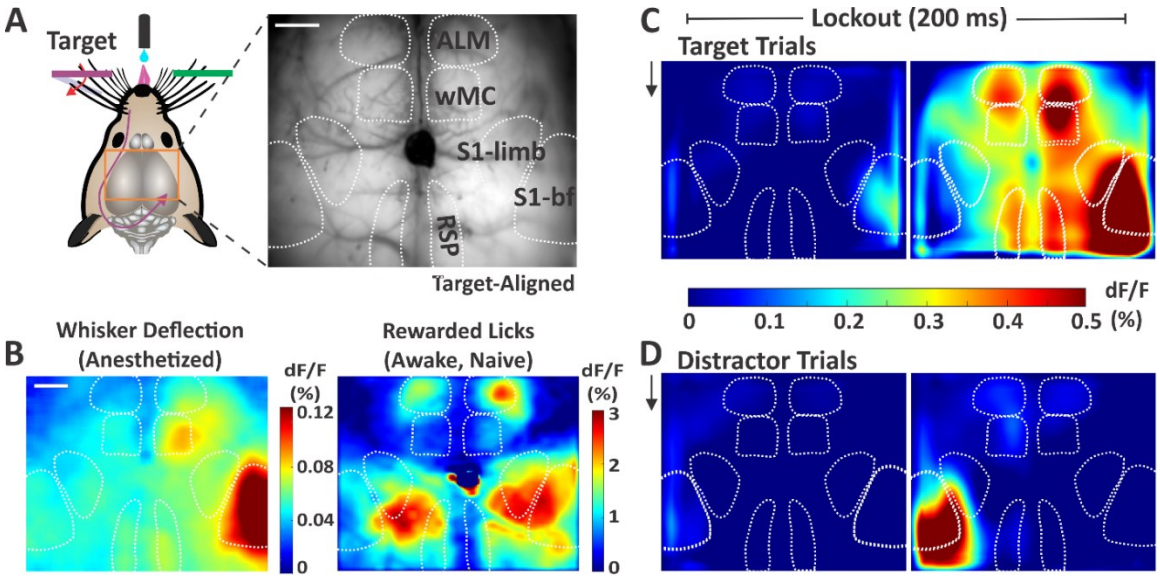

(A) Illustration of the imaging setup (left) and example frame from the through-skull GCaMP6s imaging (right). Surface vessels appear as dark striations overlaying the brain parenchyma. Bregma is indicated by the central ink blot. ALM, anterior lateral motor cortex; wMC, whisker region of primary motor cortex; S1, primary somatosensory cortex; bf, barrel field; RSP, retrosplenial cortex. (B) Cortical activity (dF/F) following whisker deflections in an anesthetized mouse (left), to localize the sensory and motor whisker representations. Cortical activity following reward-triggered licking in a naïve mouse (right), to localize licking-related activity. (C) Cortical activity on target trials during the two sequential imaging frames of the lockout period in expert mice performing the detection task (grand average, n=39 sessions). Black arrow indicates whisker stimulus onset, which coincides with the start of the first imaging frame. (D) Same as [C], but for distractor trials. Note the differential propagation of cortical activity depending on trial type. Scale bars in [A] and [B] are 1mm.

Figure 2.4: Cortical Activity Patterns across All Trial Types

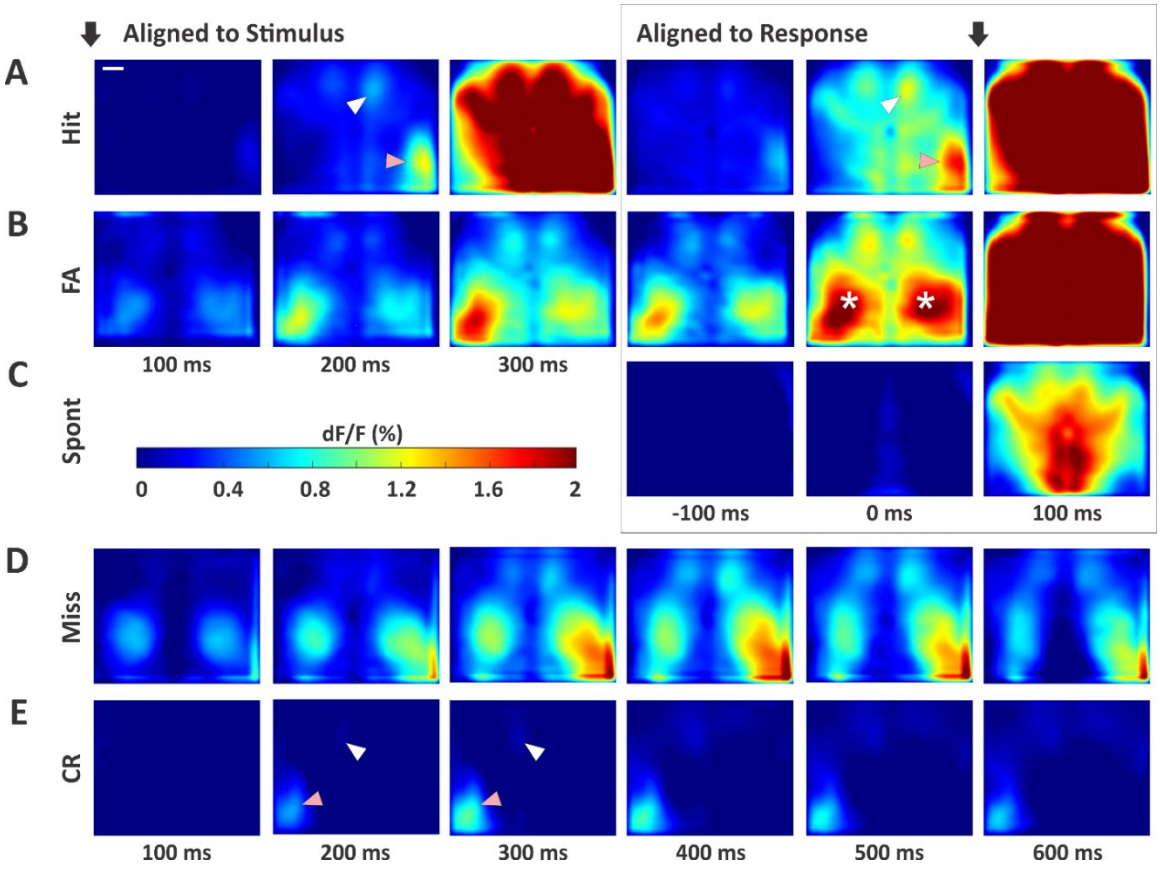

(A) Hit trials. Black arrows indicate alignment to stimulus onset (left three panels) or response onset (right three panels). The third frame aligned to stimulus (300 ms) is the first frame after the lockout and within the response window. Note the strong activity in contralateral S1 (pink arrows) with propagation to wMC (white arrows) and ALM, prior to response generation. (B) False alarm trials, with the same plot structure as in [A]. Asterisks mark elevated activity in the S1-limb regions, bilaterally. (C) Spontaneous trials (no stimulus alignment). (D) Miss trials. As there is no response on these trial types, we plot an extended series of post-stimulus activity. (E) Correct rejection trials, with the same plot structure as in [D]. Note the strong activity in S1 (pink arrow) yet lack of propagation to wMC (white arrow) and ALM. Scale bar in [A] is 1 mm.

Figure 2.5: Spatial Maps of Stimulus Encoding

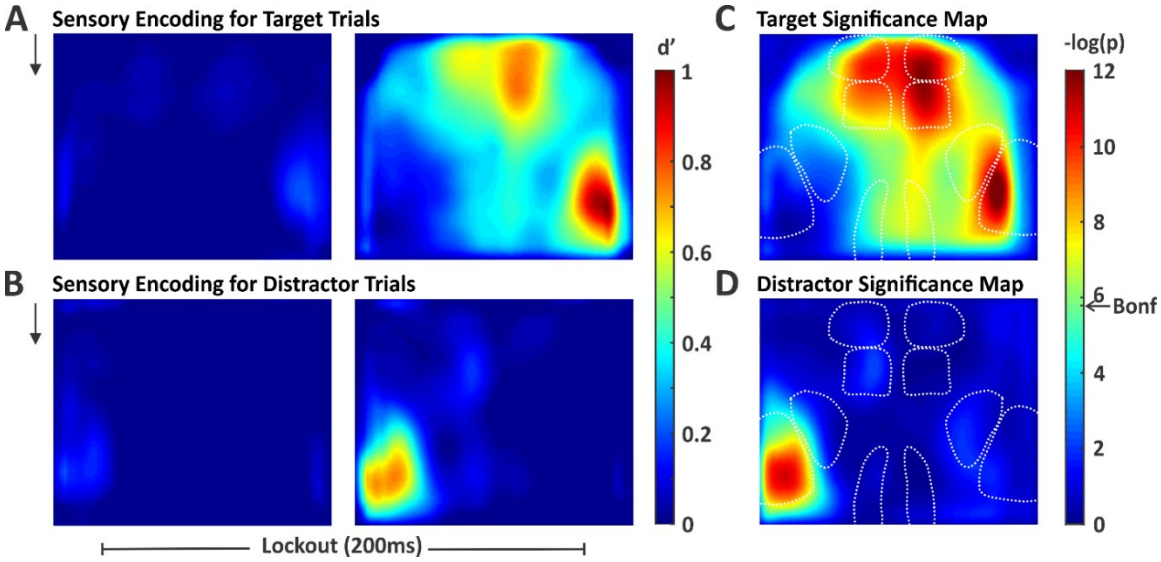

We quantified stimulus encoding as the separation between stimulus absent and stimulus present d', computed pixel-by-pixel. (A) Map of target stimulus encoding during the two sequential frames of the lockout period (black arrow represents stimulus onset). (B) Map of distractor stimulus encoding during the same time windows as in [A]. (C) and (D) Significance maps of the right panels of [A] and [B], respectively. The significance threshold determined by the Bonferroni correction for multiple comparisons is indicated by the arrow on the color bar (Bonf). Pixels with smaller p-values (warmer colors) have d' values significantly above 0. For target stimuli, we observed widespread stimulus encoding including in multiple frontal and parietal regions. For distractor stimuli, significant stimulus encoding is restricted to S1.

Figure 2.6: Quantification of Target vs Distractor Stimulus Propagation within Cortex

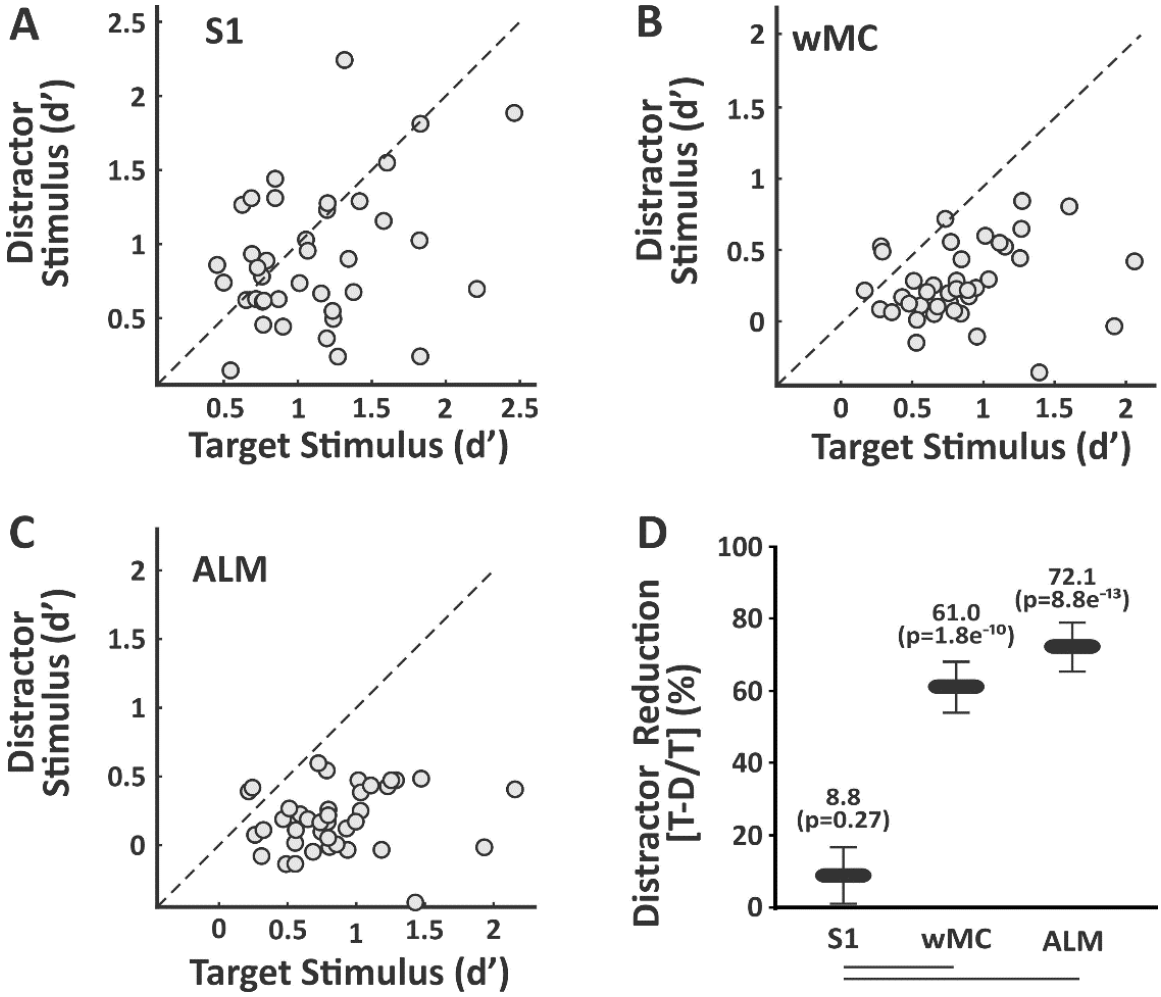

For each session, we compared target stimulus encoding in target aligned cortices to distractor stimulus encoding in distractor aligned cortex. (A-C) Scatter plots of target versus distractor encoding in S1 (A), wMC (B) and ALM (C). Each data point is one session (n=39 sessions). Note that the data are broadly distributed in S1, and highly biased towards stronger target encoding in wMC and ALM. (D) Summary data, comparing reductions in distractor encoding within each region (values above each data point) and between regions (lines below graph denote statistical significance). Reductions in distractor encoding are significantly larger in wMC and ALM compared to S1.

Figure 2.7: Similar Behavior and Neural Activity Across Target Assignments and Trial Structures

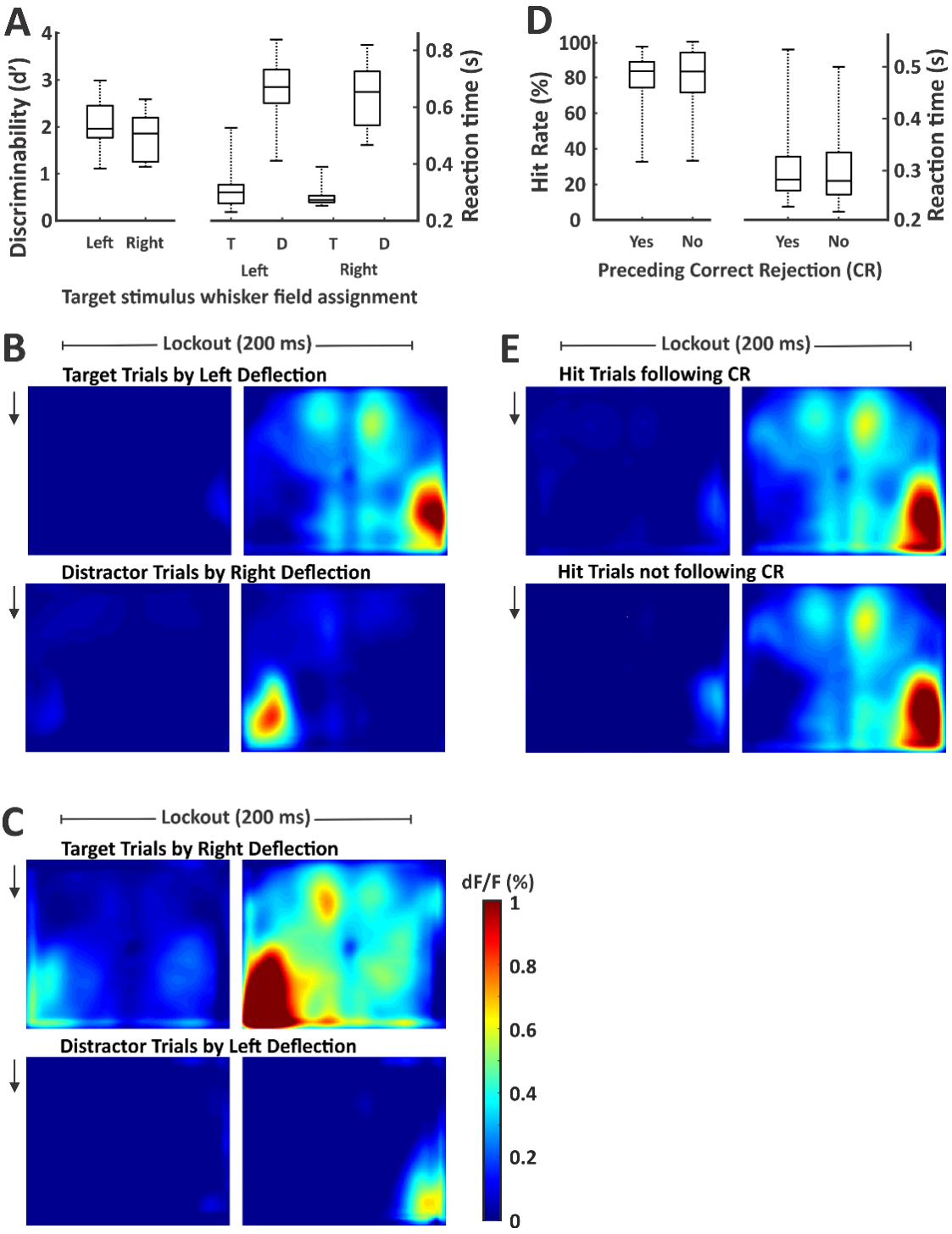

(A) Discriminability d' and reaction times reported (box and whisker plots) separately for mice with left or right target whisker field assignment. None of the behavioral measures were significantly different between these two populations. (B) Cortical activity during the lockout period for target trials (top) and distractor trials (bottom) for sessions in which the target was assigned to the left whisker field (represented by the right cortical hemisphere) (n = 3 mice, n = 25 sessions). (C) Same as [B], but for sessions in which the target was assigned to the right whisker field (represented by the left cortical hemisphere) (n = 2 mice, n = 14 sessions). Signal propagation to frontal cortex correlated with target assignment. (D) Hit rates and reaction times reported (box and whisker plots) separately for target trials with and without a preceding correct rejection. None of the behavioral measures were significantly different between these two trial structures. (E) Cortical activity during the lockout period for hit trials following a correct rejection (top) and hit trials not following a correct rejection (bottom) (n=39 sessions for both).

Figure 2.8: LFP Signal Transformation across S1, wMC and ALM

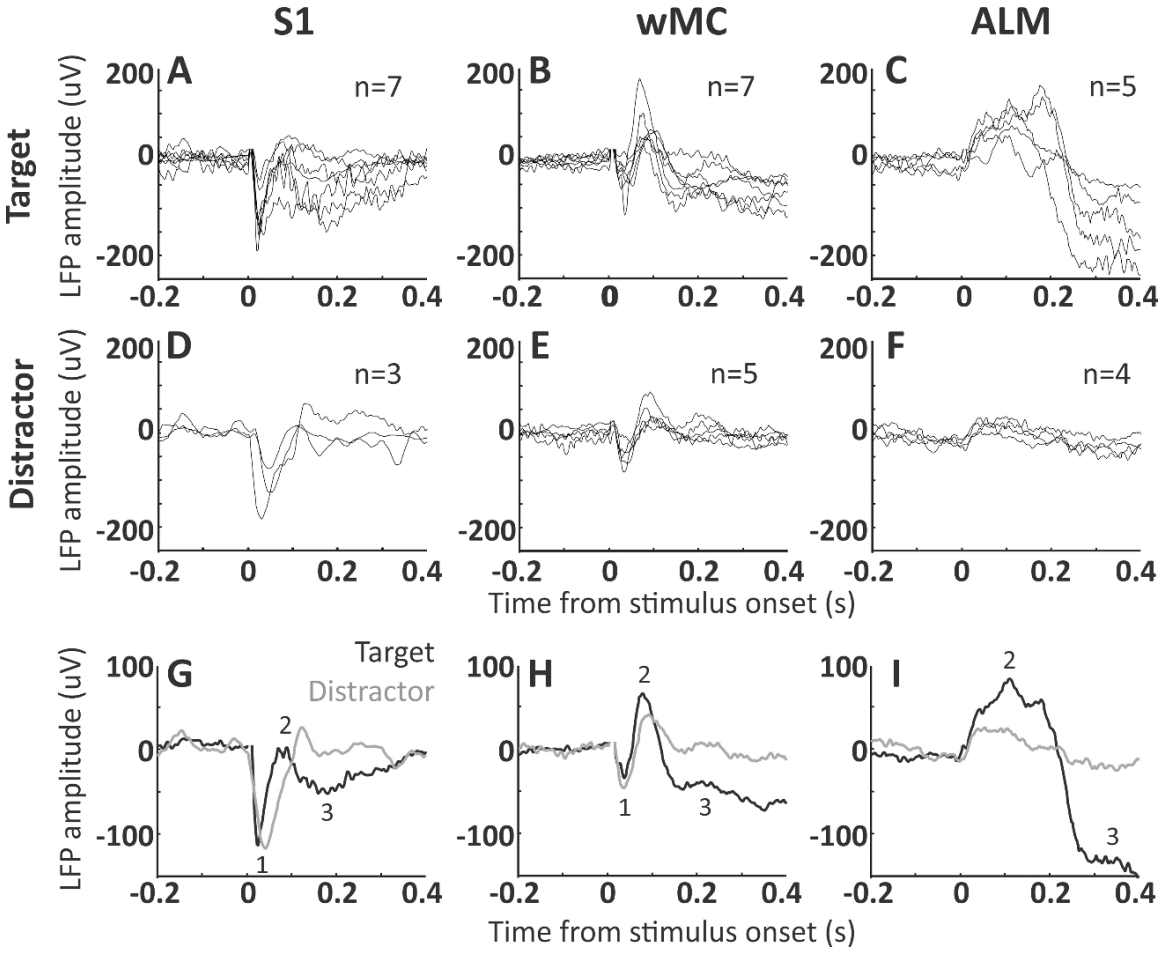

LFP signals were recorded from layer 5 of S1, wMC and ALM. (A-F) Each trace reflects average LFP signals from one session, across all target trials in target aligned cortices (A-C) and across all distractor trials in distractor aligned cortices (D-F). The count in each panel refers to the number of recorded sessions included. (G-I) Target aligned (black) and distractor aligned (grey) LFP signals, averaged across sessions. We observed three distinct event-related potentials, two negative-going (1 and 3) and one positive-going (2). Event 1, which is large in S1, small in wMC and absent in ALM, likely reflects the initial feedforward sensory sweep. This event is similar in target and distractor recordings. Event 3, which is large in ALM and moderate in wMC and S1, is highly dissimilar between target and distractor recordings.

Figure 2.9: Bilateral Whisker Movements on Target Trials

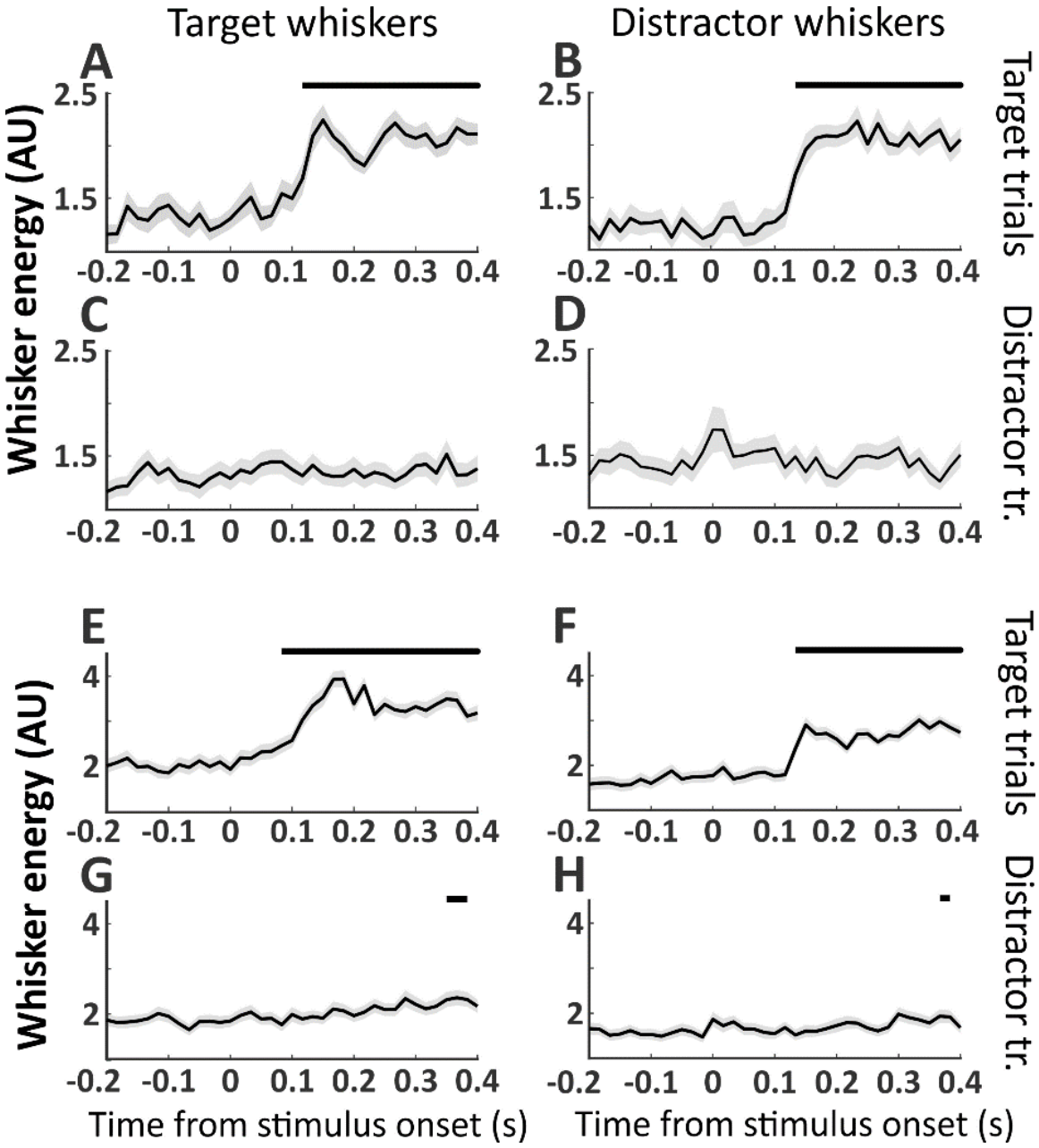

Whisker movement energy was calculated from target or distractor whisker fields and plotted separately for target and distractor trials. Significant changes in post-stimulus compared to pre-stimulus whisker movements are indicated as black bars above each plot. Two example sessions are shown, session 1 (A-D) and session 2 (E-H). (A, E) Target whisker energy on target trials; (B, F) distractor whisker energy on target trials; (C, G) target whisker energy on distractor trials; (D, H) distractor whisker energy on distractor trials. Significant increases in whisker movements occurred for both target and distractor whiskers approximately 0.1 seconds after target stimulus onset (A, B, E, F). Target and distractor whisker movements to distractor stimuli were either non-significant throughout the trial (C, D) or delayed (G, H).

Figure 2.10: Spatial Maps of Choice Encoding

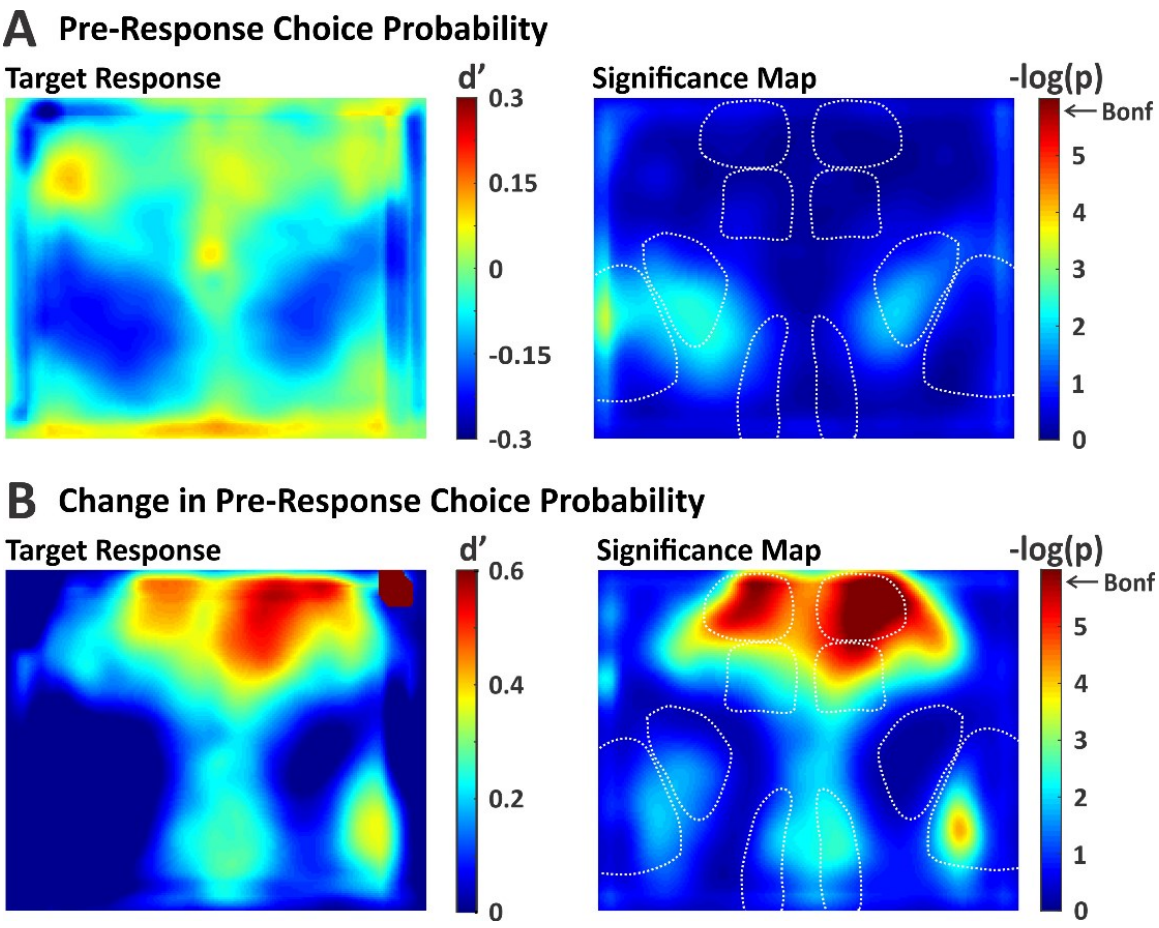

We quantified choice encoding as the separation between response absent and response present d', computed pixel-by-pixel. ***(A)*** *Choice encoding map (left) and significance map (right) during the last frame of the lockout period. None of the pixels reached significance after correcting for multiple comparisons (Bonferroni).* ***(B)*** *Same as in [A], except with choice encoding computed on the difference in activity between the two lockout frames. With this approach, significant choice encoding was observed in target aligned wMC and bilateral ALM.*

Figure 2.11: Spatial Correlation Analysis

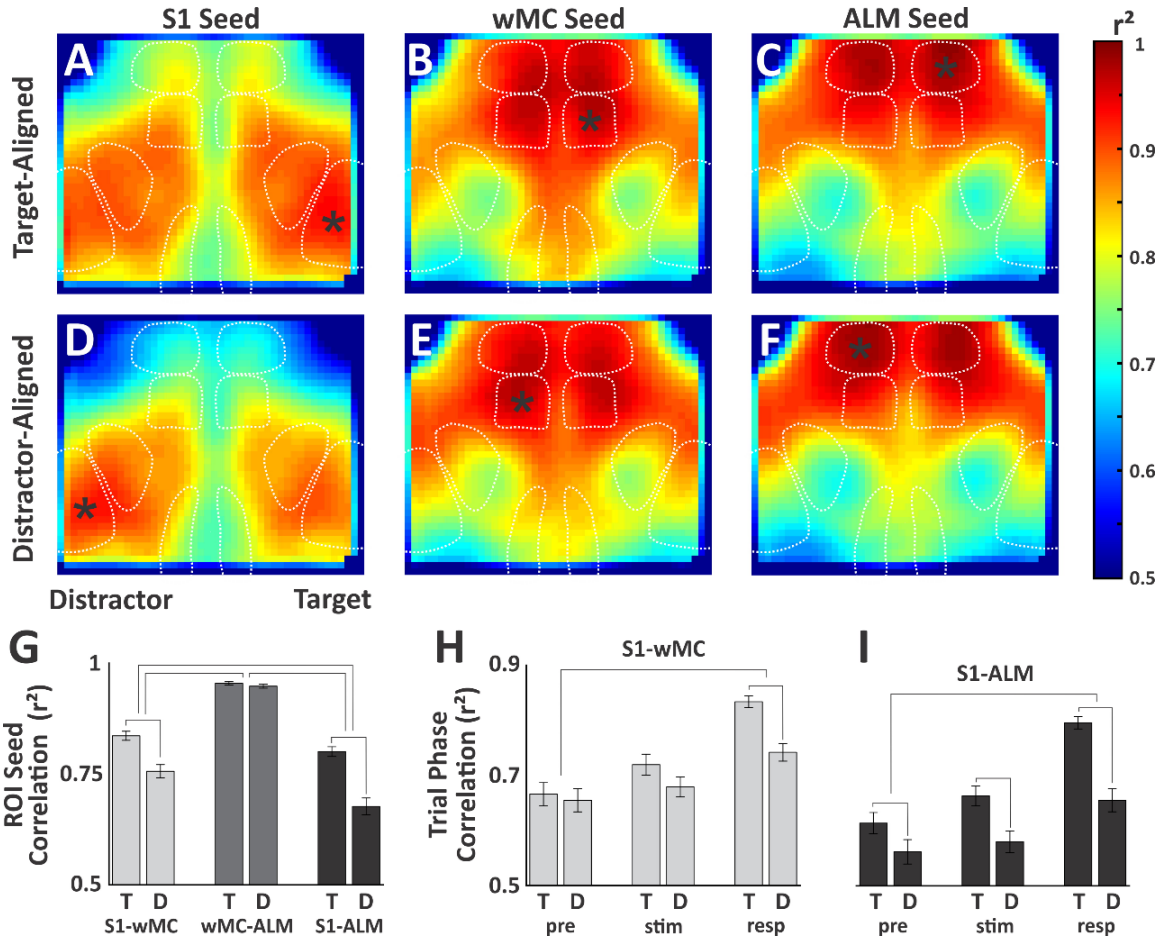

(A-F) *Correlation maps for full trial data. Seed regions of interest (marked by asterisk) included S1, wMC and ALM, in target aligned* ***(A-C)*** *and distractor aligned* ***(D-F)*** *cortices.* ***(G)*** *Summary data of average pairwise correlation values between S1-wMC, wMC-ALM and S1-ALM. Statistical comparisons were made between target aligned (T) and distractor aligned (D) correlations, with significance denoted by lines connecting adjacent columns. Statistical comparisons were also made based on the differences in target aligned and distractor aligned correlations between regions, with significance denoted by lines connecting pairs of columns. (H, I) Similar structure as in [G], except for comparisons of target aligned and distractor aligned correlations (H, S1-wMC; I, S1-ALM) for different trial phases (pre, pre-stimulus; stim, peri-stimulus; resp, response).*

Chapter 3: Global, Low Amplitude Cortical State

The prestimulus manuscript was an effort to address the underlying activity before a successful versus unsuccessful trial outcome. Does an animal subject prepare a response before a stimulus arrives or is the decision making process entirely reliant on neuronal signaling after the stimulus presentation? We anticipated that a predictive prestimulus condition; we termed the potential condition a prestimulus 'state.' Although we discussed whether we could defend this state as an optimal state, we resolved that without presenting an optimal versus suboptimal state, our interpretation on whether cortical optimality had been achieved was beyond the purview of the investigation. Nevertheless, by evaluating the cortical activity in the prestimulus period, we were determined that prestimulus activity did predict trial outcome; specifically, as presented here, the prestimulus activity predicted a response outcome.

As this work was built upon the previous widefield manuscript, my contributions to this work were similar in nature to the attenuation work: animal surgery and behavior, fluorescence data analyses, and stimulus encoding. Importantly, we defended a prestimulus analysis using the sliding window method with optimized sliding window parameters for our data analysis. Consistent results with regards to previously reported post-stimulus localization and stimulus encoding were essential for defending this work.

A minor change has been made regarding this adapted chapter. All statements using the terminology 'in a selective detection task' have been replaced with 'for a

selective detection task'. This was changed for this work only, purely based on consistency with previous works. The changes adapted are noted in blue.

An attempt was made regarding choice encoding in the prestimulus epoch. Because we identified a low amplitude cortical state preceding all responses, we would expect prestimulus activity to show negative choice encoding (lower than chance choice probability). We found marginal negative choice probability in target aligned single unit analyses, which confirmed our manuscript claims. When the choice probability analysis was performed for the widefield calcium imaging, we found additional evidence for global prestimulus choice probability (not in manuscript). This data was not included in the original manuscript because we are still pondering its interpretation. When this analysis was initially run across mice, we identified more significance in lower than chance choice probability for focal distractor aligned regions in the prestimulus epoch for target trials only. We would then expect negative choice encoding in the identified distractor aligned regions. Still to be explored, focal localization of negative choice encoding may indicate evidence for region-specific suppression preceding successful outcome trials. To note, the significance was observed in distractor aligned and task-related motor cortices and retrosplenial cortex. The results, however, have not yet been reproduced. Therefore, the original figure is included in **Appendix Figure 1** and can be further discussed as a possible future direction. As the widefield choice probability analysis still yielded global significance, it did not change our prestimulus interpretations, but may point to additional prestimulus mechanisms for a prestimulus cortical state.

Functional Localization of an Attenuating Filter

Adapted from:

Global, Low Amplitude Cortical State Predicts Response Outcomes for a Selective Detection Task in Mice

Running title: Prestimulus Cortical State on Selective Detection

Authors: Krista Marrero[1*], Krithiga Aruljothi[2*], Behzad Zareian[2], Chengchun Gao[3], Zhaoran Zhang[1], Edward Zagha[1,2]

[1]Neuroscience Graduate Program, [2]Department of Psychology, [3]Department of Bioengineering, University of California Riverside, 900 University Avenue, Riverside CA 92521 USA

* equal contributors

Correspondence to: edward.zagha@ucr.edu

Acknowledgements

This work was supported by the Whitehall Foundation (Research Grant 2017-05-71 to E.Z.) and the National Institutes of Health (R01NS107599 to E.Z.). We thank Drs. Hongdian Yang and David Salkoff for many helpful discussions throughout the project. The authors declare no competing financial interests.

Abstract

Spontaneous neuronal activity strongly impacts stimulus encoding and behavioral responses. We sought to determine the effects of neocortical prestimulus activity on stimulus detection. We trained mice for a selective whisker detection task, in which they learned to respond (lick) to target stimuli in one whisker field and ignore distractor stimuli in the contralateral whisker field. During expert task performance, we used widefield Ca^{2+} imaging to assess prestimulus and post-stimulus neuronal activity broadly across frontal and parietal cortices. We found that lower prestimulus activity correlated with enhanced stimulus detection: lower prestimulus activity predicted response versus no response outcomes and faster reaction times. The activity predictive of trial outcome was distributed through dorsal neocortex, rather than being restricted to whisker or licking regions. Using principal component analysis, we demonstrate that response trials are associated with a distinct and less variable prestimulus neuronal subspace. For single units, prestimulus choice probability was weak yet distributed broadly, with lower than chance choice probability correlating with stronger sensory and motor encoding. These findings support a low amplitude, low variability, optimal prestimulus cortical state for stimulus detection that presents globally and predicts response outcomes for both target and distractor stimuli.

Keywords

Neocortex, widefield imaging, sensory detection, choice probability, prestimulus

Introduction

The brain is never silent. Throughout sleep and wakefulness, spontaneous neuronal activity reflects dynamic, self-organized states that affect the generation and propagation of neuronal signals (Arieli et al., 1995; Arieli et al., 1996; Ferezou et al., 2007; McCormick et al., 2015; McGinley, David, et al., 2015; McGinley, Vinck, et al., 2015; Niell & Stryker, 2010; Poulet et al., 2012; Zagha & McCormick, 2014). Changes in spontaneous activity impact the amplitude of neuronal sensory responses (S. Crochet & C. C. Petersen, 2006; Haider & McCormick, 2009; Poulet & Petersen, 2008; Sachdev et al., 2004; Shimaoka et al., 2018) and behavioral outcomes (Boly et al., 2007; Fiebelkorn & Kastner, 2021; Kim & Sejnowski, 2021; Mazaheri et al., 2011; McGinley, David, et al., 2015; van Kempen et al., 2020). In awake subjects, these changes correlate with changes in task engagement, movement, and internal (cognitive or egocentric) versus external (perceptive or allocentric) processing modes (Andreou & Borgwardt, 2020; Boly et al., 2007; de Lange et al., 2013; Murphy et al., 2018; Musall et al., 2020; Salkoff et al., 2020; Stringer et al., 2019). However, most studies of sensory processing and sensory detection normalize post-stimulus by prestimulus activity, thereby obscuring the impacts of spontaneous activity. And yet, understanding how spontaneous activity impacts neuronal signaling and task performance will reveal important principles of context-dependent sensory and motor processing.

This study focuses on prestimulus activity during a sensory detection task, for which many open questions remain. First, is the ability to detect a stimulus improved by

high or low prestimulus activity (Figure 3.1A)? A common model of decision-making is integration to bound, which proposes that a decision is made once neuronal activity reaches a specific threshold (Gold & Shadlen, 2007; Hanes & Schall, 1996; Roitman & Shadlen, 2002). Within this model, higher prestimulus activity may bring a network closer to decision threshold and/or increase the gain of a network and therefore promote stimulus detection (Haider & McCormick, 2009). Consistent with this framework, studies in primary visual cortex demonstrate that higher prestimulus activity leads to larger amplitude stimulus responses (Haider et al., 2007). However, higher prestimulus activity may reduce cortical stimulus responses (Hasenstaub et al., 2007), due to increased cortical inhibition and reduced intrinsic and synaptic excitability. Studies in the primary somatosensory and primary auditory cortices support this alternative noise suppression framework, demonstrating that lower prestimulus activity, or activity in a low-arousal synchronized state, leads to larger amplitude stimulus responses (McGinley, David, et al., 2015; Petersen et al., 2003; Sachdev et al., 2004).

In somatosensory (whisker) detection tasks, impacts of prestimulus activity on stimulus encoding and detection have been studied at the level of membrane potential through whole cell patch clamp recordings. While prestimulus membrane potential activity of primary somatosensory cortical neurons did predict sensory response amplitudes (Sachidhanandam et al., 2013), it did not predict trial outcome (e.g., hit versus miss) (Sachidhanandam et al., 2013; Yang et al., 2016). However, these whole cell recording studies are limited by relatively small samples sizes (10s of neurons) which may

obscure the ability to resolve small yet widespread contributions of prestimulus activity to task performance.

A second open question is whether the prestimulus activity that impacts stimulus encoding and detection is focal and restricted to specific cortical regions or global and observed throughout neocortex (Figure 3.1B). Global activity may reflect changes in arousal and movement (Musall et al., 2020; Salkoff et al., 2020; Stringer et al., 2019) whereas focal changes may reflect shifts in, for example, attentional focus or response preparation (Fries et al., 2001; Ghose & Maunsell, 2002; Luck et al., 1997; Moore & Armstrong, 2003). It is currently unknown whether prestimulus activity in sensory compared to motor cortices have larger impacts on task performance, and whether the directionality of that impact is the same across neocortical regions (Shimaoka et al., 2018). In addition to considering different cortices individually, is there an 'optimal state' of prestimulus activity that includes the contributions of multiple cortices (Figure 3.1C)? A third open question is whether prestimulus activity has the same or different impacts on target (attended) versus distractor (unattended) stimulus encoding and detection (Figure 3.1A, C). For example, the same prestimulus activity may promote discrimination (response to targets, no response to distractors) or bias responses for detection (respond to or ignore all stimuli). Lastly, do the neurons that express task-relevant changes in prestimulus activity overlap with or are they distinct from the neuronal populations that express strong post-stimulus sensory and/or motor activity (Figure 3.1D)?

We address these questions in the context of a selective whisker detection task in mice. We trained mice to respond (lick) to deflections on one whisker field (target) and ignore deflections in the contralateral whisker field (distractor) (Aruljothi et al., 2020; Zareian et al., 2021). Using widefield Ca^{2+} imaging, we previously identified the cortical regions that are highly active post-stimulus and pre-response, and therefore may contribute to stimulus detection: the whisker region of primary somatosensory cortex (S1), the whisker region of primary motor cortex (wMC), and the pre-motor licking region anterior lateral motor cortex (ALM) (Aruljothi et al., 2020). We consider these cortical regions to be 'task-related' and all other cortical regions to be 'task-unrelated'. Here, we implement a sliding window normalization to preserve prestimulus fluctuations. We investigate the impacts of prestimulus activity levels on trial outcome, for both target and distractor stimuli. Additionally, we use dimensionality reduction of the imaging data to assess prestimulus variability across cortices. Lastly, we assess prestimulus choice probability of single units in task-related cortices to determine the distribution of these signals across the neuronal population.

Materials and Methods

The experimental datasets in this study were previously published, including the whisker monitoring, widefield GCaMP6 imaging (Aruljothi et al., 2020) and single unit recordings (Zareian et al., 2021). Below, we summarize these experimental methods and describe the new analyses used in this study.

Animal Subjects

Experiments were approved by the IACUC of University of California, Riverside. Both male and female adult mice were used, either wild type (C57BL/6J, BALB/cByJ) or transgenic (Snap25-2A-GCaMP6s-D, backcrossed to BALB/cByJ). GCaMP6s expressing transgenic mice were used for widefield Ca^{2+} imaging; wild type mice were used for whisker imaging and electrophysiology. Mice were housed in a 12-hour light/dark cycle; experiments were conducted during the light cycle.

Animal Surgery

For headpost implantation, mice were placed under isoflurane (1-2%), ketamine (100 mg/kg), and xylazine (10 mg/kg) anesthesia. The scalp was cut (10 mm x 10 mm) and resected to expose the skull. A lightweight metal headpost was fixed onto the skull using cyanoacrylate glue. An 8 mm × 8 mm headpost window exposed most of the dorsal cortex. The skull was covered with a thin layer of cyanoacrylate gap-filling medium (Insta-Cure, Bob Smith Industries) to seal the exposed skull and enhance skull transparency; the window was sealed with a quick-dry silicone gel (Reynolds Advanced Materials). Mice were administered meloxicam (0.3 mg/kg) and enrofloxacin (5 mg/kg) for three days post-

op. Water restriction began after recovery from surgery (minimum of three days). Training on the behavior rig began after one day of water restriction. For electrophysiological recordings, craniotomies and durotomies (< 0.5 mm diameter) were performed under isoflurane anesthesia. Full recovery from anesthesia was allowed (up to 60 minutes) before placement on the behavioral rig.

Animal Behavior

Training stages, metrics of learning, and criterion for expert performance in the Go/NoGo selective whisker detection task were previously reported (Aruljothi et al., 2020). Briefly, head-fixed and water deprived mice were placed on a behavioral apparatus controlled by Arduino and custom MATLAB (MathWorks) scripts. Two paddles were placed in whisker fields on the opposite sides of the face, designated as target or distractor. Target and distractor designations were assigned at the beginning of training and remained constant. Following variable intertrial intervals, mice could receive a target trial (rapid deflection of the target paddle), distractor trial (rapid deflection of the distractor paddle) or catch trial (no whisker stimulus). Mice responded by licking at a central lick port. Hits (responses to target stimuli) were rewarded with ~5 µL of water, correction rejections (not responding to distractor stimuli) and correct withholdings (not responding during the catch trial) were rewarded with a shortened intertrial-interval (ITI) and a subsequent target trial. Licking during the ITI was punished by resetting the ITI, effectively a time-out.

Mice were considered expert once they achieved a discriminability *d'* > 1 (separation of hit and false alarm response rates) for three consecutive days:

$$disiminability\ d' = \phi^{-1}_{Hit\ rate} - \phi^{-1}_{False\ alarm\ rate}$$

d' Discriminability - Equation 4

All recordings were conducted in expert mice while performing the task.

Widefield Imaging

Widefield imaging during expert task performance was conducted as previously reported. The dataset consists of 38 behavioral/imaging sessions, recorded from 5 mice. The through-skull imaging window included bilateral dorsal parietal and frontal cortices. Illumination from a 470 nm LED source (Thorlabs) was band-pass filtered for excitation (Chroma ET480/40x) and directed onto the skull via a dichroic mirror (Chroma T510lpxrxt). Emitted fluorescence was band-pass filtered (Chroma ET535/50m) and collected using an RT sCMOS camera (Diagnostic Imaging, SPOT Imaging software). Images were acquired at 10 Hz with a final resolution of 142 x 170 pixels (41 µm per pixel). Image sequences were imported to MATLAB for subsequent analyses.

Electrophysiology

Single unit recordings during expert task performance were conducted as previously reported (Zareian et al., 2021). The dataset consists of 32 behavioral/recording sessions, recorded from 22 mice, yielding a total of 936 single units from three cortical regions (target aligned whisker region of primary somatosensory cortex [S1], whisker region of motor cortex [wMC], and anterior lateral motor cortex [ALM]). Coordinates (mm, from

bregma): S1 3.2-3.7 lateral, 1-1.5 posterior; wMC 0.5-1.5 lateral, 1-2 anterior; ALM 1-2 lateral, 2-2.5 anterior. Recordings were targeted to layer 5 of S1, wMC, and ALM, approximately 500 to 1100 µm below the pial surface. Electrophysiological recordings were conducted using a silicon multielectrode probe (NeuroNexus A1x16-Poly2-5mm-50s-177), positioned using a Narishige micro-manipulator. Neuralynx amplifier (DL 4SX 32ch System) and software were used for data acquisition and spike sorting.

Whisker imaging

Whisker imaging during expert task performance was conducted as previously reported (Aruljothi et al., 2020). The dataset consists of 9 behavioral/recording sessions, recorded from 4 mice. Images were acquired with a CMOS Camera (Thorlabs DCC3240M camera with Edmund Optics lens 33-301) at either 20 or 60 Hz. No systematic difference between 20 and 60 Hz was observed (data not presented). The imaging field of view included both paddles and the mouse's head (including whiskers and snout).

Data Analysis

Data analyses were performed in MATLAB using custom scripts.

Engagement period

To ensure that analyses were conducted during task engagement, 'engaged periods' were defined as continuous behavioral performance of at least 10 minutes without 60 seconds of no responding. For sessions with more than one engaged period, the longest engaged period was used for further analyses. Furthermore, sessions were included in subsequent analyses only if performance was at expert level: discriminability d'>1. For sessions with

multiple stimulus amplitudes, trials were combined for further analyses only when the differences in response rates were 15% or less.

Sliding Window Normalization and Trial-Based Neuronal Activity

The trial-based imaging time window consisted of the prestimulus epoch (1 s), the stimulus and lockout epoch (0.2 s), and the allowable response epoch (1 s), a total of 2.2 s. A raw movie F was created by concatenating fluorescence activity from consecutive trials, where $F_n(i,j,f)$ is the fluorescence of each pixel (row *i* and column *j*) in frame *f* for each trial *n*. To generate normalized fluorescence values, we first determined the sliding window local mean for each pixel, computed every 2 s using a +/- 200 s window size [$F_{SW}(i,j,n)$]. Then, we calculated the normalized fluorescence (Salkoff et al., 2020) (see also Supplemental Figure 3.1) for each pixel at each frame as:

$$dF_{SW}/F_{SW}(i,j,n) = [F_n(i,j,f) - F_{SW}(i,j,n)]/F_{SW}(i,j,n)$$

Sliding Window Fluorescence - Equation 5

Trialwise average movies were then compiled by first indexing outcome type (*hit*, *miss*, *false alarm*, *correct rejection*) and then by averaging pixelwise activity across corresponding frames of corresponding trials. Frames were aligned to the stimulus onset frame (stimulus aligned) where stimulus occurred or aligned to the first frame containing the response (response aligned) where response occurred. Trials with responses during the lockout period were considered *premature* and excluded from the analysis. Trials with responses before the stimulus but within the prestimulus imaging period were considered *spontaneous*, dF/F reported but not further analyzed. Grand average movies (n = 38

sessions) were aligned to bregma, flipped at bregma according to target-distractor assignment, and then averaged across all sessions. Trialwise average, standard deviations, and differences in averages and standard deviations were compiled and aligned as above, but across the full 1 s prestimulus epoch (n = 38 sessions).

Difference in Prestimulus Fluorescence

Fluorescence differences for target and distractor assignment were calculated per trial type per session. Prestimulus frames 6 to 10 (capturing the last 500 ms of the prestimulus window, before stimulus onset) were trialwise and pixelwise averaged per session. Session data were excluded from this analysis if there were fewer than 5 incorrect trials in the session (excluding 9 sessions for target Miss, 6 sessions for distractor FA). For target fluorescence difference frames (n = 29 sessions), Hits fluorescence mean frame was subtracted from Miss fluorescence mean frame. For distractor fluorescence difference frames (n = 32 sessions), FA fluorescence mean frame was subtracted from CR fluorescence mean frame. Response prestimulus frames were subtracted from no response prestimulus frames because no response fluorescence activity was generally higher than response fluorescence activity. Prestimulus difference frames were aligned, assigned, and averaged across all sessions (as above). To normalize for differences in changes in fluorescence across regions, we indexed the pixelwise mean of fluorescence map differences across sessions normalized by the pixelwise deviation in fluorescence map differences across sessions ($\mu_{i,j}/\sigma_{i,j}$). For quantification of target versus distractor

prestimulus difference, normalized difference (index), and significance, frames were averaged across pixels for scalar values.

Regression Analyses between Prestimulus Activity and Reaction Time for Response Trials

The correlation between activity during prestimulus period (dF/F) and reaction times (RT) for response trials (Hits and FAs) were computed as a linear regression from which we obtained the slope of the linear fit with 95% confidence interval and coefficient of determination, R^2, as the goodness of fit (B. Zareian et al., 2020) (Curve Fitting Toolbox in Matlab). For this analysis, we assigned prestimulus dF/F as the independent variable and reaction time as the dependent variable.

Defining Cortical Regions of Interest

For task relevant and task irrelevant cortical regions, we defined a center pixel according to pixel resolution (41 μm) and alignment with bregma as center pixel value = [coordinates from bregma (in mm)]/0.041 mm. Thus, we converted coordinates from bregma (mm) [wS1 ±3.4 lateral, 1.2 posterior; wMC ±1.2 lateral, 1.2 anterior; ALM ±1.5 lateral, 2.3 anterior; RSP ±0.4 lateral, 2.4 posterior; limb S1 ±2.0 lateral, 0.6 posterior] to coordinates from bregma (pixels); we then systematically defined rectangles about the center pixel with width (±medial/lateral) and height (±anterior/±posterior) in pixels [wS1 10, 25 ; wMC 15, 15; ALM 15, 15; RSP 10, 25; limb S1 25, 25]. Rectangles that fell off-frame were cropped at frame borders instead of shifted. Subsequent analyses for region specific Hits-Miss, dF/F versus RT, and seed correlation used these defined ROIs (n = 29 sessions, target; n = 32 sessions, distractor).

Seed Correlation Analysis

Correlation maps were trialwise generated for target and distractor hemispheres and for wS1, wMC, ALM, RSP, and limb S1 seed regions of interest (ten maps per session). Seed regions were defined as the mean of the pixels in the indicated ROI (rectangles defined above). Pairwise correlation coefficients were calculated between the defined seed region and all other pixels. The R^2 values are reported as the square of the pixelwise correlation coefficient.

Stimulus Encoding in Post-Stimulus Fluorescence

Stimulus encoding was quantified as the neurometric *d'* (K. Britten et al., 1992) of prestimulus fluorescence (stimulus absent) and post-stimulus fluorescence (stimulus present) during the lockout epoch, as previously applied to imaging data (Aruljothi et al., 2020). We excluded session data from this analysis if there were fewer than 4 incorrect trials in the session (excluding 5 sessions for target Miss, 2 sessions for distractor FA). Neurometric *d'* was calculated separately according to target and distractor assignment and then according to trial type outcome. This resulted in 6 different datasets for stimulus encoding: all target, all distractor, hit trials, miss trials, false alarm trials, and correct rejection trials. Prestimulus and post-stimulus fluorescence histograms were plotted into receiver operating characteristic (ROC) curves and the area under the curve (AUC) was converted to *d'* as the neurometric:

$$fluorescence\ d'_{Stimulus} = \sqrt{2} * Z_{AUC}$$

d' Stimulus Encoding - Equation 6

Region specific pixel values for stimulus encoding were identified as the maximum value within the defined regions of interest (ROI), performed for target aligned and distractor aligned regions of S1, wMC, and ALM. The difference in stimulus encoding in S1 between the response and the no response trials for both target and distractor stimuli was calculated as the percentage:

$$\%_{difference} = \frac{response\ trial - no\ respse\ trial}{(response\ trial + no\ response\ trial)/2} * 100$$

% diff Stimulus Encoding - Equation 7

Whisker Motion Energy During Behavior

The imaging window was cropped by region of interest: target or distractor paddle stimulus or whisker fields. The function *vision.VideoFileReader* was used for optimal reading of video frames into MATLAB. Whisker movement per frame (*Δframe*) was calculated as the pixelwise frame by frame mean gray value (*MGV*) difference (ΔMGV_{pixel}). Whisker motion energy (*WME*) was defined as the sum of the squares across pixels:

$$WME = (\Delta l)^2 = \sum_{pixels} \left(\frac{\Delta MGV_{pixel}}{\Delta frame}\right)^2$$

Whisker Motion Energy - Equation 8

WME traces of the cropped videos of the paddles were used to detect stimulus events (target/distractor). This was performed by using a constant threshold and aligning detected events from the video to their temporally closest events recorded using Arduino. The traces from the cropped videos of whisker fields were transformed (z-scored) to have a mean of zero and standard deviation of 1 for the purpose of comparison across sessions. Subsequently, WME data were temporally aligned by trial type to

stimulus onset (target/distractor) determined from the videos. The prestimulus analysis window was the 500 ms preceding stimulus onset.

Principal Component Analysis of Fluorescence

Fluorescence was averaged across anatomic masks [target and distractor S1, wMC, ALM, and retrosplenial (RSP) cortex] per frame per trial per session. Mean regions were normalized and placed into a covariance matrix. The covariance matrix was decomposed into an eigenmatrix, eigenvectors were sorted by eigenvalue weight, and eigenvectors were projected into component space. All frames were separated by trial type, plotted in PC space, and differentiated by trial epoch (prestimulus, post-stimulus and pre-response lockout, and allowable response window). Component data for prestimulus frames were further analyzed: confidence area ellipses of 1 standard deviation, σ, was defined by the ellipsoid distribution of prestimulus frames in PC space per session. Centroids were defined as the geometric means of prestimulus frames in PC space per session.

Spike Sort and Cluster of Single Units

Using Neuronalynx recording system, signals were sampled at 32 kHz, band-pass filtered from 0.1 Hz to 8000 Hz (wideband), and high pass filtered at 600 Hz to 6000 Hz (for spike detection). Putative spikes crossed thresholds of 20 to 40 μV, isolated from baseline noise. KlustaKwik algorithm in SpikeSort3D software was used for spike sorting and clustering. Clusters were defined by waveform and cluster location in feature space (peaks and valleys); movement artifacts (atypical waveforms or those occurring across all channels) were removed, as previously reported (Zareian et al., 2021). Subsequent analyses were

conducted using MATLAB software (MathWorks). For analyses of population data, spike times of single units from each recording session were combined into a multiunit.

Sensory and Motor Encoding of Single Units

Sensory and motor encoding of single units was performed as previously reported (Zareian et al., 2021). Sensory encoding was quantified by the neurometric *d'* using stimulus absent spiking (300 ms prestimulus) and stimulus present spiking (100 ms post-stimulus). Motor encoding was quantified by the neurometric *d'* using response absent spiking (300 ms prestimulus) and response present spiking (100 ms pre-response). Distributions were plotted into ROC curves and the AUC was converted to *d'* as a neurometric:

$$spike\ d'_{sensory}\ or\ d'_{motor} = \sqrt{2} * Z_{AUC}$$

d' Single Unit Encoding - Equation 9

Choice Probability of Single Units

For choice probability analyses, we ensured that there was a minimum of 5 trials per trial type (minimum 5 Hits and 5 Miss). Choice probability (%) was quantified as the separation of prestimulus spiking in Hits versus Miss trials. ROC and AUC were calculated from the distributions of Hits and Miss across trials, 500 ms to 0 ms before stimulus onset, averaged over 50 ms nonoverlapping intervals, as previously reported (Zareian et al., 2021).

Local Field Potential Analyses

A single middle site from each silicon probe recording was used for local field potential (LFP) analyses; use of other sites led to qualitatively similar results (data not shown). To

obtain the LFP, wideband signals were down sampled to 200 Hz using MATLAB function decimate. Power spectral densities were calculated using the welch method (MATLAB function *pwelch*). Frequency resolution step for calculating power was 0.78 Hz. Subsequently, trial-by-trial spectral densities were averaged from a one second period before stimulus onset and pooled across all trials and sessions. For spike triggered average (STA) analyses, we used the 400 ms window surrounding each prestimulus spike (±200 ms) for power analyses. We included spikes from 1 sec to 200 ms before the stimulus so that STA windows would not overlap with the stimulus onset. For STA power calculation, LFP signals and spikes were not analyzed from the same recording site to minimize spike waveform artifacts (Fries et al., 2001).

Statistical Analyses

For imaging statistics, threshold for statistical significance was corrected for multiple comparisons with a Bonferroni correction. For all dF/F and dF/F differences (Miss–Hits, CR–FA, means, standard deviations), statistical analyses determined whether dF/F frames were significantly different than zero across sessions (one sample t-test). For region specific dF/F of Hits-Miss trials across defined ROIs, statistical analysis determined whether dF/F within ROIs was significantly different from zero (one-sample t-test) and whether dF/F across ROIs was significantly different from each other (one-way ANOVA and multiple comparison Tukey-Kramer test). For analyses of correlations between dF/F and RT within ROIs, statistical analyses of region-specific linear regression determined whether slopes within ROIs were significantly different from zero (one-sample t-test) and

whether slopes across ROIs were significantly different from each other (one-way ANOVA). For whisker analyses statistics, since the number of samples in the whisking data were low, we used one-sample Kolmogorov-Smirnov test (*kstest* in MATLAB) to test for normality assumptions. Since the data mostly violated the normality assumption, Wilcoxon signed rank (*signrank* in MATLAB) and rank sum (*ranksum* in MATLAB) tests were used for comparisons between prestimulus and post-stimulus whisking and between trial types (Hits vs. Miss, FA vs. CR), respectively. For stimulus encoding (neurometric d'), statistical analyses determined whether the trialwise (Hits, Miss, FA, CR) maximum pixel value in S1 was significantly different than zero across sessions (one sample t-test). For differences in stimulus encoding, statistical analyses determined whether the stimulus aligned S1 maximum pixel value was significantly different between response (Hits, FA) and no response (Miss, CR) outcome types across sessions (two sample t-test). For PCA ellipsoid variance and centroid distribution, statistical analysis determined whether ellipsoid variance or centroid distribution was significantly different between response and no response prestimulus frames, evaluated per component. Box whisker plots show the distribution of prestimulus frames or ellipsoid centroids per trial type with outliers, evaluated per component. For choice probability of single units, statistical analysis determined whether distributions within regions were significantly different from chance (one-sample t-test, chance level 50%) and whether distributions between regions were significantly different from each other (ANOVA and post-hoc Tukey test). For the significance assessment of sensory and motor encoding of single units, one-

sample t-test was used to compare d-prime distributions to zero. For the relationship between sensory and motor encoding and choice probability of single units, statistical analysis determined whether regression slopes were significantly different from zero (95% confidence bounds for slopes). Box whisker plots were used to show distributions of sensory encoding, motor encoding, and choice probability of single units evaluated within regions. Single unit and multi-unit average data are presented as mean +/- standard error of the mean, unless otherwise indicated. For LFP and STA LFP power comparisons between hit and miss or FA and CR trials, statistical analysis determined whether response trials were different from no response trials for each frequency step (paired t-test, $p<0.01$).

Results

Global prestimulus activity predicts response outcomes

We considered how prestimulus activity may influence sensory detection (Figure 3.1A-D). High prestimulus activity may promote detection of target and distractor stimuli; alternatively, low prestimulus activity may promote detection of target and distractor stimuli or discrimination of target from distractor stimuli (Figure 3.1A). The prestimulus activity that influences behavioral outcomes may present focally in specific task-related regions or globally across neocortex (Figure 3.1B). A low variability, specific 'optimal state' configuration may promote stimulus detection or target/distractor discrimination (Figure 3.1C). At the level of single units, prestimulus contextual signals and post-stimulus sensory and motor signals may be carried by distinct neuronal ensembles (sparse coding) or overlapping neuronal ensembles (dense coding) (Figure 3.1D). We tested these possibilities for a selective whisker detection task, in which head-fixed mice learn to respond to rapid deflections in one whisker field (target) and ignore identical deflections in the opposite whisker field (distractor) (Figure 3.1E). In this task, the possible trial outcomes include hit (response to target), miss (no response to target), false alarm (FA, response to distractor), and correct rejection (CR, no response to distractor) (Figure 3.1F). Prior to each stimulus was a variable inter-trial interval (ITI), in which mice were required to withhold responding or else reset the ITI. The prestimulus epoch we used for analyses is the last 1 second of the ITI immediately prior to stimulus onset (Figure 3.1G).

We used widefield Ca^{2+} imaging to measure neuronal activity during expert task performance in frontal and parietal cortices, bilaterally (Figure 3.1F). Our imaging dataset consists of 38 imaging sessions from 5 mice, using a single task-engaged period per session (see Methods). Due to the highly lateralized cortical whisker representation, we could clearly define target aligned and distractor aligned cortical regions, contralateral to the side of the whisker stimulus. To preserve activity fluctuations prestimulus, we normalized raw fluorescence activity using a sliding window method (400 s sliding window, see Methods and Supplemental Figure 3.1).

In Figure 3.2 we present grand average fluorescence activity for each trial outcome, aligned to the onsets of both the stimulus and response. In the first column of Figure 3.2 we show the last prestimulus frame, which is representative of the full prestimulus epoch (Supplemental Figure 3.2A). We note stark differences in prestimulus activity for different trial outcomes, particularly when comparing hit (Figure 3.2A) and miss (Figure 3.2D) trials. We observed lower prestimulus activity for hit versus miss and for FA versus CR trials, indicating that lower prestimulus activity precedes 'response' compared to 'no response' outcomes. Interestingly, low prestimulus activity appears to be specifically related to stimulus detection rather than response preparation. This is evidenced by higher activity preceding spontaneous responses (Spont, a response during the ITI, Figure 3.2C) compared to stimulus-related responses (hits and FA, Figures 3.2A and 3.2B). The magnitude of the prestimulus differences is large, on the same scale as the post-stimulus activity. Additionally, prestimulus activity suppression preceding response

trials appears to be widely distributed throughout dorsal neocortex, rather than being focused on the task-related regions of S1, wMC and ALM.

We quantified the differences in prestimulus activity between response and no response trials for target and distractor stimuli (Figure 3.3A-F). Shown in this figure are data from the last 500 ms of the prestimulus (similar results were obtained using 1 s prestimulus epochs, Supplemental Figure 3.2C, E). We subtracted the average prestimulus fluorescence activity of hit from miss trails (Figure 3.3A). The positive values indicate higher activity preceding miss compared to hit trials (n=29 sessions, averaged across the entire field of view: dF/F $\mu_{[\text{Miss-Hits}]}$=2.1%±0.3%; one-sample t-test, t(28)=8.1, p=7.9e-09). The largest differences were not in the task-related whisker or licking regions but appear to be focused on the limb regions of somatosensory cortex. While dF/F is already a normalized metric, we sought to further control for possible regional differences in imaging sensitivity. Therefore, we conducted the same subtraction analysis, but on normalized dF/F values, indexed using the pixelwise mean and standard deviation across sessions. With this analysis (Figure 3.3B), the activity differences are more uniformly distributed across frontal and parietal cortices, with an average miss-hit difference of 1.2 standard deviations.

To determine the spatial regions of significance, on each pixel we performed a paired, two-sample t-test on average prestimulus fluorescence activity in hit versus miss sessions (p-value of each pixel shown in Figure 3.3C). All neocortical regions within our field of view demonstrated statistical significance, even with a Bonferroni corrected alpha

level to control for multiple comparisons (28,960 pixels). Thus, lower prestimulus activity on upcoming target trials is predictive of hit versus miss outcomes. This is observed for all cortical regions within our field of view, including task-related and task-unrelated regions. Similar findings were obtained for measures of variability (Supplemental Figure 3.2B,D,F), with increased standard deviation of prestimulus activity on miss compared to hit trials globally throughout dorsal cortex.

There were some notable similarities and differences for distractor trials (Figure 3.3D-F). Similar to target trials, higher activity was observed preceding no response (CR) versus response (FA) trials (n=32 sessions, averaged across the entire field of view: dF/F $\mu_{[CR-FA]}$= 0.36± 0.11% one-sample t-test, t(31)=3.38, p=0.002). However, the fluorescence differences were approximately 5-fold higher for target trials compared with distractor trials (dF/F $\mu_{[Miss-Hits]}$=2.1% versus $\mu_{[CR-FA])}$=0.36%). A second difference is that for distractor trials, the focus on the somatosensory limb regions was observed in dF/F, standard deviation, indexed, and p-value maps (Figure 3.3D-F, Supplemental Figure 3.2B,D,F). The regions with the lowest p-value were slightly above the Bonferroni corrected alpha level. Thus, while lower activity preceding distractor trials was also predictive of a response, the effect size was smaller and less widespread.

In addition to predicting response outcome, we also sought to determine whether prestimulus activity levels predict reaction time on response trials (Figure 3.3G-J). For these analyses, we determined the slope and coefficient of determination (R^2) of linear fits for prestimulus dF/F versus reaction time for Hit and FA trials (separately) for each

session. As shown in the example session in Figure 3.3G, a positive slope indicates a correlation between higher prestimulus activity and longer post-stimulus reaction times. Across all sessions, we found a significant positive correlation (positive slope) on Hit trials between prestimulus activity and reaction time (n=30 sessions, slope=0.64±0.23, one-sample t-test: t(29)=2.73, p= 0.011; R^2=0.074±0.023) (Figure 3.3H). Thus, for target stimuli, lower prestimulus activity predicts both Hit versus Miss outcomes and faster reaction times. We performed the same regression analyses for FA trials (Figure 3.3I,J). In contrast to Hit trials, FA trials across sessions did not show a consistent correlations between prestimulus activity and reaction time (n=32 sessions, slope=-0.45±1.48, one-sample t-test: t(31)=-0.3, p=0.76; R^2=0.12±0.021) (Figure 3.3J).

The above analyses demonstrated that lower prestimulus activity broadly across dorsal cortex predicted response (versus no response) outcomes and faster reaction times (for hit trials). Subsequent analyses determined if these correlations displayed regional differences. We defined regions of interest (ROIs) bilaterally (target aligned and distractor aligned: wS1, wMC, ALM, retrosplenial cortex (RSP), limb S1). For Hits-Miss prestimulus dF/F, parietal regions (wS1, RSP, and limb S1) showed significantly larger differences compared to frontal regions (wMC and ALM) (one-way ANOVA, F(289)=7.53, p=7.1e-10, post-hoc multiple comparisons) (Supplemental Figure 3.3). However, we did not observe differences amongst these ROIs in the relationships between prestimulus activity and reaction time (Supplemental Figure 3.4, one-way ANOVA, Hits: F(149)=0.63, p=0.64, FA: F(159)=0.2, p=0.94).

In addition to analyzing these regions individually, we also determined whether their prestimulus spatial correlations predicted response outcomes. We defined seed ROIs as above and determined the pairwise correlations across prestimulus frames for each pixel (Supplemental Figure 3.5). Interestingly, this analysis revealed widespread spatial correlations preceding no response trials (higher R^2 values outside of the seed region). Inversely, our data demonstrate spatial *decorrelation* preceding response trials. Similar patterns were observed for both target and distractor trials (Supplemental Figure 3.5A and B, respectively).

Contributions of stimulus encoding and movement on trial outcomes

Next, we assessed whether the differences in trial outcome were reflected in differences in stimulus responses in the neocortex. We quantified the stimulus encoding during the lockout period (200 ms post-stimulus and pre-response) for each trial type (Figure 3.4). For each pixel, we measured stimulus encoding as the neurometric sensitivity index d' (Figure 3.4A-F) and determined whether these values were significantly different from zero (Figure 3.4G-L). We observed significant stimulus encoding in the stimulus aligned primary somatosensory cortex (S1) for each trial type (one-sample t-test, n= 38, hits: 38, miss: 33, FA: 36, CR: 38, hits: d' μ_{S1}=0.98±0.06, t(37)=15.58, p=7.79e-18; miss: d' μ_{S1}=0.69±0.08, t(32)=9.08, p=2.26e-10; FA: d' μ_{S1}=1.05±0.09, t(35)=12.08, p=4.87e-14; CR: d' μ_{S1}=0.58±0.049, t(37)= 11.89, p=3.32e-14). Thus, significant stimulus responses occur in S1 for both response and no response trials. However, we did observe a 40-60% reduction in S1 stimulus encoding in no response compared to response trials for target

and distractor stimuli (hits vs. miss: d' $\mu_{\%\ difference}$=39.84±7.44%, paired-sample t-test, t(32)= 4.51, p=8.26e-05; FA vs. CR: d' $\mu_{\%\ difference}$=61.62±7.26%, paired-sample t-test, t(35)= 6.72, p=8.75e-08, see Methods). In summary, response trials are associated with reduced prestimulus activity and enhanced post-stimulus sensory responses.

Recent studies have demonstrated widespread neuronal activity increases due to movement (Musall et al., 2020; Salkoff et al., 2020; Stringer et al., 2019). Therefore, in a separate set of recordings, we determined the magnitude of prestimulus and post-stimulus whisker movements on different trial outcomes. Whisker movement was quantified as whisker motion energy (WME, normalized by z-score, see Methods). In Figure 3.5A-C we present these analyses for one example session for target stimuli. On hit trials, WME increased dramatically post-stimulus (Figure 3.5A, purple trace). We interpret this as whisking being part of the 'uninstructed' behavioral response sequence (Musall et al., 2020). Importantly, we also observed differences in WME prestimulus, with higher WME on miss compared to hit trials (mean +/- STD WME μ_{Hits}=-0.45 ± 0.32, WME μ_{Miss}=0.19 ± 0.71, rank sum=1516, p=0.001, two-sided Wilcoxon rank sum test; Figure 3.5A and 3.5B). In Figure 3.5C, we show prestimulus WME for each target trial, with the color of the bar indicating trial outcome. High prestimulus WME was more likely to result in a miss trial, even though many miss trials were not preceded by high prestimulus WME. Similar results were observed across all sessions (n=9 session, Figure 3.5D, Wilcoxon sign rank test, mean +/- STD prestimulus WME μ_{Hits}=-0.12 ± 0.17 vs. prestimulus WME

μ_{Miss}=0.12 ± 0.15, signed rank=1, p=0.008). Thus, high prestimulus movement was associated with some, but not all, of the miss trials.

Differences in prestimulus WME were not as pronounced on distractor trials (Figure 3.5E-H). We did notice a trend towards increased WME on CR trials. However, this effect was not statistically significant across sessions (n=9 session, Figure 3.5H, Wilcoxon sign rank test: prestimulus WME μ_{FA}=-0.14 ± 0.2 vs. prestimulus WME μ_{CR}=-0.04 ± 0.10, signed rank=8, p=0.098). Notably, the effects of prestimulus movement on target and distractor trial outcomes parallel the effects of prestimulus neuronal activity: low prestimulus neuronal activity and low prestimulus WME predict response outcomes, yet these effects are much more pronounced for target compared to distractor trials.

Analyses of prestimulus activity variance and subspace in reduced spatial dimensions

Next, we sought to characterize frame-by-frame variability in our imaging data. To accomplish this, we used principal component analysis (PCA) to reduce the spatial dimensionality (Figure 3.6). First, we extracted regional single-trial fluorescence activity using anatomic masks from the dorsal neocortex centered on regions of interest: target/distractor S1, RSP, wMC, and ALM (Figure 3.6A). We concatenated data from all frames, trials, sessions, and mice and performed PCA on this combined matrix. This enabled us to convert all sessions into the same lower-dimensional axes. Most of the variability in our imaging data could be explained by the first component (~91%) and the first two components explained ~96% of the variance (Figure 3.6B-D). Therefore, further analyses focused on these first two spatial components.

We determined the distributions of prestimulus activity from single frames within this PCA space (Figure 3.7). In Figure 3.7A, we plot the data from two example sessions, in which each data point is a single prestimulus frame preceding a hit (purple) or miss (yellow) trials. We noticed that the data from hit trials were more tightly clustered than the data from miss trials. To quantify this observation, first we fit the data from each trial type with a covariance ellipse. The shaded ellipses in Figure 3.7A represent a confidence area of 1 standard deviation, σ, which we used as a measure of framewise variability. Figure 3.7B plots the confidence area for prestimulus activity on hit and miss trials for all sessions (n=29 sessions). The prestimulus activity variance is significantly lower for hit compared to miss trials (effect size, Cohen's d=1.92; paired t-test, t(28)= 9.43, p=1.74e-10).

We conducted the same analyses for distractor trials and obtained similar results. The two example sessions in Figure 3.7C show more tightly clustered prestimulus activity for response (FA) compared to no response (CR) trials. Across all sessions (n=32), the confidence areas are significantly lower for FA compared to CR trials (effect size, Cohen's d=1.11; paired t-test, t(31)= 7.40, p=1.22e-8, Figure 3.7D). Thus, for both target and distractor trials, lower framewise prestimulus variability predicts response outcomes.

In addition to differences in variability, we also noticed that the prestimulus activity resides in different subspaces preceding response and no response trials. As evident in Figure 3.7A, *within* each session the centroids of the hit and miss confidence areas are offset, whereas *between* these two sessions the hit centroids occur at similar

positions. In Figure 3.7E, we plot the centroid position for all sessions (n=29 sessions). Indeed, we find that across all sessions the centroid positions preceding hit trials are separated from the centroid positions preceding miss trials. For target trials, this separation is significant, for both PC1 and PC2 axes (Figure 3.7F, PC1: d=2.19, paired t-test, t(28)=8.55, p=1.34e-9; PC2: d=1.24, t(28)=4.01, p=2.07e-4). In contrast, for distractor trials, the centroids of prestimulus activity show greater overlap for response (FA) and no response (CR) trials (Figure 3.7G). However, we do still find significantly different centroid positions on distractor trials along PC1 (Figure 3.7H, PC1: d=0.57, paired t-test, t(31)=2.99, p=0.0027; PC2: d=0.43, t(31)=1.30, p=0.10). These data indicate that the neuronal activity across dorsal neocortex preceding response trials is less variable than no response trials and occupies a separate subspace. Additionally, like prestimulus neural activity (Figure 3.3) and movement (Figure 3.5), the differences in variability and subspace position are larger for target compared to distractor trials. Taken together, these data specify an optimal neuronal and behavioral state for stimulus detection.

Distribution of prestimulus choice probability among single units

The above analyses of widefield imaging data assessed population neuronal activity. In this final series of analyses, we sought to determine the distribution of task-relevant prestimulus activities among single units (Figure 3.8). During the same selective whisker detection task, we recorded 936 single units, from target aligned S1 (377 units), target aligned wMC (338 units) and target aligned ALM (221 units). First, we quantified the prestimulus choice probability of all units on target trials. Choice probabilities (CP) of

single units in each region were marginally below chance (Figure 3.8A, CP μ_{S1}=49.10 ± 0.16, one-sample t-test, t(376)=-5.72, p=2.21e-8, CP μ_{wMC}=49.44 ±0.2, one-sample t-test, t(337)=-2.82, p=0.005, CP μ_{ALM}=49.64 ±0.19, one-sample t-test, t(220)=-1.92, p=0.06). These distributions were not significantly different across the three regions (two-way ANOVA: F(2,933)= 2.18, p=0.11 and post hoc Tukey: S1 vs. wMC, p=0.33; wMC vs. ALM, p=0.76; S1 vs. ALM, p=0.12). To increase spike density, we combined single units from each session (Behzad Zareian et al., 2020) and calculated the average prestimulus choice probability for these multiunit ensembles across all sessions. This analysis generated a slightly lower prestimulus choice probability than the analysis of single units (all regions: n=43 sessions, 47.62 ± 5.78, one-sample t-test, p=0.01). Prestimulus choice probability below chance indicates that lower activity predicts hit compared to miss outcomes, and therefore is consistent with the widefield imaging data. However, the distributions of these data indicate that only a small portion of single units show strong prestimulus choice probability.

Given this variability of single units, we next asked whether the units with strong prestimulus choice probability overlap with the units with strong post-stimulus sensory and pre-response motor encoding. To test this, we plotted prestimulus choice probability against post-stimulus sensory (Figure 3.8A) and pre-response motor (Figure 3.8B) encoding. The negative regression slopes show correlations between choice probability and sensory encoding for S1, and between choice probability and motor encoding for S1, wMC, and ALM (Figure 3.8C and 3.8D, one-sample t-test, sensory encoding slope: m_{S1}=-

1.96 ± 0.31, t(375)=-6.34, p=6.56e-10; one-sample t-test, motor encoding slope: m_{S1}=-2.05 ± 0.28, t(375)=-7.35, p=1.23e-12 , m_{wMC}=-0.64 ± 0.26, t(336)=-2.49, p=0.013, m_{ALM}=-0.96 ± 0.28, t(219)=-3.46, p=6.41e-4). Thus, units in these regions have combined neuronal representations such that those representing prestimulus behavior context overlap with those with post-stimulus (sensory) and pre-response (motor) task-relevant encoding. This overlap may be influenced by a common factor such as firing rate (Supplemental Figure 3.6). Nevertheless, these analyses demonstrate that the subset of neurons that show the largest prestimulus suppression on hit trials are the same neurons that encode post-stimulus task features.

Prestimulus LFP power and spike-LFP synchrony do not predict trial outcome

Finally, we wondered whether the low amplitude, low variability prestimulus widefield Ca^{2+} signals preceding response trials reflect changes in neuronal synchrony. Specifically, this activity profile may reflect low frequency desynchronization observed during behavioral states of high arousal (Harris & Thiele, 2011; Zagha & McCormick, 2014). To test this, we analyzed local field potentials (LFPs) recorded from layer 5 of the target aligned wS1, wMC, and ALM (Figure 3.9). First, we compared prestimulus LFP power preceding hit and miss trials. We did not observe difference in LFP power (0-50 Hz) across all regions combined and did not observe any differences in low frequencies (0-20 Hz) in each region analyzed separately (Figure 3.9A-D). Similar results were obtained for FA and CR trials (Supplemental Figure 3.7A-D). Second, we measured the prestimulus spike triggered average (STA) LFP, as a measure of spike-LFP synchrony. Similarly, we did not

observe differences in prestimulus STA LFP preceding hit and miss trials (Figure 3.9E-H) or FA and CR trials (Supplementary Figure 3.7E-H). These negative findings suggest that the global activity differences observed in widefield Ca^{2+} imaging data are not due to a difference in neuronal synchrony.

Discussion

The primary focus of this study is to determine whether and how neuronal activity before stimulus onset predicts trial outcomes during goal-directed behavior. We assessed this for both target and distractor stimulus detection. We find that lower prestimulus activity predicts detection of both target and distractor stimuli (Figures 3.2 and 3.3) and faster reaction times on Hit trials (Figure 3.3). This low activity state is distributed globally throughout dorsal cortex (Figure 3.3), maps onto a distinct, less variable subspace than activity preceding no response trials (Figure 3.7) and is represented most robustly in the subset of neurons also encoding post-stimulus sensory and pre-response motor task features (Figure 3.8). Additionally, this global low amplitude cortical state preceding response trials is associated with long-range spatial decorrelation (Supplementary Figure 3.5) without changes in local synchronization (Figure 3.9).

The impacts of spontaneous activity on stimulus responses have been explored extensively in both physiological and computational studies. Increased spontaneous activity has been proposed to increase response gain by two primary mechanisms: depolarization to reduce membrane potential distance to spike threshold and increased variance to amplify the impacts of weak inputs (Cardin et al., 2008; Haider et al., 2007; Haider & McCormick, 2009; Hô & Destexhe, 2000; Rudolph & Destexhe, 2003; Shu et al., 2003). Therefore, we were surprised to find that reduced prestimulus activity correlated with both enhanced stimulus detection (Figures 3.2 and 3.3) and increased sensory responses (Figure 3.4). And yet, our data are consistent with studies in primary

somatosensory and auditory cortices, demonstrating increased sensory responses with reduced prestimulus activity (Cardin et al., 2008; Hasenstaub et al., 2007; McGinley, David, et al., 2015; Sachdev et al., 2004). Future studies are required to determine the cellular and network mechanisms underlying increased responsiveness with low activity, with possibilities including reduced membrane conductance (Chance et al., 2002), reduced inhibition, and reduced synaptic depression.

Our study was conducted in the context of a somatosensory (whisker) detection task. It is not currently known, however, whether these findings will generalize to other sensory modalities and other types of tasks. Reduced network activity and reduced synaptic variance have been shown to predict a network with a discrete, all-or-none input-output function (Hô & Destexhe, 2000). This configuration may improve distinguishing the presence versus absence of a stimulus as needed for stimulus detection. Such a network state, though, would be predicted to poorly encode the precise features of a stimulus. Therefore, we speculate that tasks requiring discrimination of fine stimulus details may be optimal in a high activity network state with a continuous input-output function. However, this remains to be tested.

Most studies of the impacts of spontaneous activity on sensory responses focus on primary sensory areas. However, stimulus detection tasks require the contributions of multiple cortices (de Lafuente and Romo 2006). Indeed, we have recently shown that the task in this study activates multiple sensory and motor cortices, including S1, wMC, and ALM (Aruljothi et al., 2020; Zareian et al., 2021). In this study we demonstrate that the

prestimulus activity predictive of trial outcome is global, involving all regions of dorsal neocortex. This global cortical state may reflect the coordination amongst multiple cortices, to improve not just stimulus encoding in primary sensory cortex, but the propagation of task-relevant signals throughout neocortex. Interestingly, we found prestimulus activity suppression to be largest in the same neurons that also strongly encode post-stimulus sensory and pre-response motor features, in S1, wMC, and ALM. This organization may ensure coordination not just between cortical regions, but among the specific neuronal ensembles involved in this stimulus detection task. Low activity in these specific neuronal ensembles may increase excitability and transmission by increasing membrane resistance and reducing synaptic depression.

Global changes in cortical state, as observed here, are traditionally associated with changes in arousal, driven by widespread ascending neuromodulatory systems (Zagha & McCormick, 2014). More recently, studies have shown that movement is associated with global increases in neocortical activity (Musall et al., 2020; Salkoff et al., 2020; Stringer et al., 2019). As with low activity preceding response trials, we also find that whisker movements are reduced preceding hit trials (Figure 3.5), consistent with previous reports (Kyriakatos et al., 2016; Douglas R. Ollerenshaw et al., 2012). We suspect that whisker movements impair detection for multiple reasons: 1) reafference signals from self-generated movements (Fee et al., 1997) may obscure stimulus-evoked afferent signals, 2) self-generated movements may evoke top-down sensory gating and thereby suppress stimulus evoked signals (Shubhodeep Chakrabarti & Cornelius Schwarz, 2018), and 3)

centrally-mediated cortical activation associated with whisker movements (Poulet et al., 2012) may reduce network excitability. And yet, our findings support a view of cortical state as higher dimensional than stationary versus moving (Zagha and McCormick 2014;McGinley, 2015 #1163). Among Hit trials, we find a positive correlation between prestimulus activity and reaction time (Figure 3.3). This suggests that even within overt changes in arousal, the precise levels of cortical activity impact performance in our task, with the lowest prestimulus activity correlating with optimal performance.

The neural processes that underlie the low amplitude, low variable widefield Ca^{2+} imaging signals preceding response trials could be due to multiple mechanisms. One possibility is that these low amplitude signals reflect a 'desynchronized' cortical state, as observed in whole-cell recordings, EEG, or LFP signals during wakefulness and high arousal compared to sleep and low arousal (Poulet & Petersen, 2008; Tan et al., 2014; Zagha & McCormick, 2014). To test this possibility, we analyzed LFP power and spike triggered average LFP power from three different cortical areas. Overall, these measures did not identify differences in cortical state preceding response versus no response outcomes. A second possibility is that the low amplitude Ca^{2+} imaging signals reflect low spiking activity. To test this possibility, we analyzed prestimulus spike rates from the same cortical areas as in the LFP analyses. Indeed, we observed significantly reduced spike rates before response compared to no response trials. Thus, the low amplitude Ca^{2+} imaging signals can, at least in part, be accounted for by reduced spike rates. However, we do recognize a difference in magnitude: the prestimulus reductions in dF/F are larger than

the reductions in spike rate when converted to a common metric (such as d', data not shown). This may simply reflect a sub-sampling of spiking activity. However, a third possibility is that the low amplitude Ca^{2+} imaging signals reflect robust modulations of apical dendrites, with only modest impacts on axo-somatic spike rates. We suspect that most of the Ca^{2+} imaging signals reported here are derived from the apical dendrites of supragranular and infragranular pyramidal neurons. Local spikes in these apical dendrites have been shown to modulate axo-somatic spiking output (Branco & Häusser, 2011; Palmer et al., 2014; Smith et al., 2013). However, the long electrotonic distances between these compartments indicate the possibility of partial local control; robust prestimulus modulation of apical dendritic excitability may have only minor impacts on axo-somatic spike output, yet greatly impact dendritic integration and plasticity in response to sensory inputs. Recent studies have identified specific dis-inhibitory neural circuits that control the excitability of apical dendrites (Fu et al., 2015; Soohyun Lee et al., 2013; Pi et al., 2013). Future studies, recording specifically from these interneuron populations, are needed to further assess this possibility.

References

Andreou, C., & Borgwardt, S. (2020). Structural and functional imaging markers for susceptibility to psychosis. *Mol Psychiatry*, *25*(11), 2773-2785. https://doi.org/10.1038/s41380-020-0679-7

Arieli, A., Shoham, D., Hildesheim, R., & Grinvald, A. (1995). Coherent spatiotemporal patterns of ongoing activity revealed by real-time optical imaging coupled with single-unit recording in the cat visual cortex. *Journal of Neurophysiology*, *73*(5), 2072-2093. https://doi.org/10.1152/jn.1995.73.5.2072

Arieli, A., Sterkin, A., Grinvald, A., & Aertsen, A. (1996). Dynamics of Ongoing Activity: Explanation of the Large Variability in Evoked Cortical Responses. *Science*, *273*(5283), 1868-1871. https://doi.org/10.1126/science.273.5283.1868

Aruljothi, K., Marrero, K., Zhang, Z., Zareian, B., & Zagha, E. (2020). Functional Localization of an Attenuating Filter within Cortex for a Selective Detection Task in Mice. *The Journal of Neuroscience*, *40*(28), 5443-5454. https://doi.org/10.1523/jneurosci.2993-19.2020

Boly, M., Balteau, E., Schnakers, C., Degueldre, C., Moonen, G., Luxen, A., Phillips, C., Peigneux, P., Maquet, P., & Laureys, S. (2007). Baseline brain activity fluctuations predict somatosensory perception in humans. *Proceedings of the National Academy of Sciences*, *104*(29), 12187-12192. https://doi.org/10.1073/pnas.0611404104

Branco, T., & Häusser, M. (2011). Synaptic Integration Gradients in Single Cortical Pyramidal Cell Dendrites. *Neuron*, *69*(5), 885-892. https://doi.org/10.1016/j.neuron.2011.02.006

Britten, K., Shadlen, M., Newsome, W., & Movshon, J. (1992). The analysis of visual motion: a comparison of neuronal and psychophysical performance. *The Journal of Neuroscience*, *12*(12), 4745-4765. https://doi.org/10.1523/jneurosci.12-12-04745.1992

Cardin, J. A., Palmer, L. A., & Contreras, D. (2008). Cellular Mechanisms Underlying Stimulus-Dependent Gain Modulation in Primary Visual Cortex Neurons In Vivo. *Neuron*, *59*(1), 150-160. https://doi.org/10.1016/j.neuron.2008.05.002

Chakrabarti, S., & Schwarz, C. (2018). Cortical modulation of sensory flow during active touch in the rat whisker system. *Nature Communications*, *9*(1). https://doi.org/10.1038/s41467-018-06200-6

Chance, F. S., Abbott, L. F., & Reyes, A. D. (2002). Gain Modulation from Background Synaptic Input. *Neuron*, *35*(4), 773-782. https://doi.org/10.1016/s0896-6273(02)00820-6

Crochet, S., & Petersen, C. C. (2006). Correlating whisker behavior with membrane potential in barrel cortex of awake mice. *Nat Neurosci*, *9*(5), 608-610. https://doi.org/10.1038/nn1690

de Lange, F. P., Rahnev, D. A., Donner, T. H., & Lau, H. (2013). Prestimulus oscillatory activity over motor cortex reflects perceptual expectations. *J Neurosci*, *33*(4), 1400-1410. https://doi.org/10.1523/JNEUROSCI.1094-12.2013

Fee, M. S., Mitra, P. P., & Kleinfeld, D. (1997). Central Versus Peripheral Determinants of Patterned Spike Activity in Rat Vibrissa Cortex During Whisking. *Journal of Neurophysiology*, *78*(2), 1144-1149. https://doi.org/10.1152/jn.1997.78.2.1144

Ferezou, I., Haiss, F., Gentet, L. J., Aronoff, R., Weber, B., & Petersen, C. C. (2007). Spatiotemporal dynamics of cortical sensorimotor integration in behaving mice. *Neuron*, *56*(5), 907-923. https://doi.org/10.1016/j.neuron.2007.10.007

Fiebelkorn, I. C., & Kastner, S. (2021). Spike Timing in the Attention Network Predicts Behavioral Outcome Prior to Target Selection. *Neuron*, *109*(1), 177-188 e174. https://doi.org/10.1016/j.neuron.2020.09.039

Fries, P., Reynolds, J. H., Rorie, A. E., & Desimone, R. (2001). Modulation of Oscillatory Neuronal Synchronization by Selective Visual Attention. *Science*, *291*(5508), 1560-1563. https://doi.org/10.1126/science.1055465

Fu, Y., Kaneko, M., Tang, Y., Alvarez-Buylla, A., & Stryker, M. P. (2015). A cortical disinhibitory circuit for enhancing adult plasticity. *Elife*, *4*. https://doi.org/10.7554/elife.05558

Ghose, G. M., & Maunsell, J. H. R. (2002). Attentional modulation in visual cortex depends on task timing. *Nature*, *419*(6907), 616-620. https://doi.org/10.1038/nature01057

Gold, J. I., & Shadlen, M. N. (2007). The neural basis of decision making. *Annu Rev Neurosci*, *30*, 535-574. https://doi.org/10.1146/annurev.neuro.29.051605.113038

Haider, B., Duque, A., Hasenstaub, A. R., Yu, Y., & McCormick, D. A. (2007). Enhancement of Visual Responsiveness by Spontaneous Local Network Activity In Vivo. *Journal of Neurophysiology*, *97*(6), 4186-4202. https://doi.org/10.1152/jn.01114.2006

Haider, B., & McCormick, D. A. (2009). Rapid neocortical dynamics: cellular and network mechanisms. *Neuron*, *62*(2), 171-189. https://doi.org/10.1016/j.neuron.2009.04.008

Hanes, D. P., & Schall, J. D. (1996). Neural Control of Voluntary Movement Initiation. *Science*, *274*(5286), 427-430. https://doi.org/10.1126/science.274.5286.427

Harris, K. D., & Thiele, A. (2011). Cortical state and attention. *Nature Reviews Neuroscience*, *12*(9), 509-523. https://doi.org/10.1038/nrn3084

Hasenstaub, A., Sachdev, R. N. S., & McCormick, D. A. (2007). State Changes Rapidly Modulate Cortical Neuronal Responsiveness. *Journal of Neuroscience*, *27*(36), 9607-9622. https://doi.org/10.1523/jneurosci.2184-07.2007

Hô, N., & Destexhe, A. (2000). Synaptic Background Activity Enhances the Responsiveness of Neocortical Pyramidal Neurons. *Journal of Neurophysiology*, *84*(3), 1488-1496. https://doi.org/10.1152/jn.2000.84.3.1488

Kim, R., & Sejnowski, T. J. (2021). Strong inhibitory signaling underlies stable temporal dynamics and working memory in spiking neural networks. *Nat Neurosci*, *24*(1), 129-139. https://doi.org/10.1038/s41593-020-00753-w

Kyriakatos, A., Sadashivaiah, V., Zhang, Y., Motta, A., Auffret, M., & Petersen, C. C. H. (2016). Voltage-sensitive dye imaging of mouse neocortex during a whisker detection task. *Neurophotonics*, *4*(3), 031204. https://doi.org/10.1117/1.NPh.4.3.031204

Lee, S., Kruglikov, I., Huang, Z. J., Fishell, G., & Rudy, B. (2013). A disinhibitory circuit mediates motor integration in the somatosensory cortex. *Nature Neuroscience*, *16*(11), 1662-1670. https://doi.org/10.1038/nn.3544

Luck, S. J., Chelazzi, L., Hillyard, S. A., & Desimone, R. (1997). Neural Mechanisms of Spatial Selective Attention in Areas V1, V2, and V4 of Macaque Visual Cortex. *Journal of Neurophysiology*, *77*(1), 24-42. https://doi.org/10.1152/jn.1997.77.1.24

Mazaheri, A., DiQuattro, N. E., Bengson, J., & Geng, J. J. (2011). Pre-stimulus activity predicts the winner of top-down vs. bottom-up attentional selection. *PLoS One*, *6*(2), e16243. https://doi.org/10.1371/journal.pone.0016243

McCormick, D. A., McGinley, M. J., & Salkoff, D. B. (2015). Brain state dependent activity in the cortex and thalamus. *Curr Opin Neurobiol*, *31*, 133-140. https://doi.org/10.1016/j.conb.2014.10.003

McGinley, M. J., David, S. V., & McCormick, D. A. (2015). Cortical Membrane Potential Signature of Optimal States for Sensory Signal Detection. *Neuron*, *87*(1), 179-192. https://doi.org/10.1016/j.neuron.2015.05.038

McGinley, M. J., Vinck, M., Reimer, J., Batista-Brito, R., Zagha, E., Cadwell, C. R., Tolias, A. S., Cardin, J. A., & McCormick, D. A. (2015). Waking State: Rapid Variations Modulate Neural and Behavioral Responses. *Neuron*, *87*(6), 1143-1161. https://doi.org/10.1016/j.neuron.2015.09.012

Moore, T., & Armstrong, K. M. (2003). Selective gating of visual signals by microstimulation of frontal cortex. *Nature*, *421*(6921), 370-373. https://doi.org/10.1038/nature01341

Murphy, M. C., Chan, K. C., Kim, S. G., & Vazquez, A. L. (2018). Macroscale variation in resting-state neuronal activity and connectivity assessed by simultaneous calcium imaging, hemodynamic imaging and electrophysiology. *Neuroimage*, *169*, 352-362. https://doi.org/10.1016/j.neuroimage.2017.12.070

Musall, S., Kaufman, M. T., Juavinett, A. L., Gluf, S., & Churchland, A. K. (2020). Single-trial neural dynamics are dominated by richly varied movements. *Nat Neurosci*, *22*(10), 1677-1686. https://doi.org/10.1038/s41593-019-0502-4

Niell, C. M., & Stryker, M. P. (2010). Modulation of visual responses by behavioral state in mouse visual cortex. *Neuron*, *65*(4), 472-479. https://doi.org/10.1016/j.neuron.2010.01.033

Ollerenshaw, D. R., Bari, B. A., Millard, D. C., Orr, L. E., Wang, Q., & Stanley, G. B. (2012). Detection of tactile inputs in the rat vibrissa pathway. *Journal of Neurophysiology*, *108*(2), 479-490. https://doi.org/10.1152/jn.00004.2012

Palmer, L. M., Shai, A. S., Reeve, J. E., Anderson, H. L., Paulsen, O., & Larkum, M. E. (2014). NMDA spikes enhance action potential generation during sensory input. *Nature Neuroscience*, *17*(3), 383-390. https://doi.org/10.1038/nn.3646

Petersen, C. C. H., Grinvald, A., & Sakmann, B. (2003). Spatiotemporal Dynamics of Sensory Responses in Layer 2/3 of Rat Barrel Cortex MeasuredIn Vivoby Voltage-Sensitive Dye Imaging Combined with Whole-Cell Voltage Recordings and Neuron Reconstructions. *The Journal of Neuroscience*, *23*(4), 1298-1309. https://doi.org/10.1523/jneurosci.23-04-01298.2003

Pi, H.-J., Hangya, B., Kvitsiani, D., Sanders, J. I., Huang, Z. J., & Kepecs, A. (2013). Cortical interneurons that specialize in disinhibitory control. *Nature*, *503*(7477), 521-524. https://doi.org/10.1038/nature12676

Poulet, J. F., Fernandez, L. M., Crochet, S., & Petersen, C. C. (2012). Thalamic control of cortical states. *Nat Neurosci*, *15*(3), 370-372. https://doi.org/10.1038/nn.3035

Poulet, J. F., & Petersen, C. C. (2008). Internal brain state regulates membrane potential synchrony in barrel cortex of behaving mice. *Nature*, *454*(7206), 881-885. https://doi.org/10.1038/nature07150

Roitman, J. D., & Shadlen, M. N. (2002). Response of Neurons in the Lateral Intraparietal Area during a Combined Visual Discrimination Reaction Time Task. *The Journal of Neuroscience*, *22*(21), 9475-9489. https://doi.org/10.1523/jneurosci.22-21-09475.2002

Rudolph, M., & Destexhe, A. (2003). A Fast-Conducting, Stochastic Integrative Mode for Neocortical NeuronsInVivo. *The Journal of Neuroscience*, *23*(6), 2466-2476. https://doi.org/10.1523/jneurosci.23-06-02466.2003

Sachdev, R. N. S., Ebner, F. F., & Wilson, C. J. (2004). Effect of Subthreshold Up and Down States on the Whisker-Evoked Response in Somatosensory Cortex. *Journal of Neurophysiology*, *92*(6), 3511-3521. https://doi.org/10.1152/jn.00347.2004

Sachidhanandam, S., Sreenivasan, V., Kyriakatos, A., Kremer, Y., & Petersen, C. C. H. (2013). Membrane potential correlates of sensory perception in mouse barrel cortex. *Nature Neuroscience*, *16*(11), 1671-1677. https://doi.org/10.1038/nn.3532

Salkoff, D. B., Zagha, E., McCarthy, E., & McCormick, D. A. (2020). Movement and Performance Explain Widespread Cortical Activity in a Visual Detection Task. *Cereb Cortex*, *30*(1), 421-437. https://doi.org/10.1093/cercor/bhz206

Shimaoka, D., Harris, K. D., & Carandini, M. (2018). Effects of Arousal on Mouse Sensory Cortex Depend on Modality. *Cell Reports*, *22*(12), 3160-3167. https://doi.org/10.1016/j.celrep.2018.02.092

Shu, Y., Hasenstaub, A., Badoual, M., Bal, T., & McCormick, D. A. (2003). Barrages of Synaptic Activity Control the Gain and Sensitivity of Cortical Neurons. *The Journal of Neuroscience*, *23*(32), 10388-10401. https://doi.org/10.1523/jneurosci.23-32-10388.2003

Smith, S. L., Smith, I. T., Branco, T., & Häusser, M. (2013). Dendritic spikes enhance stimulus selectivity in cortical neurons in vivo. *Nature*, *503*(7474), 115-120. https://doi.org/10.1038/nature12600

Stringer, C., Pachitariu, M., Steinmetz, N., Reddy, C. B., Carandini, M., & Harris, K. D. (2019). Spontaneous behaviors drive multidimensional, brainwide activity. *Science*, *364*(6437), 255. https://doi.org/10.1126/science.aav7893

Tan, A. Y. Y., Chen, Y., Scholl, B., Seidemann, E., & Priebe, N. J. (2014). Sensory stimulation shifts visual cortex from synchronous to asynchronous states. *Nature*, *509*(7499), 226-229. https://doi.org/10.1038/nature13159

van Kempen, J., Gieselmann, M. A., Boyd, M., Steinmetz, N. A., Moore, T., Engel, T. A., & Thiele, A. (2020). Top-down coordination of local cortical state during selective attention. *Neuron*. https://doi.org/10.1016/j.neuron.2020.12.013

Yang, H., Kwon, S. E., Severson, K. S., & O'Connor, D. H. (2016). Origins of choice-related activity in mouse somatosensory cortex. *Nat Neurosci*, *19*(1), 127-134. https://doi.org/10.1038/nn.4183

Zagha, E., & McCormick, D. A. (2014). Neural control of brain state. *Curr Opin Neurobiol*, *29*, 178-186. https://doi.org/10.1016/j.conb.2014.09.010

Zareian, B., Maboudi, K., Daliri, M. R., Abrishami Moghaddam, H., Treue, S., & Esghaei, M. (2020). Attention strengthens across-trial pre-stimulus phase coherence in visual cortex, enhancing stimulus processing. *Sci Rep*, *10*(1), 4837. https://doi.org/10.1038/s41598-020-61359-7

Zareian, B., Zhang, Z., & Zagha, E. (2020). *Cortical Localization of the Sensory-Motor Transformation in a Whisker Detection Task in Mice*. Cold Spring Harbor Laboratory. https://dx.doi.org/10.1101/2020.07.08.194555 https://www.biorxiv.org/content/biorxiv/early/2020/07/09/2020.07.08.194555.full.pdf

Zareian, B., Zhang, Z., & Zagha, E. (2021). Cortical Localization of the Sensory-Motor Transformation in a Whisker Detection Task in Mice. *eNeuro*, ENEURO.0004-0021. https://doi.org/10.1523/eneuro.0004-21.2021

Figures and Legends

Figure 3.1: Predictions and Experimental Design for Testing Impacts of Prestimulus Activity on Sensory Detection and Discrimination

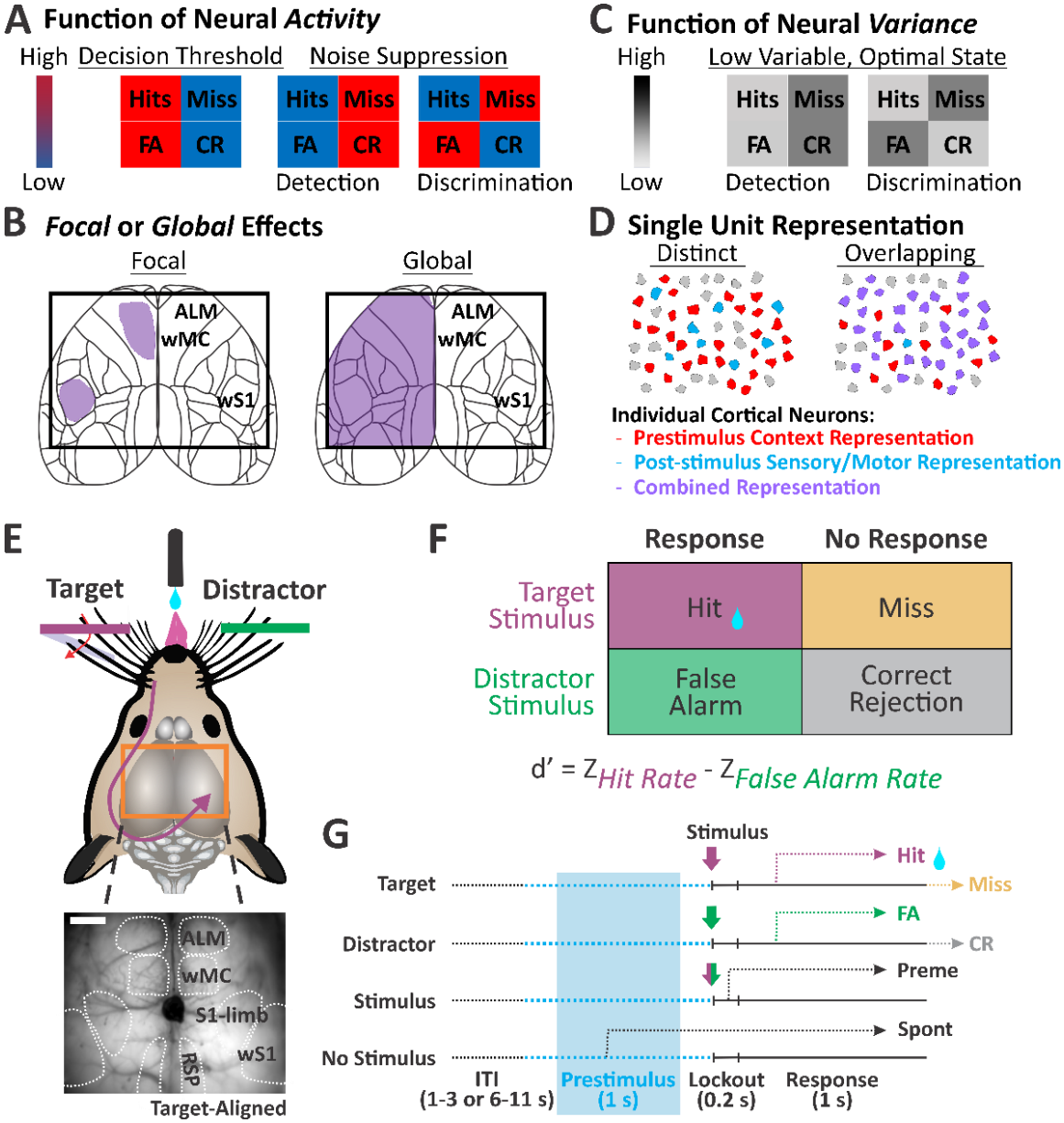

(A-D) Potential mechanisms of task-relevant prestimulus activity. (E-G) Experimental design. (E). Head-fixed mice are trained to discriminate between target whisker deflections (purple) and distractor whisker deflections (green), within opposite whisker fields. Mice report detection by licking a central lickport. The orange rectangle reflects the widefield Ca^{2+} imaging window. The inset below is a sample imaging frame, demarcating neocortical regions of interest in bilateral frontal and parietal cortices. (F) Classification of trial types and outcomes. Task performance is quantified by discrimination d' as the separation between hit and false alarm rates. z, inverse cumulative function of the normal distribution. G. Trial structure, including a variable inter-trial interval, 1 s prestimulus window, 0.2 s stimulus and lockout (delay) window, and 1 s response window. The prestimulus window of interest in this study is the last 1 s of the inter-trial interval (blue shade), immediately before stimulus onset. Spont, spontaneous responses during the prestimulus window; Preme, premature responses during the lockout window. Scale bar in (E) is 1 mm.

Figure 3.2: Sliding Window Normalized Grand Average Fluorescence Activity (dF/F)

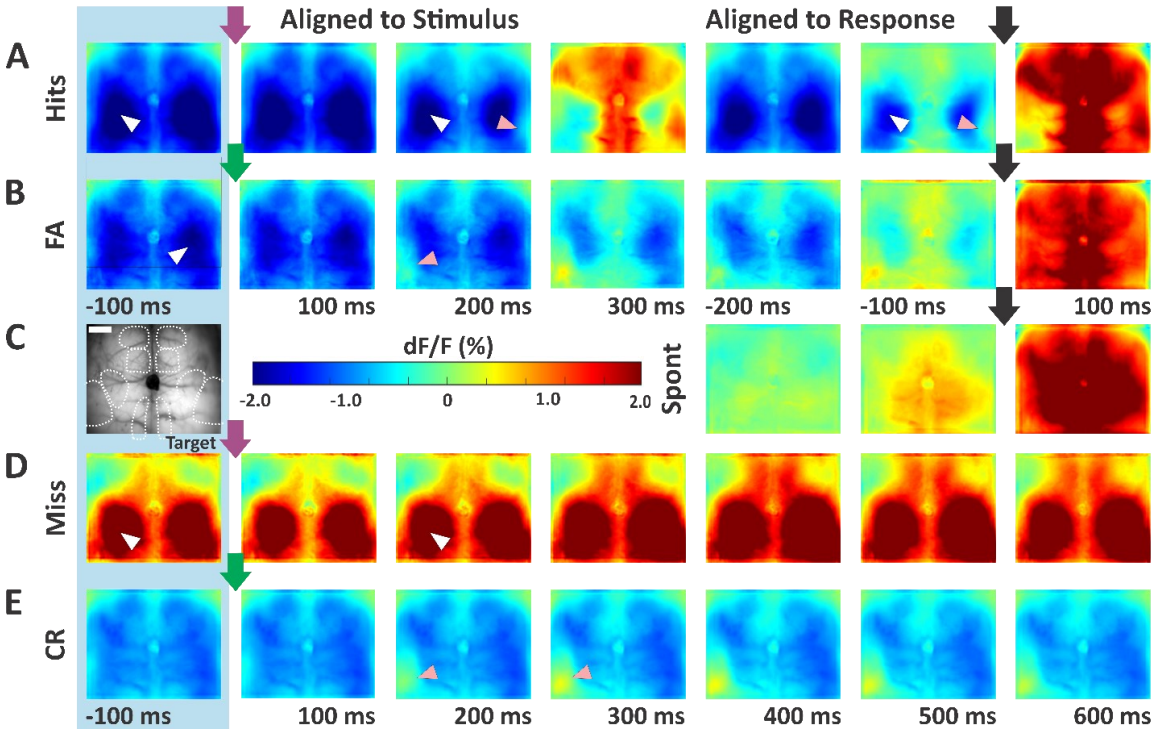

Data are averages across all mice and all sessions (n=38 sessions). Activity in specific imaging frames is aligned to the stimulus onset (left, purple and green arrows for target and distractor stimuli, respectively) or response onset (black frame, black arrows, in rows A, B, and C). Warmer colors indicate higher activity. The pink arrowheads specify stimulus aligned whisker regions of S1, whereas the white arrowheads specify limb regions of S1 (see atlas in leftmost panel in row C). The last prestimulus frame is shown in the first column (blue shade). Shown are hit trials (A), false alarm trials (B), spontaneous trials (C), miss trials (D), and correct rejection trials (E). Note the low (negative due to normalization) dF/F prestimulus activity in response trials (hit and false alarm), compared to the high dF/F prestimulus activity in miss trials. Scale bar in (C) is 1 mm.

Figure 3.3: Prestimulus Neuronal Activity Differences between Response and No Response Trials and Correlations with Reaction Time

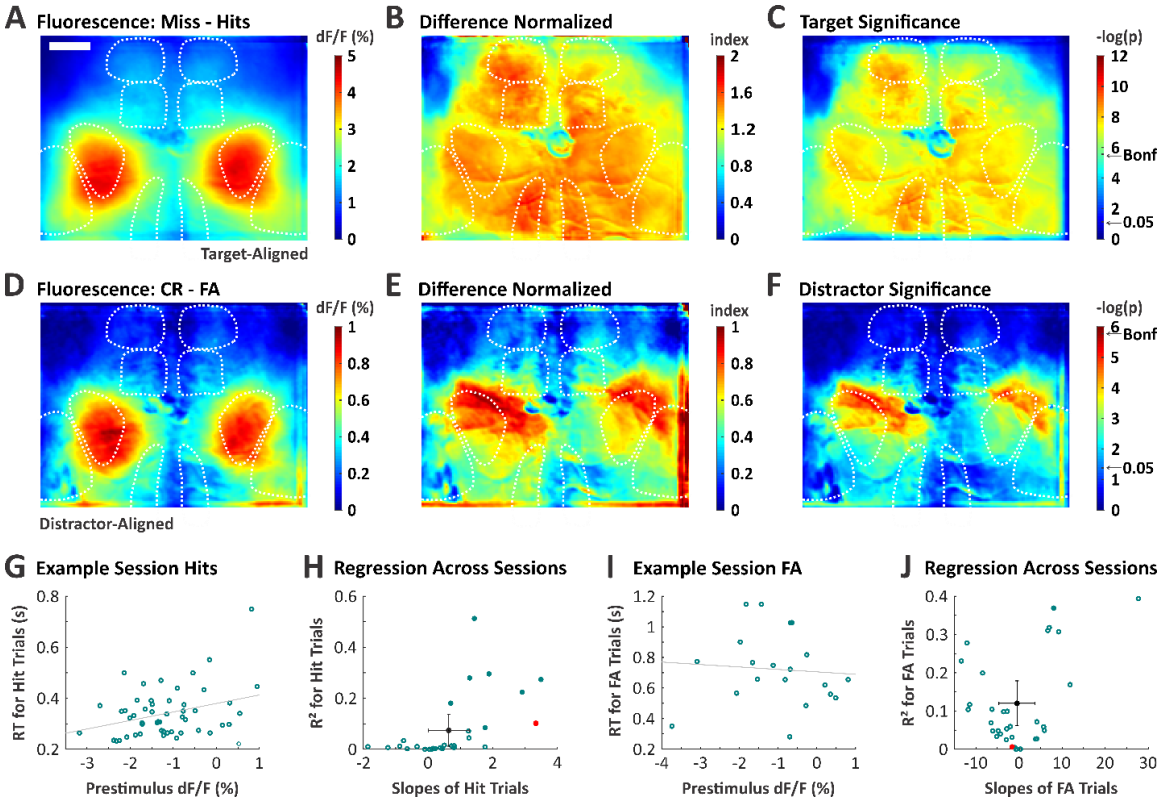

(A) Grand average of prestimulus dF/F for miss minus hit trials. All pixel values within neocortex are greater than 0, indicating higher global activity preceding miss trials. (B) Similar to [A], except that the individual session dF/F signals were further indexed (μ/σ) to normalize for differences in fluorescence fluctuations. (C) Significance map for the data in [A]. Significance threshold with Bonferroni correction for multiple comparisons is indicated by the arrow (Bonf). For target trials, higher activity preceding no response trials is statistically significant throughout dorsal cortex. (D-F) Same structure as [A-C], except for CR minus FA trials. Note the more restricted range of scale bars in each panel, compared to target data. For distractor trials, higher activity preceding no response trials is marginally significant, most prominent in the S1 limb regions. Scale bar in (A) is 1 mm. (G) An example session showing a positive correlation between prestimulus activity (dF/F) and reaction time for individual Hit trials (slope=3.34, R^2=0.10, dotted line is the linear regression). (H) Regression analyses across all sessions for Hit trials. The red data point is the example session in [G], the black data reflect the mean ± standard deviation across sessions (n=30 sessions). (I) FA trials in an example session, with a non-significant negative correlation between prestimulus activity and reaction time (slope=-1.6, R^2=0.006). (J) Same as H but for FA trials (n=32 sessions).

Figure 3.4: Quantification of Stimulus Encoding for Each Trial Type

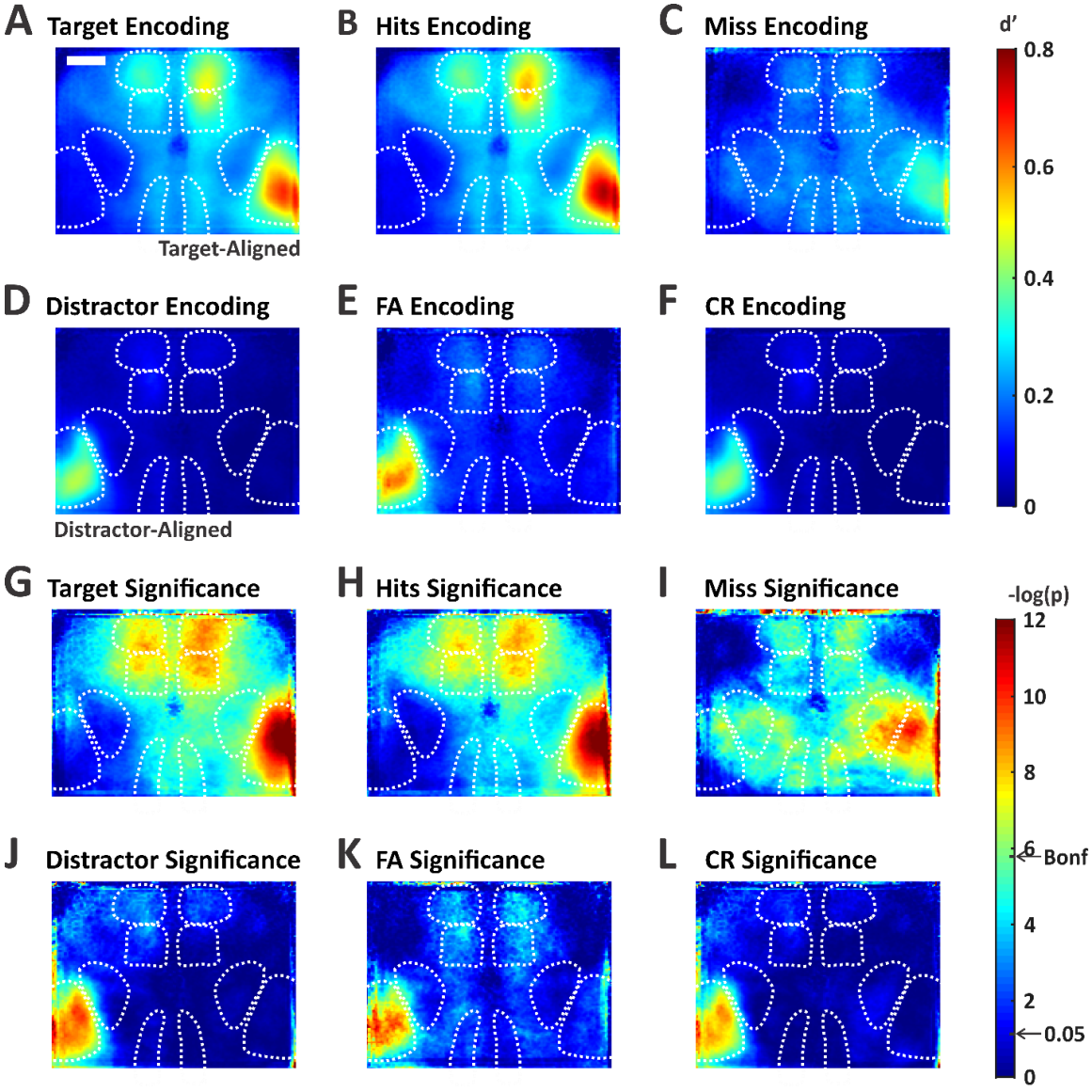

(A-F) Neurometric d' values were calculated for each pixel during the last frame of the lockout: after stimulus presentation and before the allowed response window. Data are grand average d' maps from all sessions, showing all target trials (A), hit trials (B), miss trials (C), all distractor trials (D), FA trials (E), and CR trials (F). Note the larger stimulus encoding in response trials (B and E compared to C and F). Significance maps of the data in [A-F], respectively. Significance threshold with Bonferroni correction for multiple comparisons is indicated by the arrow (Bonf). For all trial types there is significant stimulus encoding in the stimulus aligned S1 whisker region. Scale bar in (A) is 1 mm.

Figure 3.5: Prestimulus and Post-Stimulus Whisker Movements in Each Trial Type

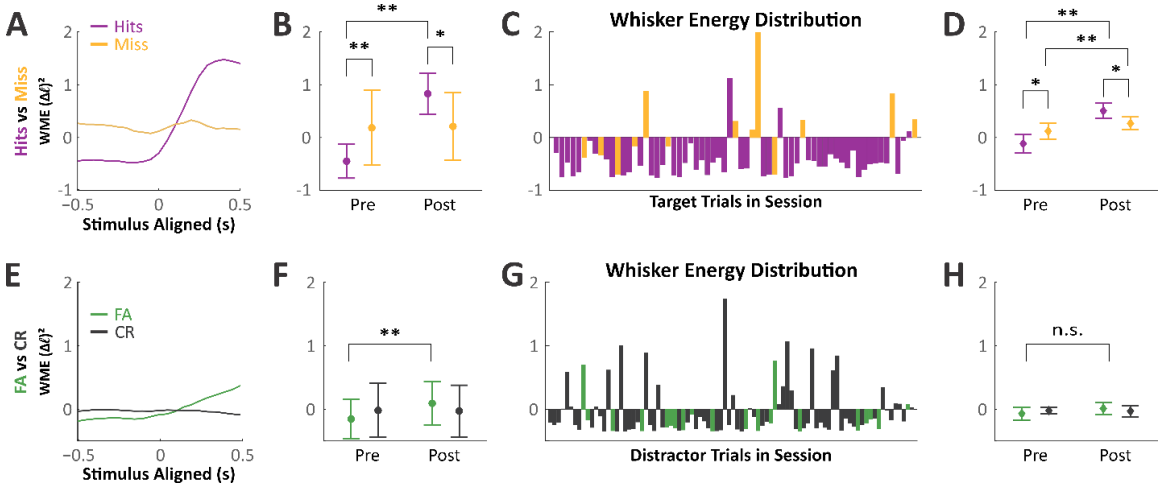

*(A) Peristimulus whisker motion energy (WME) on target trials in an example session, hits (purple) and misses (orange). On hits trials there was a dramatic increase in WME post-stimulus and during the response window. Prestimulus, however, WME on hits trials was reduced compared to miss trials. (B) Quantification of data in [A], comparing prestimulus (pre) and post-stimulus WME for hit and miss trials. (C) Prestimulus WME values for each trial in the example session. (D) Summary data for all sessions (n=9). Note the reduced WME preceding hit compared to miss trials. (E-H) Same as above, but for distractor trials. While this example session shows moderately reduced WME preceding false alarm trials (E-G), this trend was not statistically significant across the full dataset (H). Data are presented as mean +/- STD, *p<0.05, **p<0.005.*

Figure 3.6: Spatial Dimensionality Reduction for Single Trial Analyses

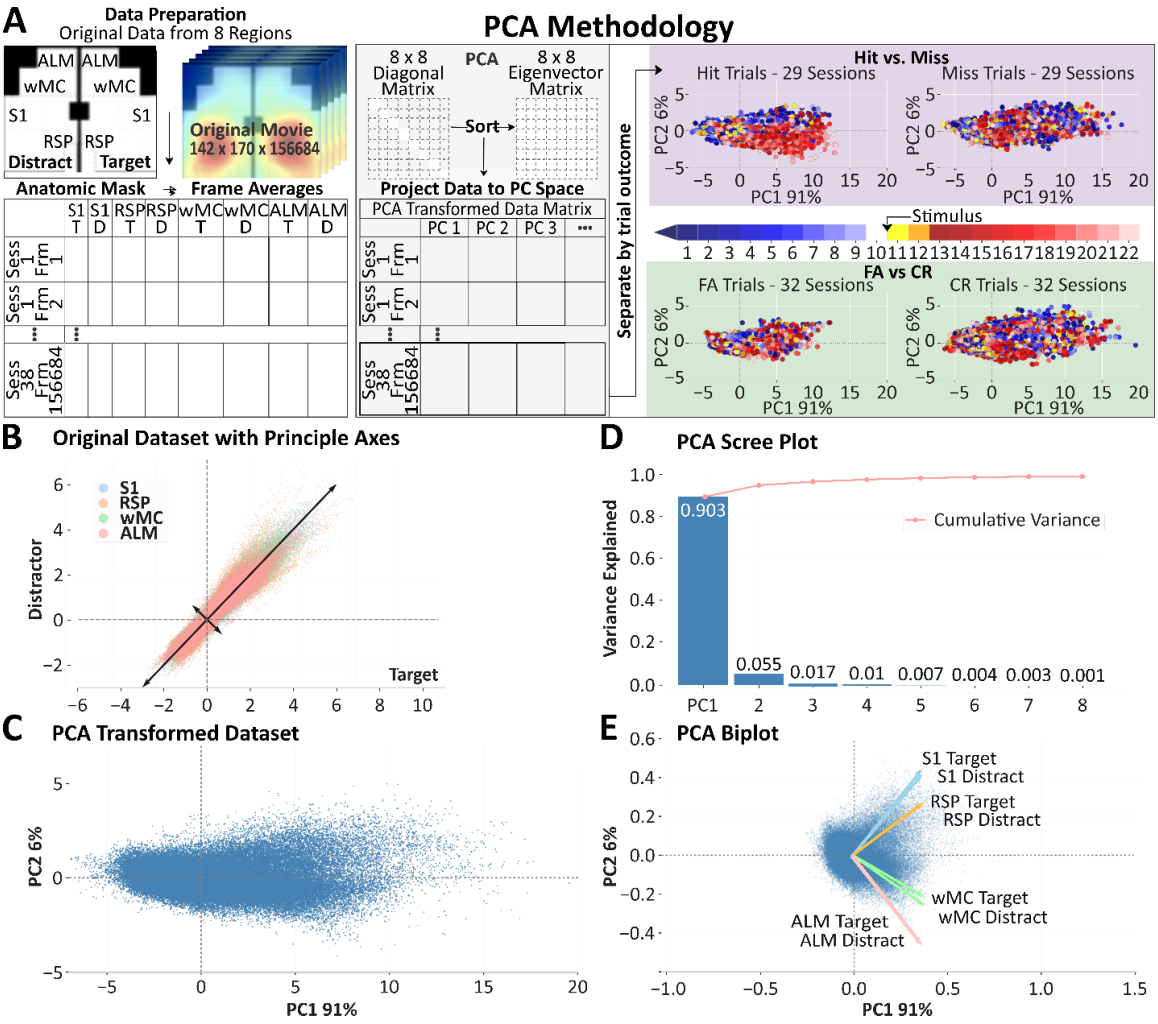

(A) Methodology for using principal component analysis (PCA) to reduce spatial dimensionality. Left, full images were parsed into 8 regional masks. Average dF/F within each mask for all trials and all sessions were appended into a single matrix, upon which PCA was performed. Right, frames with different trial outcomes were back projected to the first principal component (PC1) and plotted against their projection onto the second principal component (PC2). Transformed samples are colored based on their frame index: prestimulus (blue to white), post-stimulus and pre-response (yellow and orange), response (red to pink). (B) Original dataset, each data point represents a sample frame ROI-specific average, plotted against its change in fluorescence (dF/F) between target (x-axis) and distractor (y-axis) hemispheres. Black arrows represent the first two principal vectors. (C) Transformed dataset, each data point represents a sample frame plotted against its projection onto PC1 and PC2. (D) PCA scree plot. PCs are plotted according to their rank in variance, with accumulated variance plotted in red. The first two PCs were chosen for further analysis as they explain >95% variance of the untransformed dataset (PC1, 91%, PC2, 6%). (E) PCA biplot. Samples plotted against their normalized projection onto PC1 and PC2, with vectors representing individual ROIs according to their loadings.

Figure 3.7: Single Trial Analyses of Prestimulus Subspace Variance and Position According to Trial Outcomes

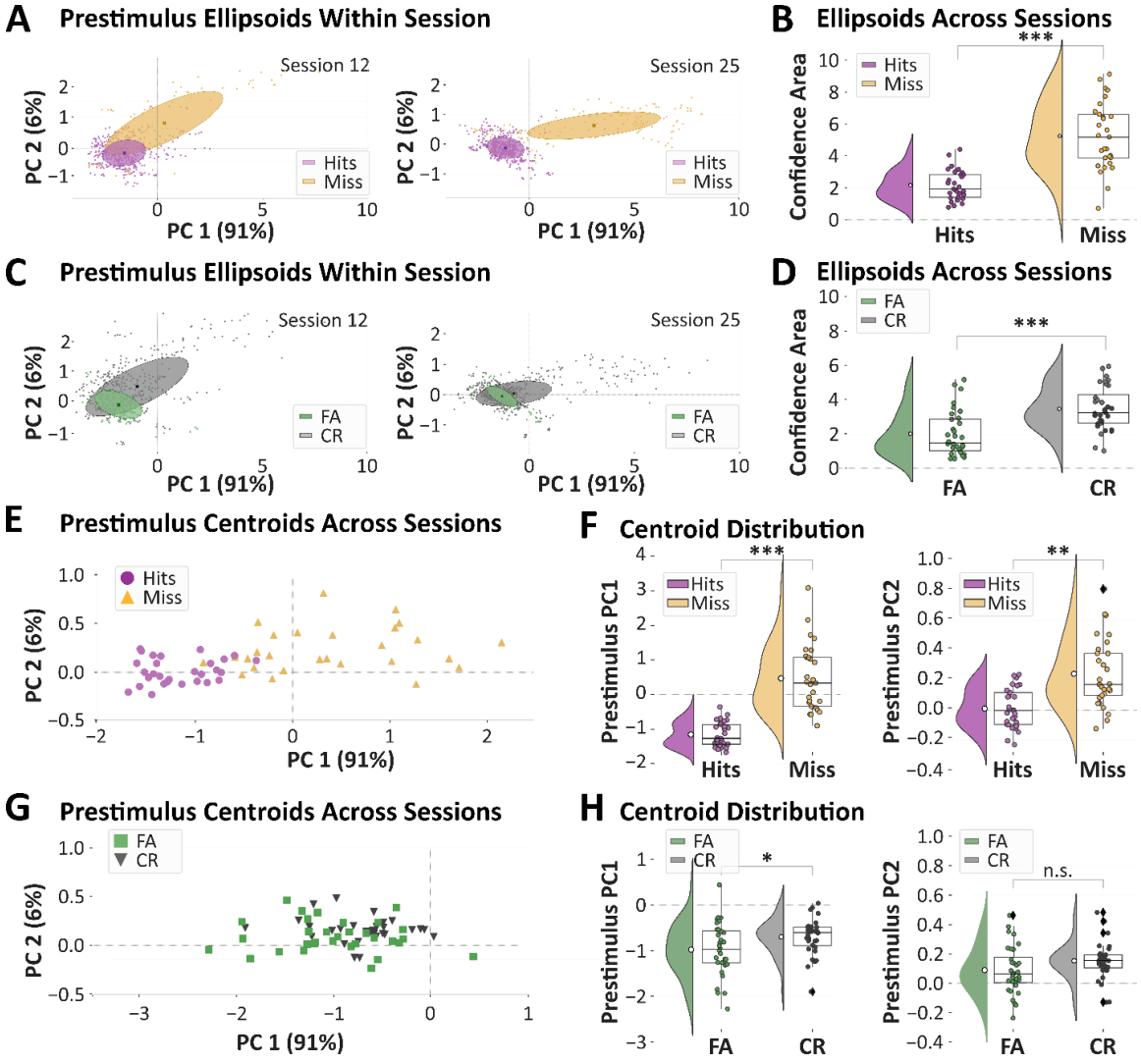

*All data presented are from the last 500 ms of the prestimulus window (frames 6 to 10 of Figure 3.6A). (A) Prestimulus activity in PC space for hit (purple) and miss (yellow) trials of two example sessions. Each data point represents a single prestimulus frame. Overlaid are covariance ellipses for both trial outcome types (major radius, 1σ along PC1; minor radius, 1σ along PC2). Note the reduced area and distinct position of the covariance ellipses for hit compared to miss trials. (B) Comparison of the ellipse area, as a measure of variability, across all sessions. (C and D) Same as [A] and [B], except for FA (green) and CR (gray) trials. Response trials (hit and FA) are preceded by less variable prestimulus activity compared to no response trials (miss and CR). (E) Centroid positions of the covariance ellipses in PC space for all sessions, for hit and miss trials (same color designation as above). Each data point represents the hit or miss centroid from one session. (F) Quantification of centroid positions on axes PC1 (left) and PC2 (right). (G and H) Same as [E] and [F], except for FA and CR trials. Prestimulus activity occupies distinct subspaces for response and no response trials, along both PC1 and PC2 for target trials and along PC 1 for distractor trials. *p<0. 01; **p<0.001; ***p<0.0001; n.s., non-significant.*

Figure 3.8: Distribution of Prestimulus Choice Probability, Post-Stimulus Sensory, and Pre-Response Motor Encoding across Single Units in S1, wMC and ALM

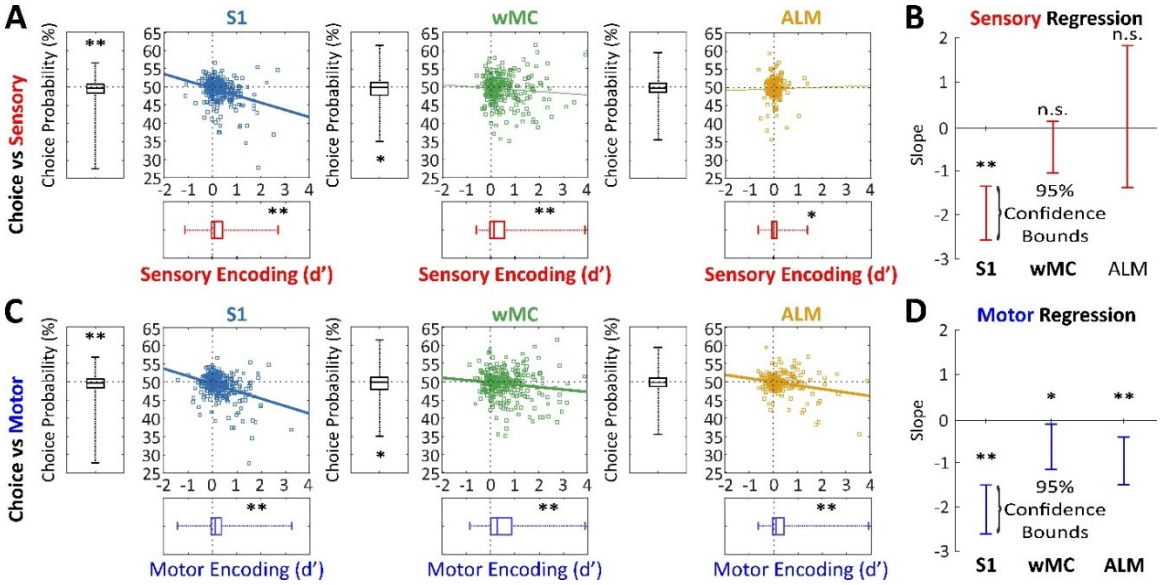

*(A) Plots of sensory encoding (d') versus choice probability (%) for single units in target aligned S1 (left), wMC (center), and ALM (right). Asterisks above box plots reflect comparisons of individual measures to chance (d'=0 and choice probability=50%). Scatter plots include linear fits of the single unit data. Single units in each of these three cortical regions show below chance prestimulus choice probability (tending yet not significant for ALM (p=0.06), significant for S1 and wMC) and positive post-stimulus sensory encoding. (B) 95% confidence bounds of the linear regression slope values. (C and D) Same as [A] and [B], but for pre-response motor encoding. The significant negative slope values indicate an overlap between the single units with lower than chance prestimulus choice probability and positive post-stimulus sensory encoding (for S1) and pre-response motor encoding (for S1, wMC, and ALM). *p<0.05; **p<0.005; n.s., non-significant.*

Figure 3.9: Lack of differences in LFP power and spike triggered average LFP power preceding hit compared to miss trials

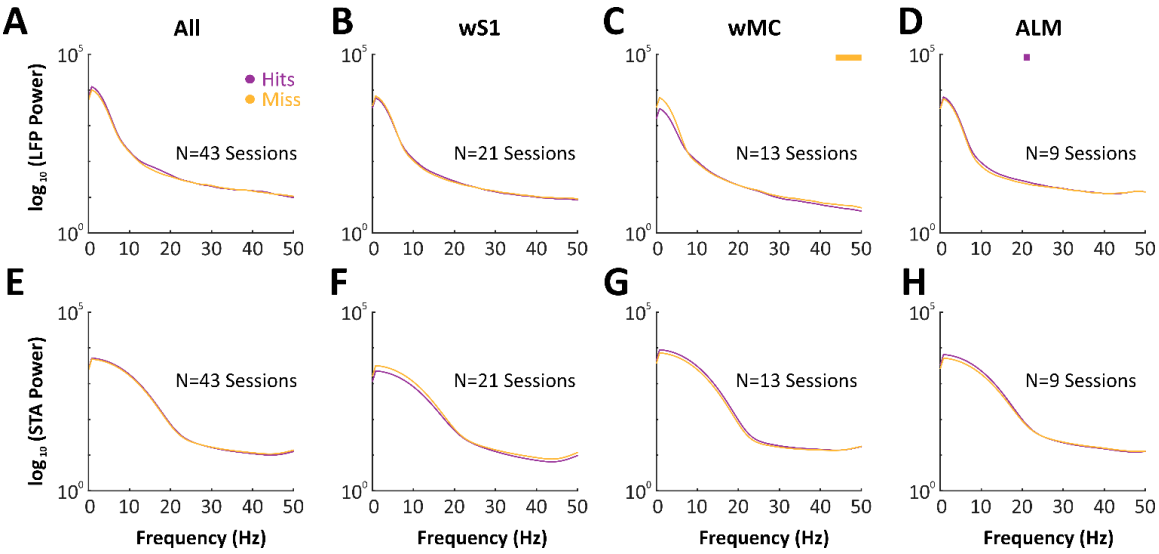

(A-D) Power spectra for local field potentials (LFPs) recorded from layer 5 across target aligned regions combined (A) and separately calculated for (B) wS1, (C) wMC, and (D) ALM. Bars above plots reflect significance using paired t-test ($p<0.01$) for each frequency. Color of bar indicates direction of difference between LFP traces (purple for hits larger than miss, yellow for miss larger than hits). (E, F, G, and H) Same as in [A, B, C, and D], except for power spectra calculated from spike triggered average (STA) LFPs.

Supplementary Figures

Supplemental Figure 3.1, Related to Methods, Figures 3.1-3: Sliding Window Normalization Method and Robustness of Window Size

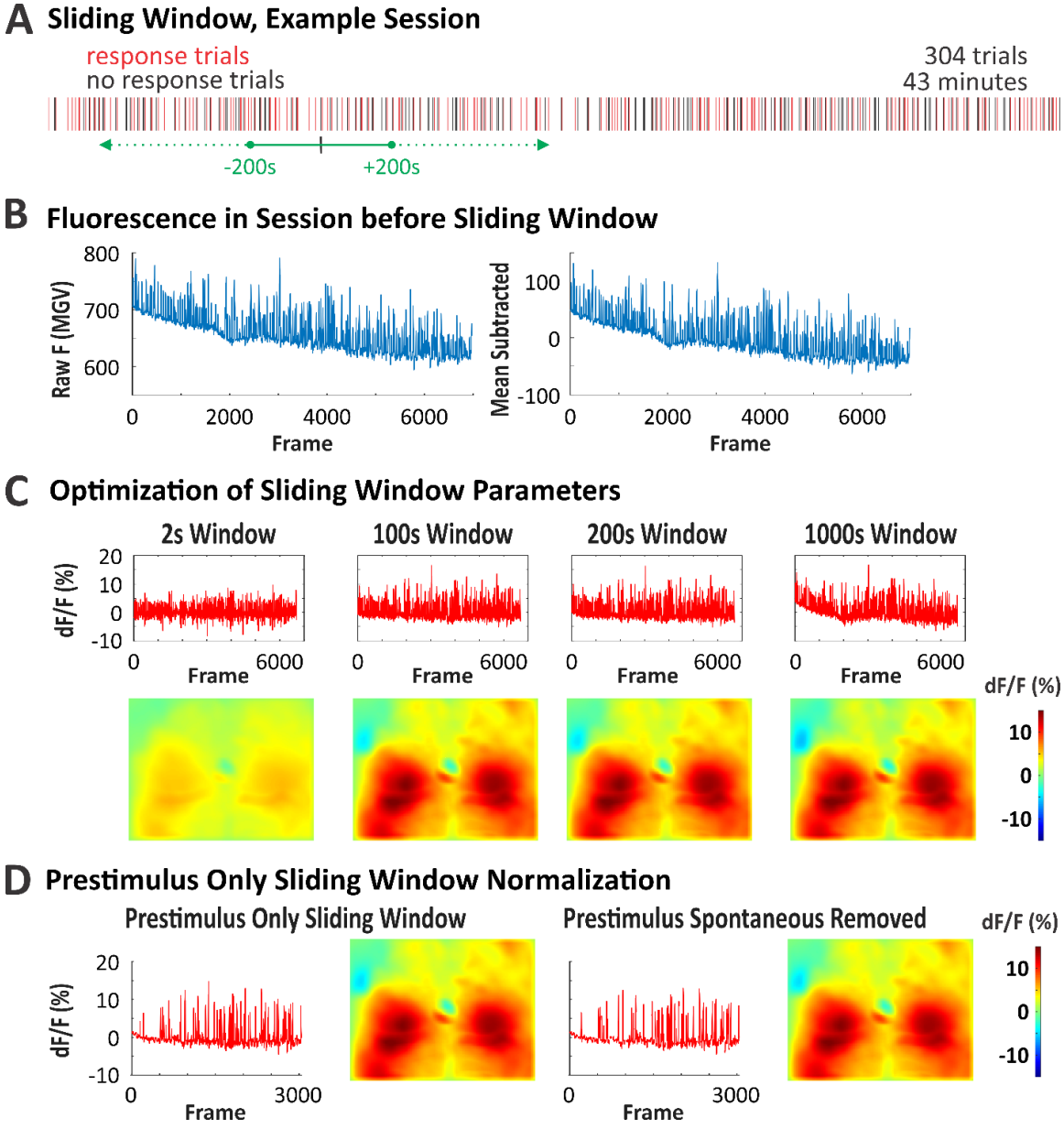

(A) Depiction of response trials (red), no response trials (black) and sliding window (green) used for an example session. This session consisted of 304 trials over 43.4 minutes. Each sliding window segment included an average of 46 trials. (B) Rundown in raw fluorescence per frame and mean subtracted raw fluorescence per frame acquired across example session. (C) Different sliding windows considered for optimization of method used in this study. Top row: dF/F using a sliding window every 2s; 2s half-width (far left), 100s half-width (center left), 200s half-width (center right), 1000s half-width (far right). Bottom row: Mean to Hits difference using sliding window indicated in top row. This normalization method is robust to a range of sliding window sizes, between 50s to 200s. If the window is too small (left) single trial differences are normalized out. If the window is too large (right) fluorescence rundown is not corrected. (D) Sliding window method (200s) applied to prestimulus frames only and applied to prestimulus frames with spontaneous trials removed. Left to right: dF/F per frame across prestimulus frames in example session (far left), Miss to Hits difference using only prestimulus frames (left center), dF/F per frame across prestimulus frames, spontaneous trials removed, in example session (right center), Miss to Hits difference using prestimulus frames, spontaneous trials removed (far right). Excluding post-stimulus frames and spontaneous trials does not impact our sliding window prestimulus analyses.

Supplemental Figure 3.2, Related to Figure 3.2: Prestimulus mean and standard deviation is larger for no response trials compared to response trials

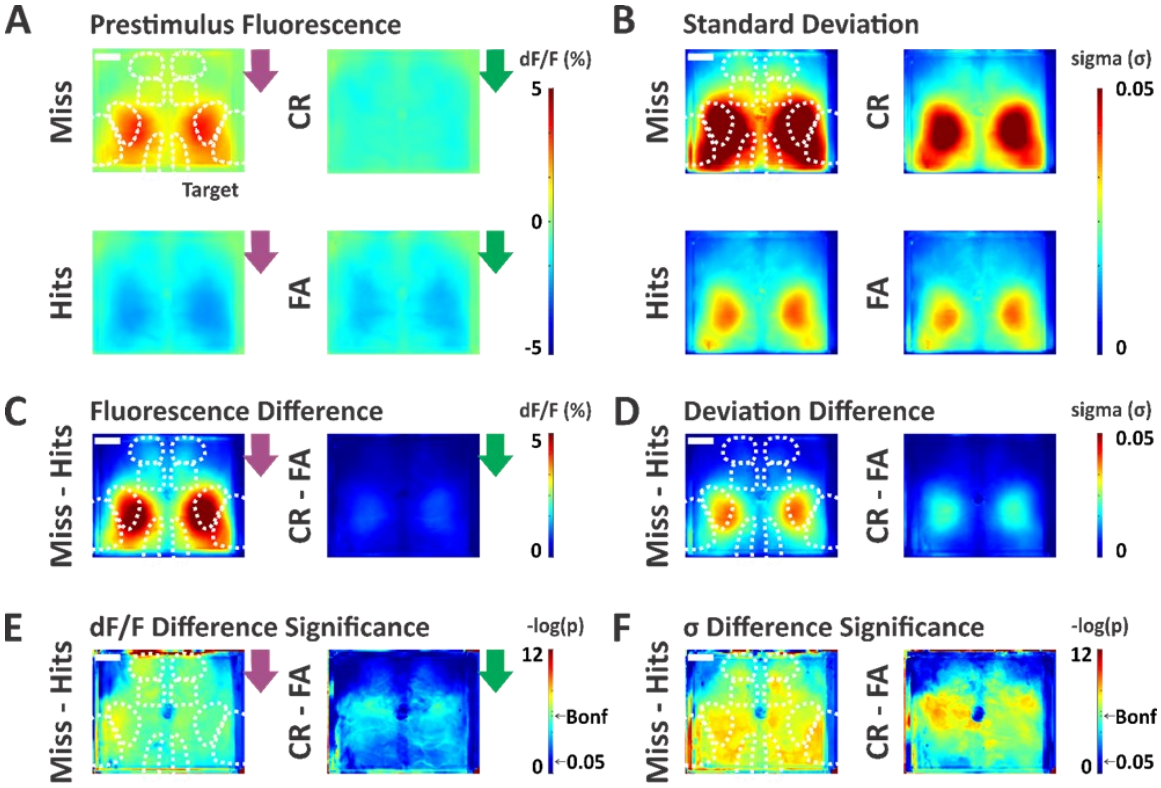

(A) Trialwise prestimulus average across full prestimulus window (1s), across all mice, all sessions (n=38 sessions). Prestimulus mean is shown aligned to the stimulus onset (left, purple for target stimuli and right, green for distractor stimuli). First row includes no response trials (Miss and CR), second row includes response trials (Hits and FA). (B) Trialwise prestimulus standard deviation across full prestimulus window as in [A]. (C) No response minus response prestimulus mean for target (left) and distractor (right) trials. (D) No response minus response prestimulus standard deviation for target (left) and distractor (right) trials. (E) Significance maps for data in [C]. (F) Significance maps for data in [D]. Significance threshold with Bonferroni correction for multiple comparisons is indicated by the arrow (Bonf). Prestimulus fluorescence amplitude and variability are larger preceding no response compared to response trials, which is broadly significant for target trials and more focused on the limb S1 regions for distractor trials. Wire frames (dotted white) in top left of each subpanel indicate regions of interest as in Figure 3.2. Scale bar is 1 mm for all maps.

Supplemental Figure 3.3, Related to Figure 3.3: Prestimulus fluorescence activity differences in parietal cortices are larger than in frontal cortices for hit versus miss trials

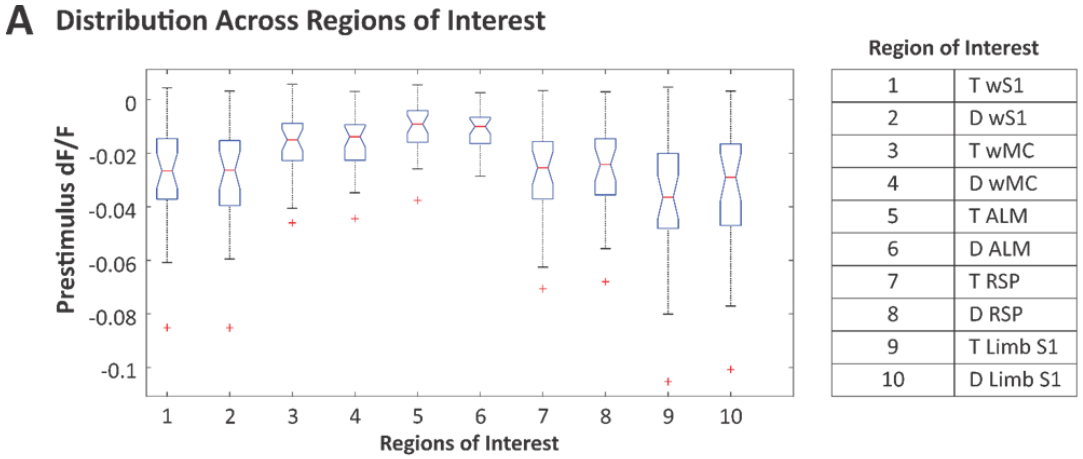

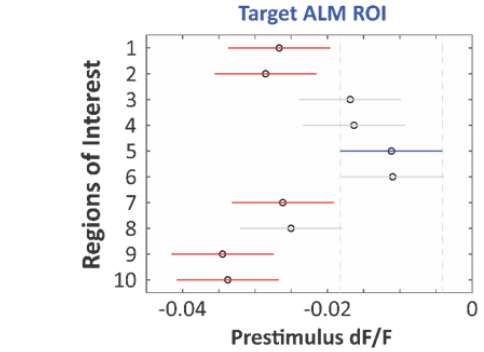

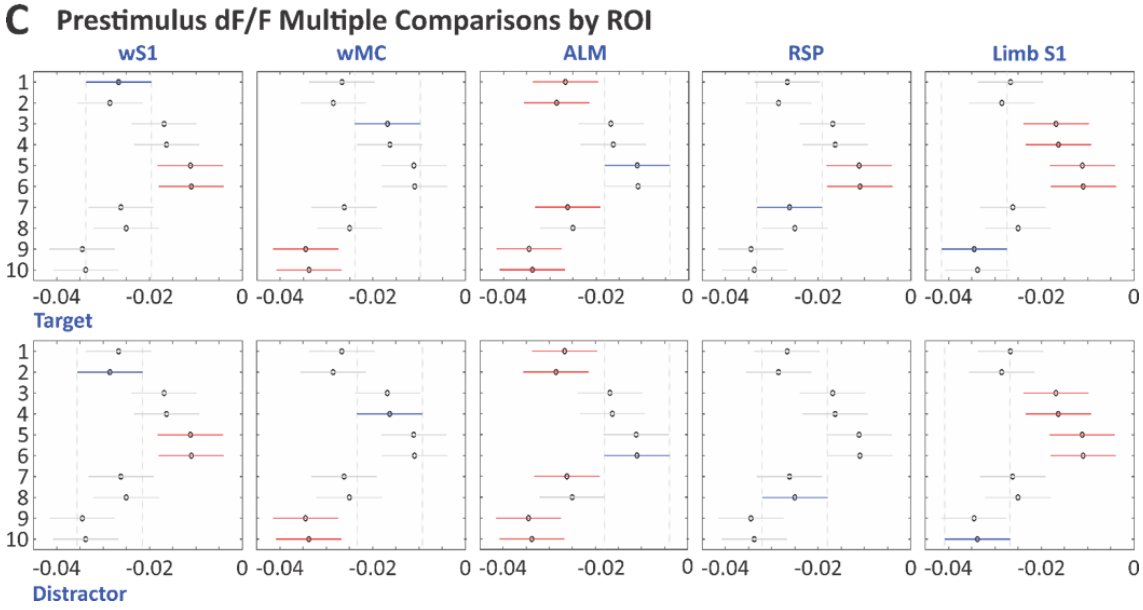

(A) Distribution of prestimulus fluorescence activity (dF/F) for Hits-Miss across target and distractor regions of interest (ROIs). Note that negative Hits-Miss indicates higher dF/F for no response trial. Outliers (+) in red. Defined ROIs are significantly different from zero (one-sample t-test, $p<0.01$) and significantly different across regions (one-way ANOVA, $p<0.01$). Table lists ROIs by corresponding number [A-C]. (B) Example multiple comparison (Tukey-Kramer) test on example ROI (target ALM). (C) Multiple comparison (Tukey-Kramer) test across ROIs shows that bilateral dF/F Hit-Miss differences in frontal cortical regions (wMC and ALM) are significantly smaller (as shown in A) than parietal cortical regions (wS1, RSP, and limb S1). ROI selected for comparison (blue); ROIs significantly different from selected ROI (red); ROIs not significantly different from selected ROI (gray).

Supplemental Figure 3.4, Related to Figure 3.3: Absence of regional differences in correlations between prestimulus fluorescence activity and reaction times

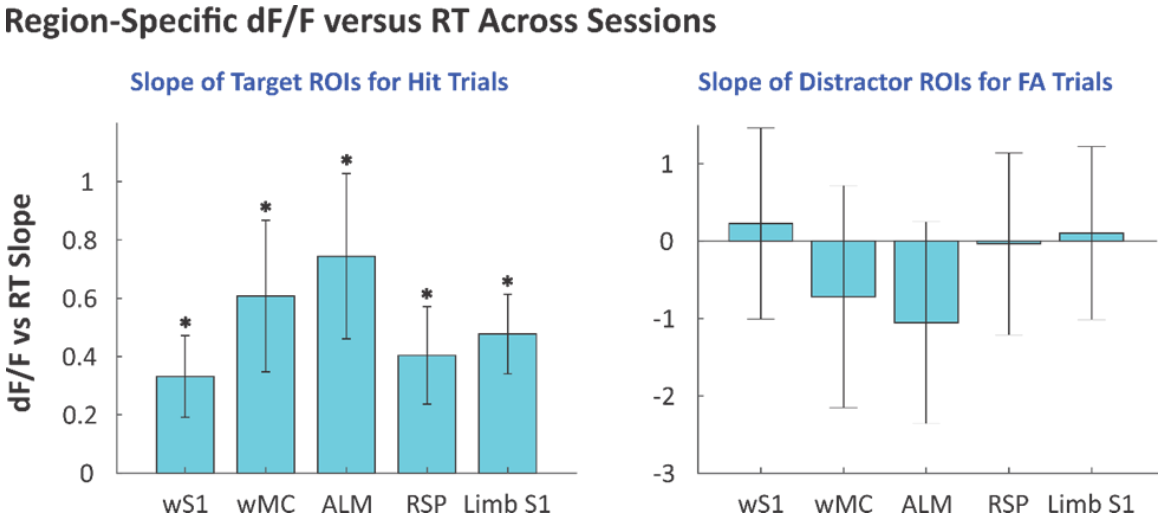

Prestimulus fluorescence activity (dF/F) versus reaction time (RT) slopes are calculated based on linear regression of each region of interest (ROI) across sessions for Hits (left) and FA (right). Hit trials across sessions show that all target aligned ROIs have significantly positive slopes (one-sample t-test) but not different slopes (one-way ANOVA), indicating a lack of regional differences in the relationships between prestimulus dF/F and post-stimulus RT. In contrast, for FA trials, none of the distractor aligned ROIs demonstrated significant correlations between prestimulus dF/F and post-stimulus RT.

Supplemental Figure 3.5, Related to Figure 3.3: Long-range spatial correlations preceding no response trials are larger and more widespread than preceding response trials

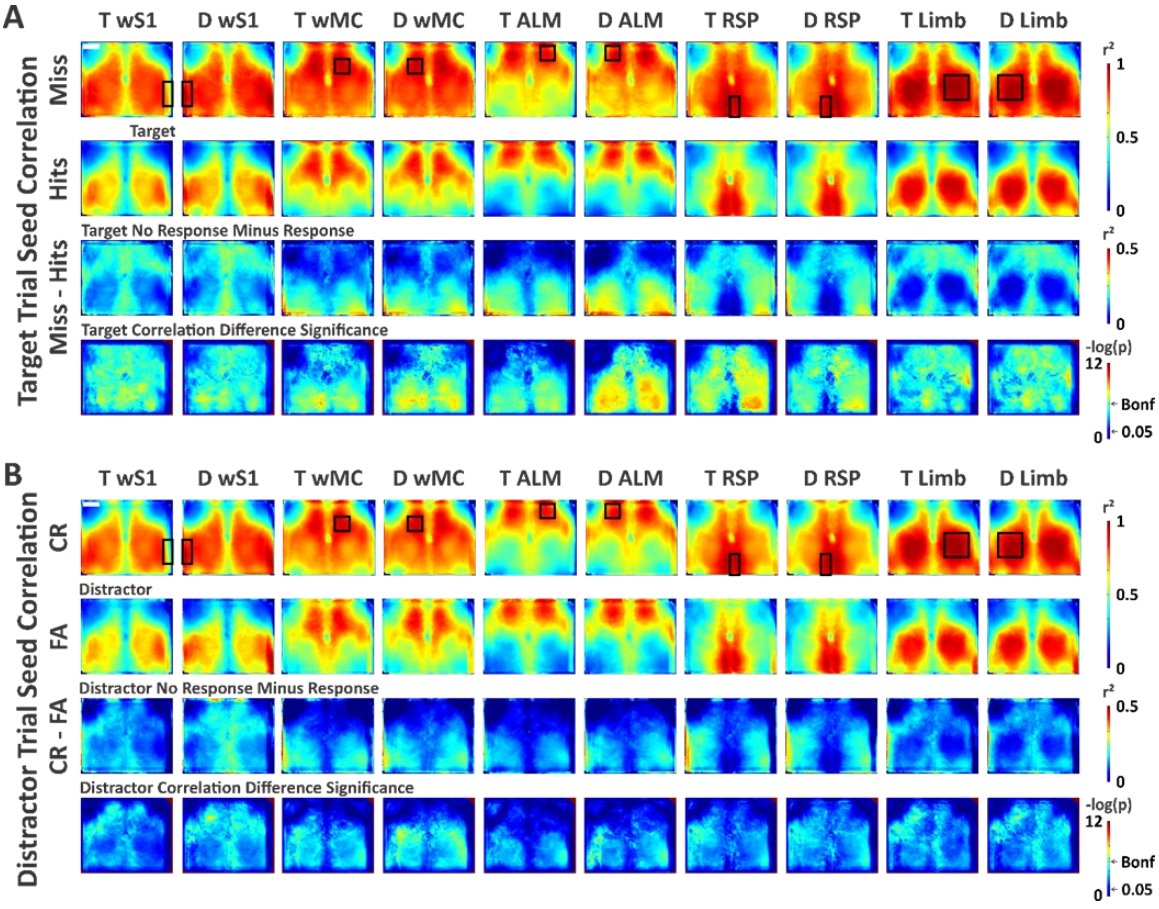

(A) Seed regions of interest are marked and labeled according to target (T) or distractor (D) stimulus alignment: wS1, wMC, ALM, RSP, and limb S1 seed rectangles (black). First row is no response target trials (miss), second row is response target trials (hits), third row is difference in correlation between no response and response trial types, fourth row is significance map for data in third row. (B) Same structure as [A], except for CR and FA trials.

Supplemental Figure 3.6, Related to Figure 3.8: Relationship between Spike Rate and Prestimulus Choice Probability and Post-Stimulus Sensory and Pre-Response Motor Encoding across Single Units in S1, wMC and ALM

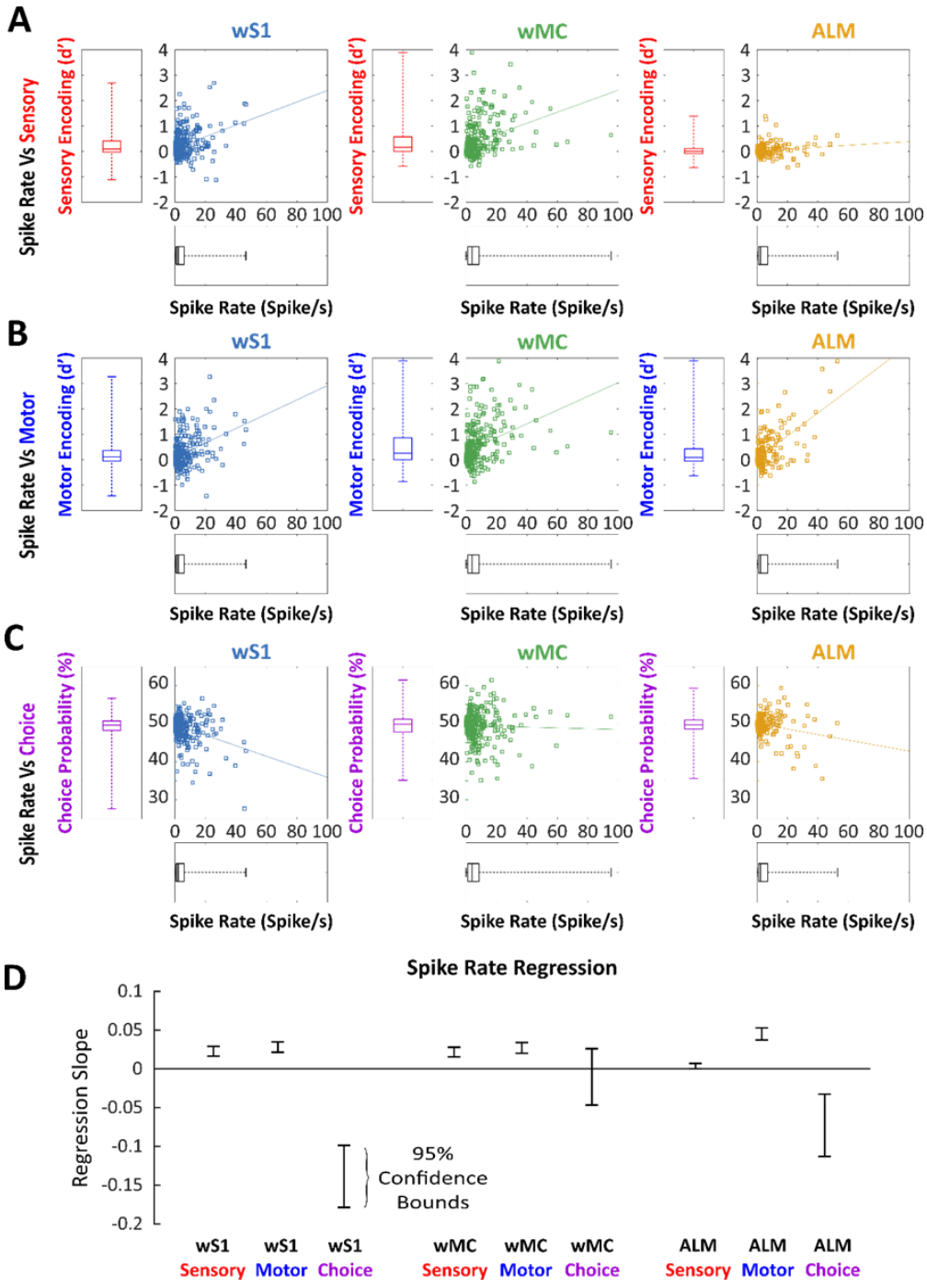

(A) Plots of sensory encoding (d') versus spike rate (Hz) for single units in target aligned S1 (left), wMC (center), and ALM (right). Scatter plots include linear fits of the single unit data. Single units in each of these three cortical regions show a positive relationship between spike rate and post-stimulus sensory encoding. (B and C) Same as [A], but for pre-response motor encoding (B) and prestimulus choice probability (C). (D) 95% confidence bounds of the linear regression slope values for all scatter plots. These data identify spike rate as a common factor that correlates with both post-stimulus sensory and motor encoding (positive correlation) and prestimulus choice probability (negative correlation).

Supplemental Figure 3.7, Related to Figure 3.9: Lack of differences in LFP power and spike triggered average LFP power preceding FA compared to CR trials

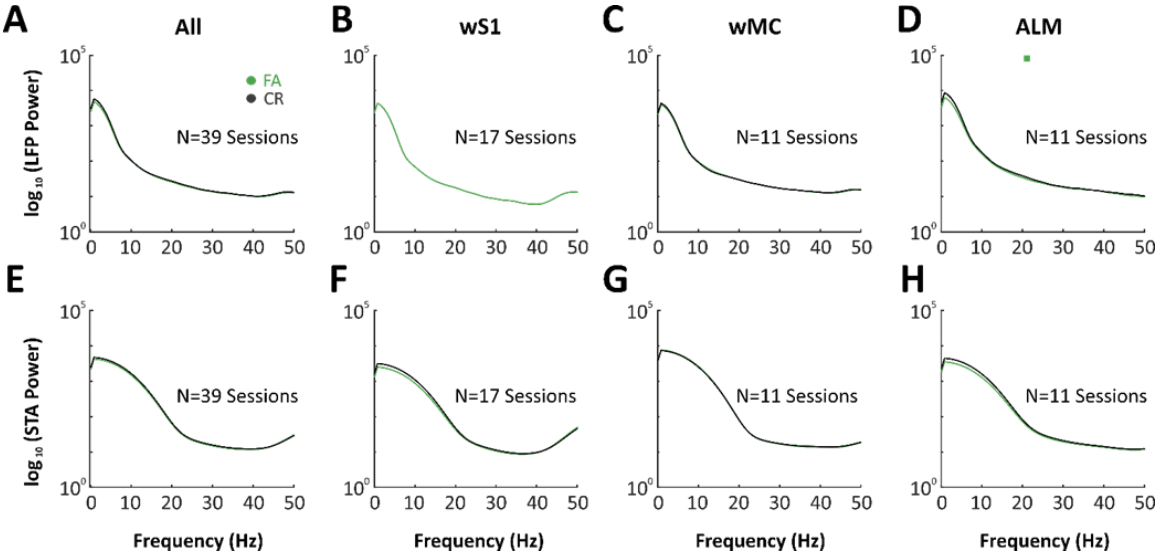

(A-D) Power spectra for local field potentials (LFPs) recorded from layer 5 across target aligned regions combined (A) and separately calculated for (B) wS1, (C) wMC and (D) ALM. Bars above plots reflect significance using paired t-test ($p<0.01$) for each frequency. Color of bar indicates direction of difference between LFP traces (green for FA larger than CR, black for CR larger than FA). (E, F, G, and H) Same as in [A, B, C, and D], except for power spectra calculated from spike triggered average (STA) LFPs.

Chapter 4: Multiple Object-Based and Temporal Strategies Across Learning

Most of the previous work investigated expert performing mice (as defined by a threshold of discrimination between target and distractor stimulus greater than one for three days in a row). The discrimination threshold was crucial in standardizing lab wide interpretations of decision making behavior in mice, and therefore neural correlates of their behavior. However, especially when presenting widefield imaging results, we were often asked about behavior and neuronal investigation into both learning and sex specificity. This working manuscript addresses learning strategies as observed in behavior readouts for a selective detection task. We took a longitudinal dataset and investigated not only discrimination, but multiple alternate and/or hybrid strategies that mice could employ across learning. We also further explored potential sex differences in these learning strategies.

Here, we establish learning behavior of mice as they transition from naïve to expert status for the selective detection task. Importantly, the consideration of both object-based and temporal features in learning allows us to interpret mouse behavior more comprehensively. By identifying multiple strategy transitions and how they play out across learning, we set a stage to further investigate complex strategy formation for decision making paradigms.

Minor changes to this adapted chapter include ongoing edits as part of the pre-published work. Note: this manuscript has not yet been peer-reviewed.

Multiple Temporal and Object-Based Strategies Across Learning

Adapted from:

Multiple Temporal and Object-Based Strategies Across Learning for a Selective Detection Task in Mice

Abbreviated title: Temporal and object-based selective detection strategies across learning.

Authors: Krista Marrero[1], Krithiga Aruljothi[2], Behzad Zareian[2], Zhaoran Zhang[1], Edward Zagha[1,2]

[1] Neuroscience Graduate Program, [2] Department of Psychology, University of California Riverside, 900 University Avenue, Riverside CA 92521 USA

Correspondence to: edward.zagha@ucr.edu

Acknowledgements: This work was supported by the Whitehall Foundation (Research Grant 2017-05-71 to E.Z.) and the National Institutes of Health (R01NS107599 to E.Z.). We thank Drs. Hongdian Yang and Anubhuti Goel for many helpful discussions throughout the project. We thank Angelina Lam and Dr. Manas Kinra for valuable critique and collegial support.

Abstract

Goal-directed behavior paradigms inevitably involve temporal processes, such as anticipation, expectation, timing, waiting, and withholding. And yet, amongst the vast use of object-based task paradigms, characterizations of temporal features are often neglected. Here, we longitudinally analyzed mice from naïve to expert performance in a somatosensory selective detection task. In addition to tracking standard measures from signal detection theory, we also characterized learning of temporal features. We find that mice transition from general sampling strategies to stimulus detection and stimulus discrimination. During these transitions, mice learn to wait as they anticipate an expected stimulus presentation and to time their response after a stimulus presentation. By establishing and implementing standardized measures, we show that the development of waiting and timing in the task overlaps with learning of stimulus detection and discrimination. We also investigated sex differences in temporal and object-based trajectories of learning, finding that males learn strategies idiosyncratically and that females learn strategies more sequentially and stereotypically. Overall, our findings emphasize multiple temporal strategies in learning for an object-based task and highlight the importance of considering diverse temporal and object-based features when characterizing behavioral and neuronal aspects of learning.

Goal-directed behavior paradigms inevitably involve temporal processes, such as anticipation, expectation, timing, waiting, and withholding. And yet, amongst the vast use of object-based task paradigms, characterizations of temporal features are often

neglected. Here, we longitudinally analyzed mice from naïve to expert performance in a somatosensory selective detection task. In addition to tracking standard measures from signal detection theory, we also characterized learning of temporal features. We find that mice transition from general sampling strategies to stimulus detection and stimulus discrimination. During these transitions, mice learn to wait as they anticipate an expected stimulus presentation and to time their response after a stimulus presentation. By establishing and implementing standardized measures, we show that the development of waiting and timing in the task overlaps with learning of stimulus detection and discrimination. We also investigated sex differences in temporal and object-based trajectories of learning, finding that males learn strategies idiosyncratically and that females learn strategies more sequentially and stereotypically. Overall, our findings emphasize multiple temporal strategies in learning for an object-based task and highlight the importance of considering diverse temporal and object-based features when characterizing behavioral and neuronal aspects of learning.

Introduction

All behavior operates within a temporal structure. Moreover, temporal processes, such as anticipation, expectation, timing, waiting, and withholding, significantly impact performance on object-based tasks (Cravo et al., 2017; Grabenhorst et al., 2019; Guo et al., 2014). And yet, object-based versus temporal processes in behavioral tasks are often investigated in isolation from each other (Buhusi & Meck, 2005; Dent & Neill, 2012; Murakami et al., 2017; Narayanan et al., 2012; Paton & Buonomano, 2018; Richter & von Kortzfleisch, 2020; Womelsdorf & Fries, 2007). Understanding temporal processes may be particularly important in the study of neuropsychiatric disease. In disorders such as autism spectrum disorder (ASD), attention deficit hyperactivity disorder (ADHD), learning disorders, and schizophrenia, greater disparities are observed across temporal (interval estimation, perception) compared to object-based (frequency, localization, categorization, orientation, spatial) features (F. Bayard et al., 2020; Carroll et al., 2009; Eden et al., 1995; Lee et al., 2009; Meilleur et al., 2020; Pardey et al., 2009; Rubia et al., 2009; Toplak et al., 2006). For example, in a study of ADHD versus control children, deficits were not found in reporting visual stimulus detection. Rather, deficits were found in fixation and countermanding: ADHD children tended to demonstrate larger and more frequent breaks in visual fixation and increased errors, faster responses to go signals, and slower responses to stop signals (Hanisch et al., 2006).

For training in any object-based task, learning must occur for both object-based and temporal features. Object-based paradigms such as detection (Huber et al., 2012),

discrimination (Erlich et al., 2011; Pai et al., 2011; Rudebeck & Murray, 2008; Song et al., 2020), categorization (Freedman et al., 2003; Reinert et al., 2021), and sequencing (Jin & Costa, 2010; Smits-Bandstra & De Nil, 2007) require learning of temporal features such as anticipation (Chen et al., 2017; McClure et al., 2003), evidence accumulation (Churchland et al., 2011; Erlich et al., 2015; Roitman & Shadlen, 2002), impulse control (Peterson et al., 1999; Robbins & Dalley, 2017; Winstanley et al., 2004), reward discounting (Kable & Glimcher, 2007; Mar et al., 2011; Mobini et al., 2002), starting and stopping (Bari & Robbins, 2013; Hanisch et al., 2006), and temporal uncertainty (Daw et al., 2005; Fiorillo et al., 2003; Lawson et al., 2021; Mendonça et al., 2020). Moreover, learning may not track along a single continuum from naïve to expert but may involve transitions between intermediate strategies. For instance, just as optimal temporal strategies are learned, such as fast reaction times for a detection paradigm (Baunez & Robbins, 1997, 1999), suboptimal strategies must be unlearned, such as fast reaction times for a waiting paradigm (Narayanan et al., 2006; Reyes et al., 2020).

This investigation explores the relationship between learning of temporal and object-based features from naïve to expert performance for a selective sensory detection task in mice. Along with traditional measures of sensory detection, we address two specific temporal processes, waiting and timing, which are not typically studied in object-based tasks (Komiyama et al., 2010; McBurney-Lin et al., 2020; Ruff & Cohen, 2019; Xiong et al., 2015; Yang et al., 2019) and vice versa (Bakhurin et al., 2017; Droit-Volet et al., 2007; Kawai et al., 2015; Lak et al., 2014; Namboodiri et al., 2015; Shuler & Bear, 2006).

1) *Sampling versus Waiting*: naïve behavior involves high sampling and low waiting before stimulus presentation (Dickinson & Balleine, 1994; O'Doherty et al., 2003; Schoenbaum & Roesch, 2005). The null hypothesis predicts that sampling behavior and waiting behavior do not change while learning sensory detection and discrimination. An alternative hypothesis predicts that sampling behavior decreases and waiting behavior increases as performance improves. 2) *Reacting versus Timing*: due to response sampling, post-stimulus reaction times in naïve behavior are long and broadly distributed (Laubach et al., 2000; van Maanen et al., 2012). A reactive hypothesis predicts that with learning of sensory detection, reaction times decrease towards a biophysical response limit (Duan et al., 2015; Romo & Schultz, 1990; Schultz et al., 1993). An alternative timing hypothesis predicts the convergence of reaction times to a task-specific optimal response latency.

Additional questions addressed in this study focus on learning trajectories. During learning of a sensory detection task, do mice transition in stages of intermediate strategies? Do mice learn temporal features before, after, or in tandem with object-based features? Are there sex-specific transitions, intermediates, or orders of learning? By addressing these questions, we strive to better understand the temporal and object-based features that mice learn during different phases of training. With this knowledge, we will be better equipped to determine the neural mechanisms underlying temporal and object-based learning.

Here, we use temporal and object-based measures to track learning for a whisker-based selective detection task, with target or distractor whisker stimuli presented in

individual trials. We find transitions from suboptimal *sampling* to optimal *waiting* before a stimulus and to optimal *timing* after a stimulus. Additionally, we identify learning trajectories in which temporal and object-based feature learning overlap. Lastly, we identify sex-based differences in the order of learning, transition magnitudes, and intermediate strategies. These findings emphasize the importance of tracking multiple measures through learning, for a more comprehensive understanding of both learning behavior and its neural mechanisms.

Materials and Methods

Animals

Animal subjects

Experimental protocols have been approved by the IACUC of University of California, Riverside. The dataset used here include behavioral studies that have been previously reported (Aruljothi et al., 2020; Marrero et al., 2022; Zareian et al., 2023; Zareian et al., 2021; Zhang & Zagha, 2022). A wide variety of wild type and transgenic mice were considered for behavioral learning data. Male and female, wild type (C57BL/6J, JAX #000664; BALB/cByJ, JAX #001026), transgenic (Snap25-2A-GCaMP6s-D, JAX #025111; Thy1-ChR2-YFP, JAX #007612; VGAT-ChR2-EYFP, JAX #014548), and virus-injected adult mice were used (Arenkiel et al., 2007; Zhao et al., 2011). Mice were not under transgenic manipulation (e.g., optogenetic activation or Ca^{2+}-sensor imaging) during behavioral training. Mice were maintained in a 12-h light/dark cycle and animal behavior occurred during the light cycle. Mice were head-fixed before behavioral training began, as previously reported (Aruljothi et al., 2020; Zareian et al., 2021; Zhang & Zagha, 2022). Mice started behavioral training after a minimum of a 4-day recovery period from surgery.

Animal behavior

Training stages, metrics of learning, and criterion for expert performance in the Go/NoGo selective whisker detection task were as previously reported (Aruljothi et al., 2020). Briefly, head-fixed and water deprived mice learned on customized behavioral rigs. Behavioral data was collected using Arduino and custom MATLAB scripts (MathWorks,

MA). Target and distractor paddles were positioned symmetrically within the mouse whisker fields bilaterally. Mice reported stimulus detection by licking a centrally located lick port, positioned under the snout. Mice progress through classical conditioning (2-5 days) and operant conditioning (2-5 days) stages before entering the full task (Figure 4.1, see Aruljothi et al., 2020 for details). Data presented in this paper are exclusively from the full task, in which the task structure did not change through training.

In the full task, we implemented a variable intertrial interval (ITI) before a stimulus presentation to discourage spontaneous sampling. Lick bouts within the ITI were punished by ending the trial and beginning the next trial with a new ITI, randomly selected from a negative exponential distribution between 5.5 and 9.5 s. Target stimuli and distractor stimuli were presented on a probabilistic schedule, 20% and 80% respectively. Following the correct rejection of a distractor stimulus, the next ITI was randomly selected from a negative exponential between 0.2 and 1.9 s. We also implemented a short lockout period (200-300 ms) after a stimulus presentation to isolate sensory versus response-related activity. Responding during the lockout ended the current trial and initiated a full ITI. Lick bouts, reaction times, stimulus types, and trial outcome types were recorded throughout the task. Lick bouts were considered spontaneous (sampling) if they occurred within the ITI. Post-stimulus licking responses were considered hits if they occurred after a target whisker stimulus and during the response window (after the lockout). Post-stimulus licking responses were considered false alarms (FA) or premature (Preme) if they occurred after a distractor whisker stimulus or during the lockout window, respectively.

Hits (responses to target stimuli) were rewarded with ~5 µL of water, correct rejections (not responding to distractor stimuli) and correct withholdings (not responding during the catch trial) were rewarded with a shortened intertrial-interval (ITI) and a subsequent target trial. Only trials of task engagement periods within sessions were analyzed, with 'task engagement' defined as a minimum block of 10 minutes without a pause in licking greater than 60 seconds. If more than one engagement period was identified within a session, the longest engagement period was chosen for the subsequent analyses. Spontaneous rates per session were calculated as the percentage of trial types in which the mouse responded within 1 second before an impending stimulus. Response rates per session were calculated as the percentage of response trial outcome types across all stimulus trials. Measures based on signal detection theory were calculated,

$$d'_{Stimulus\ Detection} = z_{Response\ Rate} - 1.2 * (z_{Spontaneous\ Rate})$$
$$d'_{Discrimination\ Performance} = z_{Hit\ Rate} - z_{False\ Alarm\ Rate}$$
$$d'_{Target\ Detection} = z_{Hit\ Rate} - z_{Spontaneous\ Rate}$$
$$d'_{Distractor\ Detection} = z_{False\ Alarm\ Rate} - z_{Spontaneous\ Rate}$$
$$d'_{Premature\ Detection} = z_{Premature\ Rate} - 0.2 * (z_{Spontaneous\ Rate})$$
$$C_{Criterion\ Bias} = -0.5 * (z_{Hit\ Rate} + z_{False\ Alarm\ Rate})$$

Signal Detection - Equations 10-15

where z is the inverse normal distribution function.

Data inclusion criteria

We examined 120 mice with potential learning data but included only the 52 mice who met all criteria described below. First, mice were included if they learned the task, as defined by discrimination performance (d' between hit rate and false alarm rate) greater than one for three consecutive days. Second, mice were included if they learned

progressively: from naïve to expert performance in less than three weeks of training. Third, the data required a minimum of seven training sessions with a maximum 7-day gap between sessions. No more than seven sessions of consecutive expert behavior were analyzed.

For tercile and quintile learning data per mouse, each session was binned according to the exclusive integer value of total sessions divided by three and five, respectively. For performance learning data per mouse, each session was defined as naïve ($d'<0.8$), intermediate ($0.8<d'<1.2$), and expert ($d'>1.2$). The intermediate performance was considered because it highlighted performance near our learning threshold. This allowed for comparison of time in training (tercile or quintile) versus learning stage (performance), with the potential of identifying intermediate behavioral strategies. Sex-specificity in learning was studied according to available data on the sex of each mouse (available for 48 of the 52 total mice).

Behavioral learning analyses

Analyses were performed using standard MATLAB scripts. Linear regression analyses were used to determine slopes of behavioral outcome measures across sessions per mouse (Figures 4.2, 4.3, and Supplementary 4.1, 4.2). If linear slopes across mice were significantly positive, the transition was identified as 'increasing'; if linear slopes across mice were significantly negative, the transition was identified as 'decreasing'.

For individual trajectory analyses (Figures 4.4 and 4.5), interquintiles of maximum change were determined as the differential slopes across quintiles ($\Delta_{Trajectory}/\Delta_{quintile}$) per

mouse. Interquintiles were then binned categorically for interquintile analysis. Order of learning was specified by ordering the mean interquintiles across mice per measure.

Behavioral measures with non-redundant dynamics (Figure 4.6) were identified by correlation analyses (MATLAB function *corrcoef*) for measures across quintiles per mouse, and then averaged across mice. We considered the absolute value of the correlations to determine magnitude of correlation (or anticorrelation). High correlations indicated measures with similar dynamics; low correlations indicated measures with unique dynamics and were therefore included in pairwise trajectory analyses.

For pairwise trajectory analyses (Figures 4.6 and 4.7), innerquintile curvature was determined by first rectifying quintile points such that quintiles increased by the absolute value of consecutive interquintile changes, $+\text{abs}(\Delta_{\text{Trajectory}})$; rectified quintile points were then scaled to the interval [0 1]. Then, pairwise transition quintiles were plotted against each other. Innerquintile curvature was defined as the mean distance of pairwise quintile points 2, 3, and 4 to the line segment between pairwise quintile points 1 and 5 per mouse.

Strategies in Figure 4.8 were identified as combinations of individual measures, based on assessments of both individual and pairwise trajectory analyses.

Statistical analyses

Reproducibility of learning data

Session performance was reported for all learning sessions per mouse, jittered only for visualization and not for quantification. For interlick interval (ILI) analysis, the term 'sampling' was defined by the percent area under the histogram curve of spontaneous

lick bouts between zero and the minimum ITI per session. For most sessions, this was between zero and 5.5 seconds. The term 'waiting' was defined by the percent area under the histogram curve of stimulus responses between the minimum ITI per session and the maximum possible wait time for engaged behavior per session. For most sessions, this was between 5.5 and 14.6 seconds (9.5 s maximum ITI for distractor stimulus, 2.2 s for subsequent correct rejection trial, 1.9 s for maximum shortened ITI, 1 s for prestimulus trial window preceding a target stimulus). For rection time analyses, reaction times in premature trials were defined by the lockout period per session. For most mice, this was 0.2 seconds (0.3 seconds for 3 mice). Stimulus response trials were determined by reaction times greater than the lockout period and during the 1 second response window. Data are reported as mean ± standard error of the mean (SEM) unless otherwise noted. Cumulative probabilities per session, per tercile, per tercile per mouse, and by performance level were determined by cumulative distribution functions (CDFs), the normalized cumulative sum under ILI or RT distributions. Because interlick and reaction time distributions were not gaussian, the median values (instead of means) are reported. To report spread in reaction time distributions, the spread of ±34.1% from the median was used to emulate one standard deviation in the nongaussian distribution.

Statistics for learning data

All analyses, including statistics, were performed using standard and custom MATLAB scripts and visualized using CorelDRAW. One sample t-tests were used to determine if slopes across mice were significantly different from zero (MATLAB function *ttest*).

Nonparametric (interquintile of maximum change in trajectory) data were analyzed using the chi-square (χ^2) Kruskal-Wallis rank sum test (MATLAB function *kruskalwallis*) across all measures for all mice, male mice, and female mice. For the waiting measure specified by sex, Kruskal-Wallis rank sum was performed on the nonparametric waiting data for all males versus all females. Cross correlation analyses were performed for interquintiles of maximum change across all mice, across male mice, and across female mice, separately, by determining the correlation coefficient (MATLAB function *corrcoef*). Reported correlations are calculated from the mean correlation. One sample t-test was used for analyses of innerquintile curvature across all mice to test significant curvature difference from zero, Bonferroni corrected for multiple comparisons. For analysis of variance (ANOVA) statistical tests (balanced and unbalanced one-way ANOVA, two-way ANOVA, and longitudinal RANOVA), Tukey-Kramer post-hoc multiple comparisons were generated using function *multcompare* in MATLAB. Significance was assigned according to p-values <0.05. For visualization, asterisks are shown according to orders of p-values: *$p<0.05$, **$p<0.005$, ***$p<0.0005$.

Results

Learning strategies for a selective detection task. We used an object-based selective detection paradigm to investigate concurrent temporal strategies across learning in mice (Figure 4.1A). In this task, water-restricted mice learn to selectively respond to target paddle deflections in one whisker field (hit, rewarded with water delivery) and ignore distractor paddle deflections in the opposite whisker field (correct rejection). We impose a variable intertrial interval (ITI) between 5.5 and 9.5 s, chosen to reduce spontaneous sampling before stimulus presentation. Target and distractor stimuli were presented probabilistically; the correct rejection of a distractor stimulus initiated the next trial, a target trial preceded by a shortened 0.2 to 1.9 s ITI. Overall, mice must wait (withhold licking) across a duration of minimum 5.5 s (ITI_{min}) to maximum 14.6 s (ITI_{max}) to be presented with a target stimulus and opportunity for reward (Figure 4.1B). Prepotent responses during the ITI were defined as spontaneous sampling (Spont) and resulted in a resetting of the ITI. Additionally, we implemented a minimum 200 ms lockout period after a stimulus presentation. Therefore, mice were required to respond on target trials after this lockout period to trigger a reward. In our previous studies of this task, expert performance was determined solely by target and distractor stimulus discrimination. Given the temporal structures described above, here, we additionally test a waiting strategy by exploring interlick interval (ILI) distributions for all lick responses and we test a timing strategy by exploring reaction time (RT) distributions for responses to stimuli (Figure 4.1C).

In this study we present longitudinal data from 52 mice. An increase in discrimination (separation of hit rate and false alarm rate) across terciles of training sessions indicated a learning trajectory from naïve to expert performance (Figure 4.1D, unbalanced one-way $ANOVA_{d'TercDiscrim}$ $F(2,573)=167.49$, $p<0.0005$). Across the same training sessions, we also observed a decrease in criterion bias, indicating an increased tendency to respond across target and distractor trials (Figure 4.1E, unbalanced one-way $ANOVA_{TercCriterion}$ $F(2,573)=59.47$, $p<0.0005$).

Transition in waiting behavior. We next investigated the temporal strategy of sampling versus waiting across learning. We tested the hypothesis that, due to the variable ITI imposition, suboptimal sampling behavior (ILI shorter than ITI_{min}) decreases while optimal waiting behavior (ILI longer than ITI_{min} and shorter than ITI_{max}) increases across learning. These analyses address a temporal phenotype before target stimulus presentation. The null hypothesis is that mice do not change their sampling and waiting behavior across learning (Figure 4.2A). Alternatively, we expect a divergence in sampling and waiting behavior across learning (Figure 4.2B), indicating an improvement in waiting.

We identified sampling and waiting by defining a sampling criterion (spontaneous responding within the minimum ITI before a stimulus) and a waiting criterion (responding after successfully waiting for a stimulus). We investigated sampling versus waiting behavior across sessions binned as early, middle, and late tercile stages of training (Figure 4.2C-E). For 'all responses' (Figure 4.2C, including sampling and waiting), we note that early and late tercile counts of all lick responses are not significantly different; however,

responses increased significantly from early to middle terciles (Figure 4.2C, unbalanced one-way $ANOVA_{TercILICount}$ $F(2,573)=4.45$, $p=0.0121$). Sampling responses ($ILI<ITI_{min}$) significantly decreased from middle to late terciles with a nonsignificant increase between early and middle terciles (Figure 4.2D, unbalanced one-way $ANOVA_{TercSampCount}$ $F(2,573)=3.72$, $p=0.0249$). Waiting responses ($ITI_{min}<ILI<ITI_{max}$) increased significantly from early to middle terciles and remained elevated, with a nonsignificant increase from middle to late terciles (Figure 4.2E, unbalanced one-way $ANOVA_{TercWaitCount}$ $F(2,573)=22.20$, $p<0.0005$). Thus, all response distributions increased from early to middle terciles; sampling responses then decreased while waiting responses remained high from middle to late terciles.

To quantify sampling and waiting distributions, we calculated the area under the sampling curve and the area under the waiting curve and normalized by the total area under the 'all response' curve. This analysis generated sampling % AUC values and waiting % AUC values (Figure 4.2F). Sampling % AUC decreased significantly across all terciles (unbalanced one-way $ANOVA_{TercSamp\%AUC}$ $F(2,573)=24.19$, $p<0.0005$) and waiting % AUC increased significantly across all terciles (unbalanced one-way $ANOVA_{TercWait\%AUC}$ $F(2,573)=42.15$, $p<0.0005$). We also quantified waiting strategies per mouse by plotting % AUC for each session across learning and determining the slopes of a linear fit (Figure 4.2F). We found that sampling % AUC decreased significantly across sessions per mouse (one sample t-test $\mu_{mSamp\%AUC}=-2.003\pm0.386$, $p<0.0005$, $n=52$ mice) and that waiting % AUC increased significantly across sessions per mouse (one sample t-test

$\mu_{mWait\%AUC}$=2.248±0.353, p<0.0005, n=52 mice). Overall, these analyses demonstrate robust changes in prestimulus behavior, with progressive decreases in sampling and increases in waiting.

As waiting behavior improves, we would expect the ILI distribution to shift towards longer intervals (Figure 4.2G). We investigated the ILI cumulative distribution function (CDF) and found that it shifted rightward towards longer ILIs (plotted for all sessions across mice, averaged terciles for all mice, and averaged terciles across mice, Figure 4.2H-J, respectively). In addition to simply considering sessions (by terciles) in training, we also plotted these CDFs according to target-distractor stimulus discrimination performance, for naïve (d'<0.8), intermediate (0.8<d'<1.2), and expert (d'>1.2) behavior. Interestingly, we found that CDF curves during naïve and intermediate performance were similar, and markedly different from CDF curves during expert performance (Figure 4.2K). We quantified the shift in CDF curves by the median ILI across terciles and across performance (Figure 4.2L, unbalanced one-way $ANOVA_{TercMedSessILI}$ F(2,573)=14.87, p<0.0005; balanced one-way $ANOVA_{TercMedMiceILI}$ F(2,153)=7.34, p=0.0009; unbalanced one-way $ANOVA_{PerfMedSessILI}$ F(2,573)=20.34, p<0.0005; balanced one-way $ANOVA_{PerfMedMiceILI}$ F(2,141)=9.92, p<0.0005). These analyses indicate that mice do show improvements in waiting, but only during expert target-distractor discrimination performance. These comparisons of waiting and discrimination indicate potentially non-uniform learning trajectories for different task features, which we explore further below.

Transition in timing behavior. Next, we investigated the temporal strategy of reacting versus timing across learning. We test the hypothesis that, due to the post-stimulus lockout window, mice will transition from broad RT distributions to optimal timing behavior that aligns with the lockout duration. This addresses a temporal phenotype after a stimulus presentation. The null hypothesis predicts that mice learn to respond to a stimulus with the fastest RT distribution possible (reactive strategy, Figure 4.3A). Alternatively, we predict RT distributions to cluster at the lockout duration with decreased variance across learning (Figure 4.3B), indicating an improvement in timing.

We investigated reactive versus timing behavior by analyzing RT distributions across sessions and across tercile stages of training. We compared RT distributions for all stimulus responses (Figure 4.3C), for target premature responses (Figure 4.3D), and for target hit responses (Figure 4.3E). First, we describe response counts across training. Stimulus responses increased across training for all three distributions. For all stimulus responses, this was significant across all terciles (Figure 4.3C, unbalanced one-way $ANOVA_{TercStimResp}$ $F(2,573)=52.42$, $p<0.0005$; unbalanced one-way $ANOVA_{TercStimRT}$ $F(2,573)=51.11$, $p<0.0005$). Target premature responses increased significantly from early to middle terciles with a nonsignificant increase from middle to late terciles (Figure 4.3D, unbalanced one-way $ANOVA_{TercPremeTResp}$ $F(2,573)=9.90$, $p<0.0005$). Target hit responses increased across terciles as well (Figure 4.3E, unbalanced one-way $ANOVA_{TercHitsResp}$ $F(2,573)=105.66$, $p<0.0005$). Second, we note the timing of these distributions. All three response types increased their peak RT distribution at the 200 ms lockout restriction

across terciles. To quantify this, we measured the mean reaction time across sessions and terciles (Figure 4.3F). As predicted by both the reactive and timing hypotheses, hits RTs significantly decreased across terciles (unbalanced one-way $ANOVA_{TercHitsRT}$ $F(2,569)=100.51$, $p<0.0005$). As uniquely predicted by the timing hypothesis, target premature RTs significantly increased from early to late terciles (unbalanced one-way $ANOVA_{TercPremeTRT}$ $F(2,545)=5.09$, $p=0.0065$). We also quantified timing per mouse by plotting outcome-based RT for each session across learning and determining the slopes of a linear fit (Figure 4.3F). We found that target premature RTs significantly increased while target hit RTs significantly decreased across sessions per mouse (one sample t-test $\mu_{mPremeTRT}=0.003\pm0.001$, $p=0.0008$; $\mu_{mHitsRT}=-0.023\pm0.002$, $p<0.0005$, $n=52$ mice). Although false alarm counts increased from early to middle tercile, all other distractor counts and RTs showed no difference across sessions or terciles (Supplementary Figure 4.1, unbalanced one-way $ANOVA_{TercFAResp}$ $F(2,573)=5.64$, $p=0.0038$). Additionally, distractor RTs did not change with training (Supplementary Figure 4.1C). These analyses demonstrate robust changes in post-stimulus behavior, with a bidirectional target RT change for precise timing as required by the lockout window.

As timing behavior improves, we would expect an RT distribution to shift towards the lockout duration with decreased variance (Figure 4.3G). We investigated the RT CDF and found it to shift left and decrease in variance across sessions, across mice, and across terciles towards the lockout period (Figure 4.3H-J). As described above, we also plotted CDF curves according to target-distractor stimulus discrimination. Interestingly, we found

that RT CDF curves during naïve performance differed dramatically from CDF curves during intermediate and expert performance (Figure 4.3K). We quantified the shift in CDF curves by the median RT for both terciles and performance (Figure 4.3L, unbalanced one-way $ANOVA_{TercMedSessRT}$ $F(2,573)=48.44$, $p<0.0005$; balanced one-way $ANOVA_{TercMedMiceRT}$ $F(2,153)=22.77$, $p<0.0005$; unbalanced one-way $ANOVA_{PerfMedSessRT}$ $F(2,573)=159.34$, $p<0.0005$; balanced one-way $ANOVA_{PerfMedMiceRT}$ $F(2,141)=34.35$, $p<0.0005$). We quantified the variance in CDF curves by the spread from the median RT for both terciles and performance (unbalanced one-way $ANOVA_{TercSpreadSessRT}$ $F(2,573)=103.59$, $p<0.0005$; balanced one-way $ANOVA_{TercSpreadMiceRT}$ $F(2,153)=44.73$, $p<0.0005$; unbalanced one-way $ANOVA_{PerfSpreadSessRT}$ $F(2,573)=304.11$, $p<0.0005$; balanced one-way $ANOVA_{PerfSpreadMiceRT}$ $F(2,141)=68.69$, $p<0.0005$). These analyses indicate that mice do show improvements in timing. Unlike waiting behavior, improvements in timing appeared to lead expert target-distractor discrimination, providing further evidence for potential intermediate stages in learning.

Order of learning for individual transition trajectories. Mice improved through training in object-based measures as determined by the slopes of their linear fits across sessions (Supplementary Figure 4.2). Hit rates significantly increased across sessions and FA rates significantly decreased across sessions (one sample t-test $\mu_{mHitRate}=5.141\pm0.525$, $p<0.0005$; $\mu_{mFARate}=-0.686\pm0.266$, $p=0.0128$, $n=52$ mice). As expected, suboptimal sampling decreased, as determined by reductions in spontaneous response rates (one sample t-test $\mu_{mSpontRate}=-0.448\pm0.168$, $p=0.0101$, $n=52$ mice). Additionally, we found that

overall target detection significantly increased across sessions (one sample t-test $\mu_{md'Target}$=0.178±0.018, p<0.0005; $\mu_{mTPremed'}$=0.036±0.020, p=0.0737, n=52 mice). Also expected, target-distractor discrimination significantly increased and target-distractor criterion bias significantly decreased (one sample t-test $\mu_{md'Discrim}$=0.183±0.016, p<0.0005; μ_{mCBias}=-0.070±0.012, p<0.0005, n=52 mice).

While analyzing temporal and object-based measure through training, we noticed that different measures displayed distinct learning trajectories across mice (Figure 4.4A). Furthermore, some trajectories appeared to lag or lead others; for example, stimulus responding increased before waiting with discrimination increasing in between the two (Figure 4.4B). We investigated these learning dynamics using two methods. For both analyses we segregated training sessions into quintiles. In our first analysis, for individual measures per mouse, we determined the interquintile showing the maximum change. For example, early learning would be reflected in a maximum change between the first two quintiles, late learning between the last two quintiles (Figure 4.4B). Next, we binned the interquintile of maximum change for all mice (Figure 4.4C). We found that some distributions clustered towards the 1st interquintile (e.g., stimulus response rate), some towards the 4th interquintile (e.g., waiting), and others appeared evenly distributed across mice (e.g., distractor d', Figure 4.4C).

We compared the distributions of interquintiles of maximum change. This analysis yielded an ordered learning across our selected measures (Figure 4.4D). We interpret this as evidence for sequential transitions in strategy across learning. Maximum increases in

stimulus response rates occurred significantly earlier than maximum increases in waiting ($\mu_{Resp\Delta max}$=1.98±0.13 versus $\mu_{Wait\Delta max}$=2.69±0.16, Kruskal-Wallis p=0.03, n=52 mice). Maximum increases were not significantly different between other paired trajectories. We acknowledge three contributing explanations for the partially overlapping sequence. First, a number of these transitions co-fluctuate and may reflect overlapping learning strategies (explored further below). Second, different learning strategies may occur in overlapping time windows. Notably, the overlapping trajectories include both temporal and object-based measures. Third, lack of separation between measures may be due to variation in learning transitions across mice. Cross-correlations for interquintiles of maximum change demonstrated a statistically significant correlation across mice (p=0.0003) but with high variability (μ_{CorrR}=0.03, n=52 mice). Overall, this analysis demonstrates a partially structured learning sequence across multiple outcome measures, well beyond the single measure (target-distractor discrimination) that initially motivated this task design.

The broad distribution in interquintiles of maximum change led us to question whether biological differences accounted for learning variability. We therefore performed the same analyses as above, but separately for sex and genotype. We observed significant differences in interquintile distributions for male versus female mice (Figure 4.5). The mean interquintiles of maximum change for males appeared to be substantially clustered in comparison with females; females show a progression of learning where stimulus responding leads and waiting lags (Figure 4.5A, rank sum Kruskal-Wallis$_{Male}$ p=0.949, rank

sum Kruskal-Wallis$_{Female}$ p=0.0119). Notably, the interquintile of maximum change for waiting differed between males and females (Figure 4.5B, $\mu_{MaleWait\Delta max}$=2.39±0.20, $\mu_{FemaleWait\Delta max}$=3.24±0.26; rank sum Kruskal-Wallis$_{WaitMale|Female}$, p=0.0123). Main sex differences were found in stimulus responding, distractor detection, and prestimulus waiting (Figure 4.5C, unbalanced two-way ANOVA$_{Resp|Sex}$, p=0.034; ANOVA$_{d'Distract|Sex}$, p=0.0007; ANOVA$_{Wait|Sex}$, p=0.007). Additionally, we observed an interaction effect between sex and waiting (Figure 4.5C, bottom right, unbalanced two-way ANOVA$_{MaleWait|FemaleWait}$, p=0.024; longitudinal RANOVA$_{Sex|Wait}$, p=0.037), indicating different learning trajectories in males versus females for this measure. We recognize that the overlapping distributions of male mice could reflect either coincident learning or high variability across subjects resulting in broad distributions across the population. We find evidence for the latter. Female mice showed a small yet significant correlation in their interquintiles of maximum changes ($\mu_{CorrRFemale}$=0.104, p=0.0001, n=17 mice), indicating a shared learning structure. In contrast, male mice did not have correlated interquintiles of maximum change ($\mu_{CorrRMale}$=-0.027 p=0.53, n=31 mice), suggesting more variable (and idiosyncratic) learning profiles. Analyses of temporal and object-based measures identified significant genotype differences in timing, spontaneous response rates, and waiting across learning quintiles, but we did not pursue this further (Supplementary Figure 4.3, RANOVA$_{Gene|Time}$, p=0.0049, RANOVA$_{Gene|Spont}$, p=0.045, RANOVA$_{Gene|Wait}$, p=0.0045).

Order of learning for pairwise transition trajectories. Our second method of quantifying learning dynamics involved pair-wise comparisons of temporal or object-based measures. First, we used pairwise correlation analyses to determine patterns of shared variance between measures within individual mice (Figure 4.6A). For further pairwise analyses, we selected measures with low shared variance: stimulus responding, discrimination, timing, distractor detection, and waiting. For these measures, we determined their relational order of learning by plotting their trajectories against each other. Based on the curvature of the pairwise comparisons, we could identify leading, lagging, or co-occurring learning transitions (Figure 4.6B). We defined an inner (within) quintile distance per mouse by calculating the mean of the 2^{nd}, 3^{rd}, and 4^{th} quintile points to the linear fit between the 1^{st} and 5^{th} pairwise quintile segment. A significant deviation from zero of innerquintile distances would indicate a 'curvature' and thereby an order of learning between the pairwise measures.

By summing curvature columns across pairwise comparisons, we could approximate orders of learning across mice (Figure 4.6C). Consistent with the binned interquintile order of learning, the pairwise curvature analysis ordered stimulus responding before waiting (Figure 4.6D, $d_{Resp|Wait}$=-0.25 a.u., p=0.0001). Additionally, this analysis identified that stimulus responding leads discrimination and distractor detection, and that waiting lags timing (Bonferroni corrected: $d_{Resp|Discrim}$=-0.32 a.u., p<0.0005; $d_{Resp|d'Distract}$=-0.19 a.u., p=0.011; $d_{Time|Wait}$=-0.12 a.u., p=0.022). While we do observe some differences in the precise ordering of learning, both approaches indicate a learning structure where

stimulus responding leads and waiting lags. Accordingly, potential intermediates consist of both temporal and object-based measures.

As with interquintile of maximum change distributions, the broad distribution of innerquintile curvature led us to analyze sex-specific differences in learning variability (Figure 4.7). Therefore, we conducted the curvature analyses separately for male and female mice, and again observed substantial differences in the ordering and clustering of the learned measures (Figure 4.7A). For the normalized quintile magnitudes, analyzing sex-specific longitudinal trajectories revealed that male mice transitioned their timing, distractor detection, and waiting behavior differently in comparison with female mice (Figure 4.7B, $RANOVA_{Sex|Time}$, p=0.042; $RANOVA_{Sex|d'Distract}$, p=0.038; $RANOVA_{Sex|Wait}$, p=0.0046). Like the interquintile findings, innerquintile curvature analyses showed that female mice, but not male mice, increased their stimulus response rates before they increased waiting (Figure 4.7C, Bonferroni corrected: $d_{FemaleResp|Wait}$=-0.13 a.u., p=0.010; $d_{MaleResp|Wait}$=-0.048 a.u., p=0.19; unbalanced two-way $ANOVA_{SexResp|Wait}$, p=0.025). Thus, both analytical measures demonstrate structure in ordered learning, with prominent sex differences in learning profiles.

Discussion

In this study we have shown changes in multiple temporal and object-based measures across learning as mice transition from naïve to expert performance during a whisker-based selective detection task. Regarding temporal measures, mice learn to both wait for a target stimulus and time after a target stimulus (Figure 4.2, Figure 4.3). Using individual trajectory (Figure 4.4) and pairwise trajectory (Figure 4.6) analyses, we identify structure in the changes of these measures that suggest an order or progression of learning. Interestingly, both approaches identify notable sex differences in learning, where females show more stereotypic progressions (Figures 4.5 and 4.7).

Based on our findings, we suggest that mice to not progress uniformly from naïve to expert across a single outcome measure (in our task, target-distractor discrimination). Instead, our data are more consistent with mice progressing through intermediate strategies. Based on our learning trajectory analyses, we propose a structure of learning that involves four distinct, yet temporally overlapping, behavior strategies or profiles as mice progress from naïve to expert performance (Figure 4.8). The first strategy of "naïve sampling" involves a general increase in responding, both before and after stimulus presentation. Evidence for this strategy includes an increase in all responding between early and middle terciles (Figure 4.2C,D,E) and the consistent finding across analyses of increased stimulus responding leading all other measures (Figure 4.4C,D), followed closely by criterion bias. From a strategy of "naïve sampling", mice progress to "stimulus timing" (Figure 4.6C). The hallmark of this strategy is an improvement in RT, which

ultimately centers around the onset of the response window (Figure 4.3D,E,F). The centering of RTs indicates that mice are responding to task-relevant stimuli, even if they continue high levels of random sampling. Mice then progress to "object-based performance", indicated by increases in specific responding to target stimuli (Figures 4.4D and 4.6C). Relevant measures of this strategy include increases in target detection and target-distractor discrimination (Figure 4.4A). Last is the strategy of "waiting and withholding". This stage of learning is evidenced by decreases in distractor detection and spontaneous responding and an improvement in waiting, which consistently lags in the progression (Figures 4.4C,D and 4.6C,D). In our task design, mice must wait between 5.5 to 14.6 seconds to receive a target stimulus and opportunity for reward. Therefore, waiting (not responding) through this ITI is critical for success in the task. And yet, increased waiting is typically the lagging transition in learning. This suggests that mice do not abandon a random sampling strategy until they are proficient in stimulus discrimination.

It is currently unclear whether these four strategies are truly discrete processes involving different neural mechanisms, and the extent to which these strategies generalize to different behavioral tasks. However, our findings strongly encourage taking a broader approach to the study of learning than is typically reported in behavioral neuroscience investigations. We identify three major reasons for promoting this approach. First, if there is an orderly progression of learning, then identifying the learning stages will aid in tracking the learning process. Second, and relatedly, mouse models of neuropsychiatric

disease show learning deficits in goal-directed tasks (Goel et al., 2018; Hölter et al., 2015; Huynh et al., 2009; Remmelink et al., 2016). Are learning deficits due to failed progression across a specific stage of learning? Do different disease models fail at different learning stages, suggesting process-specific dysfunctions? Third, and perhaps most importantly, a growing number of studies are aimed at revealing the neuronal mechanisms underlying task learning (Huber et al., 2012; Lacefield et al., 2019; Le Merre et al., 2018; Makino et al., 2017; Roy et al., 2021). For example, increased activity in a brain region across learning in our task may be interpreted as a mechanism of target-distractor discrimination. However, considering this study, we recognize that changes in neuronal activity may also be related to general responding, timing, or impulse control (for both spontaneous and sensory-evoked responding). In future studies, correlating the trajectories of behavioral and neuronal measures may vastly improve our ability to identify the neuronal mechanisms underlying specific learning processes, and make more precise predictions about the effects of causal neuronal manipulations on learning outcomes.

Behavior modeling can confirm this potential, tracking task related performance processes across learning (Roy et al., 2021). Recent studies have provided great insights regarding strategies in expert performance with discrete state analyses (Ashwood et al., 2022; Pisupati et al., 2021). These types of analyses can be applied to the study of mixed (intermediate) states overlapping object-based and temporal strategies in learning. Even so, the investigation of learning strategies is often based on models presumed before interpretation. In this study, we do not predefine strategies in learning, only what can be

inferred by behavior output measures. Our findings are empirical, identifying model-free mixed strategies, which may indicate intermediate neural mechanisms. With these approaches, considering raw behavioral measures enables impartial identification of diverse behavioral strategies across animal models and task paradigms.

Another insight from this study is the importance of considering temporal processes in object-based tasks. Our ITI distributions were meant to reduce temporal expectancy of target stimulus delivery (Coull et al., 2011; Fiorillo et al., 2008; Ghose & Maunsell, 2002; Nobre et al., 2007; Zariwala et al., 2013). Nevertheless, there remains temporal regularity in the structure of all behavioral tasks. Subjects may learn these temporal regularities to improve task performance by predicting windows of opportunity in task structure (Komiyama et al., 2010). However, subjects may also exploit these temporal regularities to solve a task in a way that was unintended (Kawai et al., 2015). By considering temporal processes in object-based tasks, researchers may reveal understudied task dimensions that are critical for optimal performance and strongly contribute to behavioral dysfunctions in neuropsychiatric disease (Emmons et al., 2017; Grondin, 2010; Toplak et al., 2006).

Across mice we recognize high variability in changes in performance measures, suggesting high variability in the progression through learning strategies. While expert mice converge to the same strategy (high discrimination, improved waiting, improved timing), individual mice do vary in their paths to expert performance. We are just beginning to explore the reasons for these individual differences. We note sex-based similarities and differences

in learning trajectories. In both male and female mice, the strategy of naïve sampling tended to lead the other three strategies. For acquisition of the other three strategies, male mice were more idiosyncratic resulting in overlapping distributions of outcome measures, whereas females displayed more sequential stereotypy (Figure 4.5A, Figure 4.7A, Figure 4.8). Another interesting difference is a dissociation in two types of impulse control; female mice displayed lower distractor detection whereas male mice displayed higher ability to wait (Figure 4.5C). We do not know the cause of these sex differences, but they may relate to reported differences in novel environment exploration, in which females demonstrate more cautious (systematic) versus more risky (exploratory) decision-making behavior (Gagnon et al., 2016; Gagnon et al., 2018).

References

Arenkiel, B. R., Peca, J., Davison, I. G., Feliciano, C., Deisseroth, K., Augustine, George J. J., Ehlers, M. D., & Feng, G. (2007). In Vivo Light-Induced Activation of Neural Circuitry in Transgenic Mice Expressing Channelrhodopsin-2. *Neuron*, *54*(2), 205-218. https://doi.org/10.1016/j.neuron.2007.03.005

Aruljothi, K., Marrero, K., Zhang, Z., Zareian, B., & Zagha, E. (2020). Functional Localization of an Attenuating Filter within Cortex for a Selective Detection Task in Mice. *The Journal of Neuroscience*, *40*(28), 5443-5454. https://doi.org/10.1523/jneurosci.2993-19.2020

Ashwood, Z. C., Roy, N. A., Stone, I. R., International Brain, L., Urai, A. E., Churchland, A. K., Pouget, A., & Pillow, J. W. (2022). Mice alternate between discrete strategies during perceptual decision-making. *Nat Neurosci*, *25*(2), 201-212. https://doi.org/10.1038/s41593-021-01007-z

Bakhurin, K. I., Goudar, V., Shobe, J. L., Claar, L. D., Buonomano, D. V., & Masmanidis, S. C. (2017). Differential Encoding of Time by Prefrontal and Striatal Network Dynamics. *J Neurosci*, *37*(4), 854-870. https://doi.org/10.1523/JNEUROSCI.1789-16.2016

Bari, A., & Robbins, T. W. (2013). Inhibition and impulsivity: behavioral and neural basis of response control. *Prog Neurobiol*, *108*, 44-79. https://doi.org/10.1016/j.pneurobio.2013.06.005

Baunez, C., & Robbins, T. W. (1997). Bilateral Lesions of the Subthalamic Nucleus Induce Multiple Deficits in an Attentional Task in Rats [https://doi.org/10.1111/j.1460-9568.1997.tb01376.x]. *European Journal of Neuroscience*, *9*(10), 2086-2099. https://doi.org/https://doi.org/10.1111/j.1460-9568.1997.tb01376.x

Baunez, C., & Robbins, T. W. (1999). Effects of transient inactivation of the subthalamic nucleus by local muscimol and APV infusions on performance on the five-choice serial reaction time task in rats. *Psychopharmacology*, *141*(1), 57-65. https://doi.org/10.1007/s002130050806

Bayard, F., Nymberg Thunell, C., Abe, C., Almeida, R., Banaschewski, T., Barker, G., Bokde, A. L. W., Bromberg, U., Buchel, C., Quinlan, E. B., Desrivieres, S., Flor, H., Frouin, V., Garavan, H., Gowland, P., Heinz, A., Ittermann, B., Martinot, J. L., Martinot, M. P., . . . Consortium, I. (2020). Distinct brain structure and behavior related to ADHD and conduct disorder traits. *Mol Psychiatry*, *25*(11), 3020-3033. https://doi.org/10.1038/s41380-018-0202-6

Buhusi, C. V., & Meck, W. H. (2005). What makes us tick? Functional and neural mechanisms of interval timing. *Nat Rev Neurosci*, *6*(10), 755-765. https://doi.org/10.1038/nrn1764

Carroll, C. A., O'Donnell, B. F., Shekhar, A., & Hetrick, W. P. (2009). Timing dysfunctions in schizophrenia as measured by a repetitive finger tapping task. *Brain Cogn*, *71*(3), 345-353. https://doi.org/10.1016/j.bandc.2009.06.009

Chen, T. W., Li, N., Daie, K., & Svoboda, K. (2017). A Map of Anticipatory Activity in Mouse Motor Cortex. *Neuron*, *94*(4), 866-879 e864. https://doi.org/10.1016/j.neuron.2017.05.005

Churchland, A. K., Kiani, R., Chaudhuri, R., Wang, X. J., Pouget, A., & Shadlen, M. N. (2011). Variance as a signature of neural computations during decision making. *Neuron*, *69*(4), 818-831. https://doi.org/10.1016/j.neuron.2010.12.037

Coull, J. T., Cheng, R. K., & Meck, W. H. (2011). Neuroanatomical and neurochemical substrates of timing. *Neuropsychopharmacology*, *36*(1), 3-25. https://doi.org/10.1038/npp.2010.113

Cravo, A. M., Rohenkohl, G., Santos, K. M., & Nobre, A. C. (2017). Temporal Anticipation Based on Memory. *J Cogn Neurosci*, *29*(12), 2081-2089. https://doi.org/10.1162/jocn_a_01172

Daw, N. D., Niv, Y., & Dayan, P. (2005). Uncertainty-based competition between prefrontal and dorsolateral striatal systems for behavioral control. *Nat Neurosci*, *8*(12), 1704-1711. https://doi.org/10.1038/nn1560

Dent, M. F., & Neill, D. B. (2012). Dose-dependent effects of prefrontal dopamine on behavioral state in rats. *Behav Neurosci*, *126*(5), 620-639. https://doi.org/10.1037/a0029640

Dickinson, A., & Balleine, B. W. (1994). Motivational control of goal-directed action. *Animal Learning & Behavior*, *22*, 1-18.

Droit-Volet, S., Meck, W. H., & Penney, T. B. (2007). Sensory modality and time perception in children and adults. *Behav Processes*, *74*(2), 244-250. https://doi.org/10.1016/j.beproc.2006.09.012

Duan, C. A., Erlich, J. C., & Brody, C. D. (2015). Requirement of Prefrontal and Midbrain Regions for Rapid Executive Control of Behavior in the Rat. *Neuron*, *86*(6), 1491-1503. https://doi.org/10.1016/j.neuron.2015.05.042

Eden, G. F., Stein, J. F., Wood, H. M., & Wood, F. B. (1995). Temporal and Spatial Processing in Reading Disabled and Normal Children. *Cortex*, *31*(3), 451-468. https://doi.org/https://doi.org/10.1016/S0010-9452(13)80059-7

Emmons, E. B., De Corte, B. J., Kim, Y., Parker, K. L., Matell, M. S., & Narayanan, N. S. (2017). Rodent Medial Frontal Control of Temporal Processing in the Dorsomedial Striatum. *J Neurosci*, *37*(36), 8718-8733. https://doi.org/10.1523/JNEUROSCI.1376-17.2017

Erlich, J. C., Bialek, M., & Brody, C. D. (2011). A cortical substrate for memory-guided orienting in the rat. *Neuron*, *72*(2), 330-343. https://doi.org/10.1016/j.neuron.2011.07.010

Erlich, J. C., Brunton, B. W., Duan, C. A., Hanks, T. D., & Brody, C. D. (2015). Distinct effects of prefrontal and parietal cortex inactivations on an accumulation of evidence task in the rat. *Elife*, *4*. https://doi.org/10.7554/eLife.05457

Fiorillo, C. D., Newsome, W. T., & Schultz, W. (2008). The temporal precision of reward prediction in dopamine neurons. *Nat Neurosci*, *11*(8), 966-973. https://doi.org/10.1038/nn.2159

Fiorillo, C. D., Tobler, P. N., & Schultz, W. (2003). Discrete Coding of Reward Probability and Uncertainty by Dopamine Neurons. *Science*, *299*(5614), 1898-1902. https://doi.org/doi:10.1126/science.1077349

Freedman, D. J., Riesenhuber, M., Poggio, T., & Miller, E. K. (2003). A Comparison of Primate Prefrontal and Inferior Temporal Cortices during Visual Categorization. *The Journal of Neuroscience*, *23*(12), 5235-5246. https://doi.org/10.1523/jneurosci.23-12-05235.2003

Ghose, G. M., & Maunsell, J. H. R. (2002). Attentional modulation in visual cortex depends on task timing. *Nature*, *419*(6907), 616-620. https://doi.org/10.1038/nature01057

Goel, A., Cantu, D. A., Guilfoyle, J., Chaudhari, G. R., Newadkar, A., Todisco, B., de Alba, D., Kourdougli, N., Schmitt, L. M., Pedapati, E., Erickson, C. A., & Portera-Cailliau, C. (2018). Impaired perceptual learning in a mouse model of Fragile X syndrome is mediated by parvalbumin neuron dysfunction and is reversible. *Nature Neuroscience*, *21*(10), 1404-1411. https://doi.org/10.1038/s41593-018-0231-0

Grabenhorst, M., Michalareas, G., Maloney, L. T., & Poeppel, D. (2019). The anticipation of events in time. *Nature Communications*, *10*(1), 5802. https://doi.org/10.1038/s41467-019-13849-0

Grondin, S. (2010). Timing and time perception: a review of recent behavioral and neuroscience findings and theoretical directions. *Atten Percept Psychophys*, *72*(3), 561-582. https://doi.org/10.3758/APP.72.3.561

Guo, Z. V., Li, N., Huber, D., Ophir, E., Gutnisky, D., Ting, J. T., Feng, G., & Svoboda, K. (2014). Flow of cortical activity underlying a tactile decision in mice. *Neuron*, *81*(1), 179-194. https://doi.org/10.1016/j.neuron.2013.10.020

Hanisch, C., Radach, R., Holtkamp, K., Herpertz-Dahlmann, B., & Konrad, K. (2006). Oculomotor inhibition in children with and without attention-deficit hyperactivity disorder (ADHD). *J Neural Transm (Vienna)*, *113*(5), 671-684. https://doi.org/10.1007/s00702-005-0344-y

Hölter, S. M., Garrett, L., Einicke, J., Sperling, B., Dirscherl, P., Zimprich, A., Fuchs, H., Gailus-Durner, V., Hrabě de Angelis, M., & Wurst, W. (2015). Assessing Cognition in Mice [https://doi.org/10.1002/9780470942390.mo150068]. *Current Protocols in Mouse Biology*, *5*(4), 331-358. https://doi.org/https://doi.org/10.1002/9780470942390.mo150068

Huber, D., Gutnisky, D. A., Peron, S., O'Connor, D. H., Wiegert, J. S., Tian, L., Oertner, T. G., Looger, L. L., & Svoboda, K. (2012). Multiple dynamic representations in the motor cortex during sensorimotor learning. *Nature*, *484*(7395), 473-478. https://doi.org/10.1038/nature11039

Huynh, D. P., Maalouf, M., Silva, A. J., Schweizer, F. E., & Pulst, S. M. (2009). Dissociated Fear and Spatial Learning in Mice with Deficiency of Ataxin-2. *PLoS One*, *4*(7), e6235. https://doi.org/10.1371/journal.pone.0006235

Jin, X., & Costa, R. M. (2010). Start/stop signals emerge in nigrostriatal circuits during sequence learning. *Nature*, *466*(7305), 457-462. https://doi.org/10.1038/nature09263

Kable, J. W., & Glimcher, P. W. (2007). The neural correlates of subjective value during intertemporal choice. *Nat Neurosci*, *10*(12), 1625-1633. https://doi.org/10.1038/nn2007

Kawai, R., Markman, T., Poddar, R., Ko, R., Fantana, A. L., Dhawale, A. K., Kampff, A. R., & Olveczky, B. P. (2015). Motor cortex is required for learning but not for executing a motor skill. *Neuron*, *86*(3), 800-812. https://doi.org/10.1016/j.neuron.2015.03.024

Komiyama, T., Sato, T. R., O'Connor, D. H., Zhang, Y. X., Huber, D., Hooks, B. M., Gabitto, M., & Svoboda, K. (2010). Learning-related fine-scale specificity imaged in motor

cortex circuits of behaving mice. *Nature*, *464*(7292), 1182-1186. https://doi.org/10.1038/nature08897

Lacefield, C. O., Pnevmatikakis, E. A., Paninski, L., & Bruno, R. M. (2019). Reinforcement Learning Recruits Somata and Apical Dendrites across Layers of Primary Sensory Cortex. *Cell Rep*, *26*(8), 2000-2008 e2002. https://doi.org/10.1016/j.celrep.2019.01.093

Lak, A., Costa, G. M., Romberg, E., Koulakov, A. A., Mainen, Z. F., & Kepecs, A. (2014). Orbitofrontal cortex is required for optimal waiting based on decision confidence. *Neuron*, *84*(1), 190-201. https://doi.org/10.1016/j.neuron.2014.08.039

Laubach, M., Wessberg, J., & Nicolelis, M. A. L. (2000). Cortical ensemble activity increasingly predicts behaviour outcomes during learning of a motor task. *Nature*, *405*(6786), 567-571. https://doi.org/10.1038/35014604

Lawson, R. P., Bisby, J., Nord, C. L., Burgess, N., & Rees, G. (2021). The Computational, Pharmacological, and Physiological Determinants of Sensory Learning under Uncertainty. *Curr Biol*, *31*(1), 163-172 e164. https://doi.org/10.1016/j.cub.2020.10.043

Le Merre, P., Esmaeili, V., Charriere, E., Galan, K., Salin, P. A., Petersen, C. C. H., & Crochet, S. (2018). Reward-Based Learning Drives Rapid Sensory Signals in Medial Prefrontal Cortex and Dorsal Hippocampus Necessary for Goal-Directed Behavior. *Neuron*, *97*(1), 83-91 e85. https://doi.org/10.1016/j.neuron.2017.11.031

Lee, K. H., Bhaker, R. S., Mysore, A., Parks, R. W., Birkett, P. B., & Woodruff, P. W. (2009). Time perception and its neuropsychological correlates in patients with schizophrenia and in healthy volunteers. *Psychiatry Res*, *166*(2-3), 174-183. https://doi.org/10.1016/j.psychres.2008.03.004

Makino, H., Ren, C., Liu, H., Kim, A. N., Kondapaneni, N., Liu, X., Kuzum, D., & Komiyama, T. (2017). Transformation of Cortex-wide Emergent Properties during Motor Learning. *Neuron*, *94*(4), 880-890 e888. https://doi.org/10.1016/j.neuron.2017.04.015

Mar, A. C., Walker, A. L., Theobald, D. E., Eagle, D. M., & Robbins, T. W. (2011). Dissociable effects of lesions to orbitofrontal cortex subregions on impulsive choice in the rat. *J Neurosci*, *31*(17), 6398-6404. https://doi.org/10.1523/JNEUROSCI.6620-10.2011

Marrero, K., Aruljothi, K., Zareian, B., Gao, C., Zhang, Z., & Zagha, E. (2022). Global, Low-Amplitude Cortical State Predicts Response Outcomes in a Selective Detection Task in Mice. *Cereb Cortex*, *32*(9), 2037-2053. https://doi.org/10.1093/cercor/bhab339

McBurney-Lin, J., Sun, Y., Tortorelli, L. S., Nguyen, Q. A. T., Haga-Yamanaka, S., & Yang, H. (2020). Bidirectional pharmacological perturbations of the noradrenergic system differentially affect tactile detection. *Neuropharmacology*, *174*, 108151. https://doi.org/10.1016/j.neuropharm.2020.108151

McClure, S. M., Berns, G. S., & Montague, P. R. (2003). Temporal Prediction Errors in a Passive Learning Task Activate Human Striatum. *Neuron*, *38*(2), 339-346. https://doi.org/10.1016/S0896-6273(03)00154-5

Meilleur, A., Foster, N. E. V., Coll, S. M., Brambati, S. M., & Hyde, K. L. (2020). Unisensory and multisensory temporal processing in autism and dyslexia: A systematic review and meta-analysis. *Neurosci Biobehav Rev*, *116*, 44-63. https://doi.org/10.1016/j.neubiorev.2020.06.013

Mendonça, A. G., Drugowitsch, J., Vicente, M. I., DeWitt, E. E. J., Pouget, A., & Mainen, Z. F. (2020). The impact of learning on perceptual decisions and its implication for speed-accuracy tradeoffs. *Nature Communications*, *11*(1), 2757. https://doi.org/10.1038/s41467-020-16196-7

Mobini, S., Body, S., Ho, M. Y., Bradshaw, C. M., Szabadi, E., Deakin, J. F., & Anderson, I. M. (2002). Effects of lesions of the orbitofrontal cortex on sensitivity to delayed and probabilistic reinforcement. *Psychopharmacology (Berl)*, *160*(3), 290-298. https://doi.org/10.1007/s00213-001-0983-0

Murakami, M., Shteingart, H., Loewenstein, Y., & Mainen, Z. F. (2017). Distinct Sources of Deterministic and Stochastic Components of Action Timing Decisions in Rodent Frontal Cortex. *Neuron*, *94*(4), 908-919 e907. https://doi.org/10.1016/j.neuron.2017.04.040

Namboodiri, V. M., Huertas, M. A., Monk, K. J., Shouval, H. Z., & Hussain Shuler, M. G. (2015). Visually cued action timing in the primary visual cortex. *Neuron*, *86*(1), 319-330. https://doi.org/10.1016/j.neuron.2015.02.043

Narayanan, N. S., Horst, N. K., & Laubach, M. (2006). Reversible inactivations of rat medial prefrontal cortex impair the ability to wait for a stimulus. *Neuroscience*, *139*(3), 865-876. https://doi.org/10.1016/j.neuroscience.2005.11.072

Narayanan, N. S., Land, B. B., Solder, J. E., Deisseroth, K., & DiLeone, R. J. (2012). Prefrontal D1 dopamine signaling is required for temporal control. *Proc Natl Acad Sci U S A*, *109*(50), 20726-20731. https://doi.org/10.1073/pnas.1211258109

Nobre, A. C., Correa, A., & Coull, J. T. (2007). The hazards of time. *Current Opinion in Neurobiology*, *17*(4), 465-470. https://doi.org/https://doi.org/10.1016/j.conb.2007.07.006

O'Doherty, J. P., Dayan, P., Friston, K., Critchley, H., & Dolan, R. J. (2003). Temporal Difference Models and Reward-Related Learning in the Human Brain. *Neuron*, *38*(2), 329-337. https://doi.org/10.1016/S0896-6273(03)00169-7

Pai, S., Erlich, J. C., Kopec, C., & Brody, C. D. (2011). Minimal impairment in a rat model of duration discrimination following excitotoxic lesions of primary auditory and prefrontal cortices. *Front Syst Neurosci*, *5*, 74. https://doi.org/10.3389/fnsys.2011.00074

Pardey, M. C., Homewood, J., Taylor, A., & Cornish, J. L. (2009). Re-evaluation of an animal model for ADHD using a free-operant choice task. *J Neurosci Methods*, *176*(2), 166-171. https://doi.org/10.1016/j.jneumeth.2008.09.009

Paton, J. J., & Buonomano, D. V. (2018). The Neural Basis of Timing: Distributed Mechanisms for Diverse Functions. *Neuron*, *98*(4), 687-705. https://doi.org/10.1016/j.neuron.2018.03.045

Peterson, B. S., Skudlarski, P., Gatenby, J. C., Zhang, H., Anderson, A. W., & Gore, J. C. (1999). An fMRI study of stroop word-color interference: evidence for cingulate subregions subserving multiple distributed attentional systems. *Biological Psychiatry*, *45*(10), 1237-1258. https://doi.org/https://doi.org/10.1016/S0006-3223(99)00056-6

Pisupati, S., Chartarifsky-Lynn, L., Khanal, A., & Churchland, A. K. (2021). Lapses in perceptual decisions reflect exploration. *Elife*, *10*. https://doi.org/10.7554/eLife.55490

Reinert, S., Hubener, M., Bonhoeffer, T., & Goltstein, P. M. (2021). Mouse prefrontal cortex represents learned rules for categorization. *Nature*, *593*(7859), 411-417. https://doi.org/10.1038/s41586-021-03452-z

Remmelink, E., Smit, A. B., Verhage, M., & Loos, M. (2016). Measuring discrimination- and reversal learning in mouse models within 4 days and without prior food deprivation. *Learning & Memory*, *23*(11), 660-667. http://learnmem.cshlp.org/content/23/11/660.abstract

Reyes, M. B., de Miranda, D. H., Tunes, G. C., Cravo, A. M., & Caetano, M. S. (2020). Rats can learn a temporal task in a single session. *Behav Processes*, *170*, 103986. https://doi.org/10.1016/j.beproc.2019.103986

Richter, S. H., & von Kortzfleisch, V. (2020). It is time for an empirically informed paradigm shift in animal research. *Nat Rev Neurosci*, *21*(11), 660. https://doi.org/10.1038/s41583-020-0369-0

Robbins, T. W., & Dalley, J. W. (2017). *Impulsivity, risky choice, and impulse control disorders: Animal models*. Elsevier Inc. https://doi.org/10.1016/B978-0-12-805308-9.00007-5

Roitman, J. D., & Shadlen, M. N. (2002). Response of Neurons in the Lateral Intraparietal Area during a Combined Visual Discrimination Reaction Time Task. *The Journal of Neuroscience*, *22*(21), 9475-9489. https://doi.org/10.1523/jneurosci.22-21-09475.2002

Romo, R., & Schultz, W. (1990). Dopamine neurons of the monkey midbrain: contingencies of responses to active touch during self-initiated arm movements. *Journal of Neurophysiology*, *63*(3), 592-606. https://doi.org/10.1152/jn.1990.63.3.592

Roy, N. A., Bak, J. H., International Brain, L., Akrami, A., Brody, C. D., & Pillow, J. W. (2021). Extracting the dynamics of behavior in sensory decision-making experiments. *Neuron*. https://doi.org/10.1016/j.neuron.2020.12.004

Rubia, K., Halari, R., Christakou, A., & Taylor, E. (2009). Impulsiveness as a timing disturbance: neurocognitive abnormalities in attention-deficit hyperactivity disorder during temporal processes and normalization with methylphenidate. *Philos Trans R Soc Lond B Biol Sci*, *364*(1525), 1919-1931. https://doi.org/10.1098/rstb.2009.0014

Rudebeck, P. H., & Murray, E. A. (2008). Amygdala and orbitofrontal cortex lesions differentially influence choices during object reversal learning. *J Neurosci*, *28*(33), 8338-8343. https://doi.org/10.1523/JNEUROSCI.2272-08.2008

Ruff, D. A., & Cohen, M. R. (2019). Simultaneous multi-area recordings suggest that attention improves performance by reshaping stimulus representations. *Nat Neurosci*, *22*(10), 1669-1676. https://doi.org/10.1038/s41593-019-0477-1

Schoenbaum, G., & Roesch, M. (2005). Orbitofrontal cortex, associative learning, and expectancies. *Neuron*, *47*(5), 633-636. https://doi.org/10.1016/j.neuron.2005.07.018

Schultz, W., Apicella, P., & Ljungberg, T. (1993). Responses of monkey dopamine neurons to reward and conditioned stimuli during successive steps of learning a delayed response task. *The Journal of Neuroscience*, *13*(3), 900-913. https://doi.org/10.1523/jneurosci.13-03-00900.1993

Shuler, M. G., & Bear, M. F. (2006). Reward timing in the primary visual cortex. *Science*, *311*(5767), 1606-1609. https://doi.org/10.1126/science.1123513

Smits-Bandstra, S., & De Nil, L. F. (2007). Sequence skill learning in persons who stutter: implications for cortico-striato-thalamo-cortical dysfunction. *J Fluency Disord*, *32*(4), 251-278. https://doi.org/10.1016/j.jfludis.2007.06.001

Song, Y.-H., Hwang, Y.-S., Kim, K., Lee, H.-R., Kim, J.-H., Maclachlan, C., Dubois, A., Jung, M. W., Petersen, C. C. H., Knott, G., Lee, S.-H., & Lee, S.-H. (2020). Somatostatin enhances visual processing and perception by suppressing excitatory inputs to parvalbumin-positive interneurons in V1. *Science Advances*, *6*(17), eaaz0517. https://doi.org/doi:10.1126/sciadv.aaz0517

Toplak, M. E., Dockstader, C., & Tannock, R. (2006). Temporal information processing in ADHD: findings to date and new methods. *J Neurosci Methods*, *151*(1), 15-29. https://doi.org/10.1016/j.jneumeth.2005.09.018

van Maanen, L., Grasman, R. P., Forstmann, B. U., & Wagenmakers, E. J. (2012). Pieron's Law and Optimal Behavior in Perceptual Decision-Making. *Front Neurosci*, *5*, 143. https://doi.org/10.3389/fnins.2011.00143

Winstanley, C. A., Theobald, D. E., Dalley, J. W., Glennon, J. C., & Robbins, T. W. (2004). 5-HT2A and 5-HT2C receptor antagonists have opposing effects on a measure of impulsivity: interactions with global 5-HT depletion. *Psychopharmacology (Berl)*, *176*(3-4), 376-385. https://doi.org/10.1007/s00213-004-1884-9

Womelsdorf, T., & Fries, P. (2007). The role of neuronal synchronization in selective attention. *Curr Opin Neurobiol*, *17*(2), 154-160. https://doi.org/10.1016/j.conb.2007.02.002

Xiong, Q., Znamenskiy, P., & Zador, A. M. (2015). Selective corticostriatal plasticity during acquisition of an auditory discrimination task. *Nature*, *521*(7552), 348-351. https://doi.org/10.1038/nature14225

Yang, G. R., Joglekar, M. R., Song, H. F., Newsome, W. T., & Wang, X. J. (2019). Task representations in neural networks trained to perform many cognitive tasks. *Nat Neurosci*, *22*(2), 297-306. https://doi.org/10.1038/s41593-018-0310-2

Zareian, B., Lam, A., & Zagha, E. (2023). Dorsolateral striatum is a bottleneck for responding to task-relevant stimuli in a learned whisker detection task in mice. *The Journal of Neuroscience*, JN-RM-1506-1522. https://doi.org/10.1523/JNEUROSCI.1506-22.2023

Zareian, B., Zhang, Z., & Zagha, E. (2021). Cortical Localization of the Sensory-Motor Transformation in a Whisker Detection Task in Mice. *eNeuro*, ENEURO.0004-0021. https://doi.org/10.1523/eneuro.0004-21.2021

Zariwala, Hatim A., Kepecs, A., Uchida, N., Hirokawa, J., & Mainen, Zachary F. (2013). The Limits of Deliberation in a Perceptual Decision Task. *Neuron*, *78*(2), 339-351. https://doi.org/https://doi.org/10.1016/j.neuron.2013.02.010

Zhang, Z., & Zagha, E. (2022). Frontal Cortex Gates Distractor Stimulus Encoding in Sensory Cortex. *bioRxiv*, 2022.2003.2031.486430. https://doi.org/10.1101/2022.03.31.486430

Zhao, S., Ting, J. T., Atallah, H. E., Qiu, L., Tan, J., Gloss, B., Augustine, G. J., Deisseroth, K., Luo, M., Graybiel, A. M., & Feng, G. (2011). Cell type-specific channelrhodopsin-2 transgenic mice for optogenetic dissection of neural circuitry function. *Nat Methods*, *8*(9), 745-752. https://doi.org/10.1038/nmeth.1668

Figures and Legends

Figure 4.1: Trial Structure, Performance Measures, and Training Data

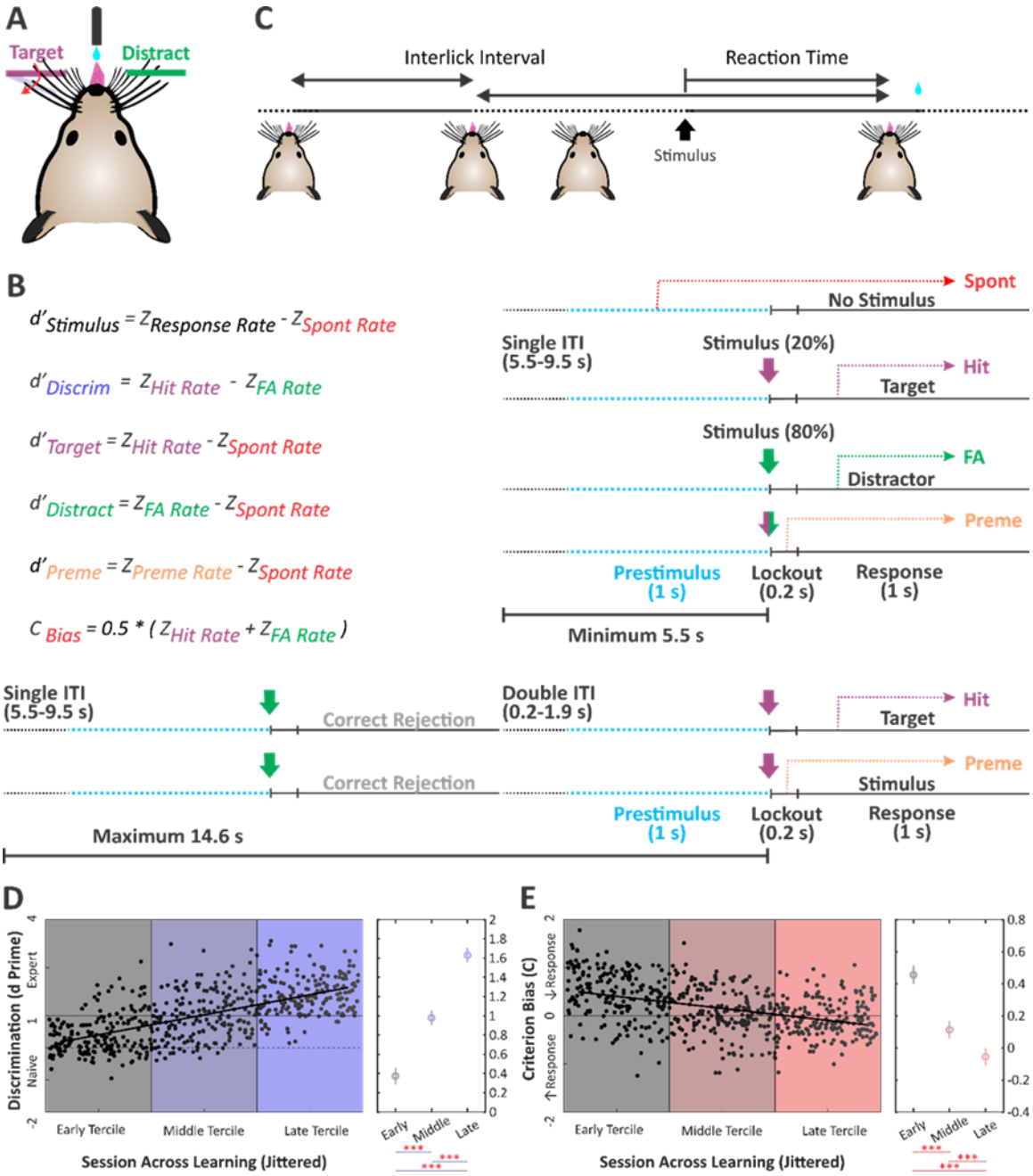

*A) Mice learn to selectively respond to target whisker deflections (fuchsia) and ignore distractor whisker deflections (green). B) Signal detection measures were quantified according to response rates: Spontaneous (Spont, red) response during the ITI and before stimulus presentation; Hit (fuchsia) response after a target stimulus during the response window; False alarm (FA, green) response after a distractor stimulus during the response window; Premature (Preme, orange) response after a stimulus during the lockout period. C) Strategies were investigated according to interlick intervals (temporal distance between consecutive licks) and reaction times (temporal distance between stimulus presentation and response). D) (Left) discrimination performance plotted across all sessions and all mice, segregated according to duration in training (early, middle, late); (right) quantification of tercile means across sessions. E) Same dataset and layout as in D, but for criterion bias. Shading denotes progression in training by tercile, dark to bright. (Unbalanced one-way ANOVA with post-hoc multiple comparisons *** $p<0.0005$).*

Figure 4.2: Mice transition from a sampling to waiting strategy before stimulus presentation across learning

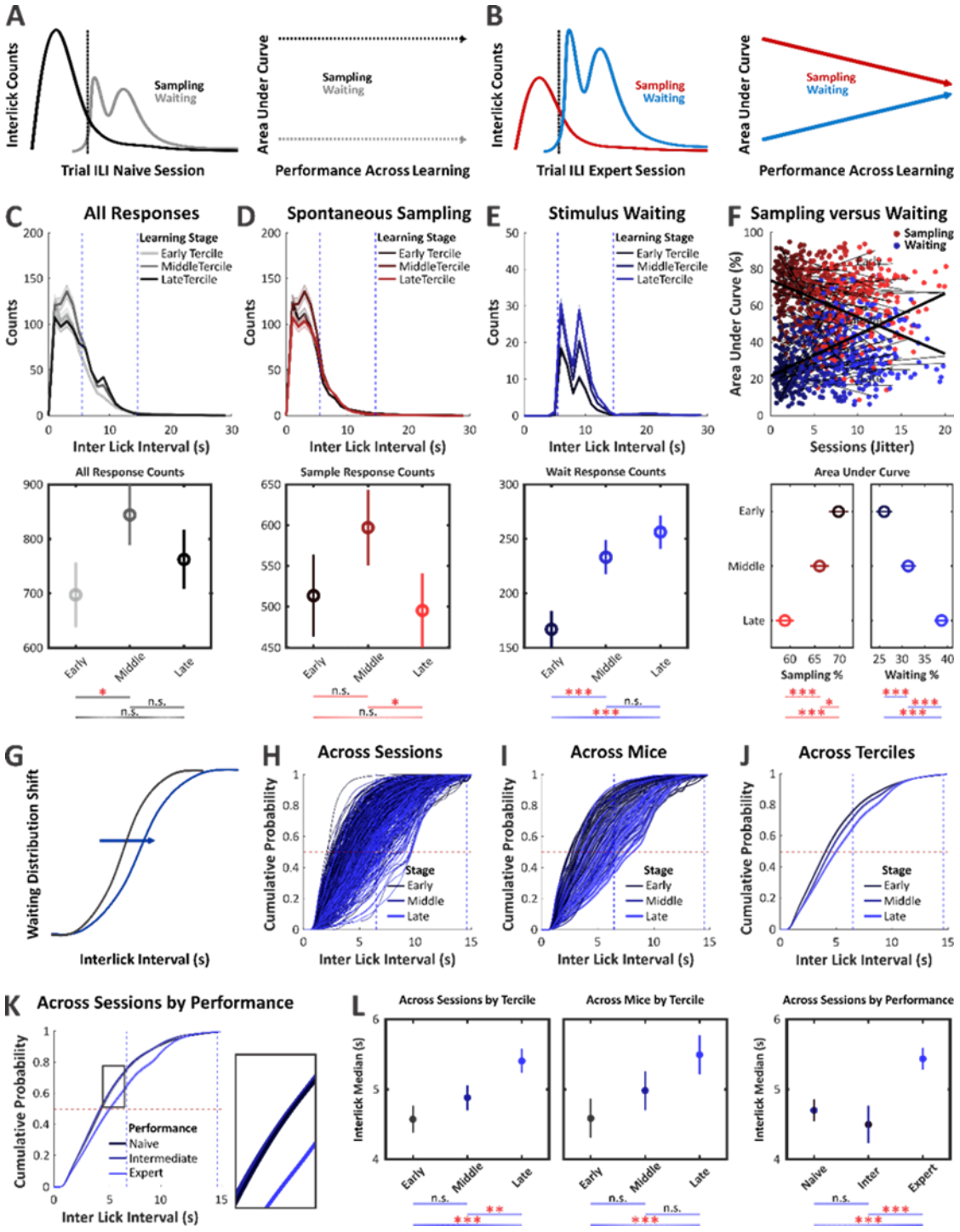

*A) (Left) hypothetical example of response distributions in naïve behavior before learning; (right) longitudinal performance if response behavior does not change across learning. B) (Left) hypothetical example of response distribution in expert behavior after learning; (right) longitudinal performance if response behavior changes across learning. C) Mice increase and then decrease all responding across terciles; shading denotes progression in training (grey to black). D) Mice decrease spontaneous prestimulus sampling from middle to late terciles. E) Mice increase stimulus responding from early to middle terciles. F) Percent area under the curve (%AUC) per session of spontaneous sampling (red) and stimulus waiting (blue) with linear fits across sessions per mouse (faint black) and mean of linear fits across mice (bold black). G) Expected cumulative distribution function shift if waiting behavior changes across learning. H) Cumulative probability distribution function (CDF) curves across all sessions. I) CDF curves across terciles per mouse. J) Mean CDF curves across tercile sessions. K) Mean CDF curves across performance sessions; inset shows overlapping of naïve and intermediate performance CDFs. L) Quantification of tercile means across sessions, tercile means across mice, and performance means across all sessions. [D-K] Shading denotes progression in training by session, dark to bright. (Balanced and unbalanced one-way ANOVA with post-hoc multiple comparisons * $p<0.05$, ** $p<0.005$, *** $p<0.0005$, n.s. $p>0.05$).*

Figure 4.3: Mice transition from a sampling to timing strategy after stimulus presentation across learning

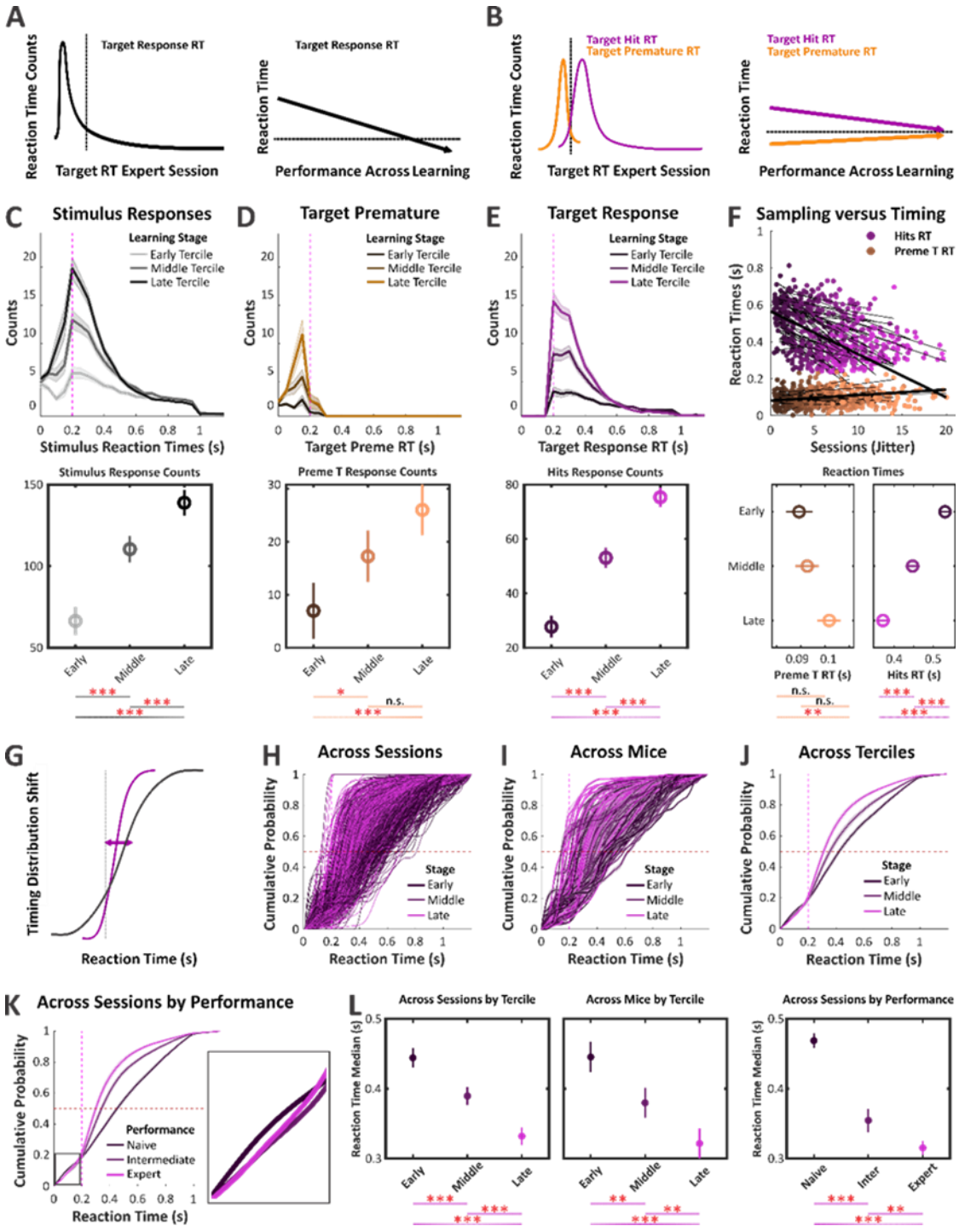

*A) (Left) hypothetical example of RT distribution in mouse behavior before and after learning if target RT improves to fastest RT possible; (right) longitudinal performance if RTs decrease across learning. B) (Left) hypothetical example of RT distribution in mouse behavior after learning if RTs converge to the imposed lockout period (dashed gray line); (right) longitudinal performance if RTs converge to the lockout period across learning. C) Mice increase stimulus responses across terciles; shading denotes progression in training, grey to black. D) Mice increase target premature (orange) RT counts across terciles. E) Mice increase target hits RT counts across terciles. For all RT distributions (C-E), the maximum increase is at the time of the lockout (vertical line). F) Target stimulus RTs per session for hits and target premature trials with linear fits across sessions per mouse (faint black) and mean of linear fits across mice (bold black). G) Expected cumulative distribution function shift if timing behavior changes across learning. H) Cumulative probability distribution function (CDF) curves across all sessions. I) CDF curves across terciles per mouse. J) Mean CDF curves across tercile sessions. K) Mean CDF curves across performance sessions; inset shows overlapping of naïve and intermediate performance CDFs. L) Quantification of tercile means across sessions, tercile means across mice, and performance means across sessions. [D-K] Shading denotes progression in training, dark to bright. (Balanced and unbalanced ne-way ANOVA with post-hoc multiple comparisons * p<0.05, ** p<0.005, *** p<0.0005, n.s. p>0.05).*

Figure 4.4: Interquintile of maximum change analyses reveal order of learning

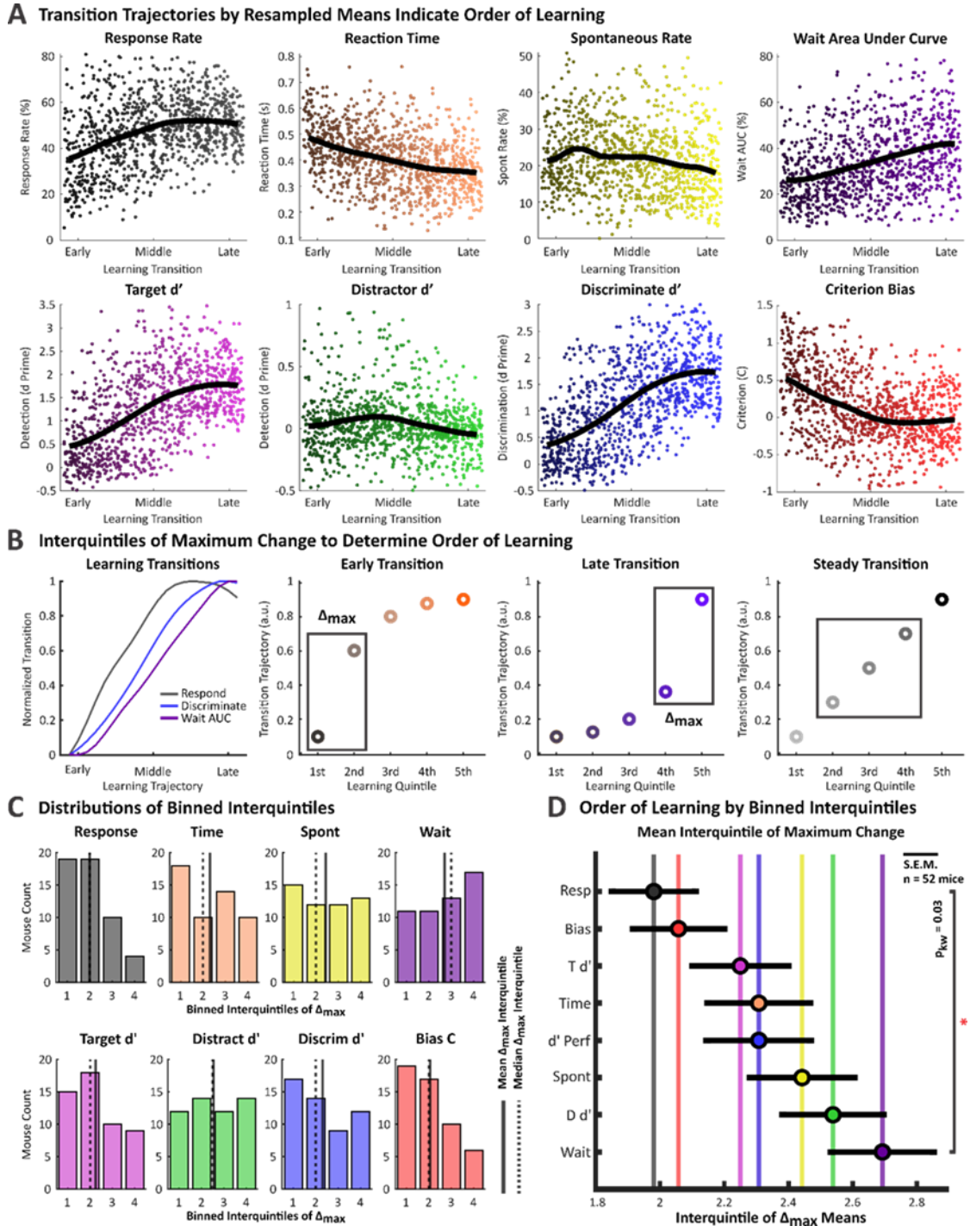

*A) Resampled means of object-based and temporal transition trajectories across mice: stimulus response rate (grey); RT (orange); spontaneous rate (yellow); wait AUC (purple); target detection (fuchsia); distractor detection (green); discrimination (blue); criterion (red); shading denotes progression in learning by resampled sessions, dark to bright. B) Normalized increasing trajectories for stimulus responding, discriminating, and waiting; example interquintile transitions: early, late, steady transitions. C) Distributions of interquintile of maximum change per measure across mice. D) Mean interquintile of maximum change ($\mu_{\Delta max}$ ± S.E.M.) sequenced by increasing order (Kruskal Wallis rank sum ANOVA * $p<0.05$).*

Figure 4.5: Order of learning by interquintile of maximum change exhibits sex specificity

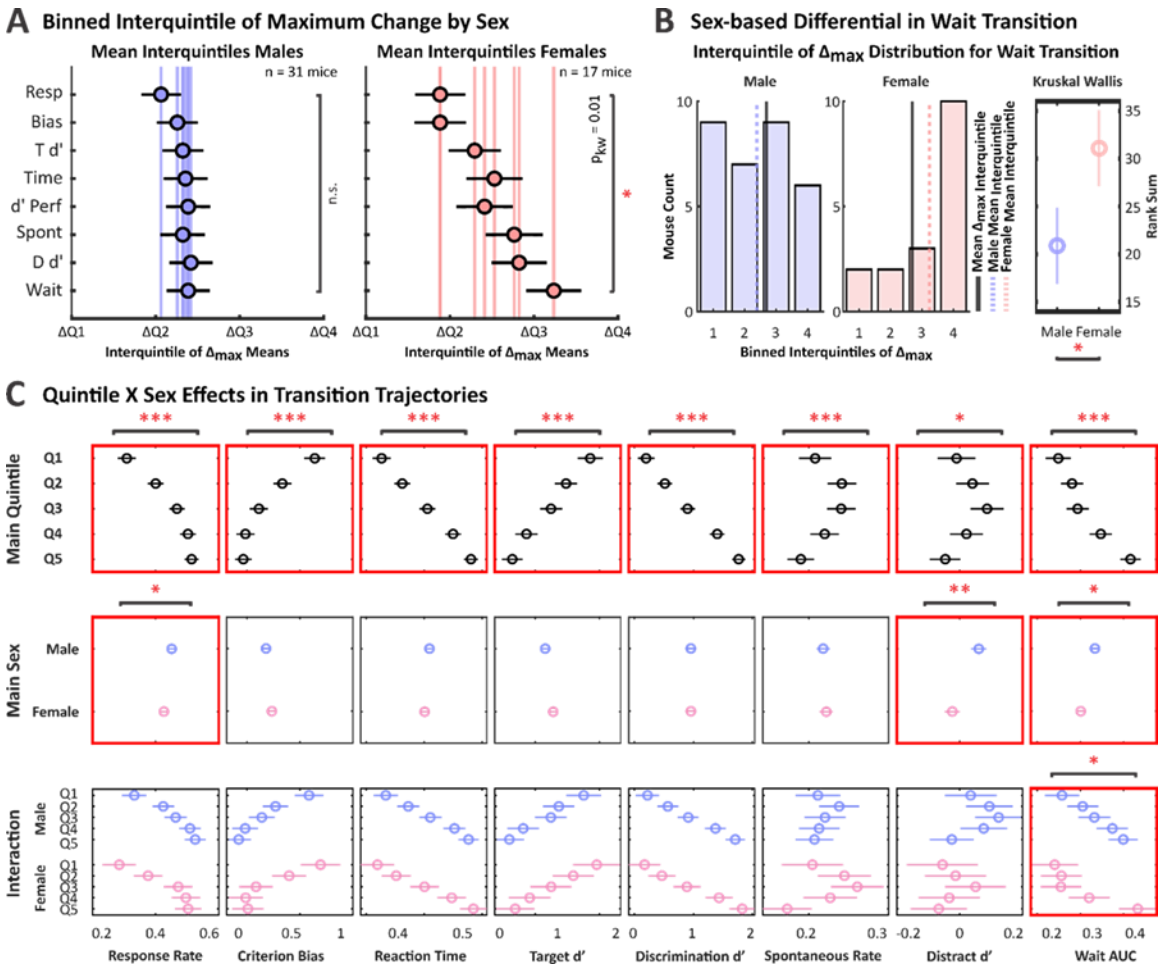

*A) Male versus female mean interquintile of maximum change ($\mu_{\Delta max}$ ± S.E.M.) sequenced as in Figure 4.4. B) Male versus female distributions of interquintile of maximum change for wait AUC; solid line, all mice mean interquintile; dashed line, male/female mean interquintile. C) Transitions of each measure by quintile (top), sex (middle), and quintile X sex interactions (bottom); colors: blue – male, pink – female. (Kruskal Wallis rank sum by sex * p<0.05; unbalanced two-way ANOVA with post-hoc multiple comparisons * p<0.05, ** p<0.005, *** p<0.0005; red borders indicate significance).*

Figure 4.6: Pairwise innerquintile curvature reveals intermediates in the order of learning

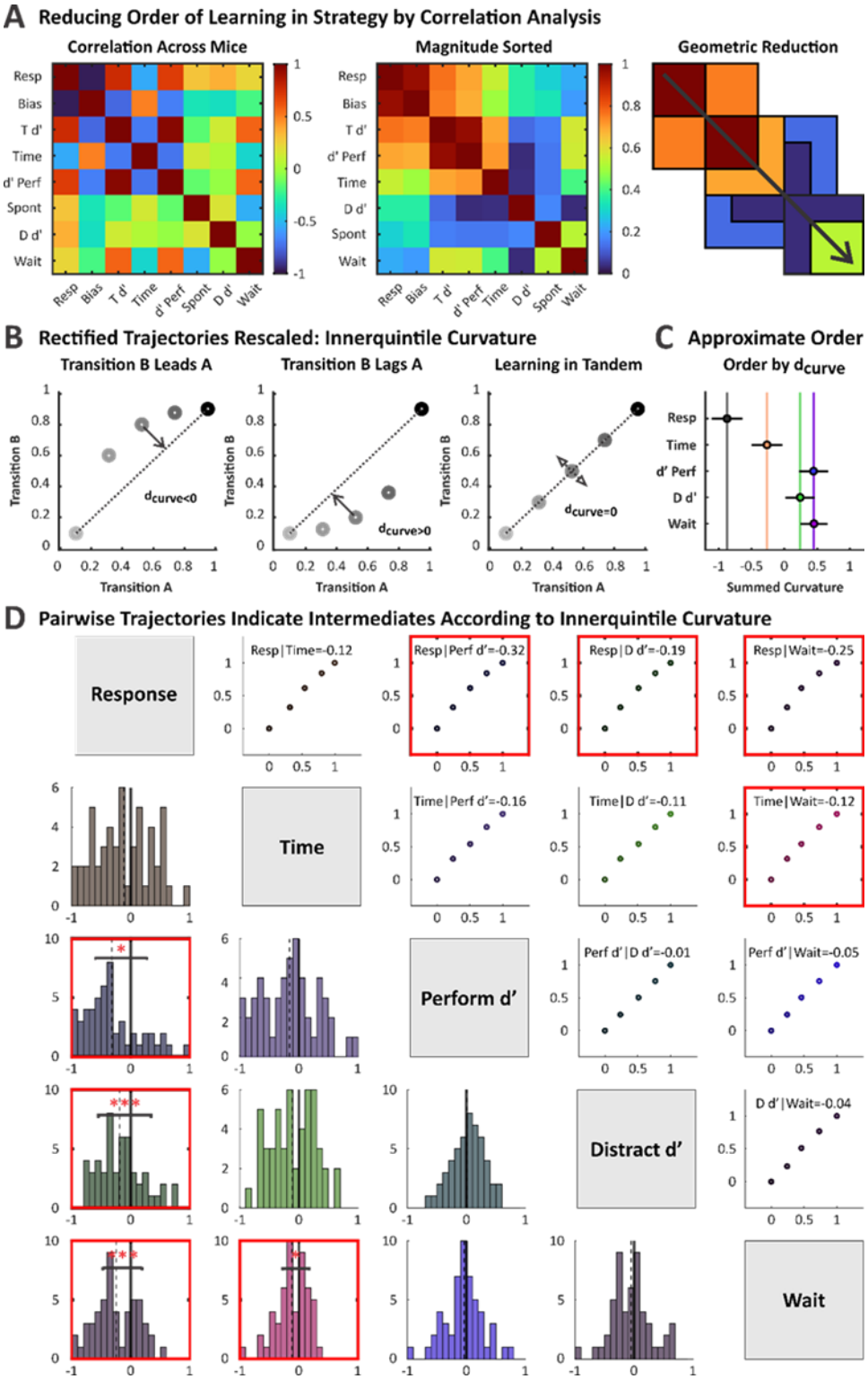

*A) Correlations of measures across mice, color scale [-1 1] (left); sorted correlation magnitudes across mice, color scale [0 1] (middle); geometric reduction model of sorted correlation magnitudes (right). B) Example analyses for innerquintile curvature (d_{curve}) between rectified pairwise measures by quintile (see Methods and Materials). C) Summed d_{curve} across columns in (D); $\sum \mu_{dcurve} \pm$ S.E.M. for learning order approximation. D) Pairwise innerquintile curvature and distributions across mice (top-right, mean d_{curve} across pairwise comparisons; bottom-left, d_{curve} distributions; dashed line, mean d_{curve} across distribution. (One sample t-test, Bonferroni corrected: * $p<0.05$, *** $p<0.0005$; red borders indicate significant curvature, denoting differences in learning trajectories).*

Figure 4.7: Order of learning by pairwise innerquintile curvature exhibits sex specificity

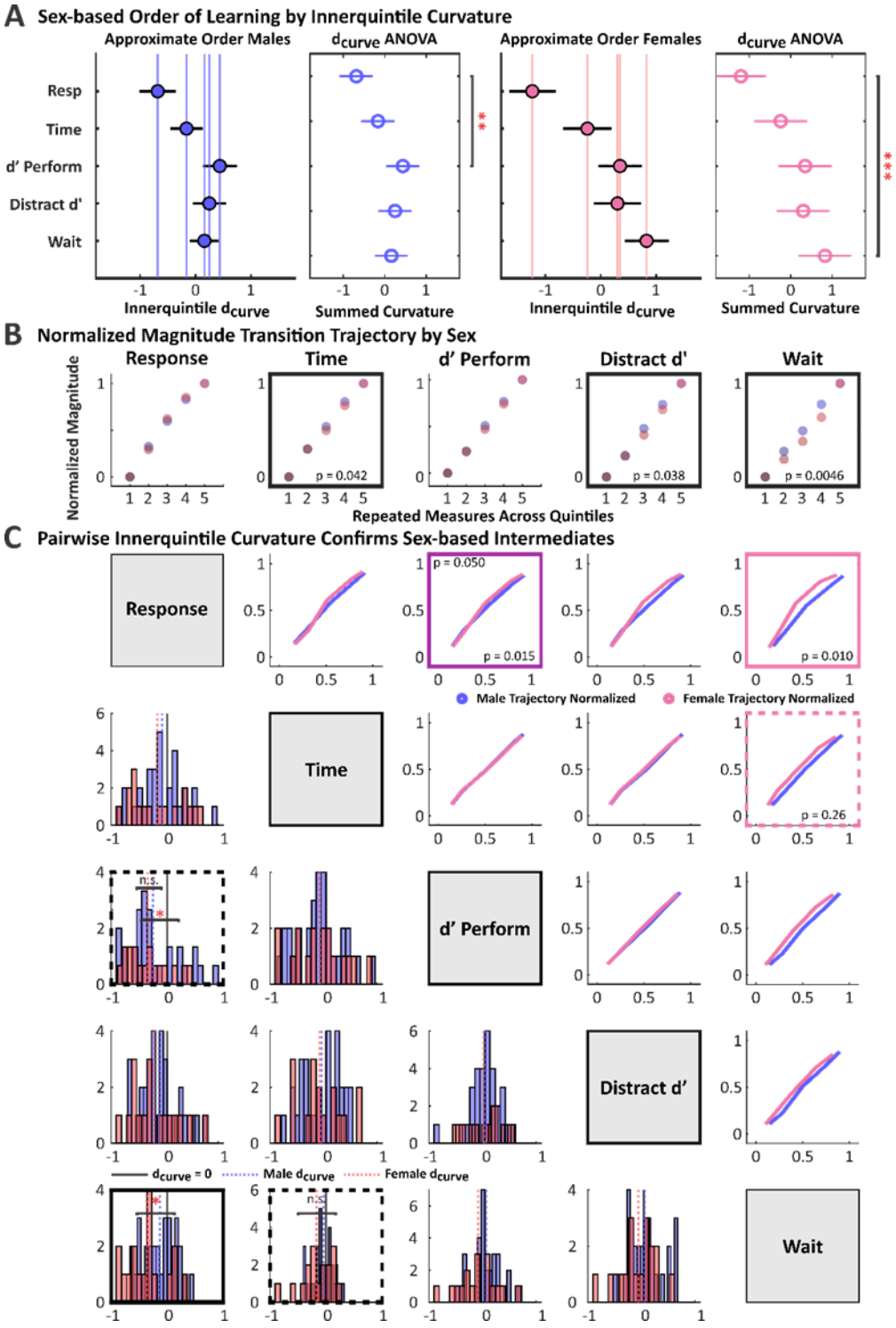

*A) Male versus female: summed d_{curve} across columns in (C); $\sum\mu$ d_{curve} ± S.E.M. for learning order approximation. B) Male versus female normalized learning trajectories across quintiles for individual measures; black borders denote statically significant differences (repeated measures ANOVA for longitudinal trajectories). C) Pairwise innerquintile curvature and distributions by sex (top-right, mean d_{curve} across pairwise comparisons by sex; bottom-left, d_{curve} distributions by sex; colored dashed lines, mean d_{curve} across distribution by sex; black dashed line, d_{curve} = 0; colors: blue – male, pink – female. (One sample t-test ** p<0.005, *** p<0.0005, border in pink denotes significant curvature in female but not male mice, border in purple denotes significant curvature in both male and female mice; unbalanced one-way ANOVA * p<0.05, n.s. p<0.10, border in black denotes significant difference between male versus female d_{curve}, dashed border denotes nonsignificant but noteworthy comparisons between male versus female d_{curve}).*

Figure 4.8: Object-based and temporal transitions overlap, forming intermediate behavioral strategies

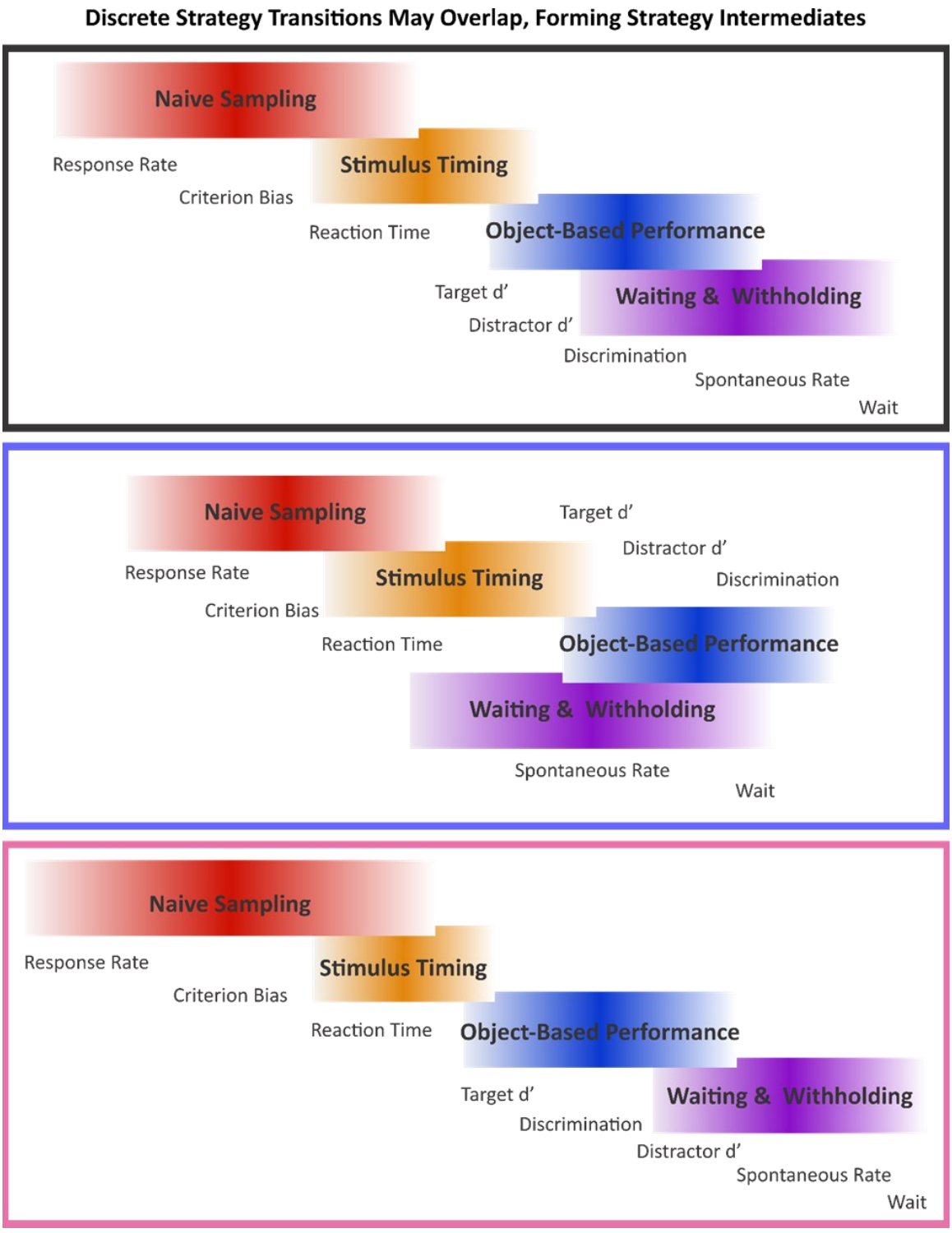

A) General learning strategy framework in which an initial strategy of naïve sampling progresses to stimulus timing, object-based performance, and ultimately waiting and withholding. B) Learning strategy framework for male mice in which naïve sampling overlaps with stimulus timing and waiting and withhold intermediates, following by object-based performance. C) Learning strategy framework for female mice in which the intermediate strategies are more temporally distinct.

Supplementary Figures

Supplementary Figure 4.1: Mice do not show transitions in timing behavior for distractor trials

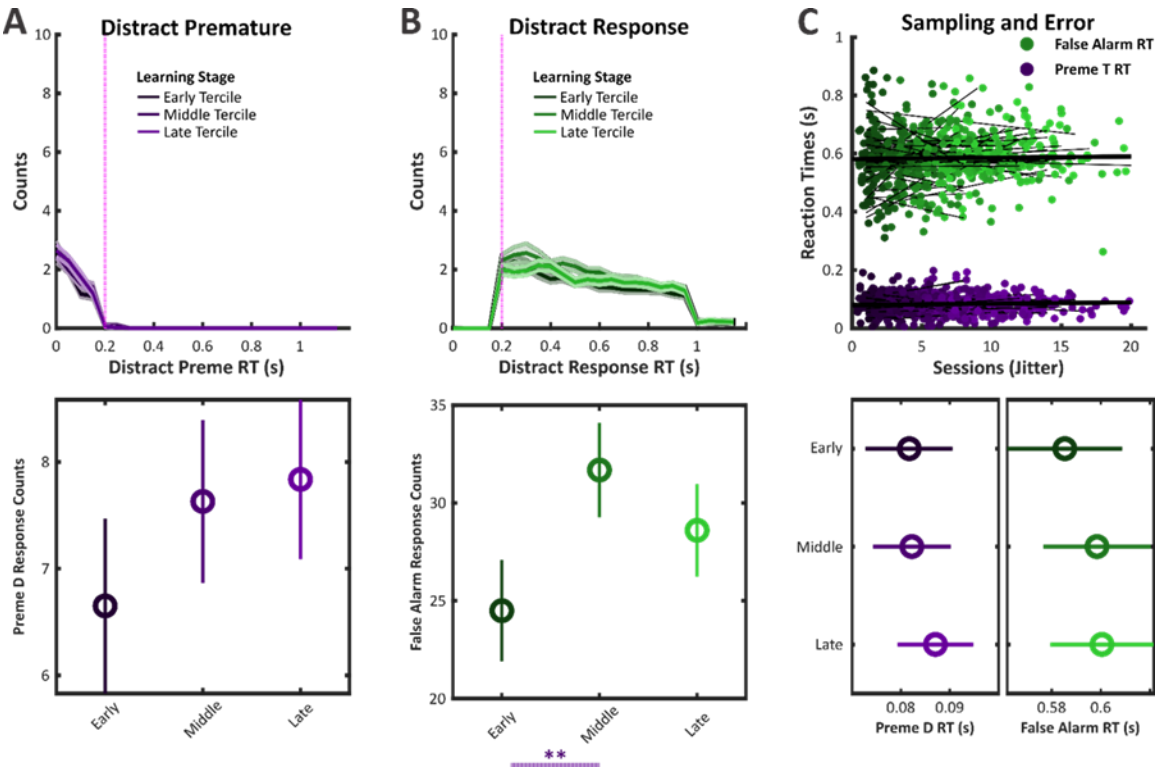

*A) Mice do not increase distractor premature (green) counts across terciles. B) Mice increase distractor false alarm counts from early to middle terciles. C) Distractor stimulus RTs per session for false alarm and distractor premature trials (circles), with linear fits across sessions per mouse (faint black) and mean of linear fits across mice (bold black); shading denotes progression in training (dark to bright; one-way ANOVA with post-hoc multiple comparisons ** p<0.005).*

Supplementary Figure 4.2: Transitions in object-based measures

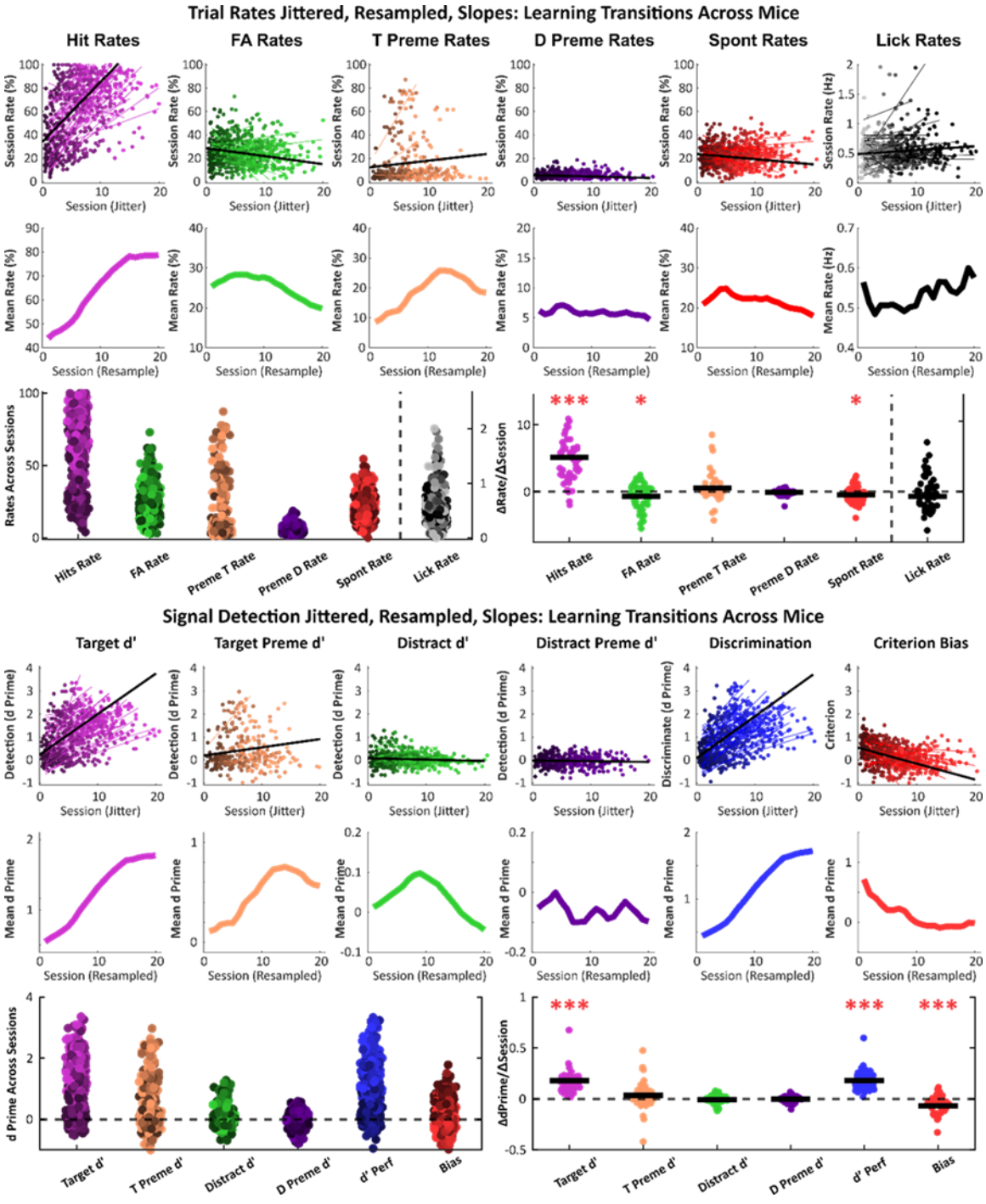

*Row 1, left to right) Object-based measures in trial rates across learning: hits (fuchsia), false alarm (green), target premature (orange), distract premature (purple), spontaneous (red), overall lick bout rates (black, in Hz). Row 2, left to right) Resampled means across mice; colors as in Row 1. Row 3) Left: session rates from Row 1; right: linear slopes of transitions per mouse. Row 4, left to right) Object-based measures from signal detection theory across learning: target detection (fuchsia), target premature detection (orange), distractor detection (green), distractor premature detection (purple), target-distractor discrimination (blue), target-distractor criterion bias (red). Row 5, left to right) Resampled means across mice; colors as in Row 4. Row 6) Left: signal detection measures from Row 4; right: linear slopes of measures per mouse (shading denotes progression in training, dark to bright, one sample t-test * p<0.05, *** p<0.0005).*

Supplementary Figure 4.3: Similar trajectories in object based measures from mice of different genotypes.

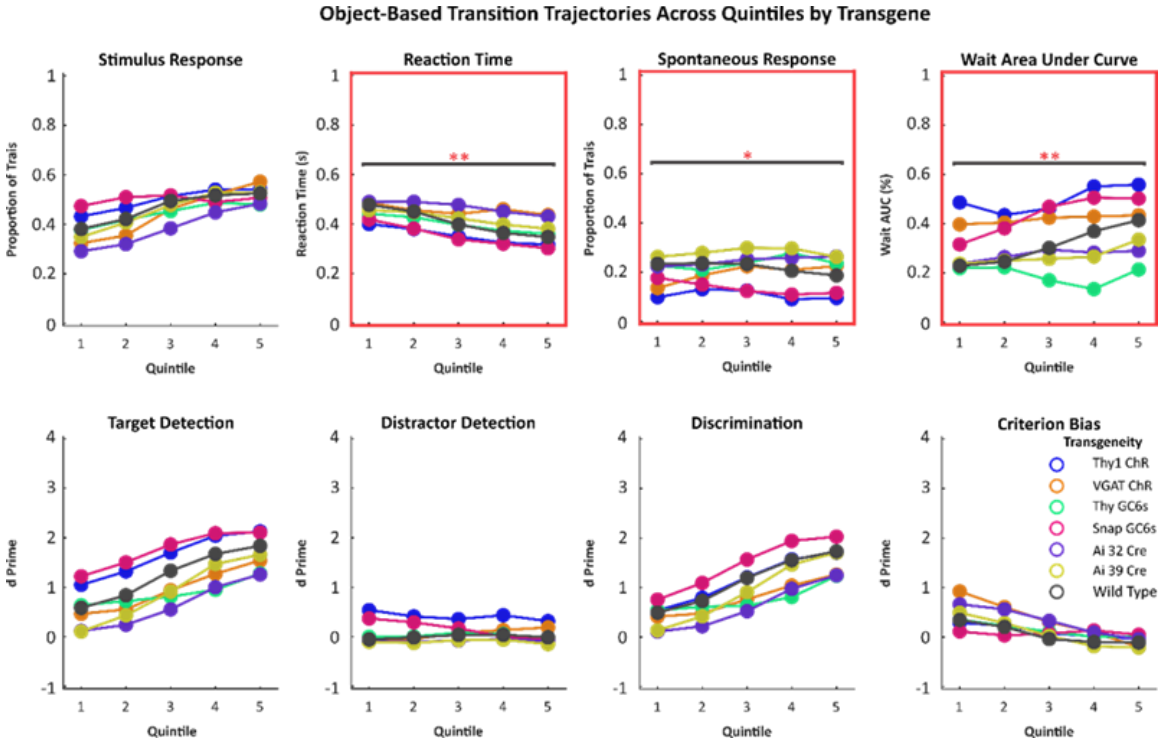

*Top row) Stimulus response rates (left) and spontaneous response rates (right) across quintiles. Bottom row) Signal detection measures across quintiles. Transgenic lines: Thy1 channelrhodopsin (blue), VGAT channelrhodopsin (orange), Thy1 GCaMP6s (green), SNAP25 GCaMP6s (fuchsia), Ai32 channelrhodopsin Cre (purple), Ai39 halorhodopsin Cre (yellow), wild type (black, repeated measures ANOVA * p<0.05, ** p<0.005; red borders indicate significance).*

Chapter 5: Conclusion, Future Directions, Retrospect

The investigations here have explored expert behavior, neuronal correlates of expert behavior across cortex, longitudinal learning behavior, and potential strategies utilized to achieve expert behavior. The outcomes reported here have only initiated more scrutiny (in the form of constructive critique), more potential investigations, more inquiries, and more awareness of the various aspects of our task. Considering this, an overall assessment adds to our retrospective understanding and potential future directions.

Behavior Paradigms

Although we have comprehensively approached the decision to selectively respond and selectively ignore competing stimuli, we have still only explored a single behavior paradigm. The methods of investigating multiple strategies and potential contributions of cortical activity across naïve, learning, and expert behavior should be utilized for many behavior paradigms. The paradigm of interest will depend on the question investigated. Developing a behavior paradigm is extensive. For instance, when first considering a timing strategy and a task that would expose timing behavior, we found that longer prestimulus wait times predicted shorter reaction times and more timing errors. We essentially reproduced the phenotype for ADHD children in a countermanding reaction time task (Hanisch et al., 2006).

We did find that consistent error reporting and audio stimuli further frustrated mice as they learned to wait for a stimulus and then respond within a target duration (Figure 5.1A versus 5.1B). Additionally, because both waiting and timing were found in

the selective detection paradigm, it would be interesting to investigate a paradigm that requires only waiting or only timing. In this way, one might be able to tease apart the two temporal strategies.

The target timing paradigm investigates the decision to target a response according to a target reward; we could implement such a paradigm to investigate pure target timing where different target windows result in different rewards (Figure 5.2A). Targeted reaction times would differ in complexity and difficulty compared to habituated response or internal representation of temporal windows (Bakhurin et al., 2017; Matell & Portugal, 2007; Namboodiri et al., 2015; Toda et al., 2017). Individual preferences would certainly vary, but the mouse's window of choice would become clear across learning. A post-stimulus lockout would differentiate between a target temporal strategy and the nontemporal reaction strategy. We should concurrently contrast a pure temporal strategy against a pure detection strategy (Figure 5.2B).

As we have found, mice learn to withhold later in training. This was shown in the late distractor withholding after a stimulus and the late prepotent response withholding before a stimulus. Deliberate exploitation of early sampling behavior may improve speed in learning. For example, the binary opportunity for mice to attain reward or lose reward based on their timed response seemed to produce more erratic behavior in training than expected. For temporal reward association to form earlier in learning, a gradient of reward based on a timed response should prove more effective. This becomes a graded reaction time task to investigate an ability to withhold a stimulus triggered response for

a larger reward (Figure 5.3A). Such a paradigm could be used to investigate reward discount behavior in normative versus diseased animal model behavior.

We also never implemented a pure waiting paradigm to investigate the decision to wait longer for a larger reward, but we could implement such a paradigm to investigate a self-initiated wait where longer waits ensure larger rewards (Figure 5.3B). A pure waiting paradigm removes the stimulus response aspect and focuses on the ability to wait for longer temporal windows based solely on prepotent withholding of response.

Cortical Attenuation and Cortical State

The investigation into widefield calcium (Ca^{2+}) imaging was initially the most challenging (yet exciting) feature of this body of work. As the investigations progressed, developing behavior paradigms became the larger challenge. Still, once behavior protocols served their purpose (i.e., our paradigm could answer the scientific inquiry and we could indeed teach the mice how to perform the task), the widefield imaging results were more consistent and more reliable. The recognition that fluorescence (mean grey value, baseline normalized, sliding window normalized, or other fluorescence interpretations) could merely contribute to qualitative interpretation was impactful.

The quantitative evaluation for widefield imaging was found in the encoding of the fluorescence data. The concept of encoded information in raw data should be expanded beyond behavior output and neurometric readouts. In this way, the signal detection application continues to enhance our neuroscientific understanding. Embracing overall encoding as a quantitative method for neural processes therefore extends to how

we think about sensory encoding (stimulus present versus stimulus absent signal), choice encoding (response present versus response absent signal), correct encoding (correct outcome versus incorrect outcome), or any other binary form of inquiry. Encoding power could be the 'engram' we so desperately seek to find.

Encoding was used to detect the presence of a stimulus and the presence of a response choice in our attenuation work (stimulus and choice encoding). As mentioned in the prestimulus work, a global state that predicts trial outcome should be evident in the prestimulus encoding. Because a great deal of effort went into the encoding analysis of the prestimulus state, **Appendix Figures 2** and **3** are included and can be further discussed concerning future directions.

Models and Modulation, Experimental and in Silico

Several future directions have not been explored in this body of work with regards to animal models of normative versus disordered conditions, potential in Silico work for data analyses, and neural correlation, function, and mechanism.

Animal models for disease and disorder are abundant. The transgenic GCaMP mice in our learning investigation had faster reaction times, higher spontaneous response rates, and lower wait AUCs. These may indicate deficits regarding attention and/or hyperactivity. These three measures, in addition to the distractor detection measure, are indicative of the ability to withhold prepotent response in the intertrial interval and the ability to target a stimulus response past the lockout of our task. We determined that larger sample sizes were required for the transgenic-specific differences across learning.

Neuronal mechanisms across disordered animal models are perhaps the most fascinating aspects of investigation: behavior task, model type, and treatment (Agster et al., 2011; Antoine et al., 2019; Pardey et al., 2009; Pardey et al., 2013; Silverman et al., 2010). Object-based versus temporal processing in ADHD children is studied across the literature, but little is dedicated to learning specifically (Frida Bayard et al., 2020; Eden et al., 1995; Hanisch et al., 2006; Jung et al., 2014; Metin et al., 2018; Toplak et al., 2006). Autism models are prevalent in human literature, but should be considered carefully when investigating comorbid phenotypes of autism, including those relating to ADHD (Meilleur et al., 2020; Murat Baldwin et al., 2021). There also exists the discussion on whether mouse models versus rat models are even appropriate for studying such disorders with social components (Berg et al., 2020; Silverman et al., 2013; Silverman et al., 2022; Till et al., 2022). These considerations are important when investigating phenotypes of animal models for mental health disorders involving hyperactivity, impulsivity, and learning.

In addition to experimental approaches, computational modeling in behavioral neuroscience has advanced due to the multiple disciplinary approach to investigation of various processes: attention, context, learning, memory, object-based, state, and temporal (Avramiea et al., 2020; Graves et al., 2016; Mante et al., 2013; Ni et al., 2018; Perez & Merchant, 2018; Pisupati et al., 2021; Ruff & Cohen, 2019). Recurrent networks, intrinsic noise, and elements of ‘chaos’ seem to be required to interpret many spatiotemporal processes (Buonomano & Maass, 2009; Sohn et al., 2019) Still, the ability

and necessity of in silico work can only contribute and confirm experimental findings. The greatest contribution of in silico methods, though, involves great strides in data analytics, machine learning, and mathematical insight (Ashwood et al., 2022; Musall et al., 2020).

The discussion on a 'brain state' before or after a stimulus presentation can be redirected towards the overall homeostatic, dynamic, or modulatory tone that potentially defines the brain state. Because our cortical work relied on a transgenic SNAP25 pan-neuronal promotor for calcium-related activity, we cannot determine excitatory versus inhibitory calcium related activity. Therefore, dynamic fluorescence observed can only indicate potential regions of interest for future investigation of task-related function and circuitry. Excitatory versus inhibitory transgenic lines have been suggested to explore this differentiation. In any case, we would expect that global low activity in the prestimulus state and post-stimulus dynamic propagation of signal would rely on a specific (potentially learned) neuromodulatory tone.

After careful review of neuromodulatory influence on function and circuitry, we can investigate a global 'blend' of monoaminergic pathways responsible for setting a correct tone for correct outcomes. These can be manipulated with systemic pharmaceuticals, focal drug application, or disordered models in animal subjects. Some discussions of interest include the development of ideal conditions across learning through synaptic plasticity, potential cross modulation and receptor dimerization in animal disorders, and reward encoding in cortical pathways (Borroto-Escuela et al., 2016; Bromberg-Martin et al., 2010; Pedrosa & Clopath, 2017; Roelfsema & Holtmaat, 2018).

Reward Association

The elements of reward processing, reward prediction, and uncertainty have also not been explored here. While reward processing is investigated in many behavior paradigms, prediction and uncertainty require precise probabilistic consideration. We introduced a temporal uncertainty in our task to minimize temporal strategies in our selective detection task. However, mice did learn that if they could wait through a temporal uncertainty, they would eventually get a target stimulus, an opportunity to respond, and a subsequent reward. The oddball paradigm is a consideration for uncertainty, reward prediction, and error signaling (Nguyen & Lin, 2014; Nonomura et al., 2018). In the oddball design, probabilistic reward or punishment is met with expectation (of a probable outcome) or prediction error (after an improbable outcome). This investigates neuronal elements of pleasant surprise upon unexpected reward, disappointment upon not receiving an expected reward, or or the difference between expected and unexpected under conditions of certainty versus uncertainty. Very careful paradigm design would exploit temporal certainty, allowing for mice to predict stimuli and reward associated outcome before introducing oddball trials.

A pure waiting paradigm involving no stimulus with a graded reward schedule emphasizes reward association with successful waiting. A pure timing paradigm that involves a predicted stimulus with targeted temporal windows emphasizes reward associations with target reaction times. Temporal windows and multimodal contexts could also be utilized to associate reward with target epochs.

Still, in any temporal consideration, it is essential to allow for hazard features associated with reward expectation in the task (Grabenhorst et al., 2019). Hazard features are evident *before a stimulus* when longer waiting predicts unintended impulse or exploratory sampling behavior; both are investigated via spontaneous lick bouts. The well-known hazard function establishes that the probability of response increases as expectation increases through a delay (Fiorillo et al., 2008; Nobre et al., 2007; Zariwala et al., 2013). Hazard features are evident *after a stimulus* when response behavior exhibits delay-dependent speeding, when reaction times to a stimulus decrease for longer delays, which is also related to the hazard function (Näätänen, 1970; Narayanan & Laubach, 2009; Parker et al., 2014). Hazards have not yet been investigated considering multiple strategies across learning for the selective detective task; it would be interesting to observe a change in hazard profiles with respect to the choice of strategy.

It would also be interesting to observe differentials in motivation with respect to the choice of strategy. Motivation in normative versus diseased models becomes the behavioral proxy via the aspects of the motivation equation: association based on value, reward discounting based on delay, and the ability to overcome hazard profiles of impulsivity across learning.

Strategies Across Learning

The application of our initial investigation into learning presents a new direction of hypothetical design. Because learning, even working memory and memory consolidation, is so extensive in behavior paradigms, it seems overwhelming. The management of big

data, longitudinally systemized and standardized, will be the hurdle to overcome (International Brain et al., 2021; Roy et al., 2021). When one considers the course of action required for a neural behavior analysis under expert behavior alone, the extension into learning seems exponential. The application, of course, reaches beyond any single experiment. It pushes the boundaries into understanding how we learn, when we learn, what we learn, which learning strategy builds upon another learning strategy, etc. to optimize goal-directed behavior.

A common understanding of stepwise learning or phasic learning should be extended into discrete or overlapping strategy formation with necessary intermediates (Ashwood et al., 2022). In this sense, we imagine the stepwise, phasic, discrete, or overlapping nature of critical periods throughout development. Case in point, critical periods may give notable insight into how we evaluate behavioral learning.

Final Remarks

In conclusion, the verdict on whether complex and dynamic spatiotemporal environments should be investigated collectively or piecewise is still up for debate. Neither nature nor nurture influence our experience and perception in a vacuum. Surely, we appreciate the initial motivation of insight into the mental health applications of this work. We should first use these findings as insight into how the normative selection process develops through learning transitions, how it may require an optimal state, and how it is used to maximize performance. We should then use such insight to investigate the selection process of the disordered or diseased model of interest. Unquestionably, the notion of

whether detection is true detection, whether learning is true learning, whether selection is true selection, whether timing is true timing, and whether waiting is true waiting should continuously be critiqued. As a final point, though, we must reconcile amongst ourselves that under no circumstances are we to answer the question of whether attention is truly attention.

References

Agster, K. L., Clark, B. D., Gao, W. J., Shumsky, J. S., Wang, H. X., Berridge, C. W., & Waterhouse, B. D. (2011). Experimental strategies for investigating psychostimulant drug actions and prefrontal cortical function in ADHD and related attention disorders. *Anat Rec (Hoboken)*, *294*(10), 1698-1712. https://doi.org/10.1002/ar.21403

Antoine, M. W., Langberg, T., Schnepel, P., & Feldman, D. E. (2019). Increased Excitation-Inhibition Ratio Stabilizes Synapse and Circuit Excitability in Four Autism Mouse Models. *Neuron*, *101*(4), 648-661 e644. https://doi.org/10.1016/j.neuron.2018.12.026

Ashwood, Z. C., Roy, N. A., Stone, I. R., International Brain, L., Urai, A. E., Churchland, A. K., Pouget, A., & Pillow, J. W. (2022). Mice alternate between discrete strategies during perceptual decision-making. *Nat Neurosci*, *25*(2), 201-212. https://doi.org/10.1038/s41593-021-01007-z

Avramiea, A. E., Hardstone, R., Lueckmann, J. M., Bim, J., Mansvelder, H. D., & Linkenkaer-Hansen, K. (2020). Pre-stimulus phase and amplitude regulation of phase-locked responses are maximized in the critical state. *Elife*, *9*. https://doi.org/10.7554/eLife.53016

Bakhurin, K. I., Goudar, V., Shobe, J. L., Claar, L. D., Buonomano, D. V., & Masmanidis, S. C. (2017). Differential Encoding of Time by Prefrontal and Striatal Network Dynamics. *J Neurosci*, *37*(4), 854-870. https://doi.org/10.1523/JNEUROSCI.1789-16.2016

Bayard, F., Nymberg Thunell, C., Abé, C., Almeida, R., Banaschewski, T., Barker, G., Bokde, A. L. W., Bromberg, U., Büchel, C., Quinlan, E. B., Desrivières, S., Flor, H., Frouin, V., Garavan, H., Gowland, P., Heinz, A., Ittermann, B., Martinot, J. L., Martinot, M. L. P., . . . Petrovic, P. (2020). Distinct brain structure and behavior related to ADHD and conduct disorder traits. *Molecular Psychiatry*, *25*(11), 3020-3033. https://doi.org/10.1038/s41380-018-0202-6

Berg, E. L., Pride, M. C., Petkova, S. P., Lee, R. D., Copping, N. A., Shen, Y., Adhikari, A., Fenton, T. A., Pedersen, L. R., Noakes, L. S., Nieman, B. J., Lerch, J. P., Harris, S., Born, H. A., Peters, M. M., Deng, P., Cameron, D. L., Fink, K. D., Beitnere, U., . . . Silverman, J. L. (2020). Translational outcomes in a full gene deletion of ubiquitin

protein ligase E3A rat model of Angelman syndrome. *Translational Psychiatry*, *10*(1), 39. https://doi.org/10.1038/s41398-020-0720-2

Borroto-Escuela, D. O., Pintsuk, J., Schäfer, T., Friedland, K., Ferraro, L., Tanganelli, S., Liu, F., & Fuxe, K. (2016). Multiple D2 heteroreceptor complexes: new targets for treatment of schizophrenia. *Ther Adv Psychopharmacol*, *6*(2), 77-94. https://doi.org/10.1177/2045125316637570

Bromberg-Martin, E. S., Matsumoto, M., & Hikosaka, O. (2010). Dopamine in motivational control: rewarding, aversive, and alerting. *Neuron*, *68*(5), 815-834. https://doi.org/10.1016/j.neuron.2010.11.022

Buonomano, D. V., & Maass, W. (2009). State-dependent computations: spatiotemporal processing in cortical networks. *Nat Rev Neurosci*, *10*(2), 113-125. https://doi.org/10.1038/nrn2558

Eden, G. F., Stein, J. F., Wood, H. M., & Wood, F. B. (1995). Temporal and Spatial Processing in Reading Disabled and Normal Children. *Cortex*, *31*(3), 451-468. https://doi.org/https://doi.org/10.1016/S0010-9452(13)80059-7

Fiorillo, C. D., Newsome, W. T., & Schultz, W. (2008). The temporal precision of reward prediction in dopamine neurons. *Nat Neurosci*, *11*(8), 966-973. https://doi.org/10.1038/nn.2159

Grabenhorst, M., Michalareas, G., Maloney, L. T., & Poeppel, D. (2019). The anticipation of events in time. *Nature Communications*, *10*(1), 5802. https://doi.org/10.1038/s41467-019-13849-0

Graves, A., Wayne, G., Reynolds, M., Harley, T., Danihelka, I., Grabska-Barwinska, A., Colmenarejo, S. G., Grefenstette, E., Ramalho, T., Agapiou, J., Badia, A. P., Hermann, K. M., Zwols, Y., Ostrovski, G., Cain, A., King, H., Summerfield, C., Blunsom, P., Kavukcuoglu, K., & Hassabis, D. (2016). Hybrid computing using a neural network with dynamic external memory. *Nature*, *538*(7626), 471-476. https://doi.org/10.1038/nature20101

Hanisch, C., Radach, R., Holtkamp, K., Herpertz-Dahlmann, B., & Konrad, K. (2006). Oculomotor inhibition in children with and without attention-deficit hyperactivity disorder (ADHD). *J Neural Transm (Vienna)*, *113*(5), 671-684. https://doi.org/10.1007/s00702-005-0344-y

International Brain, L., Aguillon-Rodriguez, V., Angelaki, D., Bayer, H., Bonacchi, N., Carandini, M., Cazettes, F., Chapuis, G., Churchland, A. K., Dan, Y., Dewitt, E., Faulkner, M., Forrest, H., Haetzel, L., Hausser, M., Hofer, S. B., Hu, F., Khanal, A., Krasniak, C., . . . Zador, A. M. (2021). Standardized and reproducible measurement of decision-making in mice. *Elife*, *10*. https://doi.org/10.7554/eLife.63711

Jung, H., Woo, Y. J., Kang, J. W., Choi, Y. W., & Kim, K. M. (2014). Visual perception of ADHD children with sensory processing disorder. *Psychiatry Investig*, *11*(2), 119-123. https://doi.org/10.4306/pi.2014.11.2.119

Mante, V., Sussillo, D., Shenoy, K. V., & Newsome, W. T. (2013). Context-dependent computation by recurrent dynamics in prefrontal cortex. *Nature*, *503*(7474), 78-84. https://doi.org/10.1038/nature12742

Matell, M. S., & Portugal, G. S. (2007). Impulsive responding on the peak-interval procedure. *Behav Processes*, *74*(2), 198-208. https://doi.org/10.1016/j.beproc.2006.08.009

Meilleur, A., Foster, N. E. V., Coll, S. M., Brambati, S. M., & Hyde, K. L. (2020). Unisensory and multisensory temporal processing in autism and dyslexia: A systematic review and meta-analysis. *Neurosci Biobehav Rev*, *116*, 44-63. https://doi.org/10.1016/j.neubiorev.2020.06.013

Metin, B., Tas, Z. C., Cebi, M., Buyukaslan, A., Soysal, A., Hatiloglu, D., & Tarhan, N. (2018). Reward Processing Deficits During a Spatial Attention Task in Patients With ADHD: An fMRI Study. *J Atten Disord*, *22*(7), 694-702. https://doi.org/10.1177/1087054717703188

Murat Baldwin, M., Xiao, Z., & Murray, A. (2021). Temporal Synchrony in Autism: a Systematic Review. *Review Journal of Autism and Developmental Disorders*. https://doi.org/10.1007/s40489-021-00276-5

Musall, S., Kaufman, M. T., Juavinett, A. L., Gluf, S., & Churchland, A. K. (2020). Single-trial neural dynamics are dominated by richly varied movements. *Nat Neurosci*, *22*(10), 1677-1686. https://doi.org/10.1038/s41593-019-0502-4

Näätänen, R. (1970). The diminishing time-uncertainty with the lapse of time after the warning signal in reaction-time experiments with varying fore-periods. *Acta Psychol (Amst)*, *34*(4), 399-419. https://doi.org/10.1016/0001-6918(70)90035-1

Namboodiri, V. M., Huertas, M. A., Monk, K. J., Shouval, H. Z., & Hussain Shuler, M. G. (2015). Visually cued action timing in the primary visual cortex. *Neuron*, *86*(1), 319-330. https://doi.org/10.1016/j.neuron.2015.02.043

Narayanan, N. S., & Laubach, M. (2009). Delay activity in rodent frontal cortex during a simple reaction time task. *J Neurophysiol*, *101*(6), 2859-2871. https://doi.org/10.1152/jn.90615.2008

Nguyen, D. P., & Lin, S. C. (2014). A frontal cortex event-related potential driven by the basal forebrain. *Elife*, *3*, e02148. https://doi.org/10.7554/eLife.02148

Ni, A. M., Ruff, D. A., Alberts, J. J., Symmonds, J., & Cohen, M. R. (2018). Learning and attention reveal a general relationship between population activity and behavior. *Science*, *359*(6374), 463-465. https://doi.org/10.1126/science.aao0284

Nobre, A. C., Correa, A., & Coull, J. T. (2007). The hazards of time. *Current Opinion in Neurobiology*, *17*(4), 465-470. https://doi.org/https://doi.org/10.1016/j.conb.2007.07.006

Nonomura, S., Nishizawa, K., Sakai, Y., Kawaguchi, Y., Kato, S., Uchigashima, M., Watanabe, M., Yamanaka, K., Enomoto, K., Chiken, S., Sano, H., Soma, S., Yoshida, J., Samejima, K., Ogawa, M., Kobayashi, K., Nambu, A., Isomura, Y., & Kimura, M. (2018). Monitoring and Updating of Action Selection for Goal-Directed Behavior through the Striatal Direct and Indirect Pathways. *Neuron*, *99*(6), 1302-1314.e1305. https://doi.org/10.1016/j.neuron.2018.08.002

Pardey, M. C., Homewood, J., Taylor, A., & Cornish, J. L. (2009). Re-evaluation of an animal model for ADHD using a free-operant choice task. *J Neurosci Methods*, *176*(2), 166-171. https://doi.org/10.1016/j.jneumeth.2008.09.009

Pardey, M. C., Kumar, N. N., Goodchild, A. K., & Cornish, J. L. (2013). Catecholamine receptors differentially mediate impulsive choice in the medial prefrontal and orbitofrontal cortex. *J Psychopharmacol*, *27*(2), 203-212. https://doi.org/10.1177/0269881112465497

Parker, K. L., Chen, K. H., Kingyon, J. R., Cavanagh, J. F., & Narayanan, N. S. (2014). D1-dependent 4 Hz oscillations and ramping activity in rodent medial frontal cortex during interval timing. *J Neurosci*, *34*(50), 16774-16783. https://doi.org/10.1523/JNEUROSCI.2772-14.2014

Pedrosa, V., & Clopath, C. (2017). The Role of Neuromodulators in Cortical Plasticity. A Computational Perspective [Perspective]. *Frontiers in Synaptic Neuroscience*, *8*. https://doi.org/10.3389/fnsyn.2016.00038

Perez, O., & Merchant, H. (2018). The Synaptic Properties of Cells Define the Hallmarks of Interval Timing in a Recurrent Neural Network. *J Neurosci*, *38*(17), 4186-4199. https://doi.org/10.1523/JNEUROSCI.2651-17.2018

Pisupati, S., Chartarifsky-Lynn, L., Khanal, A., & Churchland, A. K. (2021). Lapses in perceptual decisions reflect exploration. *Elife*, *10*. https://doi.org/10.7554/eLife.55490

Roelfsema, P. R., & Holtmaat, A. (2018). Control of synaptic plasticity in deep cortical networks. *Nature Reviews Neuroscience*, *19*(3), 166-180. https://doi.org/10.1038/nrn.2018.6

Roy, N. A., Bak, J. H., International Brain, L., Akrami, A., Brody, C. D., & Pillow, J. W. (2021). Extracting the dynamics of behavior in sensory decision-making experiments. *Neuron*. https://doi.org/10.1016/j.neuron.2020.12.004

Ruff, D. A., & Cohen, M. R. (2019). Simultaneous multi-area recordings suggest that attention improves performance by reshaping stimulus representations. *Nat Neurosci*, *22*(10), 1669-1676. https://doi.org/10.1038/s41593-019-0477-1

Silverman, J. L., Babineau, B. A., Oliver, C. F., Karras, M. N., & Crawley, J. N. (2013). Influence of stimulant-induced hyperactivity on social approach in the BTBR mouse model of autism. *Neuropharmacology*, *68*, 210-222. https://doi.org/10.1016/j.neuropharm.2012.07.042

Silverman, J. L., Thurm, A., Ethridge, S. B., Soller, M. M., Petkova, S. P., Abel, T., Bauman, M. D., Brodkin, E. S., Harony-Nicolas, H., Wöhr, M., & Halladay, A. (2022). Reconsidering animal models used to study autism spectrum disorder: Current state and optimizing future [https://doi.org/10.1111/gbb.12803]. *Genes, Brain and Behavior*, *21*(5), e12803. https://doi.org/https://doi.org/10.1111/gbb.12803

Silverman, J. L., Tolu, S. S., Barkan, C. L., & Crawley, J. N. (2010). Repetitive self-grooming behavior in the BTBR mouse model of autism is blocked by the mGluR5 antagonist MPEP. *Neuropsychopharmacology*, *35*(4), 976-989. https://doi.org/10.1038/npp.2009.201

Sohn, H., Narain, D., Meirhaeghe, N., & Jazayeri, M. (2019). Bayesian Computation through Cortical Latent Dynamics. *Neuron*, *103*(5), 934-947 e935. https://doi.org/10.1016/j.neuron.2019.06.012

Till, S. M., Hickson, R. D. L., & Kind, P. C. (2022). Cross-species considerations in models of neurodevelopmental disorders. *Trends in Neurosciences*, *45*(3), 171-172. https://doi.org/https://doi.org/10.1016/j.tins.2021.12.005

Toda, K., Lusk, N. A., Watson, G. D. R., Kim, N., Lu, D., Li, H. E., Meck, W. H., & Yin, H. H. (2017). Nigrotectal Stimulation Stops Interval Timing in Mice. *Curr Biol*, *27*(24), 3763-3770 e3763. https://doi.org/10.1016/j.cub.2017.11.003

Toplak, M. E., Dockstader, C., & Tannock, R. (2006). Temporal information processing in ADHD: findings to date and new methods. *J Neurosci Methods*, *151*(1), 15-29. https://doi.org/10.1016/j.jneumeth.2005.09.018

Zariwala, Hatim A., Kepecs, A., Uchida, N., Hirokawa, J., & Mainen, Zachary F. (2013). The Limits of Deliberation in a Perceptual Decision Task. *Neuron*, *78*(2), 339-351. https://doi.org/https://doi.org/10.1016/j.neuron.2013.02.010

Figures and Legends

Figure 5.1: Target Timing with Delay Paradigm

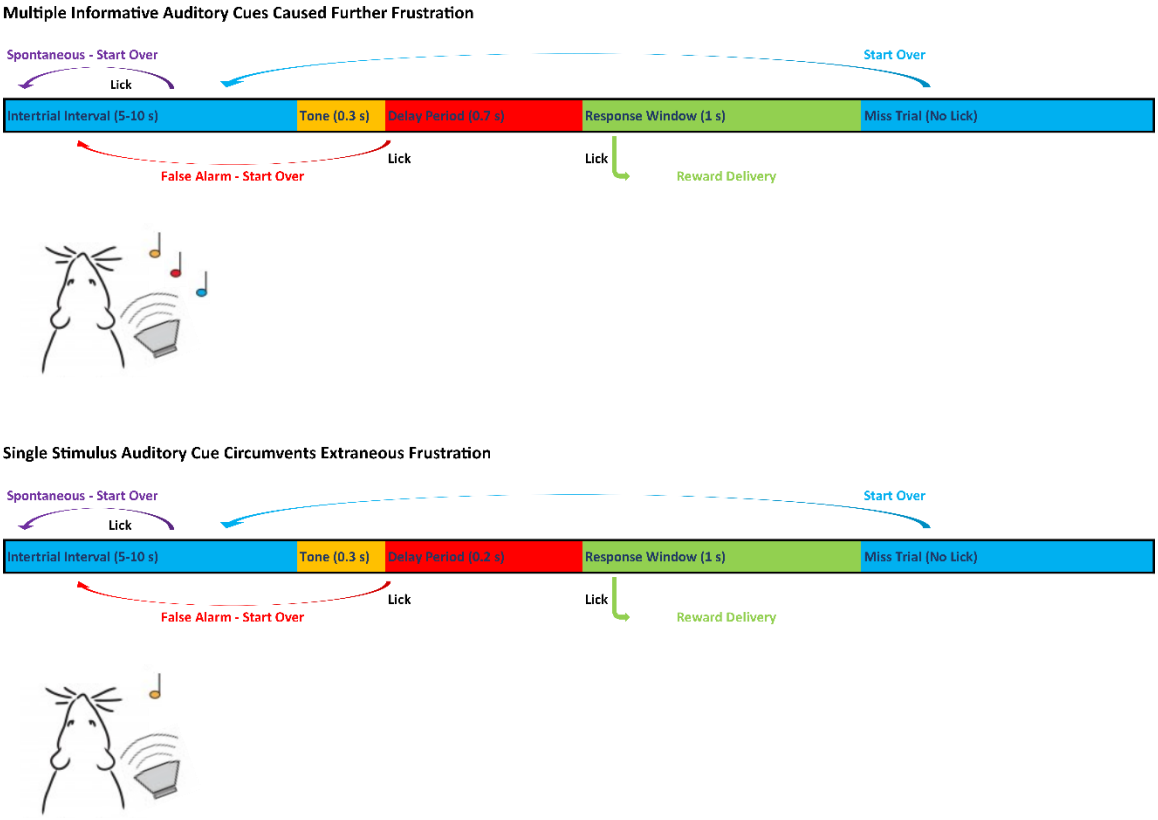

Above) Initial task structure to investigate interval timing with delay and penalty; mice performed poorly; auditory cues were adjusted to minimize a startle effect; mice seemed most frustrated with the reporting of trial outcome by differential pure tones. Below) Revised task structure to investigate interval timing with delay and penalty; mice performed better without multiple auditory cues but had difficulty with the penalty during the delay due to spontaneous responding.

Figure 5.2: Target Timing versus Detection Paradigm

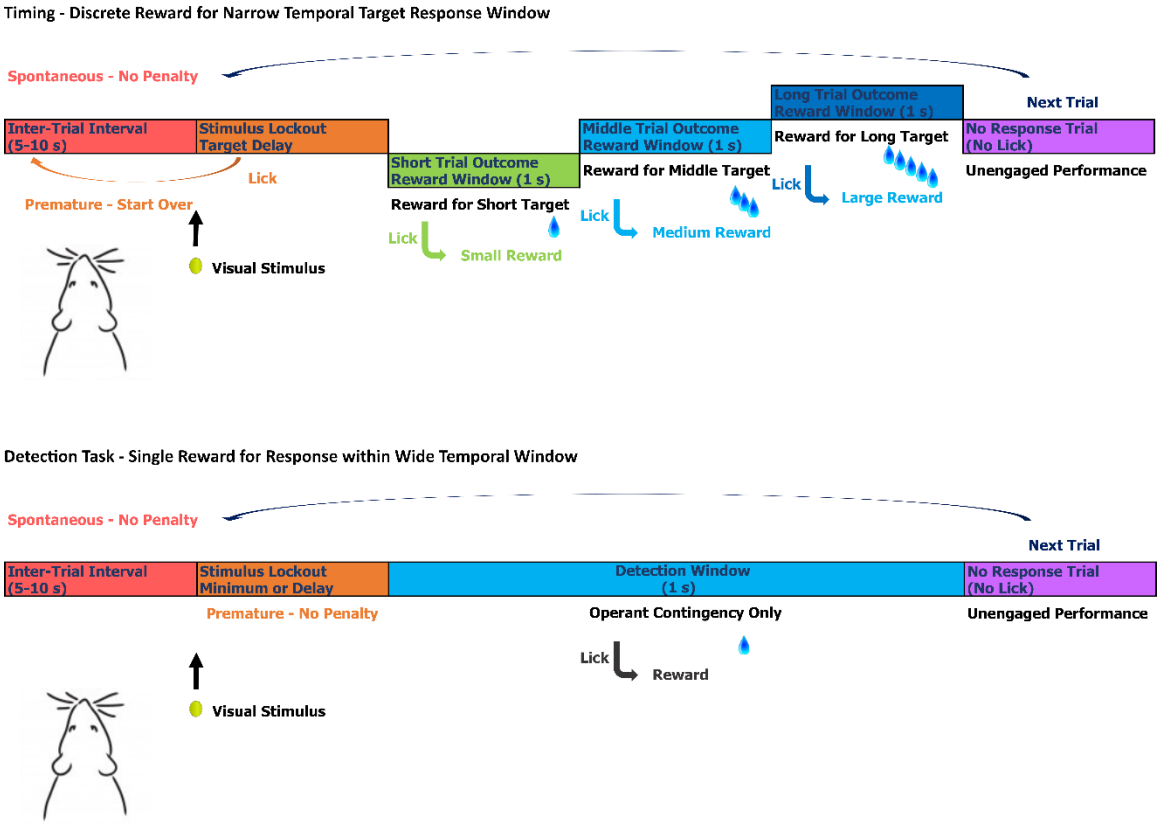

Above) A timing task would include a stimulus presentation followed by a reported response with a reaction time readout; preferred target reward per mouse may vary but should shift towards preferred target window and become less variable in RT CDF curves as mouse improves performance. Below) A detection task also includes a stimulus presentation followed by a reported response with a reaction time readout; with no penalty and no delay, the RT CDF curves shift towards fastest reaction time possible as mouse improves performance.

Figure 5.3: Withhold Before versus After Stimulus Paradigm

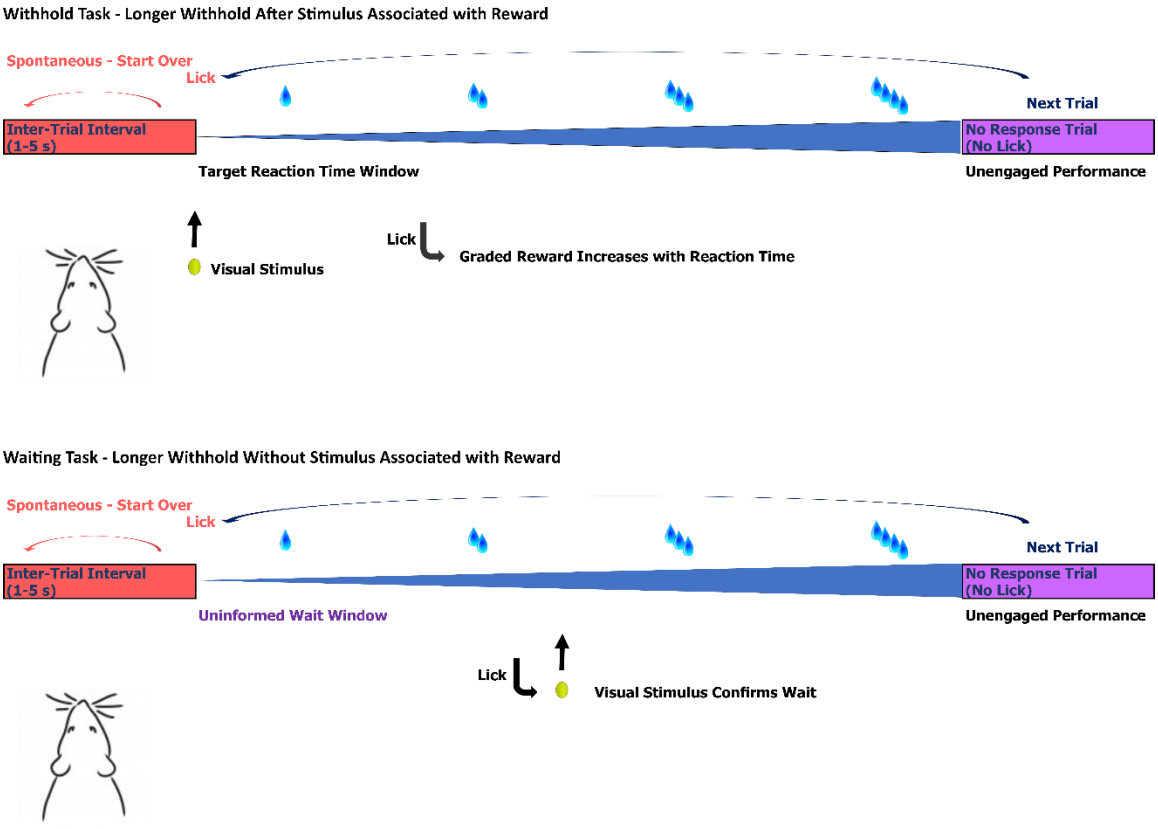

Above) A stimulus withhold task requires a stimulus where longer reaction times indicate reward association with longer withholding; we would expect that the intertrial interval influences the hazard effect. Below) A wait withhold task requires no stimulus where longer interlick intervals indicate reward association with longer waiting; we would expect that the interlick interval influences the hazard effect.

APPENDIX

Appendix Figure 1: Target Choice Probability Maps in the Prestimulus Cortical State

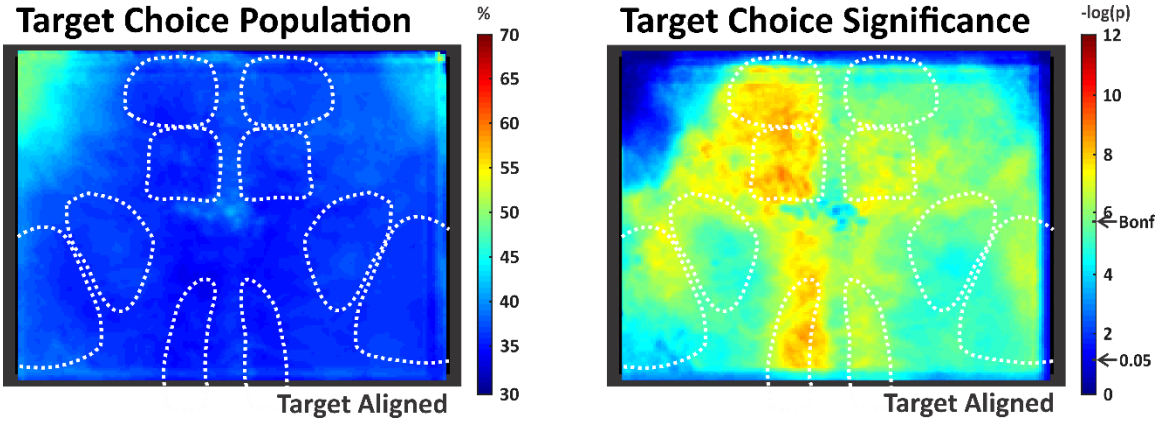

Left) Target response choice probability map; color scale [30% 70%]; lower than chance choice probability in the prestimulus epoch for target trials only; additional evidence for global, low amplitude, prestimulus cortical state. Right) Significance map for target response choice probability; greater significance in lower than chance choice probability for distractor aligned regions: whisker motor cortex, anterolateral motor cortex, and retrosplenial cortex.

Appendix Figure 2: Encoding Maps in the Prestimulus Cortical State

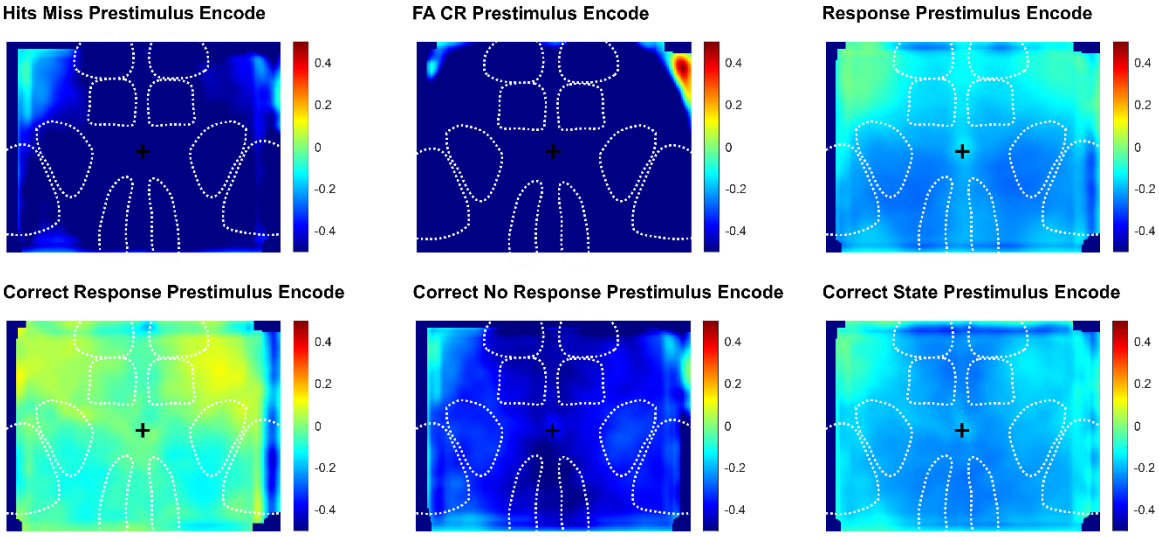

Top Left) Hit response choice encoding map; low encoding indicates low fluorescence predicts a hit response outcome versus a miss no response outcome. Top Middle) FA response choice encoding map; low encoding indicates low fluorescence predicts a FA response outcome versus a CR no response outcome. Top Right) Response choice encoding map; low encoding indicates low fluorescence predicts a response outcome versus a no response outcome. Bottom Left) Correct response choice encoding map; high encoding indicates higher fluorescence predicts a correct response (hit) versus an incorrect response (FA). Bottom Middle) Correct no response choice encoding map; low encoding indicates lower fluorescence predicts a correct no response (CR) versus an incorrect no response (Miss). Bottom Right) Correct state choice encoding map; low encoding indicates lower fluorescence predicts a correct state (Hit or CR) versus an incorrect state (Miss or FA; color scale for all maps [-0.5% 0.5%]).

Appendix Figure 3: Significant Encoding in the Prestimulus Cortical State

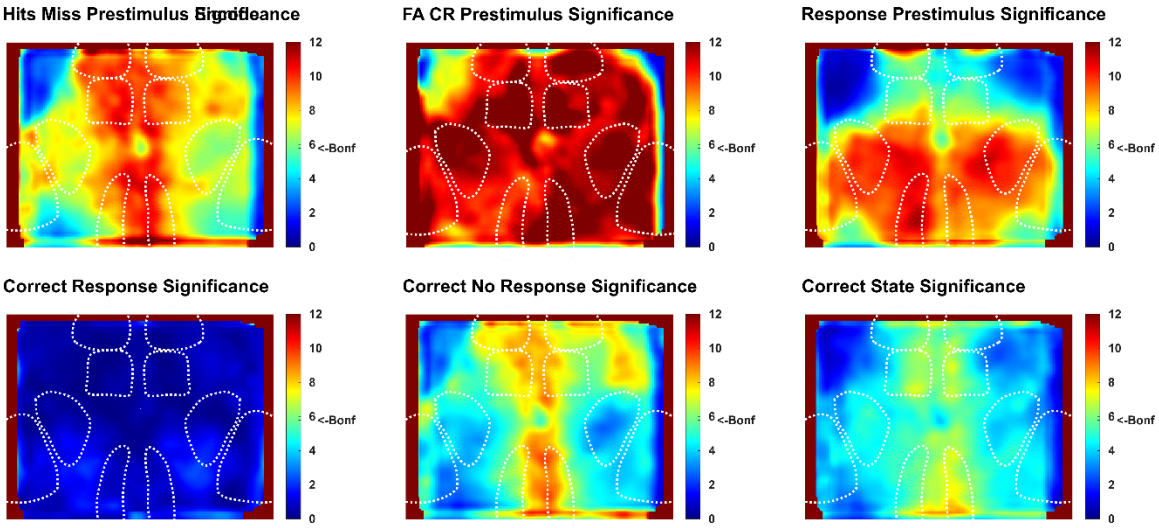

Top Left) Hit response choice significance map; focal midline effect predicts hit response outcome versus miss no response outcome. Top Middle) FA response choice significance map; global effect predicts FA response outcome versus CR no response outcome. Top Right) Response choice significance map; global sensory effect predicts response outcome versus no response outcome. Bottom Left) Correct response choice significance map; Hit response outcomes cannot be differentiated from FA response outcomes. Bottom Middle) Correct no response choice significance map; focal midline effect, higher in distractor aligned cortices, predicts a CR no response outcome versus a miss no response outcome. Bottom Right) Correct state significance map; focal frontal midline effect, with potential RSP effect, predicts Hit or CR outcome versus Miss or FA outcome (color scale for all maps [0 12], Bonferroni corrected; error indicates threshold for p=0.05 significance with a Bonferroni correction).